

Republic of Iraq
Ministry of Higher Education
and Scientific Research
University of Anbar
College of Engineering
Civil Engineering Department



Nonlinear Finite Element Analysis of Strengthened Reinforced Concrete Columns

A THESIS

**SUBMITTED TO THE CIVIL ENGINEERING DEPARTMENT
OF THE COLLEGE OF ENGINEERING OF ANBAR
UNIVERSITY IN PARTIAL FULFILLMENT OF THE
REQUIREMENTS FOR THE DEGREE OF MASTER OF
SCIENCE IN CIVIL ENGINEERING**

By

Zahraa Talib S. Al-Khatib

B.Sc. Civil Engineering 2014

Supervised By:

Asst. Prof. Dr. Akram S. Mahmoud

2018 A.D.

1439 A.H.

بِسْمِ اللَّهِ الرَّحْمَنِ الرَّحِيمِ

قُلْ إِنَّ صَلَاتِي وَنُسُكِي وَمَحْيَايَ وَمَمَاتِي لِلَّهِ رَبِّ
الْعَالَمِينَ ﴿١٦٢﴾ لَا شَرِيكَ لَهُ ۗ وَبِذَلِكَ أُمِرْتُ وَأَنَا أَوَّلُ
الْمُسْلِمِينَ ﴿١٦٣﴾

صدق الله العظيم

سورة الأنعام الآية (١٦٢-١٦٣)

Supervisor's Certificate

I certify that this thesis entitled "**Nonlinear Finite Elements Analysis of Strengthened Reinforced Concrete Columns**" was prepared by **Zahraa Talib S. Al-Khatib** under my supervision at the Civil Engineering Department, College of Engineering, University of Anbar as a partial fulfillment of the requirements for the degree of Master of Science in Civil Engineering.

Supervisor

Signature: _____

Name: **Assist. Prof. Dr.Akram S. Mahmoud**

Date: / / 2018

Report of Language Advisor

I certify that this thesis titled "**Nonlinear Finite Element Analysis of Strengthened Reinforced Concrete Columns**", which was prepared by **Zahraa Talib S. Al-Khatib** at the University of Anbar, College of Engineering, Civil Engineering Department has been revised linguistically by me and thus the thesis is now ready for discussion as far as language and style are concerned.

Signature: _____

Name: **Prof. Ayad Hammad Al-Duleimi**

Date: / / 2018

Report of the Head of the Civil Engineering Department

According to the recommendation presented by the supervisor and chairman of the postgraduate studies, I forward this thesis for discussion.

Signature: _____

Name: **Assist. Prof. Dr. Akram S. Mahmoud**

Date: / / 2018

Examining Committee Certificate

We certify that we have read this thesis entitled " **Nonlinear Finite Element Analysis of Strengthened Reinforced Concrete Columns** ", and as examining committee, examined the student **Zahraa Talib S. Al-Khatib** in its content, and that in our opinion, it meets the standard of thesis for the degree of Master of Science in Civil Engineering (Structural Engineering).

Signature: _____

Name: **Asst. Prof. Dr. Waleed A. Waryosh**
(Chairman)

Date: / / 2018

Signature: _____

Name: **Asst. Prof. Dr. Abbas A. Allawi**
(Member)

Date: / / 2018

Signature: _____

Name: **Dr. Sheelan Mahmoud Hama**
(Member)

Date: / / 2018

Signature: _____

Name: **Assist. Prof. Dr. Akram S. Mahmoud**
(Supervisor)

Date: / / 2018

Approved by the College of Engineering:

Signature: _____

Name: **Asst. Prof. Dr. Akram S. Mahmoud**
(Head of Civil Engineering Department)

Date: / / 2018

Signature: _____

Name: **Prof. Dr. Ibrahim A. Al-Jumaily**
(Dean of Engineering College)

Date: / / 2018

ACKNOWLEDGMENTS

Thanks and praise to **Allah** for inspiring and giving me the strength, willingness and patience to complete this work. Prayer and peace be upon the Messenger of **Allah Mohammed**.

It is with immense gratitude that I acknowledge the support and help of my supervisor **Asst. Prof. Dr. Akram S. Mahmoud**, who supported me with his unlimited experience, inspiration and continues valuable scientific suggestions throughout the preparation of this thesis and being patient with me in accomplishing this work.

I am indebted to my colleagues and friends for their support, advice and unlimited help along the entire steps of the master course.

I am also grateful for my brother **Hassan Al-Khatib** for his unlimited support and help during my study. In addition, I would like to express my gratitude to my brother in-law **Aws Al-Rawi** for his help.

Finally, I would like to thank my family: my parents, my brothers and sister for their patience and spiritual supporting through writing this thesis and my life in general.

Zahraa Talib S. Al-Khatib

ABSTRACT

The demand for strengthening structures became necessary when an increase in load was inevitable. Columns are an important element that needs strengthening because the degradation of these columns causes total failure of structures.

This research studied the behavior of nonlinear analysis of strengthening reinforced concrete column by finite element method used ANSYS package.

The verification models in this research consist of eight specimens; three of these specimens subjected to short-term loading, and other five remained specimens subjected to long-term loading. A three-dimensional finite element model has been used in this work. SOLID65 element used for modeling concrete and LINK8 element for steel reinforcement modeling in the analysis of reinforced concrete columns under short-term loading. In the analysis of concrete columns under long-term loading used VISCO89 element for concrete modeling and SHELL41 element for FRP modeling.

This study achieved a good agreement between numerical and available experimental results, it was found that the percentage of error of specimens which subject to short-term loading between (0.5-5.7)% for displacement and about (1.1-7.7)% for ultimate load, while the percentage of error of the other specimens that subjected to long-term loading between (2.3-5.9)% based on creep strain.

Also, this research studied the effect of some important parameters on the behavior of strengthening circular section of concrete columns. Five parameters are studied in this research the magnitude of sustained load ($7\%P_u$ - $28\%P_u$ - $72\%P_u$)kN, e/h ratio (0-0.26-0.46), length-diameter ratio (8-15-30), compressive strength (30-40-50)MPa and FRP type (glass or carbon). A 162 models were analyzed and discussed and then noticed from studying the effect of these

parameters that creep strain decreased about 13.2% and 10.4% when increased the compressive strength from (30-40)MPa and (40-50)MPa, respectively, but creep strain increased about 300% and 150% when the magnitude of sustained load increased from (7% P_u to 28% P_u)kN and (28% P_u to 72% P_u)kN respectively, while the effect of eccentricity magnitude and length - diameter ratio was very little on the creep strain.

Finally, notice that strengthened concrete columns with CFRP give a high creep strain more than thirteen times of other concrete columns which strengthened with GFRP. However, that the studied model can be represent more efficient tool for simulating long term behavior of strengthened RC column.

Notations

Symbols	Definition
ν_{xy}	Major Poisson's Ratio
ν_{yz}, ν_{xz}	Minor Poisson's Ratio
C'_b	Basic creep coefficient
$C'_b(t, t', t_0)$	Drying creep coefficient
E_c	Elastic Modulus of concrete (MPa)
E_s	Elastic Modulus of steel (MPa)
E_x	Elastic Modulus in x-direction (MPa)
E_y	Elastic Modulus in y-direction (MPa)
E_z	Elastic Modulus in z-direction (MPa)
G_{xy}	Shear Modulus in the xy Plane (MPa)
G_{xz}	Shear Modulus in the xz Plane (MPa)
G_{yz}	Shear Modulus in the yz Plane (MPa)
f_y	Yield Stress of steel (MPa)
k_σ	The ratio of stress to strength
t_0	Age of concrete at loading
ν_u	Ultimate creep coefficient
$\beta_c(t, t_0)$	Function to describe the development of creep with time after loading
ϵ_{cb}	Basic creep strain
$\phi_{0,k}$	Non-linear notional creep coefficient
ϕ_0	Notional creep coefficient.
$\Delta(\tau)$	Compliance spectrum
a	Air content
ϵ''	Inelastic strain (stress dependent)
E_0	Initial modulus (MPa)
ϵ_C	Creep strain
ϵ_E	Instantaneous strain
ϵ°	Inelastic strain (stress independent)
ϵ_{Sh}	Shrinkage strain
ϵ_T	Thermal strain
ϵ_σ	Mechanical strain (stress produced strain)
f'_c	Compressive strength (MPa)
f'_t	Splitting tensile strength (MPa)
G	Shear Modulus (MPa)

Notation and Abbreviations

h	Minimum thickness (mm)
$H(t)$	Heaviside step function
K	Bulk Modulus (MPa)
t	Current age (day)
t'	Age at loading (day)
ν	Poisson's Ratio
γ_c	Correction factors for concrete
γ_{la}	Correction factor of load age
λ	Ambient relative humidity
τ	Loading age (day)
ψ	The percent of fines by weight
D	Inverse of elastic modulus
E'	The asymptote of a plot of creep vs the logarithm of short times under load
$J(t,t')$	Creep function
Γ	Gamma function.
β_0	Open shear transfer coefficient
β_1	Closed shear transfer coefficient
$\delta(t)$	Dirac delta function
η	Newton viscosity
σ_0	Constant stress (MPa)
$\phi(t,t_0)$	Creep coefficient

Abbreviations

ACI	American Concrete Institute
AFRP	Aramid Fiber Reinforced Polymer
AS	Standards Australia
BP	Bazant-Panula
CEB	Committe European du Beton
CFFT	Concrete Filled Fiber Reinforced Polymer Tube
CFRP	Carbon Fiber Reinforced Polymer
CFST	Concrete Filled Steel Tube
EBR	External Bonded Reinforcement
EBRIG	External Bonded Reinforcement in Groves
EBROG	External Bonded Reinforcement on Groves
FEM	Finite Element Analysis
FRP	Fiber Reinforced Polymer

Notation and Abbreviations

FWCC	Fiber Warped Concrete Column
GFRP	Glass Fiber Reinforced Polymer
HSS	Hollow Steel Structural
NSM	Near Surface Mounted
RC	Reinforced Concrete

Table of Contents

<u>Subject</u>	<u>Page</u>
ACKNOLGEMENTS	I
ABSTRACT	II
Table of Contents	IV
List of Tables	VII
List of Figures	VIII
Notation and Abbreviations	XIX
<u>Chapter One: Introduction</u>	
1.1:General	1
1.2:FRP Composite for Strengthening RC Columns	2
1.3:Problem Statement	4
1.4: Objective of Research	5
1.5:Limitations of This Study	5
1.6:Thesis Outline	6
<u>Chapter Two: Literature Review</u>	
2.1:General	7
2.2:Short-Term Behavior of Concrete Columns Strengthening By Fiber Reinforced Polymer (FRP)	7
2.2.1:Strengthening By Carbon Fiber Reinforced Polymer (CFRP)	8
2.2.2 Strengthening By Glass Fiber Reinforced Polymer (GFRP)	14
2.2.3 Strengthening By Aramid Fiber Reinforced Polymer (AFRP)	16
2.3:Short-Term Behavior of Concrete Columns Enhancement By Ferrocement	17
2.4:Long-Term Behavior of Reinforced Concrete Columns	20
2.4.1:Unconfined Reinforced Concrete Columns	20
2.4.2:Confined Concrete Columns With Steel	23
2.4.3:Confined Concrete Columns With FRP	25
2.5:Mathematical Modeling of Creep of Concrete	27
2.6:Representation of Time Effects Analysis of Concrete	30
2.7:Conclusion Remark	32
<u>Chapter Three: Creep Analysis</u>	
3.1:General	33
3.2: Behavior of Concrete as a Visco-Elastic Material	33
3.2.1: Compliance Function	34
3.2.2: Viscoelastic Models	37
3.2.2.1: Maxwell Model	38
3.2.2.2: Kelvin Model	40
3.2.2.3: Standard Linear Solid	41
3.2.2.4: Maxwell-Kelvin Model	41
3.2.2.5: Power Law	42
3.2.2.6: Prony Series	43

Table of Contents

3.3: Differential Operator Form of Stress Strain Constitutive Relations	44
3.4: Concrete Aging Effects	46
3.5: Basic Theory of Viscoelasticity in ANSYS Program	47
<u>Chapter Four: Verification Models</u>	
4.1: General	49
4.2: Analysis of Reinforced Concrete Columns Subjected to Short Term Loading	49
4.2.1: Control Columns	50
4.2.1.1: Mourad and Shannag RC column	50
4.2.1.1.1: Description of Test Specimen (SC-2)	50
4.2.1.1.2: Finite Element Idealization and Material properties	50
4.2.2: Jacketed Columns:	53
4.2.2.1: Widiarsa and Hadi RC Column Strengthen with CFRP Sheet	53
4.2.2.1.1: Description of Test Specimen (1HC0)	53
4.2.2.1.2: Finite Element Idealization and Material properties	53
4.2.2.2: Benzaid et al Concrete Column Strengthened with GFRP Sheet	56
4.2.2.2.1: Description of Test Specimen (S1R1)	56
4.2.2.2.2: Finite Element Idealization and Material properties	57
4.2.3: Results of Analysis for (SC-2), (1HC0) and (S1R1) Models	59
4.3: Analysis of Columns Subjected to Long Term Loading	67
4.3.1: Control Columns	67
4.3.1.1: Katoka and Bittencourt RC column	67
4.3.1.1.1: Description of Test Specimen (F40-1.4-1)	67
4.3.1.1.2: Finite Element Idealization and Material properties	68
4.3.1.2: Hamed and Lai RC column	70
4.3.1.2.1: Description of Test Specimen (E80-C)	70
4.3.1.2.2: Finite Element Idealization and Material properties	71
4.3.2: Jacketed Columns	72
4.3.2.1: Naguib and Mirmiran column	72
4.3.2.1.1: Description of Test Specimen (FWCC)	72
4.3.2.2: Al-Chami column	73
4.3.2.2.1: Description of Test Specimen (B1C1)	73
4.3.2.3: Wang and Liu column	74
4.3.2.3.1: Description of Test Specimen (FWCC-A)	74
4.3.2.4: Finite Element Idealization and Material Properties For (FWCC), (B1C1) and (FWCC-A) Models	75
4.3.3: Results of Analysis For Columns Under Long-Term Loading	78

Table of Contents

Chapter Five: Parametric Study

5.1: General	94
5.2: Finite Element Idealization and Material Properties	94
5-3: The Parametric	98
5.3.1: Magnitude of Sustained Load Effect	102
5.3.2: Eccentricity Effect	120
5.3.3: Length Effect	121
5.3.4: Compressive Strength Effect	121
5.3.5: FRP Type Effect	140

Chapter Six: Conclusion

6.1: Introduction	155
6.2: Conclusion	155
6.2: Recommendations and Future Research	157

References

Appendix-A

Appendix-B

List of Tables

<u>Table No.</u>	<u>Page</u>
Table(3-1): Viscoelastic Models.....	39
Table (3-2): Aging Coefficient.....	47
Table (4-1): Element Type and Material Properties of (SC-2) RC Column.....	52
Table (4-2):Element Type and Material Properties of (1HC0) RC Column.....	55
Table (4-3): Element Type and Material Properties of (S1R1) Concrete Column.....	58
Table(4-4): The Results of Experimental and Finite Element Method of (SC-2), (SRCl.1L) and (Col.05.P1)Models.....	60
Table(4-5):Properties of Concrete Mix.....	69
Table (4-6): Element Type and Material Properties of (F40-1.4-1) RC Column.....	69
Table (4-7): Element Type and Material Properties of (E80-C)RC Column.....	71
Table (4-8): Element Type and Material Properties for (FWCC), (B1C1) and (FWCC-A) Models.....	76
Table(4-9): Shear Relaxation Functions For Columns Under Long-Term Loading.....	79
Table(4-10): The Results of Experimental and Finite Element Method of (F40-1.4-1), (E80-C), (FWCC), (B1C1) and (FWCC-A) Models.....	93
Table (5-1): Concrete Material Properties.....	94

List of Figures

<u>Figure No.</u>	<u>Page</u>
Fig.(1.1):Stress-Strain Relationship of Different Fibers.....	3
Fig.(1.2): Schematic of FRP Composites.....	4
Fig.(2.1):Method of Strengthening RC Square Column.....	13
Fig.(2.2):Comparision of Load vs Deflection Curves.....	13
Fig.(3.1): Creep Response of Uniaxial Loaded Specimen.....	33
Fig.(3.2): a-Creep isochrones, b-Compliance curves for various.....	36
Fig.(4.1):Details of (SC-2) RC Column.....	51
Fig.(4.2):Finite Element Model of (SC-2) RC Column.....	52
Fig.(4.3): Details of (1HC0) RC. Column.....	54
Fig.(4.4): Finite Element Model of (1HC0) RC. Column	56
Fig.(4.5): Details of (S1R1) Concrete Column.....	57
Fig.(4.6):Finite element model of (S1R1) Concrete column	59
Fig.(4.7):Experimental and Numerical Load-Displacement Curve for (SC-2) RC Column.....	60
Fig.(4.8): Displacements of (SC-2) Model at Ultimate Load.....	61
Fig.(4.9): Strains of (SC-2) model at ultimate load.....	61
Fig.(4.10): Crack pattern of (SC-2) model at ultimate load.....	62
Fig.(4.11): Experimental and numerical load-displacement curve for (SRCI.1L) RC column.....	62
Fig.(4.12): Displacements of (1HC0) Model at Ultimate Load.....	63
Fig.(4.13): Strains of (1HC0) Model at Ultimate Load.....	63
Fig.(4.14): Crack Pattern of (1HC0) Model at Ultimate Load.....	64
Fig.(4.15): Experimental and numerical Stress-Strain curve for (S1R1) Concrete Column.....	64
Fig.(4.16): Displacements of (S1R1) Model at Ultimate Load.....	65

List of Figures

Fig.(4.17): Strains of (S1R1) Model at Ultimate Load.....	65
Fig.(4.18): Crack Pattern of (S1R1) Model at Ultimate Load	66
Fig.(4-19): Details of (F40-1.4-1) RC Column.....	68
Fig.(4-20):Finite Element Model of (F40-1.4-1)RC Column.....	69
Fig.(4.21): Details of (E80-C) RC Column.....	70
Fig.(4.22):Finite Element Model of (E80-C) RC Column.....	72
Fig.(4.23): Details of (FWCC) Column.....	73
Fig.(4.24): Details of (B1C1) Column.....	74
Fig.(4.25): Details of (FWCC-A) Column.....	75
Fig.(4.26): Finite Element Model of (FWCC) Column.....	77
Fig.(4.27): Finite Element Model of (B1C1) Column.....	77
Fig.(4.28): Finite Element Model of (FWCC-A) Column.....	78
Fig.(4.29): Shear Modulus Relaxation vs Time for (F40-1.4-1) Column...	80
Fig.(4.30):Percent of Error vs Time for (F40-1.4-1) Column.....	80
Fig.(4.31): Experimental and Numerical Time-Creep Strain Curve for (F40-1.4-1) Column.....	81
Fig.(4.32): Displacements of (F40-1.4-1) Model in y-direction at 91Day..	81
Fig.(4.33): Strains of (F40-1.4-1) Model in y-direction at 91Day.....	82
Fig.(4.34): Principle Stresses of (F40-1.4-1) Model in y-direction at 91Day.....	82
Fig.(4.35): Shear Modulus Relaxation vs Time for (E80-C)Column.....	83
Fig.(4.36):Percent of Error vs Time for (E80-C) Column.....	83
Fig.(4.37): Experimental and Numerical Time-Creep Strain Curve for (E80-C) Column.....	84
Fig.(4.38): Displacements of (E80-C) Model in x-direction at 91Day.....	84
Fig.(4.39): Strains of (E80-C) Model in x-direction at 91Day.....	85
Fig.(4.40): Principle Stresses of (E80-C) Model in x-direction at 91Day...	85
Fig.(4.41): Shear Modulus Relaxation vs Time for (FWCC)Column.....	86
Fig.(4.42):Percent of Error vs Time for (FWCC) Column.....	86

List of Figures

Fig.(4.43): Experimental and Numerical Time-Creep Strain Curve for (FWCC) Column.....	87
Fig.(4.44): Displacements of (FWCC) Model in z-direction at 91Day.....	87
Fig.(4.45): Strains of (FWCC) Model in z-direction at 91Day.....	88
Fig.(4.46): Principle Stresses of (FWCC) Model in z-direction at 91Day..	88
Fig.(4.47): Shear Modulus Relaxation vs Time for (B1C1)Column.....	89
Fig.(4.48):Percent of Error vs Time for (B1C1) Column.....	89
Fig.(4.49): Experimental and Numerical Time-Creep Strain Curve for (B1C1) Column.....	90
Fig.(4.50): Displacements of (B1C1) Model in z-direction at 568Day.....	90
Fig.(4.51): Strains of (B1C1) Model in z-direction at 568Day.....	91
Fig.(4.52): Principal Stresses of (B1C1) Model in z-direction at 568Day..	91
Fig.(4.53): Shear Modulus Relaxation vs Time for (FWCC-A)Column....	92
Fig.(4.54):Percent of Error vs Time for (FWCC-A) Column	92
Fig.(4.55): Experimental and Numerical Time-Creep Strain Curve for (FWCC-A) Column.....	93
Fig.(5.1): Finite Element Model of (B1C1) with $l/d=8$	95
Fig.(5.2) Finite Element Model of (B1C1) with $l/d=15$	95
Fig.(5.3) Finite Element Model of (B1C1) with $l/d=30$	96
Fig.(5.4) Finite Element Model of (FWCC) with $l/d=8$	96
Fig.(5.5) Finite Element Model of (FWCC) with $l/d=15$	97
Fig.(5.6) Finite Element Model of (FWCC) with $l/d=30$	97
Fig.(5.7):Time vs Creep strain behavior for models(C.0.#.30.8).....	102
Fig.(5.8):Time vs Creep strain behavior for models(C.0.26.#.30.8).....	103
Fig.(5.9):Time vs Creep strain behavior for models(C.0.46.#.30.8).....	103
Fig.(5.10):Time vs Creep strain behavior for models(C. 0.#.30.15).....	103
Fig.(5.11):Time vs Creep strain behavior for models(C.0.26.#.30.15)...	104
Fig.(5.12):Time vs Creep strain behavior for models(C.0.46.#.30.15)...	104
Fig.(5.13):Time vs Creep strain behavior for models(C. 0.#.30.30).....	104

List of Figures

Fig.(5.14):Time vs Creep strain behavior for models(C.0.26.#.30.30)...	105
Fig.(5.15):Time vs Creep Strain Behavior for Models(C.0.46.#.30.30)...	105
Fig.(5.16):Time vs Creep Strain Behavior for Models(C.0.#.40.8).....	105
Fig.(5.17):Time vs Creep Strain Behavior for Models(C.0.26.#.40.8).....	106
Fig.(5.18):Time vs Creep Strain Behavior for Models(C.0.46.#.40.8).....	106
Fig.(5.19):Time vs Creep Strain Behavior for Models(C. 0.#.40.15).....	106
Fig.(5.20):Time vs Creep Strain Behavior for Models(C.0.26.#.40.15)...	107
Fig.(5.21):Time vs Creep Strain Behavior for Models(C.0.46.#.40.15)...	107
Fig.(5.22):Time vs Creep Strain Behavior for Models(C. 0.#.40.30).....	107
Fig.(5.23):Time vs Creep Strain Behavior for Models(C.0.26.#.40.30)...	108
Fig.(5.24):Time vs Creep Strain Behavior for Models(C. 0.46.#.40.30)	108
Fig.(5.25):Time vs Creep Strain Behavior for Models(C. 0.#.50.8).....	108
Fig.(5.26):Time vs Creep Strain Behavior for Models(C. 0.26.#.50.8)...	109
Fig.(5.27):Time vs Creep Strain Behavior for Models(C. 0.46.#.50.8)	109
Fig.(5.28):Time vs Creep Strain Behavior for Models(C. 0.#.50.15).....	109
Fig.(5.29):Time vs Creep Strain Behavior for Models(C. 0.26.#.50.15)...	110
Fig.(5.30):Time vs Creep Strain Behavior for Models(C. 0.46.#.50.15)	110
Fig.(5.31):Time vs Creep Strain Behavior for Models(C.0.#.50.30).....	110
Fig.(5.32):Time vs Creep Strain Behavior for Models(C. 0.26.#.50.30)...	111
Fig.(5.33):Time vs Creep Strain Behavior for Models(C. 0.46.#.50.30)	111
Fig.(5.34) :Time vs Creep Strain Behavior for Models(G.0.#.30.8).....	111
Fig.(5.35) :Time vs Creep Strain Behavior for Models(G. 0.26.#.30.8)...	112
Fig.(5.36) :Time vs Creep Strain Behavior for Models(G. 0.46.#.30.8)	112
Fig.(5.37) :Time vs Creep Strain Behavior for Models(G.0.#.30.15).....	112
Fig.(5.38) :Time vs Creep Strain Behavior for Models(G. 0.26.#.30.15)	113
Fig.(5.39) :Time vs Creep Strain Behavior for Models(G. 0.46.#.30.15)	113
Fig.(5.40) :Time vs Creep Strain Behavior for Models(G.0.#.30.30).....	113
Fig.(5.41) :Time vs Creep Strain Behavior for Models(G. 0.26.#.30.30)	114
Fig.(5.42) :Time vs Creep Strain Behavior for Models(G. 0.46.#.30.30)	114

List of Figures

Fig.(5.43) :Time vs Creep Strain Behavior for Models(G.0.#.40.8).....	114
Fig.(5.44) :Time vs Creep Strain Behavior for Models(G. 0.26.#.40.8)...	115
Fig.(5.45) :Time vs Creep Strain Behavior for Models(G. 0.46.#.40.8)	115
Fig.(5.46) :Time vs Creep Strain Behavior for Models(G.0.#.40.15).....	115
Fig.(5.47) :Time vs Creep Strain Behavior for Models(G. 0.26.#.40.15)	116
Fig.(5.48) :Time vs Creep Strain Behavior for Models(G. 0.46.#.40.15)	116
Fig.(5.49) :Time vs Creep Strain Behavior for Models(G.0.#.40.30).....	116
Fig.(5.50) :Time vs Creep Strain Behavior for Models(G. 0.26.#.40.30)	117
Fig.(5.51) :Time vs Creep Strain Behavior for Models(G. 0.46.#.40.30)	117
Fig.(5.52) :Time vs Creep Strain Behavior for Models(G.0.#.50.8).....	117
Fig.(5.53) :Time vs Creep Strain Behavior for Models(G. 0.26.#.50.8)...	118
Fig.(5.54) :Time vs Creep Strain Behavior for Models(G. 0.46.#.50.8)	118
Fig.(5.55) :Time vs Creep Strain Behavior for Models(G.0.#.50.15).....	118
Fig.(5.56) :Time vs Creep Strain Behavior for Models(G. 0.26.#.50.15)	119
Fig.(5.57) :Time vs Creep Strain Behavior for Models(G. 0.46.#.50.15)	119
Fig.(5.58) :Time vs Creep Strain Behavior for Models(G.0.#.50.30) ...	119
Fig.(5.59) :Time vs Creep Strain Behavior for Models(G. 0.26.#.50.30)	120
Fig.(5.60) :Time vs Creep Strain Behavior for Models(G. 0.46.#.50.30)	120
Fig.(5.61) :Time vs Creep Strain Behavior for Models(C.0. 7%P _u .#.8)	122
Fig.(5.62) :Time vs Creep Strain Behavior for Models(C. 0.26. 7%P _u .#.8)	122
Fig.(5.63) :Time vs Creep Strain Behavior for Models(C. 0.46. 7%P _u .#.8)	123
Fig.(5.64) :Time vs Creep Strain Behavior for Models(C.0.28%P _u .#.8)....	123
Fig.(5.65) :Time vs Creep Strain Behavior for Models(C.0.26.28%P _u .#.8)	123
Fig.(5.66) :Time vs Creep Strain Behavior for Models(C.0.46.28%P _u .#.8)	124
Fig.(5.67) :Time vs Creep Strain Behavior for Models (C.0.72%P _u .#.8)...	124
Fig.(5.68) :Time vs Creep Strain Behavior for Models(C.0.26.72%P _u .#.8)	124
Fig.(5.69) :Time vs Creep Strain Behavior for Models(C.0.46.72%P _u .#.8)	125
Fig.(5.70) :Time vs Creep Strain Behavior for Models (C.0.7%P _u .#.15)...	125
Fig.(5.71) :Time vs Creep Strain Behavior for Models(C.0.26.7%P _u .#.15)	125

List of Figures

Fig.(5.72) :Time vs Creep Strain Behavior for Models(C.0.46.7%P _u .#.15)	126
Fig.(5.73) :Time vs Creep strain Behavior for Models (C.0.28%P _u .#.15)..	126
Fig.(5.74) :Time vs Creep Strain Behavior forModels(C.0.26.28%P _u .#.15)	126
Fig.(5.75) :Time vs Creep Strain Behavior forModels(C.0.46.28%P _u .#.15)	127
Fig.(5.76) :Time vs Creep Strain Behavior for Models(C.0.72%P _u .#.15)	127
Fig.(5.77) :Time vs Creep Strain Behavior forModels(C.0.26.72%P _u .#.15)	127
Fig.(5.78) :Time vs Creep Strain Behavior forModels(C.0.46.72%P _u .#.15)	128
Fig.(5.79) :Time vs Creep Strain Behavior for Models(C.0. 7%P _u .#.30)	128
Fig.(5.80) :Time vs Creep Strain Behavior for Models(C.0.26.7%P _u .#.30)	128
Fig.(5.81) :Time vs Creep Strain Behavior for Models(C.0.46.7%P _u .#.30)	129
Fig.(5.82) :Time vs Creep Strain Behavior for Models(C.0. 28%P _u .#.30)	129
Fig.(5.83) :Time vs Creep Strain Behavior forModels(C.0.26.28%P _u .#.30)	129
Fig.(5.84) :Time vs Creep Strain Behavior forModels(C.0.46.28%P _u .#.30)	130
Fig.(5.85) :Time vs Creep Strain Behavior for Models (C.0.72%P _u .#.30)	130
Fig.(5.86) :Time vs Creep Strain Behavior forModels(C.0.26.72%P _u .#.30)	130
Fig.(5.87) :Time vs Creep Strain Behavior forModels(C.0.46.72%P _u .#.30)	131
Fig.(5.88) :Time vs Creep Strain Behavior for Models(G.0. 7%P _u .#.8)	131
Fig.(5.89) :Time vs Creep Strain Behavior for Models(G. 0.26. 7%P _u .#.8)	131
Fig.(5.90) :Time vs Creep Strain Behavior for Models(G. 0.46. 7%P _u .#.8)	132
Fig.(5.91) :Time vs Creep Strain Behavior for Models(G.0. 28%P _u .#.8)	132
Fig.(5.92) :Time vs Creep Strain Behavior for Models(G.0.26.28%P _u .#.8)	132
Fig.(5.93) :Time vs Creep Strain Behavior for Models(G.0.46.28%P _u .#.8)	133
Fig.(5.94) :Time vs Creep Strain Behavior for Models(G.0. 72%P _u .#.8)	133
Fig.(5.95) :Time vs Creep Strain Behavior for Models(G.0.26.72%P _u .#.8)	133
Fig.(5.96) :Time vs Creep Strain Behavior for Models(G.0.46.72%P _u .#.8)	134
Fig.(5.97) :Time vs Creep Strain Behavior for Models(G.0. 7%P _u .#.15)	134
Fig.(5.98) :Time vs Creep Strain Behavior for Models(G.0.26.7%P _u .#.15)	134
Fig.(5.99) :Time vs Creep Strain Behavior for Models(G.0.46.7%P _u .#.15)	135
Fig.(5.100) :Time vs Creep Strain Behavior for Models(G.0. 28%P _u .#.15)	135

List of Figures

Fig.(5.101) :Time vs Creep Strain Behavior for Models (G.0.26.28%P _u .#.15).....	135
Fig.(5.102) :Time vs Creep Strain Behavior for Models (G.0.46.28%P _u .#.15).....	136
Fig.(5.103) :Time vs Creep Strain Behavior for Models(G.0. 72%P _u .#.15)	136
Fig.(5.104) :Time vs Creep Strain Behavior for Models (G.0.26.72%P _u .#.15).....	136
Fig.(5.105) :Time vs Creep Strain Behavior for Models (G.0.46.72%P _u .#.15).....	137
Fig.(5.106) :Time vs Creep Strain Behavior for Models(G.0.7%P _u .#.30)...	137
Fig.(5.107) :Time vs Creep Strain Behavior forModels(G.0.26.7%P _u .#.30)	137
Fig.(5.108) :Time vs Creep Strain Behavior forModels(G.0.46.7%P _u .#.30)	138
Fig.(5.109):Time vs Creep Strain Behavior for Models(G.0.28%P _u .#.30)	138
Fig.(5.110):Time vs Creep Strain Behavior for Models (G.0.26.28%P _u .#.30).....	138
Fig.(5.111):Time vs Creep Strain Behavior for Models (G.0.46.28%P _u .#.30).....	139
Fig.(5.112):Time vs Creep Strain Behavior for Models(G.0.72%P _u .#.30)	139
Fig.(5.113):Time vs Creep Strain Behavior for Models (G.0.26.72%P _u .#.30).....	139
Fig.(5.114):Time vs Creep Strain Behavior for Models (G.0.46.72%P _u .#.30).....	140
Fig.(5.115):Time vs Creep Strain Behavior for Models(#.0. 7%P _u .30.8)	140
Fig.(5.116):Time vs Creep Strain Behavior for Models (#.0.26.7%P _u .30.8)	140
Fig.(5.117):Time vs Creep Strain Behavior for Models (#.0.46.7%P _u .30.8)	141
Fig.(5.118):Time vs Creep Strain Behavior for Models(#.0. 28%P _u .30.8)	141
Fig.(5.119):Time vs Creep Strain Behavior forModels(#.0.26.28%P _u .30.8)	141
Fig.(5.120):Time vs Creep Strain Behavior forModels(#.0.46.28%P _u .30.8)	141
Fig.(5.121):Time vs Creep Strain Behavior for Models(#.0. 72%P _u .30.8)	141

List of Figures

Fig.(5.122):Time vs Creep Strain Behavior forModels(#.0.26.72%P _u .30.8)	141
Fig.(5.123):Time vs Creep Strain Behavior forModels(#.0.46.72%P _u .30.8)	142
Fig.(5.124):Time vs Creep Strain Behavior for Models(#.0. 7%P _u .30.15)	142
Fig.(5.125):Time vs Creep Strain Behavior forModels(#.0.26.7%P _u .30.15)	142
Fig.(5.126):Time vs Creep Strain Behavior forModels(#.0.46.7%P _u .30.15)	142
Fig.(5.127):Time vs Creep Strain Behavior for Models(#.0.28%P _u .30.15)	142
Fig.(5.128):Time vs Creep Strain Behavior for Models (#.0.26.28%P _u .30.15).....	142
Fig.(5.129):Time vs Creep Strain Behavior for Models (#.0.46.28%P _u .30.15).....	143
Fig.(5.130):Time vs Creep Strain Behavior for Models(#.0.72%P _u .30.15)	143
Fig.(5.131):Time vs Creep Strain Behavior for Models (#.0.26.72%P _u .30.15).....	143
Fig.(5.132):Time vs Creep Strain Behavior for Models (#.0.46.72%P _u .30.15).....	143
Fig.(5.133):Time vs Creep Strain Behavior for Models (#.0.7%P _u .30.30)	143
Fig.(5.134):Time vs Creep Strain Behavior forModels(#.0.26.7%P _u .30.30)	143
Fig.(5.135):Time vs Creep Strain Behavior forModels(#.0.46.7%P _u .30.30)	144
Fig.(5.136) :Time vs Creep Strain Behavior forModels(#.0.28%P _u .30.30)	144
Fig.(5.137) :Time vs Creep Strain Behavior for Models (#.0.26.28%P _u .30.30).....	144
Fig.(5.138) :Time vs Creep Strain Behavior for Models (#.0.46.28%P _u .30.30).....	144
Fig.(5.139) :Time vs Creep Strain Behavior forModels(#.0.72%P _u .30.30)	144
Fig.(5.140) :Time vs Creep Strain Behavior for Models (#.0.26.72%P _u .30.30).....	144
Fig.(5.141) :Time vs Creep Strain Behavior for Models (#.0.46.72%P _u .30.30).....	145
Fig.(5.142) :Time vs Creep Strain Behavior for Models (#.0.7%P _u .40.8)	145

List of Figures

Fig.(5.143) :Time vs Creep Strain Behavior for Models(#.0.26.7%P _u .40.8)	145
Fig.(5.144) :Time vs Creep Strain Behavior for Models(#.0.46.7%P _u .40.8)	145
Fig.(5.145) :Time vs Creep Strain Behavior for Models(#.0.28%P _u .40.8)	145
Fig.(5.146) :Time vs Creep Strain Behavior for Models (#.0.26.28%P _u .40.8).....	145
Fig.(5.147) :Time vs Creep Strain Behavior for Models (#.0.46.28%P _u .40.8).....	146
Fig.(5.148) :Time vs Creep Strain Behavior for Models(#.0.72%P _u .40.8)	146
Fig.(5.149) :Time vs Creep Strain Behavior for Models (#.0.26.72%P _u .40.8).....	146
Fig.(5.150) :Time vs Creep Strain Behavior for Models (#.0.46.72%P _u .40.8).....	146
Fig.(5.151) :Time vs Creep Strain Behavior for Models(#.0.7%P _u .40.15)	146
Fig.(5.152) :Time vs Creep Strain Behavior for Models (#.0.26.7%P _u .40.15).....	146
Fig.(5.153) :Time vs Creep Strain Behavior for Models (#.0.46.7%P _u .40.15).....	147
Fig.(5.154) :Time vs Creep Strain Behavior for Models(#.0.28%P _u .40.15)	147
Fig.(5.155) :Time vs Creep Strain Behavior for Models (#.0.26.28%P _u .40.15).....	147
Fig.(5.156) :Time vs Creep Strain Behavior for Models (#.0.46.28%P _u .40.15).....	147
Fig.(5.157) :Time vs Creep Strain Behavior for Models(#.0.72%P _u .40.15)	147
Fig.(5.158) :Time vs Creep Strain Behavior for Models (#.0.26.72%P _u .40.15).....	147
Fig.(5.159) :Time vs Creep Strain Behavior for Models (#.0.46.72%P _u .40.15).....	148
Fig.(5.160) :Time vs Creep Strain Behavior for Models(#.0.7%P _u .40.30)	148
Fig.(5.161) :Time vs Creep Strain Behavior for Models	

List of Figures

(#.0.26.7%P _u .40.30).....	148
Fig.(5.162) :Time vs Creep Strain Behavior for Models	
(#.0.46.7%P _u .40.30).....	148
Fig.(5.163) :Time vs Creep Strain Behavior forModels(#.0.28%P _u .40.30)	148
Fig.(5.164) :Time vs Creep Strain Behavior for Models	
(#.0.26.28%P _u .40.30).....	148
Fig.(5.165) :Time vs Creep Strain Behavior for Models	
(#.0.46.28%P _u .40.30).....	149
Fig.(5.166) :Time vs Creep Strain Behavior forModels(#.0.72%P _u .40.30)	149
Fig.(5.167) :Time vs Creep Strain Behavior for Models	
(#.0.26.72%P _u .40.30).....	149
Fig.(5.168) :Time vs Creep Strain Behavior for Models	
(#.0.46.72%P _u .40.30).....	149
Fig.(5.169) :Time vs Creep Strain Behavior for Models(#.0.200.50.8)....	149
Fig.(5.170) :Time vs Creep Strain Behavior for Models(#.0.26.7%P _u .50.8)	149
Fig.(5.171) :Time vs Creep Strain Behavior for Models(#.0.46.7%P _u .50.8)	150
Fig.(5.172) :Time vs Creep Strain Behavior for Models(#.0. 7%P _u .50.8)	150
Fig.(5.173) :Time vs Creep Strain Behavior for Models	
(#.0.26.28%P _u .50.8).....	150
Fig.(5.174) :Time vs Creep Strain Behavior for Models	
(#.0.46.28%P _u .50.8).....	150
Fig.(5.175) :Time vs Creep Strain Behavior for Models(#.0. 72%P _u .50.8)	150
Fig.(5.176) :Time vs Creep Strain Behavior for Models	
(#.0.26.72%P _u .50.8).....	150
Fig.(5.177) :Time vs Creep Strain Behavior for Models	
(#.0.46.72%P _u .50.8).....	151
Fig.(5.178) :Time vs Creep Strain Behavior for Models (#.0.7%P _u .50.15)	151
Fig.(5.179) :Time vs Creep Strain Behavior for Models	
(#.0.26.7%P _u .50.15).....	151

List of Figures

Fig.(5.180) :Time vs Creep Strain Behavior for Models (#.0.46.7%P _u .50.15).....	151
Fig.(5.181) :Time vs Creep Strain Behavior for Models(#.0.800.50.15)...	151
Fig.(5.182) :Time vs Creep Strain Behavior for Models (#.0.26.28%P _u .50.15).....	151
Fig.(5.183) :Time vs Creep Strain Behavior for Models (#.0.46.28%P _u .50.15).....	152
Fig.(5.184) :Time vs Creep Strain Behavior for Models (#.0.72%P _u .50.15)	152
Fig.(5.185) :Time vs Creep Strain Behavior for Models (#.0.26.72%P _u .50.15).....	152
Fig.(5.186) :Time vs Creep Strain Behavior for Models (#.0.46.72%P _u .50.15).....	152
Fig.(5.187) :Time vs Creep Strain Behavior for Models (#.0.7%P _u .50.30)	152
Fig.(5.188) :Time vs Creep Strain Behavior for Models (#.0.26.7%P _u .50.30).....	152
Fig.(5.189) :Time vs Creep Strain Behavior for Models (#.0.46.7%P _u .50.30).....	153
Fig.(5.190) :Time vs Creep Strain Behavior for Models (#.0.28%P _u .50.30)	153
Fig.(5.191) :Time vs Creep Strain Behavior for Models (#.0.26.28%P _u .50.30).....	153
Fig.(5.192) :Time vs Creep Strain Behavior for Models (#.0.46.28%P _u .50.30).....	153
Fig.(5.193) :Time vs Creep Strain Behavior for Models (#.0.72%P _u .50.30)	153
Fig.(5.194) :Time vs Creep Strain Behavior for Models (#.0.26.72%P _u .50.30).....	153
Fig.(5.195) :Time vs Creep Strain Behavior for Models (#.0.46.72%P _u .50.30).....	154

Chapter One

Introduction

1.1: General:

A column is a compression member that has a ratio of height to least lateral dimension of three or greater (*Nilson & Winter, 1988*). It is a structural element which is used primarily to support compressive loads regardless of whether or not design calculations indicate the simultaneous bending moment to be present. A major part of the civil engineering reinforced concrete (RC) infrastructure all over the world, including: Bridges, municipal buildings, transportation systems, and parking facilities are facing problems of deficient design and/or construction practices, space, functionality or loading alterations, overuse, seismic upgrading and of course inadequate maintenance (*Al-Musawi, 2012*).

Concrete structures strengthening started with the early use of concrete as a construction material. The demand for strengthening of these structures became necessary when an increase in load was inevitable or when the structure's function is altered from its original purpose. Examples of the latter case are (i) residential buildings converted to storage and (ii) extra loads due to additional floors of an existing building (*Al-Chami, 2006*).

Due to overuse and/or inadequate maintenances, a large number of existing RC infrastructure in developed countries was suffering from distress like bridges, municipal buildings, transportation systems and parking facilities. Extending the functional service lives of different RC structures by structural strengthening is the most economical solution when compared with demolition and building new structures. The later has both cost and time consuming disadvantages. The most common methods that developed in the past to upgrade RC columns were reinforced concrete and grout-injected steel jacketing systems.

Although both methods are effective in increasing the structural capacity, they are sometimes difficult to be accomplished on site and labor consuming. In addition to that, a steel jacketing system is often heavy and poorly performs in resisting adverse environmental conditions. Therefore, an innovative, cost-effective, durable and easy to install strengthening system is required to replace outdated techniques. Recently, for upgrading deficient RC infrastructures, Fiber Reinforced Polymer (FRP) have emerged as a promising alternative strengthening material. In this technique, to increase the column's load carrying capacity, FRP sheets can be easily wrapped around a column's cross section with high –strength adhesive to provide confining stress. Many features that made FRP materials ideal for infrastructure strengthening. These features were non corrosive, non magnetic, extremely light, strong and highly versatile (*El-Maaddawy, 2009*)

Wrapping FRP laminates around concrete columns has been used in structures (such as Shinmiya Bridge in Japan and Lunensche Gasse Bridge in Germany) as a strengthening approach. This structural technique can improve both strength and ductility of columns, and it is very feasible for construction. Since concrete and the polymer-based material both show obvious time-dependent deformation characteristics, and they affect each other in the long-term deformation process, the creep of this hybrid column is a complex phenomenon. A complete understanding of its creep characteristic is necessary for the analysis and design of structural systems involving FRP-wrapped concrete columns (*Wang et al., 2011*).

1.2: FRP Composite for Strengthening RC Columns:

FRP composites consist of the two components. These components are combined at a macroscopic level and are not soluble in each other. The reinforcement is one of component, that is embedded in the second component,

a continuous polymer called the matrix (*Kaw, 1997*). The reinforcing material is in the form of fibers, i.e., carbon, glass and aramid which are typically stiffer and stronger than the matrix. Fig.(1.1) shows the stress-strain relationship of fibers.

Glass fiber has a high strength, elastic modulus (70-85) GPa, fire resistance, chemical resistance and ultimate elongation of (2-5) %, depending on quality.

Carbon fiber has a high modulus of elasticity of (200-800) GPa, ultimate elongation of (0.3-2.5) %, high tensile strength of (2500-6000) MPa and it withstands fatigue excellently. **Aramid fiber** has modulus of elasticity (70-200) GPa, very high thermal resistance, has high fracture energy and ultimate elongation

of (1.5-5) % depending on the quality (*Carlion, 2003*). The FRP composites are anisotropic materials; that is, their properties are not the same in all directions.

Fig.(1.2) shows a schematic of FRP composites.

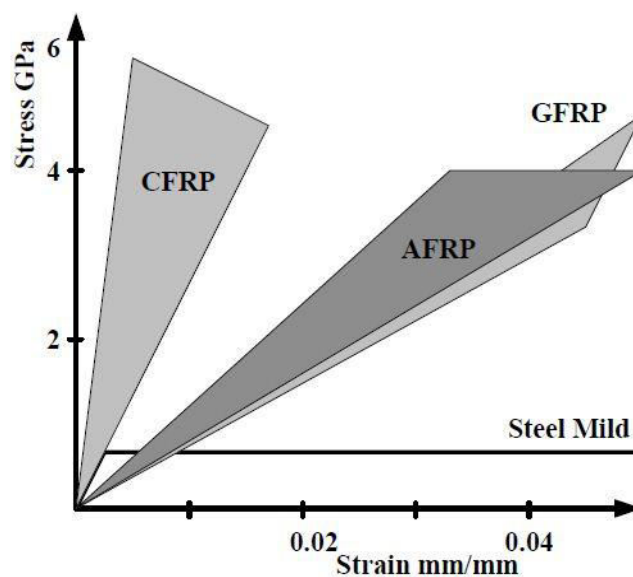


Fig.(1.1):Stress-Strain Relationship of Different Fibers (*Carlion, 2003*).

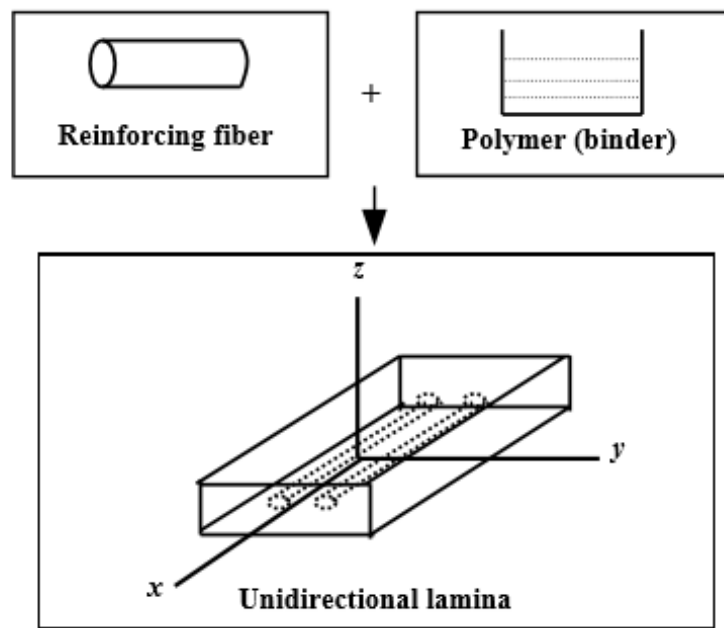


Fig.(1.2): Schematic of FRP Composites(Kaw, 1997).

1.3: Problem Statement:

The below mentioned key questions generally address the main concerns that the researchers deal with the topic of creep of FRP strengthened members. Some of these topics have been approached in previous studies while others were investigated in this study.

- Each individual material that constitutes the strengthened concrete element creep under sustained load at different magnitudes. How does the combined hybrid system of these materials will behave over long time intervals?
- How far do FRP materials creep over time? Should the creep magnitude be significant and how can it affect the strengthening effecting using these materials?
- How is the creep behavior of the concrete core of a confined column affected by the presence of an FRP wrap?

- Does creep rupture occur for FRP-strengthened concrete elements during their service life? Would this may occur at sustained load levels that normally used for the design of rehabilitated elements or at escalated levels?
- To avoid creep failure, what are the safety limits for applying sustained loads on FRP strengthened concrete columns?

1.4: Objective of Research:

The purpose of this study is to simulate the strengthened reinforced concrete columns by FRP sheets using nonlinear FEM, and the objective of the study summarized as follows:

- 1- Presenting a numerical model of analysis of reinforced concrete columns strengthened with FRP by using finite element method adopted by the ANSYS package.
- 2- Verification studies between present models and experimental models from previous studies.
- 3- Studying a parametric study of factors, such as (magnitude of sustained load, eccentricity, length - diameter ratio, compressive strength and FRP type) on the strength and ductility of columns.

1.5: Limitations of This Study:

- Studying the long term behavior of square section control reinforced concrete columns and circular section of FRP strengthening concrete columns depend on experimental researches of (*Hamid & Lai, 2016; Katoka & Bittencourt, 2014; Al-Chami, 2006; Naguib & Mirmiran, 2002; Wang et al., 2011*)

- A parametric study includes compressive strength(30-40-50)MPa, magnitude of sustained load(7.15%-28.6%-71.5%) from maximum short-term load (P_u), l/d (8-15-30), eccentricity(0-40-70)mm and FRP type.

1.6: Thesis Outline:

This thesis includes six chapters; **Chapter One** consists of an introduction which reviews introduction about strengthening columns with FRP and objectives of the research. **Chapter Two** reviews the previous researches for strengthening reinforced concrete columns under short-term and long-term loading, in addition to review the theoretical models of creep. **Chapter Three** presents the creep analysis of concrete, models of viscoelastic composite material and viscoelastic stress-strain constitutive relationship. **Chapter Four** includes the analysis and discussion of results of reinforced concrete columns. **Chapter Five** includes the parametric study of strengthening concrete columns. Finally, **Chapter Six** consists of discussion of results and recommendations and future research.

Chapter Two

Literature Review

2.1: General:

The main topic of this chapter is to give a summarized review of the previous studies on the behavior of strengthening reinforced concrete (RC) columns. Several available studies on the columns strengthening with different materials. Such as steel plates, ferrocement layers and fiber reinforced polymers (FRP) sheets or plates.

In this chapter reviewed the researches of the behavior R.C. columns under short-term and long-term loading that strengthening with FRP sheet (carbon, glass , aramid), ferrocement material and steel plates. In addition, review the mathematical model of creep of concrete.

2.2 Short-Term Behavior of Concrete Columns Strengthening by Fiber Reinforced Polymer (FRP) Sheets:

In recent years, external confinement of concrete columns by fiber reinforced polymer (FRP) has become increasing popular. This includes FRP wraps of existing columns and concrete encased in FRP tubes for new column construction. The FRP confinement is able to increase the concrete ductility because of the high tensile strain capacity of the FRP tubes in the hoop direction which increases the axial strain capacity of the confined columns (*Youssf et al., 2014*).

This method of strengthening is based on the well-known phenomenon that the axial compressive strength and ultimate axial compressive strain of concrete can significantly be increased through lateral confinement (*Hollaway & Teng, 2008*).

2.2.1 Strengthening by Carbon Fiber Reinforced Polymer (CFRP)

Sheets:

The use of CFRP in strengthening and retrofit columns became more common due to its advantage, such as easy to apply, high tension strength and light weight (*Taghia & Abu Bakar, 2013*).

(*Olivova & Bilcik, 2009*) studied the structural behavior of reinforced concrete columns strengthened with carbon fiber sheets and strengthening based on near surface mounted (NSM) laminated strips of carbon fiber reinforced polymer (CFRP). Experimental work consists of four series of reinforced concrete columns in the first series was a non-strengthening R.C columns, and the other three of these series strengthening with CFRP sheets, CFRP laminate strips, CFRP laminate strips and sheets, respectively. The result showed that the load carrying capacity increased 10%, 26% and 32% for R.C columns strengthening with CFRP sheets, CFRP laminate strips, CFRP laminate strips and sheets, respectively relative to non-strengthening R.C. columns.

(*Wu & Wei, 2010*) studied the behavior of rectangular short columns strengthened with CFRP under axially loaded. The experimental program consists of 45 specimens distributed in three groups. The main parameters observed in this study were the effect of aspect ratio, compressive strength, failure mode and the number of CFRP layers. The results showed that the increasing of aspect ratio with 25% leads to decrease compressive strength about 6% in 1-ply and 15% in 2-ply, while axial strain decrease 50% in 1-ply and 47.4% in 2-ply. In addition, the CFRP jacketing improves the performance of rectangular column. Finally, the researchers proposed new strength model for FRP confined rectangular columns depend on the results of this study.

(*Turgay et al, 2010*) studied the behavior of large scale R.C. column strengthening with CFRP. An experimental work consisted of 20 squares R.C.

columns with dimensions (200*200*1000) mm which were divided into five groups: without strengthening, partially strengthening, fully strengthening, partially strengthening with two layers and fully strengthening with two layers. The results show that increasing in strength approximately 15% for all columns partially warping of CFRP, while the ductility of fully warped one layer CFRP increased approximately 50% for columns reinforced with 8 bars and 200% for 12 bars. On the other hand, the type of failure in fully strengthening column occurred on top or bottom quarter, while the failure at partially strengthening column occurred at the end of CFRP confined regions.

(Al-Ahmad, 2011) studied finite element modeling of reinforced concrete column strengthened with CFRP under axial load and uniaxial bending ANSYS package is used to perform nonlinear finite element analysis. The researcher studied the effect of some parameter on the RC jacketed columns. These parameters include: loading eccentricity, compressive strength of concrete, thickness of CFRP layer, effect of strengthening on stress of steel reinforcement and wrapping length. The finite element model gave a very good agreement with experimental data of other researchers. The results show that increased the value of eccentricity about 28.57% leads to decrease the load carrying capacity approximately 0.22%, while the load carrying capacity increased 14.7% when the thickness of CFRP layers increased 33.3%.

(Al-Musawi, 2012) investigated the effect of eccentric load on the reinforced concrete column strengthen with CFRP sheets. Experimental work consists of twelve samples with dimensions (120*120*750)mm without corbels. This research investigated the effect of the type of concrete material, fiber orientation, FRP thickness and eccentricity. The results showed that the sample strengthen with CFRP leads to increased the strength and the approximately 100% of normal concrete strength and 112% of self compact concrete when the thickness of CFRP layer was 0.13mm, while increased the thickness to 0.26

leads to increased the strength to 108% and 132% for normal strength concrete and self compacting concrete, respectively. Also the researcher found that increase in eccentricity leads to more efficiency in CFRP confined.

(*Seffo & Hamcho, 2012*) Studied the behavior of concrete cylinders strengthening by CFRP composites experimentally and analytically under axial compression with different confinement ratios and fiber orientation with dimension (150*300) mm. The average compressive strength was 37.15MPa. Experimental works consist of 51 samples. The result showed that the CFRP confinement increased load carrying capacity approximately 45.6%, 29.8% and 56.1% for columns strengthening with one way horizontal ($\theta = 0^\circ$), one way vertical ($\theta = 90^\circ$), and two way ($\theta = 0^\circ, \theta = 90^\circ$) respectively relative to columns strengthening with four way ($\theta = 0^\circ, \theta = 90^\circ, \theta = \pm 45^\circ$). In addition increased ductility and strength. As the failure of wrapped column was marked by the rupture of CFRP layer.

(*Taghia & Abu bakar, 2013*) investigated reinforced concrete short column with carbon fiber reinforced polymer sheets under axial load. The numerical program consists of circular columns with different dimensions and these specimens were analyzed by ABAQUS software. The parameters studied included a number of applied CFRP layers, member size, ductility, volumetric ratio and mesh size. The result shows that an increased number of layers from 2-ply to 4-ply the ductility increased 62.2% and 140% for 20MPa and 40MPa compressive strength respectively.

(*Widiarsa & Hadi, 2013*) studied the performance of square reinforced concrete columns strengthened with CFRP under eccentric loading with dimensions (200*200*800) mm. The average compressive strength was 73MPa. Experimental works consist of twelve short columns which were divided into four groups. Each group consists of three columns: the first was unwrapped, the second was wrapped with one layer of CFRP, the third was wrapped with three

layers of CFRP and the fourth was wrapped with one layer of vertical strap and two layers of horizontal CFRP. The investigated parameters were carrying load capacity, failure mode and ductility. The result showed that the maximum concentric load increased 1%, 8.4% and 10.4% for column wrapped with one layer, column wrapped with one layer of vertical strap and two layers of horizontal CFRP and column wrapped with three horizontal layers of CFRP respectively, relative to non-strengthening columns, while the maximum load with 25mm eccentricity increased about 17.7% and 16.4% for column wrapped with one layer of vertical straps and two horizontal layers and column wrapped with three horizontal layers, respectively. However, column wrapped with one horizontal layer achieved only 6.5% increment in maximum load compared with unwrapped column.

(*Nasrin, 2013*) proposed a numerical model of confined concrete columns with CFRP by using ABAQUS software program, this model achieved successfully simulates for the behavior of confined concrete columns with experimental researches. The effect of important parameters in the confined concrete columns was investigated, such as thickness of FRP layers, corners radius, aspect ratio and ductility. The results show that the ultimate capacity increasing 20% and 30% when decreasing aspect ratio 30% and 50% respectively.

(*Abdel-Hay, 2014*) investigated the strengthening of the upper part of R.C square column with poor concrete by CFRP sheets. Experimental works consist of ten columns. Nine of these columns were strengthened with CFRP and the other one was a control column. The study observed the failure modes, failure load and load strain response. The results showed that using the partial strengthening by CFRP which improved the load carrying capacity.

(*Kabashi et al, 2015*) studied CFRP jacketing of (circular and rectangular) R.C. columns under centric loading with dimension (100*400) mm and

(100*100*400) mm, respectively. The average compressive strength was 38.5 MPa. Experimental works consist of 15 specimens. The column specimens were divided into five series, each series consisting of three columns, the first series was rectangular R.C columns with fully wrapped, the second series was rectangular R.C. column with partially wrapped, the third series was a non-strengthening R.C. rectangular columns, the fourth series was circular R.C. with fully wrapped and the last series was a non-strengthening R.C. circular columns. All jacketing samples were strengthened by one layer of CFRP. The investigated parameters were compressive strength, ductility and failure pattern. The results showed that compressive strength increased 28.05%, 22.62%, 155.74% and 5.9% for the first series, second series, fourth series and the last series respectively, relative to the third series.

(Rolli & Chandra, 2015) studied two methods for strengthening reinforced concrete square column by CFRP under axial compression concentric loading with dimension (150*150*750) mm. The average compressive strength was 30 MPa. Experimental works consist of 9 square R.C. columns which were divided into three groups: the first was non strengthening (Reference Column), the second was strengthening with three layers of CFRP (Column with rounded corners $R=20\text{mm}$) and the last was strengthened by circularizing with CFRP (Column Modify to Circular Shape). Fig. (2.1) stated the method of strengthening. The result showed the load-deflection slopes of third group is higher than the second and first group because the increment of the cross section area of columns modify to circular shape. Fig (2.2) showed the comparison between groups. Also, notice the circularizing method was effective for strengthening square columns because this method decreased the concentration of stresses at corners.

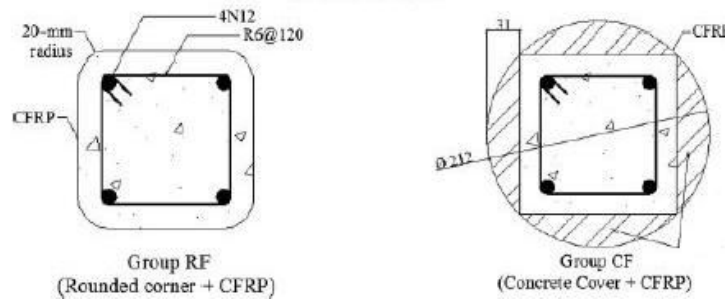


Fig.(2.1):Method of Strengthening RC Square Column (Rolli & Chandra, 2015).

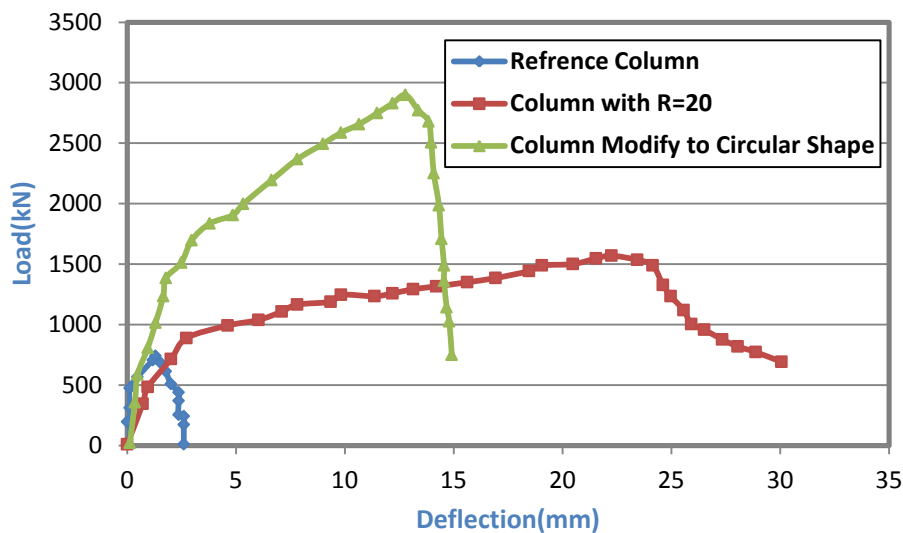


Fig.(2.2):Comparison of Load vs Deflection Curves (Rolli & Chandra, 2015).

(Moshiri et al, 2015) investigated the effect of strengthening technique by longitudinal CFRP sheets for R.C columns. The average compressive strength was 28 MPa. Experimental work consists of ten R.C columns (square and circle) with dimensions (133*500)mm and (150*500)mm respectively. The columns were divided into two series: square columns and circular columns, each series consist of five columns (Reference column, EBR, EBROG, EBRIG and NSM). The results showed that the load carrying capacity of EBROG, EBRIG and NSM strengthening methods, increasing about 10.4%, 12.7% and 4.8% compared to the reference column but EBR method is equal to reference column for square column series. On the other hand, EBROG, EBRIG and EBR

increasing about 14.1%, 18.5% and 2.6% compared to the reference column, but NSM method did not significantly increase in carrying load capacity for circular column series.

2.2.2 Strengthening by Glass Fiber Reinforced Polymer (GFRP)

Sheets:

Many investigators observed the strengthening of columns with GFRP to enhance the ductility and strength of concrete by forming a full cohesive bond between concrete and the layer of strengthening, the main advantage of GFRP including excellent resistance to corrosion and the ratio of strength to weight was high (*Raval & Dave, 2013*).

(*Benzaid et al., 2008*) investigated the effect of the strengthening square column with GFRP. The experimental program consists of twenty-one specimens. The average compressive strength of concrete was 54.8 MPa. The investigated parameters were the corner radius and the number of GFRP layers. It was stated that the increasing of corner radius and number of GFRP leads to increase the carrying load capacity was 2%, 9% and 16% for column with sharp edge square section and confined with one layer, column with corner radius equal to 8mm and confined with one layer and column with corner radius equal to 16mm and confined with two layers respectively respect to control column, while the increment of carrying load capacity for columns confined with two layers was 6%, 20% and 36% for column with sharp edge square section, column with corner radius equal to 8mm and column with corner radius equal to 16mm respectively respect to the control column. The result showed increasing in the ductility of columns when wrapped with GFRP.

(*Raval & Dave, 2013*) investigated the effect of GFRP jacketing on a different shape of R.C columns. The average compressive strength of concrete was 15 MPa. The experimental program consists of 15 R.C columns with a

different shape. The load carrying capacity of control columns for circular cross section was higher than square and rectangular. On the other hand, the increasing of carrying load capacity of columns strengthening with GFRP was 159%, 79% and 76% for circular, square and rectangular, respectively compared with control columns. The result from observed failure modes show that the failure of control was brittle, while the jacketed columns fail in one corner for square column, rupture of the GFRP material for rectangular column and the failure of a circular column without any sign of deponding. Finally, the GFRP jacketing enhanced the ductility and the strength of columns.

(*Nabil et al, 2014*) studied the effect of strengthening technique on the concrete columns under axial loaded with full scale dimensions (150*1500) mm. The experimental program consists of sixteen specimens distributed in 4 groups. The investigated parameters were numbered of GFRP layers, long steel reinforcement ratio and transverse steel reinforcement ratio. The results showed that the load carrying capacity increased when increasing the thickness of GFRP from 2 layers to 4 layers. For group (1) the increased from 755KN for plain concrete column strengthened with two layers to 831KN for plain concrete column strengthened with four layers, for group (3) the increased from 1064KN for R.C. column with two layers to 1213KN for R.C. column with four layers, while group (4) the increased from 1017KN for R.C column strengthening by NSM technique and confined with two layers to 1144KN for R.C column strengthening by NSM technique and confined with four layers.

(*Dave et al., 2014*) studied the strengthening of circular R.C. columns with GFRP laminated with dimensions (200*600) mm. The result showed that the strengthening with GFRP increased the axial load carrying capacity and transforming the failure from brittle to ductile.

(*Yehia, 2015*) investigated the effect of GFRP strengthening techniques (jacketing / strips) on the circular short columns. The experimental program

consists of six specimen's. The results showed that the load carrying capacity for plain concrete columns increased 29% for GFRP strips and 53% for GFRP jacket compared with control columns, but the increment of reinforced concrete columns was 24% for GFRP strips and 44% for GFRP jacket compared with control columns.

2.2.1 Strengthening by Aramid Fiber Reinforced Polymer (AFRP)

Sheets:

(*Toutanji & Saafi, 2001*)^a studied the stress-strain behavior of concrete columns confined with PVC-FRP tubes. The experimental program consists of thirty-eight short concrete cylinders with dimensions 305mm in length and 102mm in diameter. The average compressive strength of concrete was 45MPa. The variables of the test include the type of fiber, volume of fiber, and the spacing between the FRP hoops. The results showed that load carrying capacity increased 83.3% for concrete columns confined with PVC-AFRP tubes relative to control columns. In addition, the increased spacing between the AFRP about 26.66% leads to decrease 10% in load carrying capacity.

(*Toutanji & Saafi, 2001*)^b investigated the durability of concrete columns encased in PVC-FRP composite tubes. The average 28 days compressive strength of concrete was 32MPa and the dimensions of specimens were (305*102)mm. The variables include the spacing between the FRP hoops, the type of fiber and the environmental exposure conditions. The results show that load carrying capacity decreasing 17.5% when the spacing between AFRP hoops increased 26.66%. Also, the confined of concrete columns by PVC-FRP tubes leads to enhance compressive strength, ductility and energy absorption capacity.

(*Toutanji & Deng, 2002*) investigated the performance of concrete columns confined with AFRP sheets. Experimental work consists of 24 cylindrical

specimens with dimensions 76mm in diameter and 305mm in length, the average 28 days compressive strength was 44MPa. All confined columns strengthen with two layers of AFRP. The investigated parameters in this research was the effect of wet/dry exposure and the effect of freeze/thaw exposure. The results show enhancement load carrying capacity with value 328%.

(*Wu et al., 2009*) studied the properties of high strength concrete circular columns confined by AFRP sheets. Experimental work consists of 60 specimens. The parameters considering in this research were the compressive strength of concrete, number of AFRP layers, and the form of AFRP warping. An analytical model was predicted based on experimental results. The results showed that load carrying capacity increased 60% when increased the compressive strength 51.2%, while load carrying capacity increased 66.67% when increased the number of layers from 1 to 2 layers.

(*Silva, 2011*) investigated reinforced concrete columns with and without FRP jacketing. Experimental works consist of circular and square column with ultimate compressive strength 26.5Mpa. The square column divided into three groups depending on corner sharpness: the first group with $R=0$, the second with $R=20\text{mm}$ and the last with $R=35\text{mm}$. The test observed the ductility, axial strength and axial load capacity. He reported the AFRP and CFRP jacketing make the axial load capacity equal to cylinder columns and the ductility of AFRP jacketing higher than CFRP.

2.3 Short-Term Behavior of Concrete Columns Enhancement by Ferrocement:

Strengthening RC columns with ferrocement leads to enhance the behavior of RC columns. In addition, ferrocement material is easy to application with a low cost compared with other strengthening materials (*Wang, 2013*). Many

researchers have found that jacketing by ferrocement provided effective confinement for structural elements such as:

(Takiguchi & Abdullah, 2003) studied reinforced concrete column strengthened using ferrocement jackets. The results indicate that circular ferrocement strengthening was a good alternative material to strengthen reinforced concrete column. The ferrocement enhanced maximum shear strength of by 28%, while improving the initial stiffness about 45% and the load carrying capacity of ferrocement strengthening increased by 37%.

(Mourad & Shannag, 2012) studied ferrocement jacketing for repair and strengthening of reinforced concrete square columns. The investigated parameters were carrying load capacity, axial stress and strain, axial displacement, lateral displacement and ductility. The results showed that the behavior of jacketed column better than the control column, whereas the load carrying capacity increased by 28% as compared to control columns.

(Kaish et al, 2013) studied jacketing by ferrocement layers techniques of RC column under concentric compressive load. The investigated parameters were ultimate load carrying capacity, deflection response and failure pattern. The increased carrying capacities obtained are 28.86%, 32.22% and 44.68% for Square jacketing with single layer wire mesh, Square jacketing with single layer wire mesh and rounded column corners and Square jacketing with single layer wire mesh and two extra layer mesh at each corner respectively.

(Wang, 2013) investigated the effect of ferrocement jacketing on the behavior of reinforced concrete columns under static and cyclic loading. He proposed analytical and numerical models. Ferrocement shows significant potential for strengthening RC columns, whereas the capacity of columns increased by 20%.

(Maheswari & Soman, 2014) studied ferrocement jacketing for strengthening of reinforced concrete short square columns. The comparison between the conventional jacketed specimens and advanced jacketed square column were

observed in this test. The test results show that axial stiffness and energy absorption increased by 28.5% and 96% respectively.

(*Kaish et al., 2015*)^a investigated cylindrical concrete specimens strengthened by ferrocement jackets under axial compression. The behavior of the confined concrete with double layer of wire mesh is better than confined concrete with single layer. The results show that ferrocement jacket can enhance the load carrying capacity of concrete specimens and load carrying capacity is more enhanced in smaller size specimens which is 18 percent of non-jacketed specimen.

(*Kaish et al., 2015*)^b studied the effectiveness of external ferrocement jacket for square column and circular column as compared. The parameters studied include axial load and deflection capacities of specimens, axial stress-strain responses, lateral deflection profile of the jacketed specimens, failure patterns of specimens and absorbed energy before failure. The test results showed that the ultimate load increased by 23.22% as compared with control columns.

(*Tarkhan, 2015*) investigated reinforced concrete columns strengthening by ferrocement under concentric load. The result showed ferrocement jacket enhanced strength, performance of reinforced concrete column and increased the energy absorption and the ductility ratio about 186% and 6.25% respectively.

(*Sayan et al., 2015*) studied the behavior of R.C column encased by longitudinal steel and ferrocement under axial loading. The ferrocement can obviously increase the strength and ductility of R.C. Column and increase the load carrying capacity approximately 240%.

(*Masud & Kumar, 2016*) investigated the effect of ferrocement jacketing on circular R.C. short columns under concentric compressive load. The result showed that confinement by ferrocement increased the load carrying capacity of

R.C. columns by 23.8% and 55.2% for strengthening by ferrocement with one layer wire mesh and two layer wire mesh respectively.

(*Shafeeq, 2016*) investigated the effect of ferrocement jacketing on the behavior of circular hollow reinforced concrete columns under concentric and eccentric compression load. The results show that increasing the eccentricity value leads to decreasing the toughness, ductility and decreasing the ultimate load about 73.5%, while increasing the number of welded wire mesh layer leads to increase the toughness and decreases the ductility, whereas increased the number of welded wire mesh from zero to one and two layers results in a decreasing of the vertical displacement ductility index from (1.1%) to (39.4%) with same eccentricity.

2.4 Long-Term Behavior of Reinforced Concrete Columns:

The long-term behavior of the structure depends mainly on the deformation properties of the concrete, in particular creep and shrinkage of it, which depend on the history of load applied and environment not only on the mixing ratios and types of concrete constituents (*Gilbert & Ranzi, 2011*). This section presents research that highlight on the study of the effect of creep on columns, it includes three types of research which studied the effect of long term behavior; unconfined reinforced concrete columns, confined concrete columns with steel and confined concrete columns with FRP.

2.4.1 Unconfined Reinforced Concrete Columns:

(*Cleson & Gulltoft, 2000*) studied the behavior of slender concrete columns under sustained and short-term eccentric loading. The experimental program consist of six R.C. columns with dimensions (200*200*4000)mm. The main objective of this research was compared between high strength concrete (HSC) and normal strength concrete (NSC) under short-term and sustained loading. The results show that creep coefficients increased 2 times relative to (HSC).

(*Bradford, 2005*) studied the creep response of slender R.C. columns under eccentricity loading. Five specimens with dimensions (150*150*5000)mm was tested in this study and the average compressive strength was 29.3MPa. The main objective of this research was determining the viscoelastic response of slender numerically, eccentrically loaded R.C. columns that incorporates the time dependent effects of creep and shrinkage. So as to provide benchmark experimental results in columns under sustained loading with unequal end eccentricities, the results stated that deflections gave a good agreement with theoretical approaches.

(*Sadaoui & Khannane, 2009*) studied the effect of transient creep on the behavior of R.C. columns in fire. The investigated column design with dimensions (300*300*4800)mm and 30MPa compressive strength. The results show that load carrying capacity decreasing 75% when increase 50% in temperature. Three cases used to analyze column in this research. Transit creep considered explicitly, transit creep considered implicitly and mix both implicitly and explicitly.

(*Katoka, 2010*) studied the time dependent deformation of concrete structures. Nine short reinforced and non-reinforced columns were long term loaded for 91 days. The redistribution of internal stresses from concrete to reinforcement due to creep and shrinkage were investigated. A numerical model was performed in this study. One of creep models which best fit the experimental data of the column. Finally, an updating creep model was successfully applied to concrete experimental data.

(*Madureira et al., 2013*) investigated the effect of creep strain on rectangular reinforced concrete columns. The research studied many cases, depending on the reinforcement ratio and environmental moisture. Results showed that increasing the ratio of reinforcement leads to decreasing each of creep displacement, stress

in concrete and stress in steel, while the effect of increasing environmental moisture leads to decreasing in creep displacement.

(Kataoka & Bittencourt, 2014) studied the effect of steel ratio in concrete column on the properties of creep with dimensions (150*150*600)mm the average compressive strength was 26.2 MPa at 7days. The numerical program uses ACI- 209 model by DIANA9.3 software based on experimental test on plain concrete and plain concrete cylinders columns. The result showed that load transfers to steel reinforcement approximately 29% and 44% in the reinforcement ratio of 1.4% and 2.8%, respectively, while the increasing in reinforcement ratio leads to increase in stress relaxation of concrete about 55% and 35% for reinforcement ratio of 2.8% and 1.4%, respectively.

(Murray & Gilbert, 2015) studied the effect of creep on the slender reinforced concrete columns. The study included forty-eight column analyzed in two methods: first according to AS3600-2009 method and the second based on superposition method by using a computer. The result showed that the critical load increasing in both methods when the slenderness ratio decreasing, but the increasing of computer program was higher than AS3600-2009 method. Also, the results explained that higher compressive strength of concrete increased the critical load and having high stiffness with a little creep.

(Hamed & Lai, 2016) studied materially and geometrically nonlinear creep behavior of square reinforced concrete columns with dimensions (400*400*6000)mm. The average compressive strength was 32MPa. They study the effect of some parameters on the behavior of R.C. columns. These parameters include reinforcement ratio, slenderness ratio, level of load and eccentricity.

2.4.2 Confined Concrete Columns With Steel:

(*Uy & Das, 1997*) were used the age adjusted effective modulus method in the study of creep effect on concrete filled steel box columns in the tall buildings, the results show decreased by 35% in concrete stresses and decrease by 65% in steel stress. They study the effect of some parameters (number of levels in tall buildings and final creep values).

(*Ichinose et al., 2001*) investigated the long-term behavior of concrete filled steel pipe and they proposed analytical model based on viscoelastic model. The results show a good agreement between experiment tests and proposed model of concrete filled steel pipe. In addition, this study stated the values of creep coefficient of concrete filled steel pipe between (0.06-0.44).

(*Naguib & Mirmiran, 2003*) studied time dependent behavior of concrete filled steel tube (CFT). They proposed creep model of (CFT) columns depend on the ACI-209 creep model. The comparison of result with experimental test gives a good agreement the difference of error not pass 2.5%. To investigate the effect some factors on this model, they studied the effect of parameters such as (creep rupture and creep under service loads) on (CFT) columns. The results show that creep of bonded (CFT) much more the unbonded (CFT). This is due to the stress relaxation of concrete, while the bonded (CFT) is much more durable for creep rupture than its equivalent unbonded (CFT) for the same magnitude of sustained loads.

(*Han et al., 2004*) studied the effect of sustained load on the concrete filled hollow steel structural (HSS) columns. Six concrete specimens with dimensions 100mm in diameter and 600mm in height were investigated in this research. They proposed theoretical model included the effect of creep. By comparing results of experimental and theoretical models, they show a good agreement between these results. The test results showed that long term strain decreased

15.2% and 43% when increased aging time and steel ratio approximately 133% and 100% respectively.

(*Dong et al., 2005*) studied the long-term behavior of concrete filled steel tube (CFT) columns. Their proposed analytical model depending on the parameter viscoelastic model to study creep phenomenon. The comparison of results between the proposed model and other experimental study showed a good agreement. They investigated the effect of many factors on (CFT) columns such as (slenderness ratio, eccentricity ratio, steel ratio and long term load to strength). The results showed that increased eccentricity about 25% and the slenderness ratio about 25.6% leads to decreased 16.7% and 50% in creep coefficient respectively.

(*Kwon et al., 2007*) studied the effect of long term loading on the behavior of square concrete filled steel tubular columns, they consider four cases of loading; load applied in the concrete only, load applied in both concrete and steel tube, load applied to the steel tube and three quarters of concrete and load applied to the steel tube and a half of concrete, and they proposed an analytical model in this study. The test results showed that specific creep increased 93%, 7% and 3.6% for case1, case4 and case2 relative to case3.

(*Hassan, 2007*) studied the analysis of long term behavior of circular and square concrete filled steel tube columns (CFST) by using ANSYS package depending on the other experimental studies. The result gives a good agreement. The researcher investigated the effect of parameters such as (compressive strength of concrete, yield strength and thickness of steel tube, diameter effect and ultimate creep coefficient) on the behavior of (CFST) columns. The results show that increasing creep coefficient about 45% causes increase in the axial strain of 9%.

(*Ma & Wang, 2012*) investigated the effect of creep on the high strength concrete filled steel tube columns (HSCFT) and studied the creep difference between (HSCFT) and normal strength concrete filled steel tube columns. The experimental program consist of 8 specimens with dimensions (150*450)mm A creep model was proposed by them and show good agreement between the numerical and experimental results. The results stated that creep compliance of normal strength concrete higher than (HSCFT) approximately 14.3%.

(*Zhang et al., 2015*) studied the effect of long term loading on the compressive strength, elastic modulus and stress-strain of concrete filled steel tubular (CFT) columns. Eight cylindrical specimens with dimensions 150mm in diameter and 450mm in height was investigated in this study. A theoretical model was predicted and show good agreement between theoretical and test results. The results show that the compressive strength of (CFT) columns was decreasing, while the elastic modulus was increased.

2.4.3 Confined Concrete Columns With FRP Sheets:

(*Naguib & Mirmiran, 2002*) studied the time dependent behavior of cylinder concrete columns. This study, based on two methods to strengthening columns: concrete filled FRP tubes (CFFTs), and fiber wrapped concrete columns (FWCCs). Glass fibers are used in this study. As a result of their study, on time dependent behavior of concrete columns, Naguib and Mirmiran stated that the creep strain of FWCC higher than CFFT and as the redistribution stresses between FRP and concrete and the effect of sealing concrete, no significant effect of confinement on the creep of concrete core.

(*Al-Chami, 2006*) investigated creep behavior of confined and unconfined concrete column, cylinders with dimension 150mm in diameter and 900mm in height. The strengthening material that used in this study was CFRP sheets. The major objective of this research was illustrated the effects of the confining

pressure and the applied stress on the time dependent behavior of CFRP confined concrete columns. The result shows that confinement with CFRP delay appearance microcracking, decreasing creep strain and effective in increasing the capacity of the strengthened members.

(*Wang & Zhang, 2009*) investigated the effect of creep on the behavior of concrete columns confined by FRP. Eight cylindrical specimens with dimensions (150*450)mm was investigated in this research, specimens confined with two layers of AFRP sheets. A constitutive model that takes into account the effect of creep on behavior of concrete columns confined by FRP was presented and give a good agreement with experimental results. The results show that creep increases the elastic modulus by 24% to 77%, with a maximum difference of 6.38GPa, while the strength decreases by 7% to 11%, with a maximum difference of 9.78MPa.

(*Zhang et al., 2010*) investigated the effect of creep and shrinkage on the behavior of square concrete columns confined with AFRP sheet. The experimental program consist of four specimens with dimensions (150*150*400)mm. The results show that the creep strain increased 4.03% when decreased compressive strength about 11%. In addition, the predicted model gives a good agreement with experimental results.

(*Wang et al., 2011*)^a investigated the behavior of creep of square and circular concrete columns which were strengthened by AFRP sheet (fully and partially), the dimension of columns were (150*150*400) mm for square column and (150*450) mm for circular columns. The result shows that no cross-sectional effect on the creep behavior, while the creep of partially confined higher than fully confined with value equal to 2.2%. In addition, the creep model of confined concrete columns developed in this study and give a good agreement with test data with average of errors not pass 2.1%.

(Wang *et al.*, 2011)^b studied the long-term deformation properties of AFRP-wrapped cylindrical concrete columns with fly ash. The dimensions of test specimens were (150*450)mm. Creep model was predicted for confined concrete columns with and without fly ash. The test results show that fly ash decrease the creep strain of confined concrete columns.

(Fahmi & Karim, 2016) proposed model for creep analysis of GFRP strengthening circular section concrete column by using ANSYS package. The comparison between the experimental and numerical study gave a good agreement whereas the maximum difference of total strain about 5.5%. The effect of some parameter was studied such as (concrete compressive strength, tube wall thickness, number of fiber-wraps, column diameter, ultimate creep coefficient, and type of FRP). The results show that increased all parameters lead to decrease the creep except the ultimate creep. In addition, 22% stress reduction in the concrete and a stress increase in the FRP of 25% after 200 days of loading as a result of stress transfer.

2.5 Mathematical Modeling of Creep of Concrete:

Mathematical modeling of creep in concrete structures is a complex task, even with simplified linear forms since concrete is unique among structural materials in that it reacts to its environment, undergoing complex physical and chemical changes over time.

In order to predict the constitutive relationships of creep, mathematical models need to be used as input for FE computer program. Functions selected should meet some criteria (Bažant, 1982)

- At first, the functions should be accurately fit with available experimental data of concrete and taking into account the effect of all important factors such as; environmental humidity, curing conditions, age, temperature, and size and shape of cross section.

- The unknown coefficients in the function should be easy to calculate from the available experimental data.
- Functions must be simple enough to make the numerical evaluation in the computer program clear and effective.

Several practical models for predicting concrete creep have been developed in the following. The three main commonly used models are:

1. American Concrete Institute (ACI-209) Model

(ACI Committee 209R, 2010) recommended expression to creep as following

$$J(t, t') = \frac{1}{E(t')} \left[1 + \frac{(t-t')^{0.6}}{10+(t-t')^{0.6}} \right] v_u \quad \dots(2.1)$$

where

t = current age in days

t' = age at loading in days

$J(t, t')$ = creep function

v_u = ultimate creep coefficient

$E(t')$ = elastic modulus at loading age t'

2. Committe European du Beton (CEB-FIP) Model Code 1990

In 1993, CEB-FIP recommends expressions to creep as following

If stress $\sigma_c < 0.4f_{cm}(t_0)$, the creep is assumed to be linearly related to the stress. For constant stress was applied at the time t_0 this leads to:

$$\varepsilon_{cc}(t, t_0) = \frac{\sigma_c(t_0)}{E_{ci}} \phi(t, t_0) \quad \dots(2.2)$$

where

$f_{cm}(t, t_0)$ = mean compressive strength at an ages of days t_0

E_{ci} =elastic modulus at age 28 days

$\phi(t, t_0)$ = creep coefficient

where

$$\phi(t, t_0) = \phi_0 \beta_c(t, t_0) \quad \dots(2.3)$$

ϕ_0 =notional creep coefficient.

$\beta_c(t, t_0)$ =function to describe the development of creep with time after loading.

t =age of concrete at the moment considered in days.

t_0 =age of concrete at loading.

When $0.4f_{cm}(t_0) < \sigma_c < 0.6f_{cm}(t_0)$ the non-linearity of creep may be taken into account using the following equations:

$$\phi_{0,k} = \phi_0 \exp [\alpha_\sigma (k_\sigma - 0.4)] \quad \dots(2.4)$$

where

$\phi_{0,k}$ =non-linear notional creep coefficient, which replace ϕ_0 in eq.(2.3)

$k_\sigma = \sigma_c / f_{cm}$

k_σ :the ratio of stress to strength.

$\alpha_\sigma = 1.5$

3. Bažant-Panula (BP) Model

This model is either in its complete version or in its simplified version (*Bažant, 1982; Bažant and Baweja, 2000; Bažant, 2001*). The basic form of this model for the creep is given by the following equation:

$$\varepsilon_{cb} = \frac{1}{E'} [1 + C'_b(t, t')] \quad \dots(2.5)$$

where

ε_{cb} =basic creep strain

C'_b =basic creep coefficient

E' =the asymptote of a plot of creep vs the logarithm of short times under load

The total creep function, which is the elastic strain plus basic creep plus drying creep per unit stress expressed as

$$\varepsilon_{ct} = \varepsilon_{cb} + \frac{C'_b(t, t', t_0)}{E'} \quad \dots\dots(2.6)$$

Some expression of the drying creep coefficient $C'_b(t, t', t_0)$ are given in (Bažant, 1982).

2.6:Representation of Time Effects Analysis of Concrete:

Several practical models for predicting creep and shrinkage have been developed. An extensive review of these models was presented by (Mahmood, 2001). Most of the models used to predict the time-dependent behavior of the concrete, treat the total strain at any time (t) at a point in uniaxially loaded specimen at a constant temperature as the sum of instantaneous creep and shrinkage components. In the present study, the model of ACI Committee 209 is used. The ACI committee-209 (1992) proposed the following forms of equations to predict the compressive strength of the concrete at any time (t):

$$f'_c(t) = \frac{t}{a+bt} f'_{c(28)} \quad \dots\dots(2.7)$$

where f'_c is the 28-day strength, t is the time in days after the casting of concrete and the constants “a” and “b” from the following:

- *Moist cured concrete, type I cement: a=4, b=0.8*
- *Moist cured concrete, type II cement : a=2.3, b=0.92*
- *Steam cured concrete, type I cement : a=1.0, b=0.95*
- *Steam cured concrete, type II cement : a =0.7, b=0.92*

The ACI committee 209 proposed the following equations to calculate the direct tensile strength f'_t , and the modulus of elasticity E_o :

$$f'_t = 0.007\sqrt{w}. f'_c(t) \quad \dots\dots(2.8)$$

$$E_o(t) = 0.043w^{1.5}\sqrt{f'_c(t)} \quad \dots\dots(2.9)$$

$$\varepsilon_c(t) = \frac{2f'_c(t)}{E_o(t)} \quad \dots\dots(2.10)$$

$$\varepsilon_{cu}(t) = \frac{4f'_c(t)}{E_o(t)} \quad \dots\dots(2.11)$$

Where $\varepsilon_c(t)$ and $\varepsilon_{cu}(t)$: are maximum uniaxial compressive strains of concrete at time t , and the corresponding crushing strains at time t , respectively. On the other hand, w : is the concrete unit weight in kg/m^3 and f'_c, f'_t and E_c are in MPa.

The average values suggested for v_u is:

$$v_u = 2.35 \gamma_c \quad \dots\dots(2.12)$$

γ_c the product of the correction factors for concrete under condition other than standard, is calculated as follows:

$$\gamma_c = \gamma_{la}^c \gamma_{\lambda}^c \gamma_h^c \gamma_s^c \gamma_{\psi}^c \gamma_a^c \quad \dots\dots(2.13)$$

where γ_{la} , γ_{λ} , γ_h , γ_s , γ_{ψ} , γ_a and γ_{cm} are correction factors for loading age, humidity, minimum member thickness, slump, percent fines, air content and cement content, and the c , in the superscript mean creep. All the above correction factors assume the value of unity for the following standard condition; 102 mm or less slump, 40 percent ambient relative humidity, 152 mm or less minimum member thickness, and loading age of 7 days for moist cured concrete and 1-3 days for steam cured concrete and (279 to 445) kg/m^3 for cement content, which has a negligible effect on creep coefficient.

$$\text{For moist curing} \quad \gamma_{la}^c = 1.25\tau^{-0.118}$$

$$\text{For steam curing} \quad \gamma_{la}^c = 1.13\tau^{-0.094}$$

$$\text{For } \lambda \geq 40\% \quad \gamma_{\lambda}^c = 1.27 - 0.0067\lambda$$

$$\text{For } \leq 1 \text{ year loading} \quad \gamma_h^c = 1.14 - 0.00092h$$

For ultimate loading $\gamma_h^c = 1.1 - 0.00067h$

For slump $\gamma_s^c = 0.82 + 0.00264s$

For the percent of fines by weight $\gamma_\psi^c = 0.88 + 0.0024\psi$

For $a \leq 6\%$ $\gamma_a^c = 1$

For $a \geq 6\%$ $\gamma_a^c = 0.46 + 0.09a$

where τ is the loading age in days, λ is the ambient relative humidity in percent, h is the minimum thickness in (mm). S is the slump in (mm), ψ is the percent of fines by weight, a is the air content in percent, and (C_m) is the cement content in (kg/m^3).

2.7 Conclusion Remarks:

Most of these researches were reviewed in this chapter studied the short-term behavior of strengthening concrete columns with ferrocement and fiber reinforced polymers (FRP) including the three types, CFRP, GFRP and AFRP sheets. Through the presentation of previous research found that strengthening RC columns with FRP material improved the load carrying capacity and enhance the ductility of columns. In addition, transforming the failure from brittle to ductile. Also, this chapter included reviewing the researches that investigated the long-term behavior of reinforced concrete columns, confined concrete columns and FRP strengthening concrete columns with all types of it, CFRP, GFRP and AFRP but a little studies deal with numerical investigation including time effects. This work deals with a theoretical investigation on viscoelastic material (concrete) with the time dependent behavior of concrete columns strengthening with FRP. Finite element analysis is used in this study by utilizes ANSYS package.

Chapter Three

Creep Analysis

3.1:General:

Creep is an increase in strain under constant stress, as shown in Fig.(3.1). Analysis of creep in concrete is a complicated phenomenon, and a basic equation is in general applicable and difficult to formulate. Before the computer epoch, this assignment was not truly a problem because structural analysis problems cannot be solved by a sophisticated constituent model.

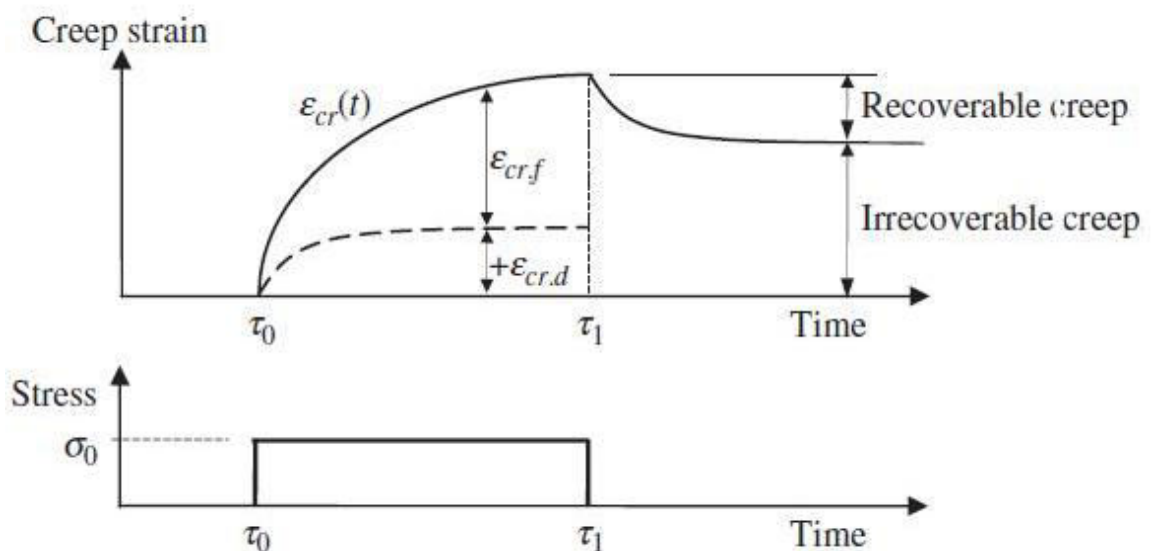


Fig.(3.1): Creep Response of Uniaxial Loaded Specimen(*Gilbert & Ranzi, 2011*).

3.2: Behavior of Concrete as a Visco-Elastic Material:

Creep is a manifestation of viscoelasticity; therefore, this study interested in viscoelasticity because it is the motivation to observe the behavior of creep. The materials response of time dependent can be classified into: elastic, viscous and viscoelastic. On application of a sudden load, which is then held constant, an **elastic material** undergoes instantaneous deformation. The elastic strain when

the state of stress in one-dimensional is $\epsilon = D\sigma$ where $D = 1/E$ is the inverse of elastic modulus E it is called, compliance. Then the deformation remains constant. The elastic strain back to its original value when the unloading state, and thus recovers all elastic deformation.

Flow of **viscous material** at a constant rate $\dot{\epsilon} = \sigma/\eta$ Where $\eta = \tau E_0$ is the Newton viscosity, E_0 is the initial modulus, and τ is the time constant of the material. When unloading, the accumulated strain $\epsilon = \int \dot{\epsilon} dt$ cannot be recovered.

A **viscoelastic material** more complex response because it combines the behavior of elastic and viscous material. H refers to Heaviside function and it's defined as: (*Barabero, 2014*)

$$\begin{aligned} H(t-t_0) &= 0 \quad \text{when } t < t_0 \\ H(t-t_0) &= 1 \quad \text{when } t \geq t_0 \end{aligned} \quad \dots(3.1)$$

When step loading $\sigma = H(t - t_0) \sigma_0$, with a constant load σ_0 , exactly like elastic material, the viscoelastic material experiences a sudden elastic deformation. Then, deformation grows through a combination of recoverable and non-recoverable viscosity flow.

3.2.1: Compliance Function:

At any age (t) , the total strain of a uniaxially loaded concrete sample consists of a number of components (*Anderson, 1982; Bažant, 1982; Bažant, 1988; Gilbert & Ranzi, 2011*):

$$\epsilon(t) = \epsilon_E(t) + \epsilon_C(t) + \epsilon_{Sh}(t) + \epsilon_T(t) \quad \dots(3.2a)$$

$$\epsilon(t) = \epsilon_E(t) + \epsilon''(t) \quad \dots(3.2b)$$

$$\epsilon(t) = \epsilon_E(t) + \epsilon_C(t) + \epsilon^0(t) \quad \dots(3.2c)$$

$$\varepsilon(t) = \varepsilon_{\sigma}(t) + \varepsilon^0(t) \quad \dots(3.2d)$$

Included (instantaneous strain $\varepsilon_E(t)$), creep strain $\varepsilon_C(t)$, shrinkage strain $\varepsilon_{sh}(t)$, thermal strain $\varepsilon_T(t)$, inelastic strain (stress independent) $\varepsilon^0(t)$, inelastic strain (stress dependent) $\varepsilon''(t)$ and mechanical strain (stress produced strain) $\varepsilon_{\sigma}(t)$. $\varepsilon_E(t)$, is reversible instantly after remaining the loads. However, because of aging that result by hydration in addition to other changes of time dependent in the microstructure.

According to the definitions of these strains, the test of creep required two similar specimens subjected to the same environment histories is one of these specimens loaded and the other for free load. The difference of the deformation in the two specimens called mechanical strain which consist of instantaneous and creep strain.

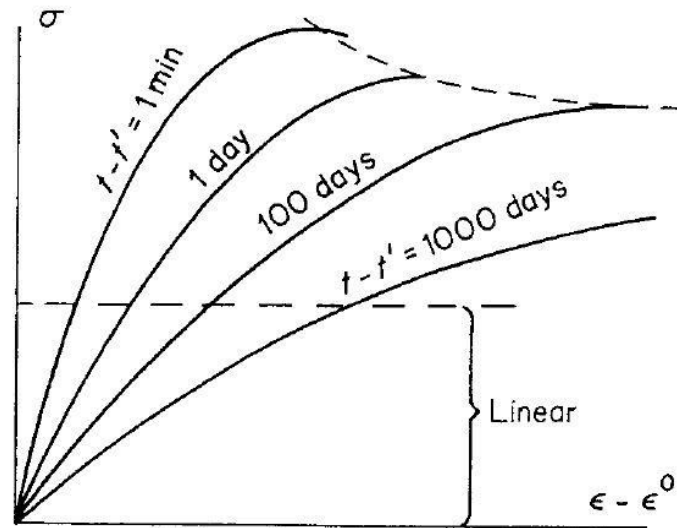
Creep is considered by measuring strain under constant stress, plotting the creep isochrones by measuring the strains of loaded specimens to different levels of stress in respect to the curves of stress versus strains (see Fig(3.2a)) one finds that within the range of services stress, i.e. the curves almost linear when stresses less than 40% on the strength. Thus;

$$\varepsilon(t) = \sigma J(t, t') + \sigma^0(t) \quad \dots\dots(3.3)$$

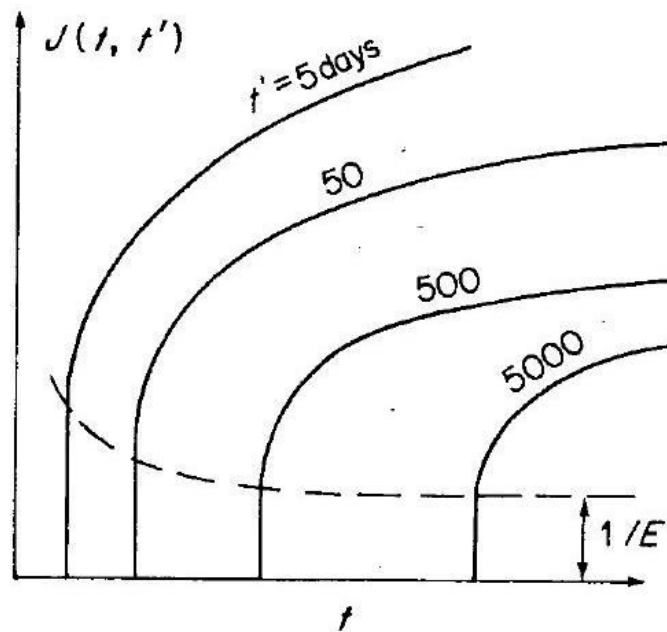
Which σ is uniaxial stress, ε is the axial strain, t is the time that represents the age of concrete, and $J(t, t')$ is the compliance function (called creep function) that represents the summation of elastic and creep strains at a time (t) produced by applying sustained unit stress at time t' . The typical shape of this function is sketched in (Fig (3.2b)). The creep function is expressed as a sum of the elastic (instant) compliance $1/E(t')$ and the creep compliance $C(t, t')$ (also called the specific creep), i.e.

$$J(t, t') = \frac{1}{E(t')} + C(t, t') = \frac{1}{E(t')} [1 + \phi(t, t')] \quad \dots\dots (3.4)$$

Where $E(t')$ is the elastic modulus at age (t'), and $\phi(t, t') = E(t') J(t, t') - 1$ is the ratio of the creep strain of the instantaneous strain, called the creep coefficient. At long times such as 30 years, the values of ϕ usually fall between 1 and 6, with 2.5 to 3 as typical values (Bažant 1982; ACI 209-92(2010); Gilbert & Ranzi, 2011).



(a)



(b)

Fig.(3.2): a-Creep Isochrones, b-Compliance Curves for Various time(Bažant 1988).

Many factors influenced the values of the compliance function, these factors are divided into internal and external. The internal factors are those that become constant when concrete is cast; they include properties of concrete mix, such as aggregate, water cement ratio and cement content as well as the design strength. Increasing all of these factors leads to decreasing creep except decrease the water cement ratio leads to reduce the creep. The external factors are those that can be changed externally after casting the concrete; they include specific humidity and the temperature (including their histories), the degree of hydration and the age when loading begins. The compliance function and the influencing factors can illustrate in a mathematical expression which are discussed in more details in (*Bažant 1982; Bažant 1988*).

The current age (t) and the age of loading (t') are important properties of the compliance function of concrete. It is a salient characteristic of concrete that the compliance function cannot be considered as a function of one variable, i.e. the time-lag ($t-t'$), as is customary in classical viscoelasticity for other material, e.g. polymers. The ageing is a considerable obstacle to analytical solution of structural problems, and necessitates that most real problems have to be solved by numerical methods.

3.2.2: Viscoelastic Models:

The models of viscoelastic materials that reviewed in this section are suitable curve fits experimental data. Creep and relaxation tests are usually tested in the time range. In creep test constant stress σ_0 is applied and measured strain, the ratio between the measured strain and stress applied is the compliance $D(t) = \varepsilon(t)/\sigma_0$. In the relaxation test constant strain ε_0 is applied and measured the stress which maintains the strain, the ratio between the measured stress and strain applied is the relaxation $E(t) = \sigma(t)/\varepsilon_0$ (*Barbero, 2014*).

3.2.2.1: Maxwell Model:

This model consists of simple series (dashpot and spring), where dashpot represent to the viscous element while the spring represent to elastic element. The relationship between stress and strain for spring and dashpot given according to Hook's law and Newton's law, respectively (*Marques & Creus, 2012*). For deriving the compliance function applying the following equations:

$$\begin{aligned}\sigma(t) &= \sigma_E(t) = \sigma_\eta(t) && \text{Equilibrium equation} \\ \varepsilon(t) &= \varepsilon_E(t) + \varepsilon_\eta(t) && \text{Compatibility equation} \\ \sigma_E(t) &= E \varepsilon_E(t) && \text{Constitutive relationship (spring)} \\ \sigma_\eta(t) &= \eta \dot{\varepsilon}_\eta(t) && \text{Constitutive relationship (dashpot)}\end{aligned}$$

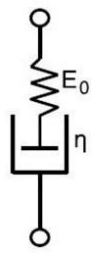
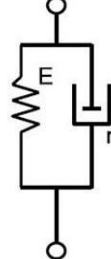
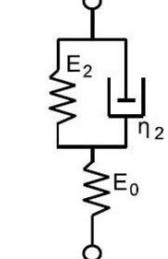
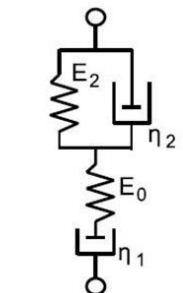
by differentiating compatibility equation with respect to time and using constitutive relationships we obtain:

$$\dot{\varepsilon}(t) = \frac{\sigma(t)}{\tau E_0} + \frac{\dot{\sigma}(t)}{E_0} \quad \dots(3.5)$$

To derive the Maxwell model compliance, a creep test is used where constant stress σ_0 is applied to the ends of the model which illustrate in Table(3.1). Integrate the equation (3.5) in respect to the time got:

$$\varepsilon(t) = \frac{1}{\tau E_0} \int_0^t \sigma_0 dt + \frac{\sigma_0}{E_0} \quad \dots(3.6)$$

Table(3-1): Viscoelastic Models (*Barbero, 2014*).

Model Name	Maxwell	Kelvin	Standard Solid	Maxwell-Kelvin
Representation				

Where τ is the time constant of the material, E_0 is the elastic constant of the spring and $\eta_0 = \tau E_0$. The same load and constant stress σ_0 subject to the dashpot and spring, thus evaluating integrated yield:

$$\varepsilon(t) = \frac{\sigma_0 t}{\tau E_0} + \frac{\sigma_0}{E_0} \quad \dots(3.7)$$

Then the compliance function given in eq.(3.8) where $D(t) = \varepsilon(t)/\sigma_0$

$$D(t) = \frac{1}{E_0} + \frac{t}{\tau E_0} \quad \dots(3.8)$$

Relaxation of the Maxwell model can be derived by taking the Laplace transform of the equation (3.8) to get:

$$D(s) = \frac{1}{sE_0} + \frac{1}{s^2\tau E_0} = \frac{s\tau + 1}{s^2\tau E_0} \quad \dots(3.9)$$

The dashpot does not move at $t=0$ and E_0 refers to initial elastic modulus of the material. In the Laplace domain, the relaxation is:

$$E(s) = \frac{1}{s^2 D(s)} = \frac{\tau E_0}{s\tau + 1} \quad \dots(3.10)$$

by taking the inverse of Laplace transformation can obtain the relaxation in time domain

$$E(t) = E_o \exp(-t/\tau) \quad \dots(3.11)$$

The relaxation decays to 36.8% of the initial value at $t = \tau$

3.2.2.2: Kelvin Model:

Simple parallel series of viscous flow and elastic fully yields recoverable deformation with no non-recoverable viscous flow, derivation of the compliance function by applying the following equations with constitutive relations of spring and dashpot (*Mehta & Monterio, 2006*).

$$\sigma(t) = \sigma_E(t) + \sigma_\eta(t) \quad \text{Equilibrium equation}$$

$$\varepsilon(t) = \varepsilon_E(t) = \varepsilon_\eta(t) \quad \text{Compatibility equation}$$

by sub constitutive relations in the equilibrium equation obtain eq. (3.12)

$$\sigma(t) = \tau E \dot{\varepsilon}(t) + E \varepsilon(t) \quad \dots(3.12)$$

but deformation does not recover immediately. This model is possible with creep test only because the relaxation required infinite large stress to extend the dashpot in Table(3.1) to a fixed value in no time. Applied constant stress $\sigma = \sigma_o$, is for creep test. Equation (3.12) is an ordinary differential equation (ODE) in $\varepsilon(t)$, which is satisfied by $\varepsilon(t) = (\sigma_o/E)[1 - \exp(-t/\tau)]$. Therefore, the compliance $D(t) = \varepsilon(t)/\sigma_o$ is:

$$D(t) = 1/E_o[1 - \exp(-t/\tau)] \quad \dots(3.13)$$

Using $E(t) = L^{-1}[E(s)]$, the relaxation can be written by using $\delta(t)$ Dirac delta function and $H(t)$ Heaviside step function as follows:

$$E(t) = EH(t) + E\tau\delta(t) \quad \dots(3.14)$$

Where $\delta(t - t_o) = \infty$ if $t = t_o$ and zero for any other time.

The compliance functions of other models can be derived in the same manner that used in Maxwell and Kelvin models.

3.2.2.3: Standard Linear Solid:

Add a spring to the Kelvin model, illustrate in Table(3.1), to have initial compliance $1/E_0$ (Mehta & Monterio, 2006). The compliance of this model is:

$$D(t) = \frac{1}{E_0} + \frac{1}{E_2} \left[1 - \exp\left(-\frac{t}{\tau_2}\right) \right] \quad \dots(3.15)$$

and

$$E(t) = E_\infty + (E_0 - E_\infty) \exp\left(\frac{-t(E_0 + E_2)}{\tau_2 E_2}\right) \quad \dots(3.16)$$

where $E_\infty = (E_0^{-1} + E_2^{-1})^{-1}$ is the equilibrium modulus as time goes to infinity.

Adding more spring-dashpot elements in series gives a better correlation, as in

$$D(t) = D_0 + \sum_{j=1}^n D_j \left[1 - \exp\left(-\frac{t}{\tau_j}\right) \right] \quad \dots(3.17)$$

where τ_j the retardation times. When $n \rightarrow \infty$

$$D(t) = \int_0^\infty \Delta(\tau) [1 - \exp(-t/\tau)] d\tau \quad \dots(3.18)$$

where $\Delta(\tau)$ is the compliance spectrum.

3.2.2.4: Maxwell-Kelvin Model:

A crude approximation of liquid material which is described in Table(3.1), called four-parameter model. This model consists of number of Maxwell and Kelvin elements placed in series. The compliance found by adding the compliances of the two models (Marques & Creus, 2012).

$$D(t) = \frac{1}{E_0} + \frac{t}{\tau_1 E_0} + \frac{1}{E_2} [1 - \exp(-t/\tau_2)] \quad \dots(3.19)$$

Where E_0 is the elastic modulus, τ_1 take place of τ in equation(3.8), and τ_2, E_2 ,

Take the place of τ, E in equation(3.13). The relaxation modulus is:

$$E(t) = (P_1^2 - 4P_2)^{-1/2} \left[\left(q_1 - \frac{q_2}{T_1} \right) \exp(-t/T_1) - \left(q_1 - \frac{q_2}{T_2} \right) \exp(-t/T_2) \right] \dots\dots(3.20)$$

$$P_1 = \frac{\eta_1}{E_0} + \frac{\eta_1}{E_2} + \frac{\eta_2}{E_2} \quad ; \quad P_2 = \frac{\eta_1\eta_2}{E_0E_2}$$

$$q_1 = \eta_1 \quad ; \quad q_2 = \frac{\eta_1\eta_2}{E_2}$$

$$T_1 = \frac{1}{2P_2} [P_1 + \sqrt{P_1^2 - 4P_2}] \quad ; \quad T_2 = \frac{1}{2P_2} [P_1 - \sqrt{P_1^2 - 4P_2}]$$

$$\eta_1 = E_0\tau_1 \quad ; \quad \eta_2 = E_0\tau_2$$

where P_1, P_2, q_1 and q_2 are the material constants, T_1 and T_2 are the roots of equation.

The long-term deformation determined if the material solid or liquid. The material is liquid if the deformation was unbounded and while the material is solid if the deformation eventually stops.

3.2.2.5: Power Law:

This model represents a short time deformation and it's popular because it is easy to fit the data and fit well the behavior of polymers (*Findley et al., 1976*)

$$E(t) = At^{-n} \dots\dots(3.21)$$

The parameters A and n adjusted with experimental data. This equation becomes a line when taking algorithm on both sides of it. Using linear regression to fit the parameters. By using $D(t) = L^{-1}[\frac{1}{s^2L[E(t)]}]$ obtained the compliance as

$$D(t) = D_0 + D_c(t)$$

$$D_c(t) = [A\Gamma(1-n)\Gamma(1+n)]^{-1}t^n \quad \dots(3.22)$$

where $D_0 = 1/E_0$ is the elastic compliance, the subscript $()_c$ refers to the creep component of compliance functions and the relaxation and Γ is the Gamma function.

3.2.2.6: Prony Series:

When the time domain became long, refined new model becomes necessary, such as Prony series that consist of n number of decaying exponentials (*Sousa et al., 2008*).

$$E(t) = E_\infty + \sum_{i=1}^n E_i \exp(-t/\tau_i) \quad \dots(3.23)$$

where E_∞ is the equilibrium modulus, E_i are the relaxation moduli and τ_i are the relaxation times.

If the Maxwell material is a liquid ($E_\infty = 0$) and decay becomes slower because the larger τ_i . At $t=0$, note that $E_0 = E_\infty + \sum E_i$. The equation(3.23) is written as follows:

$$E(t) = E_\infty + \sum_1^n m_i E_0 \exp(-t/\tau_i) \quad \dots(3.24)$$

where $m_i = E_i/E_0$ are the dimensionless moduli.

Prony Series can be expressed using a shear modulus (G) and bulk modulus (K)

$$G(t) = G_\infty + \sum_1^n g_i G_0 \exp(-t/\tau_i)$$

$$K(t) = K_\infty + \sum_1^n k_i K_0 \exp(-t/\tau_i) \quad \dots(3.25)$$

where G_0, K_0 refer to initial shear modulus and bulk modulus, respectively; $g_i = G_i/G_0$ and $k_i = K_i/K_0$ the dimensionless shear and bulk moduli and G_i, K_i represent shear and bulk modulus of the i -th term. When $t=0$, $G_\infty = G_0(1 - \sum_1^n g_i)$, $K_\infty = K_0(1 - \sum_1^n k_i)$, The Prony series written as

$$G(t) = G_0(1 - \sum_1^n g_i) + \sum_1^n g_i G_0 \exp(-t/\tau_i)$$

$$K(t) = K_0(1 - \sum_1^n k_i) + \sum_1^n k_i K_0 \exp(-t/\tau_i) \quad \dots(3.26)$$

Note Poisson's ratio usually assumed does not change over time.

The experimental results are represented by a mathematical function. On one hand, the Prony series used a mathematical curve to represent viscoelastic materials in the present study. On the other hand, the procedure to obtain Prony series from experimental data (curve fitting procedure) is not easy, involving many numerical tasks. For this reason, develop a computer program that written in **Fortran power station 4.0** to perform curve fitting of Prony series, this program depends on the least squares method to obtain the coefficient of a Prony series.

The Prony series model used in this research to represent viscoelastic materials, the fitting of compliance function will illustrate in chapter four.

3. 3: Differential Operator Form of Stress Strain Constitutive Relations:

The forms of creep and relaxation integral of stress strain constitutive relations are by no means the only possible forms. They will be given two other forms: the first involves differential operator and the second involves steady state and Fourier transform(*Christensen, 1982*).

Related to isotropic materials, from the relation between the deviatoric components of stress and strain, we consider the following differential operator form

$$p_0 s_{ij}(t) + p_1 \frac{ds_{ij}(t)}{dt} + p_2 \frac{d^2 s_{ij}(t)}{dt^2} + \dots = q_0 e_{ij}(t) + q_1 \frac{de_{ij}(t)}{dt} + q_2 \frac{d^2 e_{ij}(t)}{dt^2} + \dots$$

.....(3.27)

Or, more compactly, we write this as

$$P(D)s_{ij}(t) = Q(D)e_{ij}(t) \quad \dots(3.28)$$

where $P(D) = \sum_{k=0}^N p_k D^k$, $Q(D) = \sum_{k=0}^N q_k D^k$

with D designates the operator d/dt. The Relationship of eq.(3.28) is certainly a potential relation between stress and stress, but not clear whether this relation is important to viscoelasticity. By take the Laplace transform to eq.(3.28) to become:

$$P(s)\bar{s}_{ij}(s) - \frac{1}{s} \sum_{k=1}^N p_k \sum_{r=1}^k s^r s_{ij}^{(k-r)}(0) = Q(s)\bar{e}_{ij}(s) - \frac{1}{s} \sum_{k=1}^N q_k \sum_{r=1}^k s^r e_{ij}^{(k-r)}(0) \quad \dots(3.29)$$

where $P(s) = \sum_{k=0}^N p_k (s)^k$, $Q(s) = \sum_{k=0}^N q_k (s)^k$

and $s_{ij}^{(k-r)}(0)$ designates the $k - r$ order derivative of $s_{ij}(t)$ evaluated at $t = 0$, with a similar relationship for $e_{ij}(t)$.

$$s\bar{G}_1 = Q(s)/P(s) \quad \dots(3.30)$$

and

$$\sum_{r=k}^N p_r s_{ij}^{(r-k)}(0) = \sum_{r=k}^N q_r e_{ij}^{(r-k)}(0), \quad k = 1, 2, \dots, N \quad \dots(3.31)$$

Eq.(3.31) provides a requirement with the initial conditions, thus the initial conditions for stress and strain are not completely independent, and relationships such as eq.(3.31) may be satisfied.

The relation of eq.(3.30) gives the conditions under which the relaxation integral and differential operator forms of the deviatoric stress strain relation are equivalent. In an entirely similar manner, the independent dilatational part of the isotropic stress strain relations can be written in the differential operator form

and the equivalence with the relaxation integral form can be ascertained. This would then imply a relation of the type

$$L(D)\sigma_{kk}(t) = M(D)\varepsilon_{kk}(t) \quad \dots(3.32)$$

where $L(D)$ and $M(D)$ are operators with independent coefficients.

3.4:Concrete Aging Effects:

The main source of error is aging of concrete, which is expressed by the correction factor creep (γ_{la}) in section 2.6 and by time variation of (E_{ci}). Gradual stress changes during the service life of structure producing additional instantaneous and creep strain, which are superimposed on the creep strain due to initial stresses and to all previous stress changes. Because of concrete aging, these additional strains are much less than those which would arise if the same stress changes occur right after the instant of the first loading t_{la} . This effect can be accounted for by using the age-adjusted effective modulus method (*Bazant 1972*).

It is similar to the effective modulus method, this method consists of an elastic analysis with modified elastic modulus, E_{ca} which is defined by Eq.(3.33), and is called the age-adjusted modulus:

$$E_{ca} = E_{ci}/(1+\chi v_t) \quad \dots\dots(3.33)$$

Table (3-2), the χ values are presented for the creep function of loading age. For interpolation in the table, it is better to assume linear dependence on $\log t_{la}$ and $\log(t-t_{la})$ [*ACI 209-92(2010)*].

Table (3-2): Aging Coefficient[ACI 209-92(2010)].

(t-t _{1a})days	v _u	Time , t (days)			
		10 ¹	10 ²	10 ³	10 ⁴
10 ¹	0.5	0.525	0.804	0.811	0.809
	1.5	0.728	0.826	0.825	0.820
	2.5	0.774	0.842	0.837	0.830
	3.5	0.806	0.856	0.848	0.839
10 ²	0.5	0.505	0.888	0.916	0.915
	1.5	0.739	0.919	0.932	0.928
	2.5	0.804	0.935	0.943	0.938
	3.5	0.839	0.946	0.951	0.946
10 ³	0.5	0.511	0.912	0.973	0.981
	1.5	0.732	0.943	0.981	0.985
	2.5	0.795	0.956	0.985	0.988
	3.5	0.830	0.964	0.987	0.990
10 ⁴	0.5	0.501	0.899	0.976	0.994
	1.5	0.717	0.934	0.983	0.995
	2.5	0.781	0.949	0.986	0.996
	3.5	0.818	0.958	0.989	0.997

3.5: Basic Theory of Viscoelasticity in ANSYS Program :

A material is said to be viscoelastic if the material has elastic (recoverable) part as well as a viscous (Non-recoverable) part. Upon application of load, the elastic deformation is instantaneous, while the viscous part occurs over time (ANSYS 2011).

The viscoelastic implementation uses a quasi-static boundary value approach to solve linear viscoelastic solids undergoing mechanical deformations. The basic constitutive relationship is similar to that used in (Zienkiewicz *et al.* 1968, Zienkiewicz *et al.* 1988), as the effects of time characterized reduced or pseudo time.

The material properties are expressed in integral using the kernel function of generalized Maxwell elements as:

$$G(\zeta) = \sum_{i=1}^I G_i e^{(-\zeta/\tau_i)} + G(\infty) \quad \dots(3.34)$$

where :

$G(\zeta)$ = Current value of material property (output quantities effective shear modulus).

I = Number of Maxwell element used to approximate the material relaxation shear modulus .

$$G_i = C_i (G(0) - G(\infty)).$$

C_i = Constant associated with the instantaneous response .

$G(0)$ = Initial shear modulus .

$G(\infty)$ = Final shear modulus .

ζ = reduced or pseudo time ,equal $(t - t')$.

τ_i = Constant associated with a discrete relaxation spectrum .

The stress can be related to strain at any time by the convolution integral ,

$$\sigma(t) = \int_0^t G(\zeta - \zeta') \frac{d\zeta(t)}{dt'} dt' \quad \dots(3.35)$$

where :

σ = Stress .

ε = Total strain (includes thermal strain) .

t = Time.

ζ = pseudo time ,equal $(t - t')$.

Chapter Four

Verification Models

4.1 General:

This chapter presents some examples which are analyzed numerically of reinforced concrete columns in order to investigate the behavior of RC column under short term and long term loading (strengthening and non-strengthening). In the current work, the finite element model compared with available experimental results so as to check the accurate validation of finite element models. The simulation of columns was done by using ANSYS package according to the finite element formulation and materials idealization in Appendix A.

This chapter consists of eight models; three of these models are subjected to short term loading (control and jacketed columns), while the remained models are subjected to long term loading (control and jacketed columns).

4.2 Analysis of Reinforced Concrete Columns Subjected to Short Term Loading:

This section included the analysis of two groups of columns; the first group consists of one un-strengthened reinforced concrete column (Control Column) which was tested by (*Mourad & Shannag, 2012*), while the second group consists of two strengthening concrete columns (Jacketed Columns). One of these columns was strengthened by CFRP which was investigated by (*Widiarsa & Hadi, 2013*) and the other was strengthened by GFRP which was tested by (*Benzaid et al., 2008*).

4.2.1 Control Columns:

4.2.1.1 Mourad and Shannag RC column:

In this study, one column of ten squares reinforced concrete columns was selected which was tested by Mourad and Shannag in 2012. The selected column in the current research was analyzed by using a nonlinear finite element model where ANSYS package was utilized in this analysis, it was designed as SC-2.

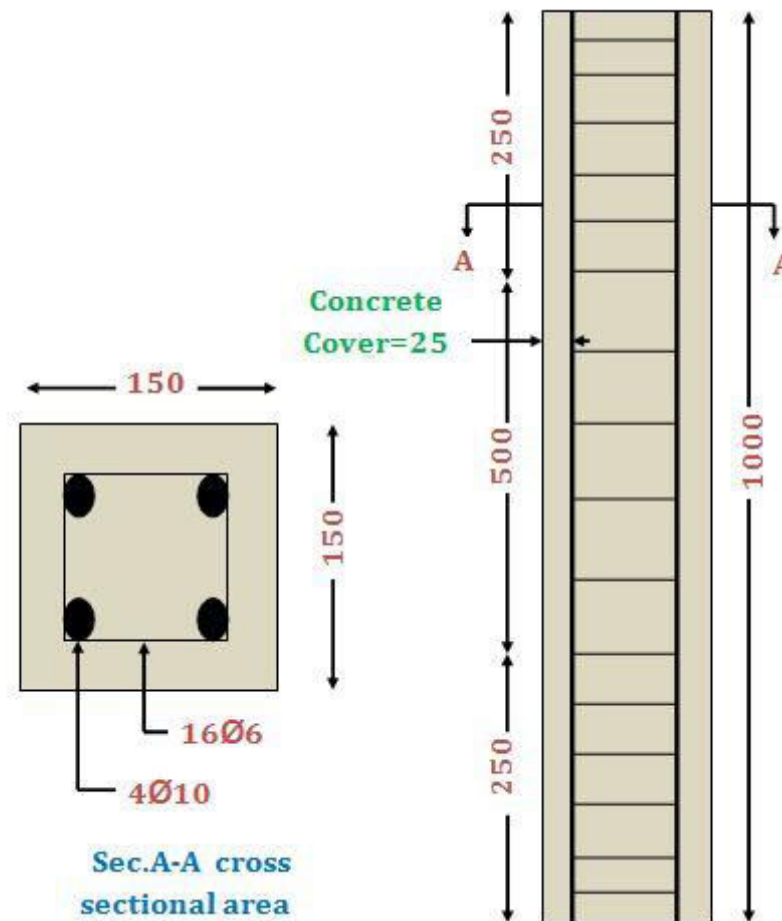
4.2.1.1.1 Description of Test Specimen (SC-2):

The test specimen was designed with a square cross section of (150*150)mm and 1000mm for height. The compressive strength of concrete cylinders were 25MPa after 28 days, tensile strength of concrete was 3.1MPa and the elastic modulus was 23.65GPa, while the steel reinforcement that was used in this specimen were 4 \varnothing 10mm and 16 \varnothing 6mm for longitudinal bar and stirrups respectively, the elastic modulus and yield stress of steel reinforcement was 210GPa and 240 MPa. The distributions of steel reinforcement and the dimensions of this column were given in Fig.(4.1)

4.2.1.1.2 Finite Element Idealization and Material properties:

This column was modeled by using 1928 elements which consist of SOLID65, LINK8 and SOLID45 elements were used for modeled concrete, steel reinforcement and steel plate (supports), consecutively. Two steel plates with dimension (150*150*25) mm was used in the support's ends for preventing local failure at the location of the load applied and support. The dimension of elements of concrete and steel plate were chosen (25* 25* 25)mm, element types and material properties that were used (SC-2) model of finite element was illustrated in Table(4-1).

In the analysis of RC column, four corner nodes in a lower plane ($y=-25$) were restrained in x and y directions to prevent motion, and applied axial compression load at the upper end of the column, whereas distributed on all the nodes in an upper plane ($y=1025$), as illustrated in Fig.(4.2).



***All dimensions in mm**

Fig.(4.1):Details of (SC-2) RC Column(Mourad and Shannag, 2012).

Table (4-1): Element Type and Material Properties of (SC-2) RC Column
(Mourad & Shannag, 2012).

Material Type	Element Type	Material Properties
Concrete	SOLID65	$E_c=23650^*$
		$\nu=0.2^{**}$
		$\beta_1=0.5^{**}$
		$\beta_0=0.9^{**}$
		$f'_c=25$
		$f_t=3.3^*$
Steel Reinforcement	LINK8	$E_s=210000^{**}$
		$\nu=0.3^{**}$
		$f_y=420^{**}$
Steel Plate	SOLID45	$E=210000^{**}$
		$\nu=0.3^{**}$

*Calculated according to ACI-318 Equations

**Assumed

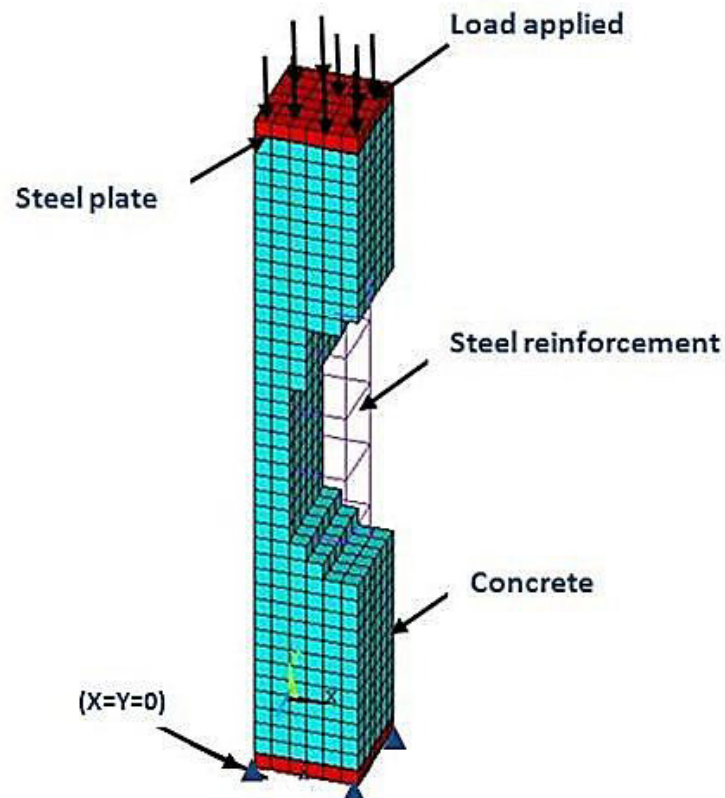


Fig.(4.2):Finite Element Model of (SC-2) RC Column.

4.2.2 Jacketed Columns:

4.2.2.1 Widiarsa and Hadi RC Column Strengthen with CFRP Sheet:

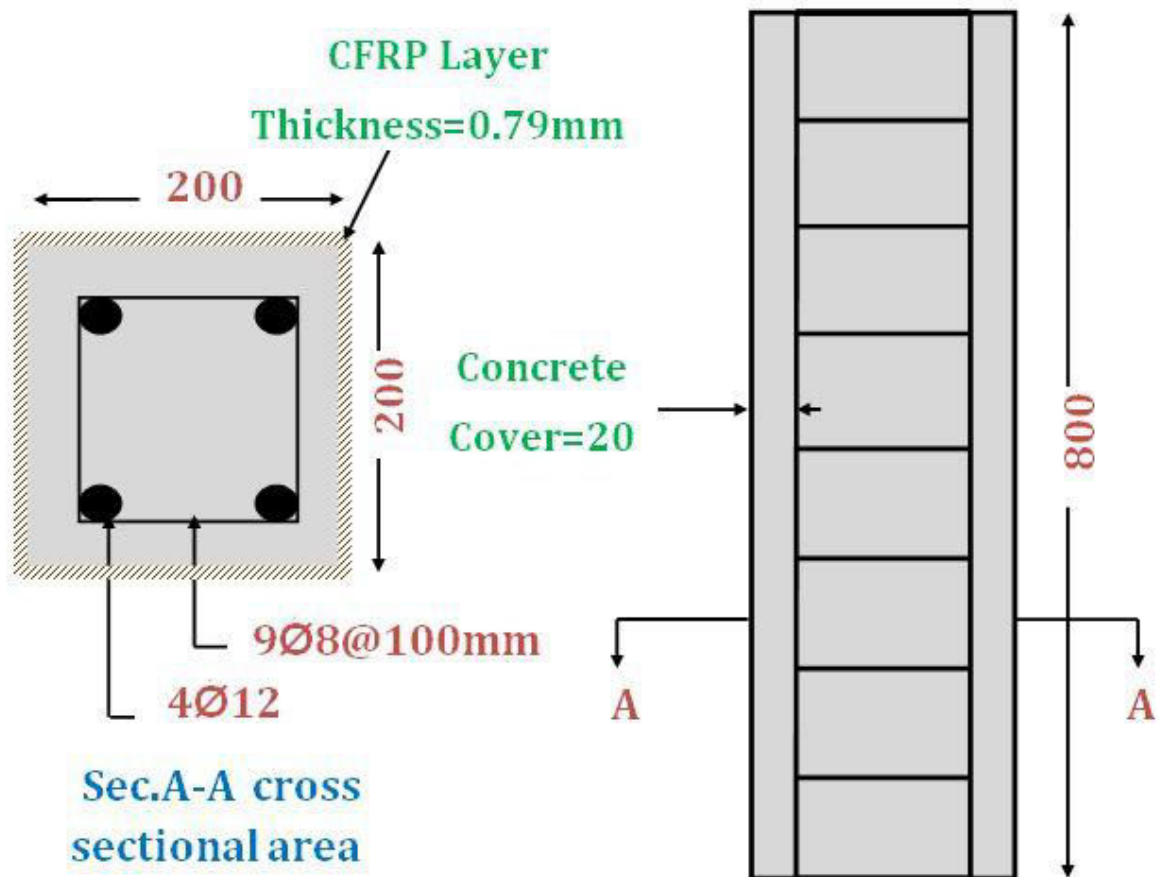
Twelve short high strength reinforced concrete columns were tested by Hadi and Widiarsa. In this study, one of jacketed specimens was selected for the analysis using a nonlinear finite element model by using ANSYS package, it was designed as 1HC0.

4.2.2.1.1 Description of Test Specimen (1HC0):

The (1HC0) RC column was cast with height of 800mm and square cross section of (200*200) mm. The column was reinforced by 4 ϕ 12mm longitudinal reinforcement bar and 9 ϕ 8mm for stirrups were distributed @100mm. The yield stress of longitudinal reinforcement bar was 564MPa, while the stirrups yield stress was 516MPa, elastic modulus of concrete was 42.174GPa. The average compressive strength and tensile strength of concrete was 73MPa and 5.5MPa respectively. This specimen strengthened by a layer of CFRP material with a thickness equal to 0.79mm. The details and distribution of steel reinforcement for (1HC0) RC column were shown in Fig.(4.3).

4.2.2.1.2 Finite Element Idealization and Material Properties:

For simulating (1HC0) RC column used SOLID65 brick element, SHELL41element and LINK8 element for modeling concrete, CFRP layer and reinforcing steel bars. This model consists of 6648 elements with dimensions (20*20*20)mm and for preventing local failure at the location of the load applied and support used two steel plates in the support's ends with dimensions (140*140*20)mm. Table (4-2) illustrates element types and material properties that were used to simulate (1HC0) RC column in FEM.



*All dimensions in mm

Fig.(4.3): Details of (1HC0) RC Column (Widiarsa & Hadi, 2013).

For investigating the behavior of (1HC0) RC column was subjected to concentrated compression load on the upper nodes in the middle lines at $y=860$ and $y=840$, while four corner nodes in the lower plane ($y=-60$) were restrained in x and y directions and the ten nodes at a height of 380mm at $x=0$ and $x=200$ were restrained in x and z directions. The finite element model of (1HC0) RC column was given in Fig. (4.4) which illustrated loading and boundary condition of the column.

Table (4-2): Element Type and Material Properties of (1HC0)
RC Column(Widiarsa & Hadi, 2013).

Material Type	Element Type	Material Properties
Concrete	SOLID65	$E_c=42174\text{MPa}$ *
		$\nu=0.2$ **
		$\beta_1=0.1$ **
		$\beta_0=0.8$ **
		$f'_c=73\text{MPa}$
		$f_t=5.5\text{MPa}$ *
Longitudinal steel reinforcement bar	LINK8	$E_s=200000\text{MPa}$ **
		$\nu=0.3$ **
		$f_y=564$
Transverse steel reinforcement bar	LINK8	$E_s=200000\text{MPa}$ **
		$\nu=0.3$ **
		$f_y=516\text{MPa}$
CFRP	SHELL41	$E_x = 62000\text{MPa}$ ***
		$E_y=4800\text{MPa}$ ***
		$E_z=4800\text{MPa}$ ***
		$G_{xy}=3270\text{MPa}$ ***
		$G_{yz}=1860\text{MPa}$ ***
		$G_{xz}=3270\text{MPa}$ ***
		$\nu_{xy}=0.22$ ***
		$\nu_{yz}=0.3$ ***
		$\nu_{xz}=0.22$ ***
		$t=0.79\text{mm}$
Steel Plate (Supports)	SOLID45	$E = 200000\text{MPa}$ **
		$\nu=0.3$ **

*Calculated according to ACI-318 Equations

**Assumed

***From [Kachlakev et al., 2001]

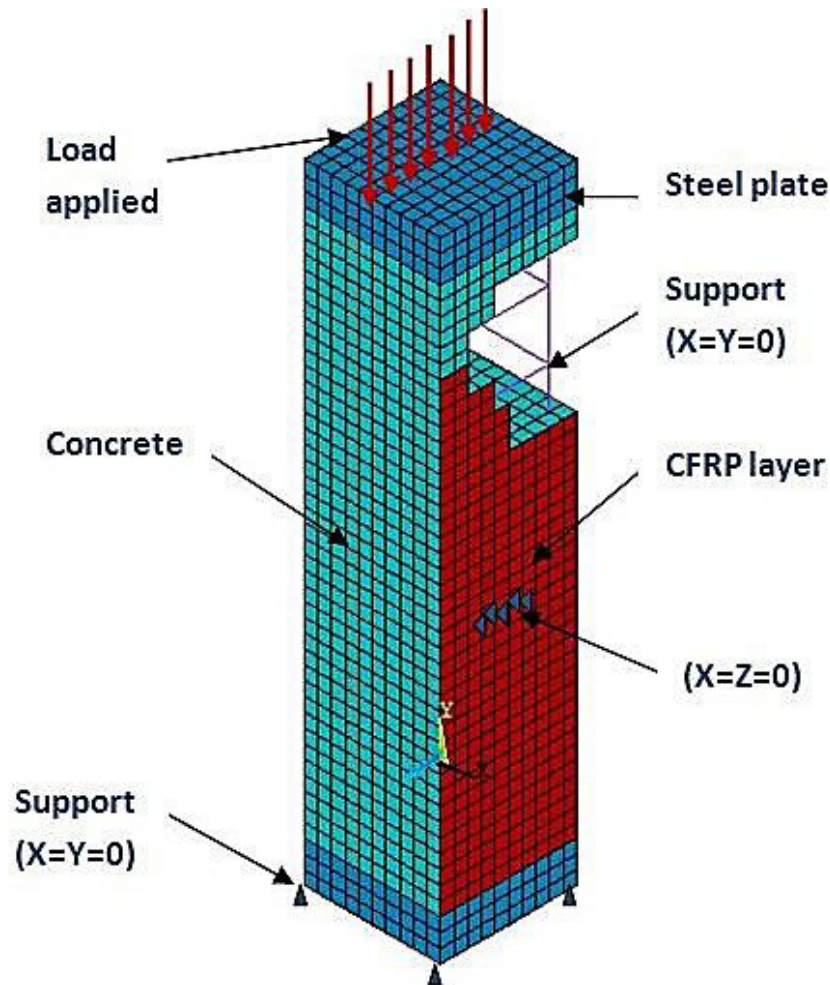


Fig.(4.4): Finite Element Model of (1HC0) RC Column.

4.2.2.2 Benzaid et al Concrete Column Strengthened with GFRP

Sheet:

An experimental program of Benzaid et al in 2008 consists of seven series to investigate the behavior of concrete square prisms confined by GFRP. In this study, analyzing one of these jacketed specimens using a nonlinear finite element model by using ANSYS package, it was designed as S1R1.

4.2.2.2.1 Description of Test Specimen (S1R1):

The test specimen with 54.8MPa average compressive strength of 28 days and 4.6MPa tensile strength was cast with dimensions (100*100) mm in cross section and height of 300mm, while the elastic modulus of concrete was

35.015GPa. GFRP layer with 23.8GPa elastic modulus and thickness equal to 0.44mm used in jacketing. Fig.(4.5) shows the details of (S1R1) RC column.

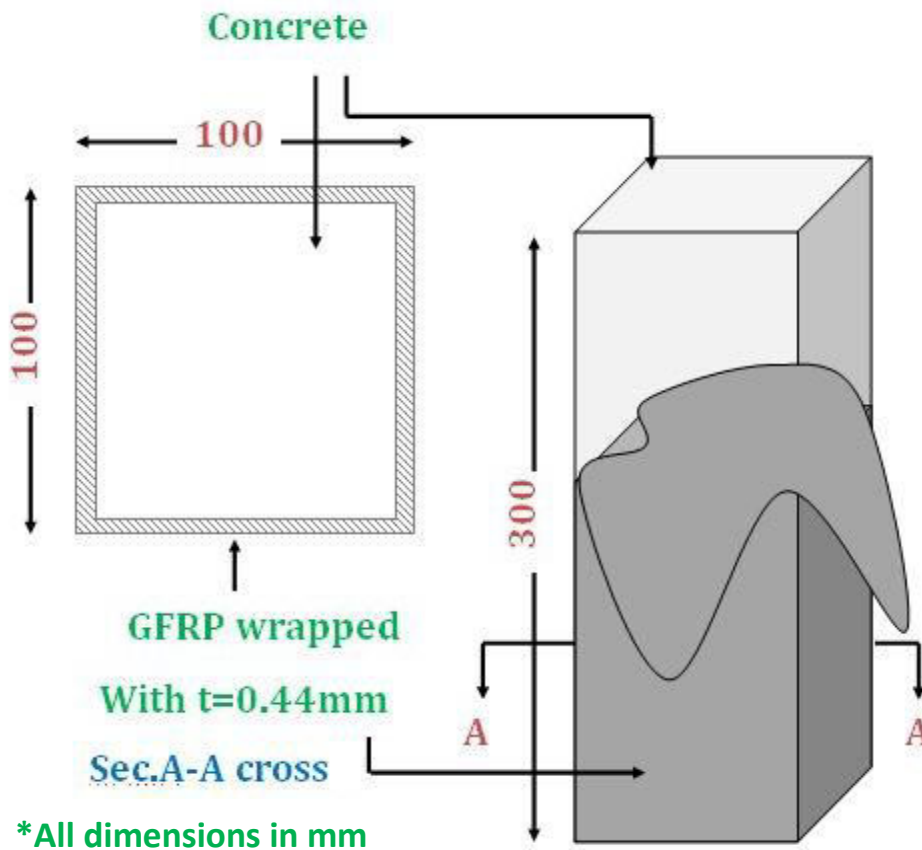


Fig.(4.5): Details of (S1R1) Concrete Column (*Benzaid et al., 2008*).

4.2.2.2.2 Finite Element Idealization and Material Properties:

The model of (S1R1) column represented by using SOLID65 and SHELL41 elements to modeling concrete and GFRP sheet, where using 4600 elements to create this model, including SOLID45 that's used for support ends (Two steel plates with dimensions (100*100*20)mm). The dimensions of the elements that was used in (S1R1) model were chosen (10*10*10)mm. Table(4-3) illustrates the element type and material properties of finite element model. The stress-

strain relationship of GFRP used in this model was stated in Fig.(A.12) in Appendix A

In a lower plane when $y=-20$, all nodes were restrained in all directions(x , y , z), in addition, two nodes at $(0,240,50)$ and $(100,240,50)$ coordinate restrained in x and y directions. The forces applied at the nodes in the middle line on the upper plane ($y=320$) of the column, as illustrated in Fig.(4.6)

**Table (4-3): Element Type and Material Properties of (S1R1)
Concrete Column (Benzaid et al., 2008).**

Material Type	Element Type	Material Properties
Concrete	SOLID65	$E_c=35015 \text{ MPa}^*$
		$\nu=0.2$
		$\beta_1=0.2^{**}$
		$\beta_0=0.55^{**}$
		$f'_c=54.8 \text{ MPa}^*$
		$f_t=4.8 \text{ MPa}^*$
GFRP Layer	SHELL41	$E_x = 21000 \text{ MPa}^{***}$
		$E_y=7000 \text{ MPa}^{***}$
		$E_z=7000 \text{ MPa}^{***}$
		$G_{xy}=1520 \text{ MPa}^{***}$
		$G_{yz}=2650 \text{ MPa}^{***}$
		$G_{xz}=1520 \text{ MPa}^{***}$
		$\nu_{xy}=0.26^{***}$
		$\nu_{yz}=0.3^{***}$
		$\nu_{xz}=0.26^{***}$
		$t=0.44 \text{ mm}$
Steel Plate (Supports)	SOLID45	$E=200000 \text{ MPa}^{**}$
		$\nu=0.3^{**}$

*Calculated according to ACI-318 Equations

**Assumed

***From [Kachlakev et al., 2001]

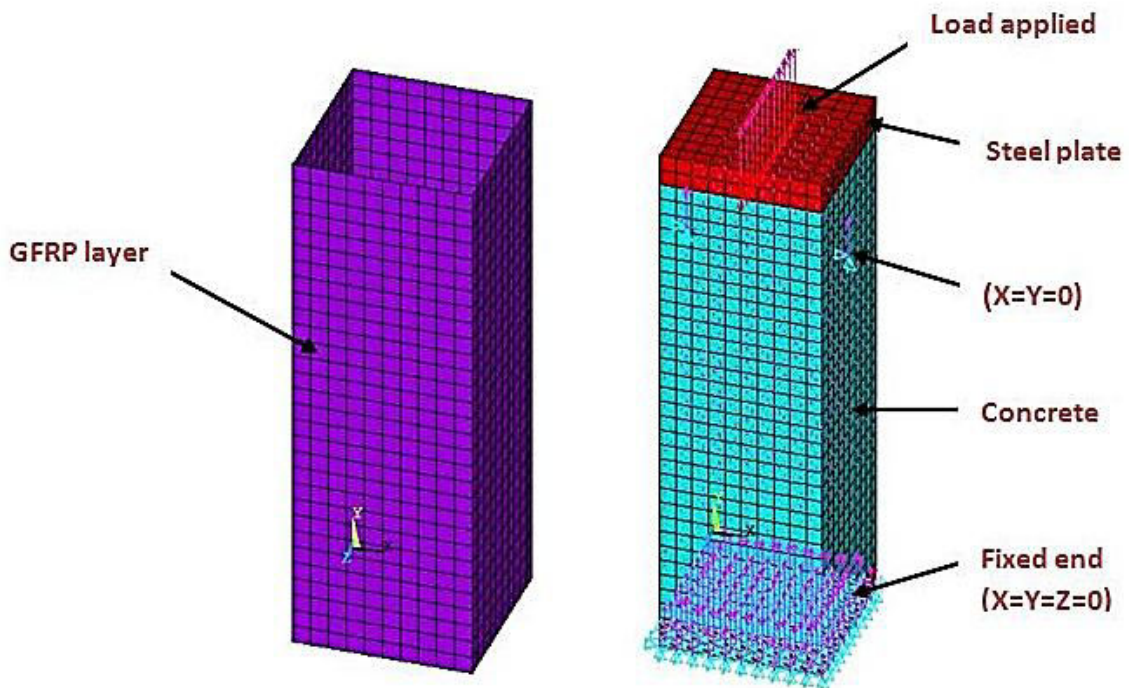


Fig.(4.6):Finite Element Model of (S1R1) Concrete Column.

4.2.3 Results of Analysis for (SC-2), (1HC0) and (S1R1) Models:

By comparing the results of (SC-2), (1HC0) and (S1R1) models that are given in the curves of Figs.(4.7), (4.11) and (4.15), it was achieved good agreements between numerical and experimental results, as illustrated in Table(4-4). The results of proposed models show that the ratio of FE to experimental is between (1.011-1.077) and (0.943-1.011) for ultimate load and vertical displacement. According to the results in Table (4-4) the percentage increase for ultimate load equal to (+7.69%), (+1.12%) and (+5.69%) for (SC-2), (1HC0) and (S1R1) models, while the percentage increase of vertical displacement equal to (+1.1%), (-5.74%) and (-0.49%) for (SC-2), (1HC0) and (S1R1) models.

The variation of deflections, and strains in the longitudinal y-direction was given in Figs.(4.8), (4.9), (4.12), (4.13), (4.16) and (4.17), these figures were given the values of deflections in (mm) and strains in (mm/mm) where the variation of

these values was shown as a colored bar at the base of figures, while the crack pattern of proposed models was illustrated in Figs.(4.10), (4.14) and (4.18).

Eventually, from these results found that the load carrying capacity of strengthening columns was higher than un-strengthening columns.

Table(4-4): The Results of Experimental and Finite Element Method of (SC-2), (1HC0) and (S1R1) Models.

Column	P _u (Exp.) (kN)	P _u (FEM) (kN)	$\frac{P_u(FEM)}{P_u(Exp.)}$	Deflection at ultimate load		
				Δ(Exp.) (mm)	Δ(FEM) (mm)	$\frac{\Delta_u(FEM)}{\Delta_u(Exp.)}$
SC-2	750	807.7	1.077	1.81	1.83	1.011
1HC0	3279	3315.8	1.011	4.53	4.27	0.943
S1R1	561	592.94	1.057	2.02	2.01	0.995

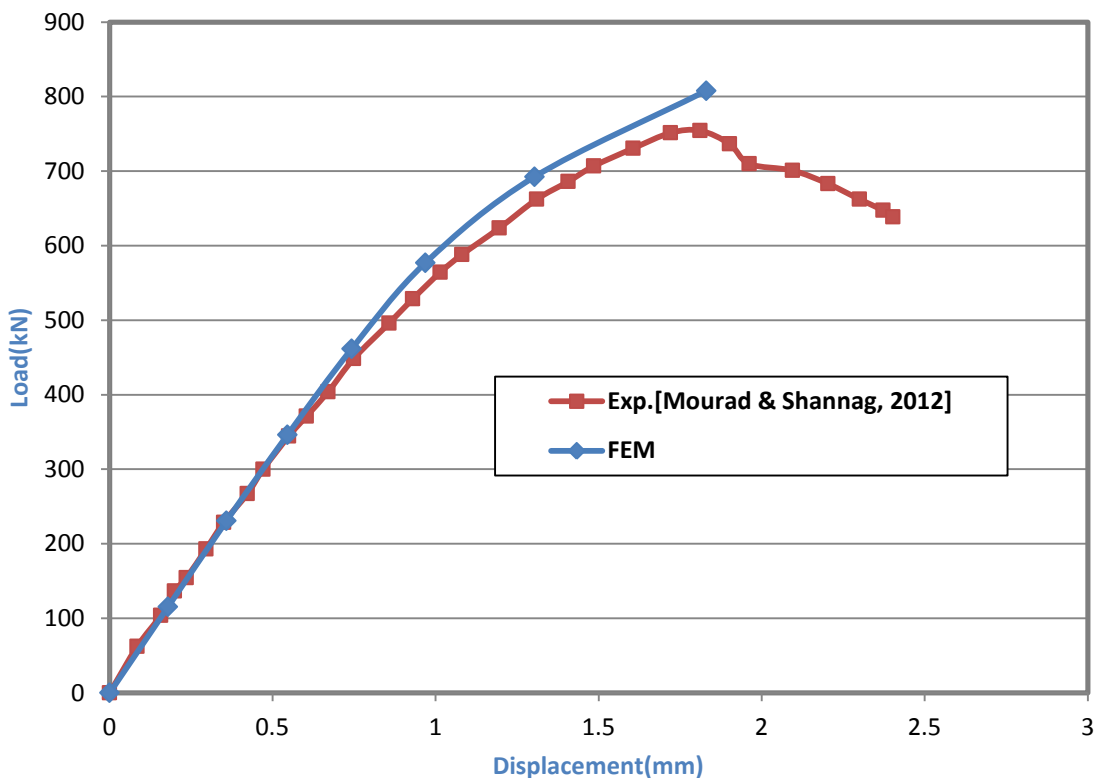


Fig.(4.7): Experimental and Numerical Load-Displacement Curve for (SC-2) RC Column.

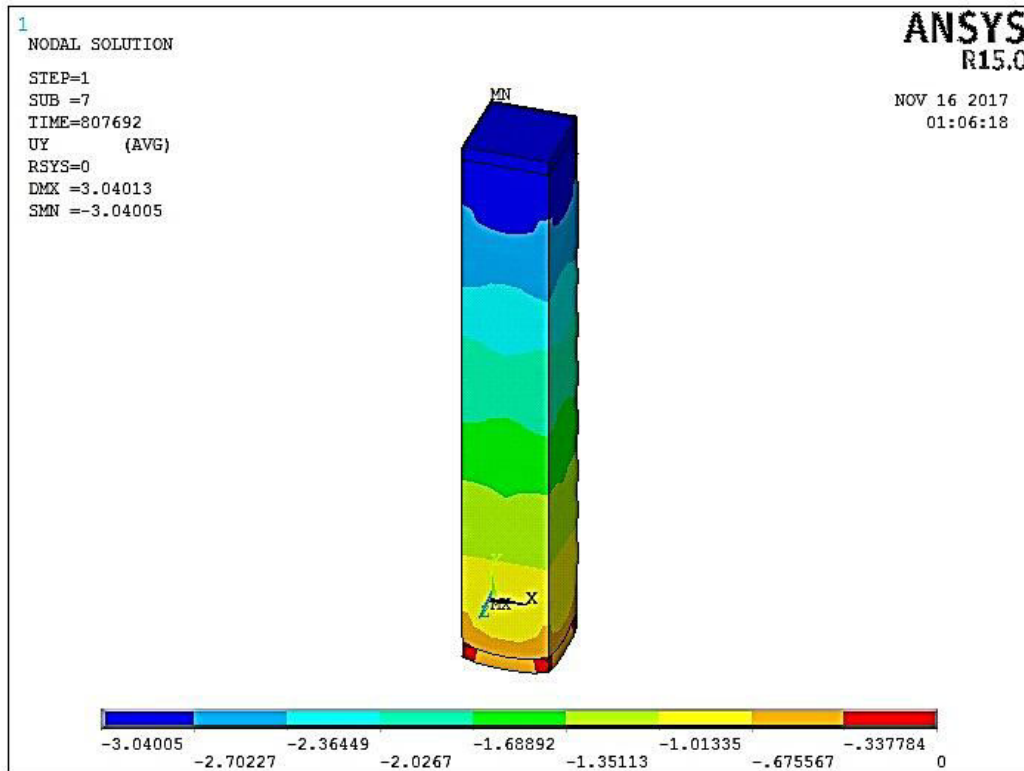


Fig.(4.8): Displacements of (SC-2) Model at Ultimate Load.

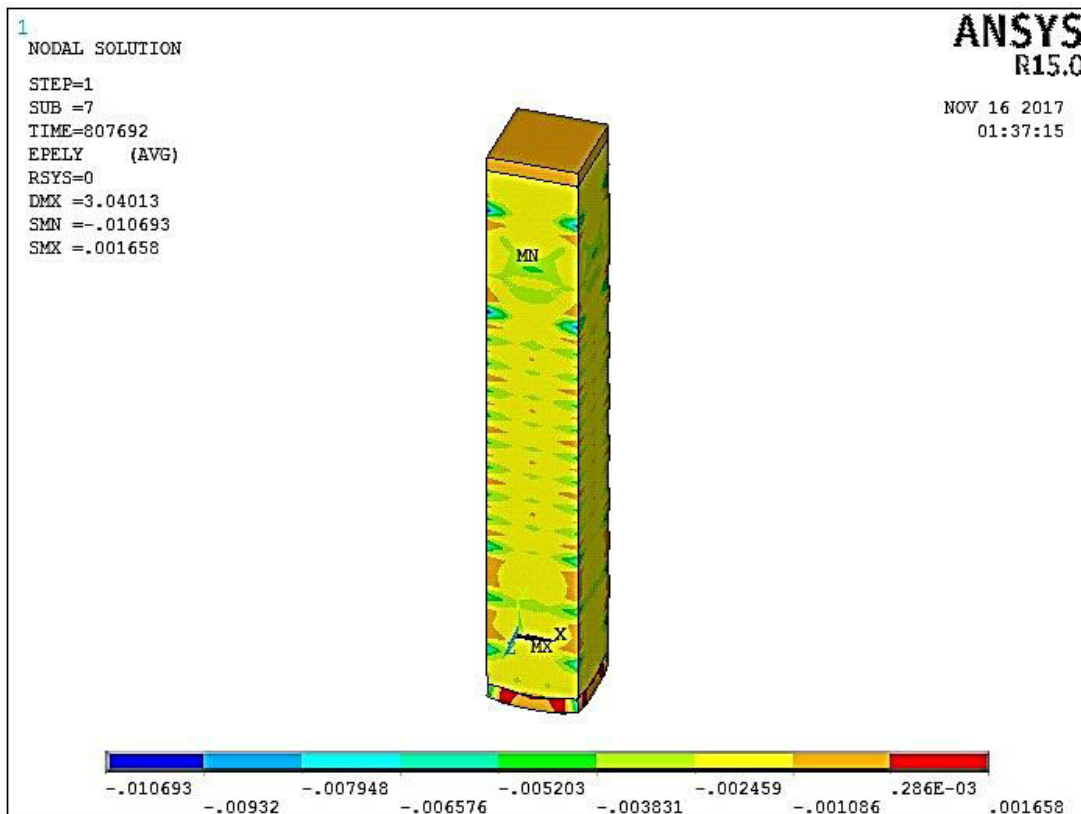


Fig.(4.9): Strains of (SC-2) Model at Ultimate Load.

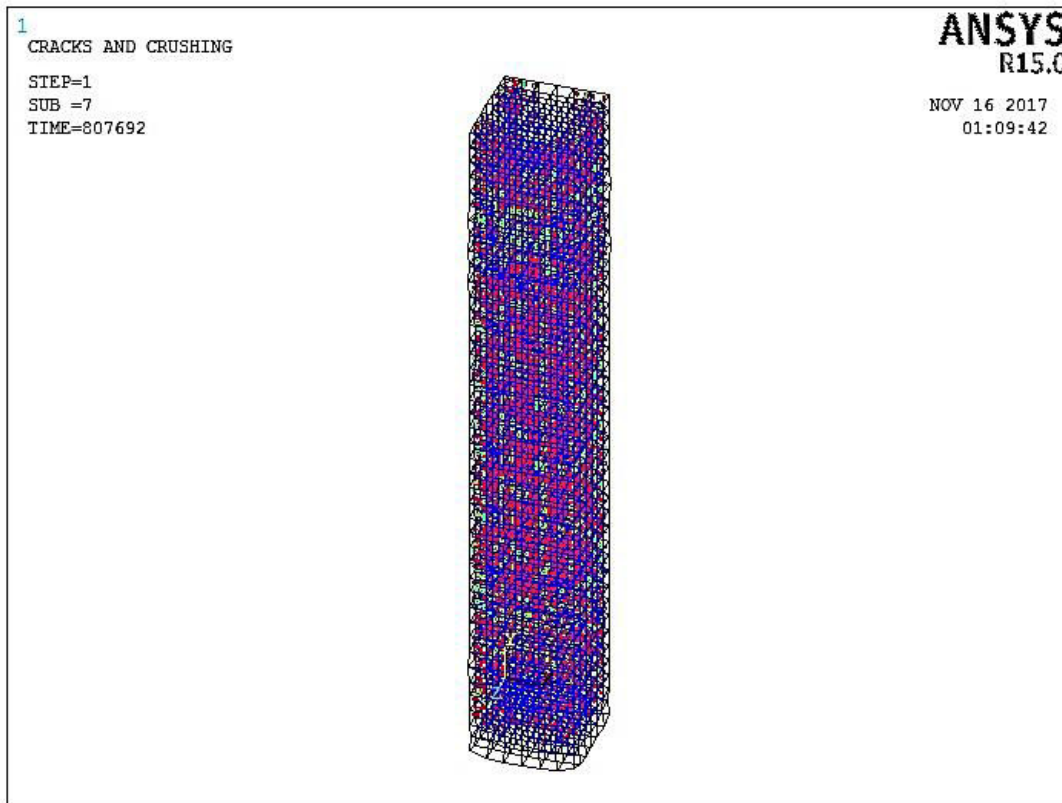


Fig.(4.10): Crack Pattern of (SC-2) Model at Ultimate Load.

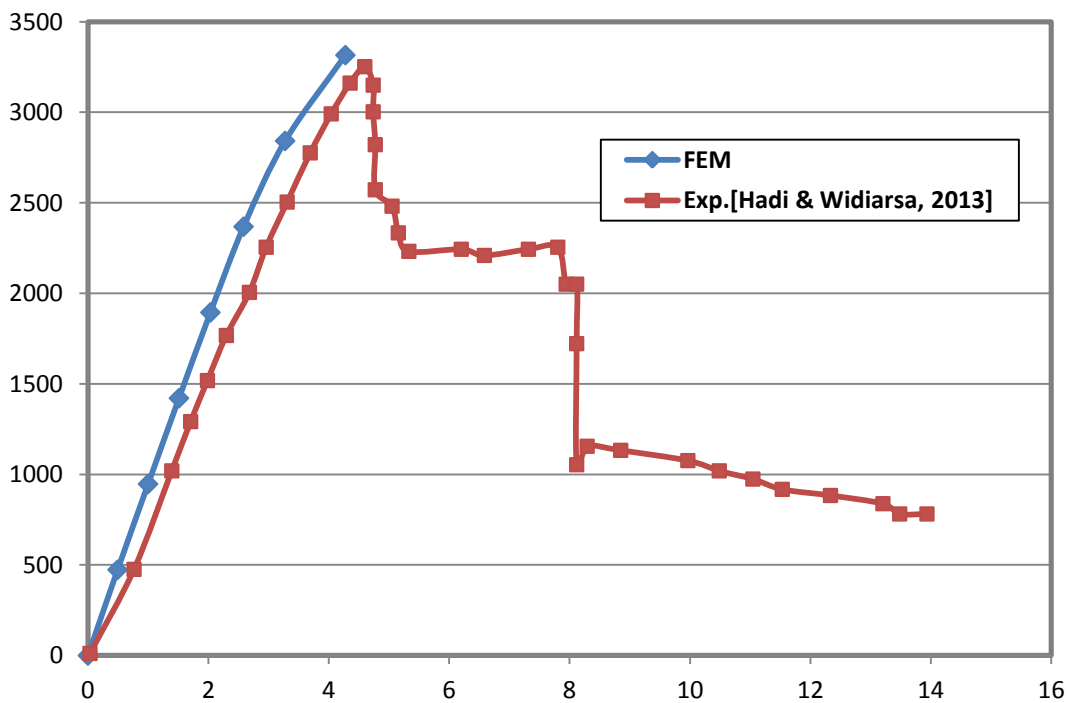


Fig.(4.11): Experimental and Numerical Load-Displacement Curve for (1HC0) RC Column.

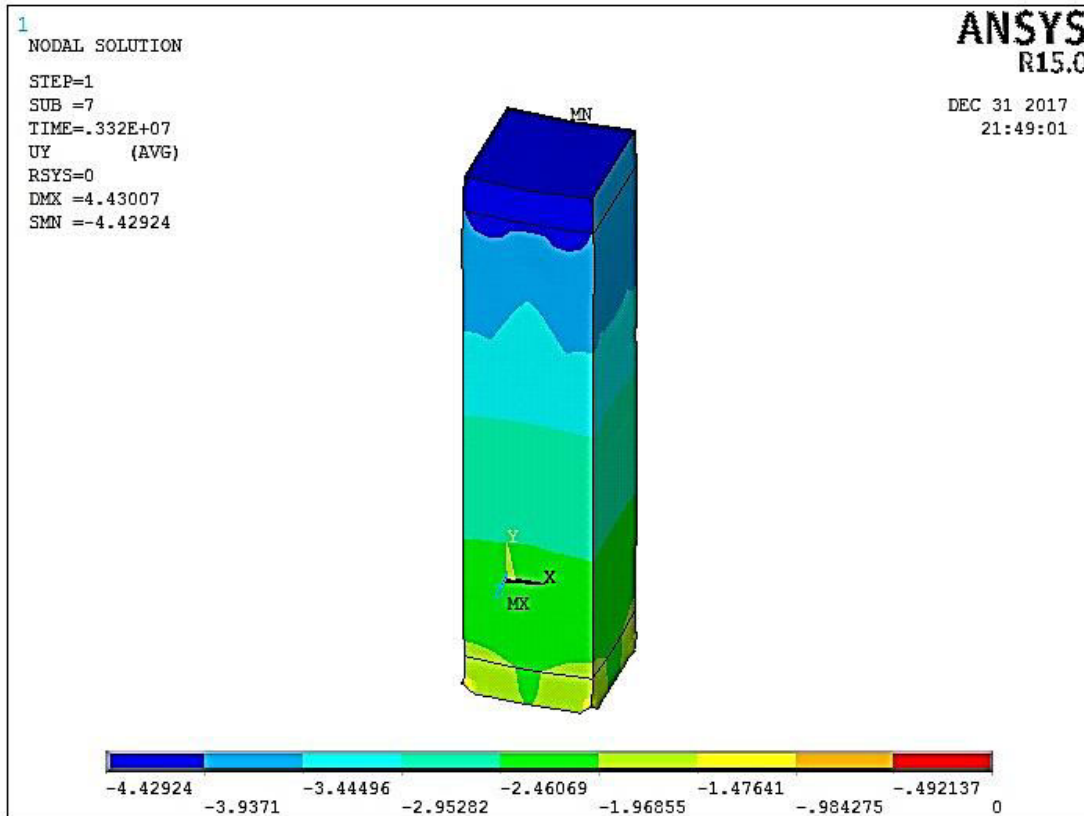


Fig.(4.12): Displacements of (1HC0) Model at Ultimate Load.

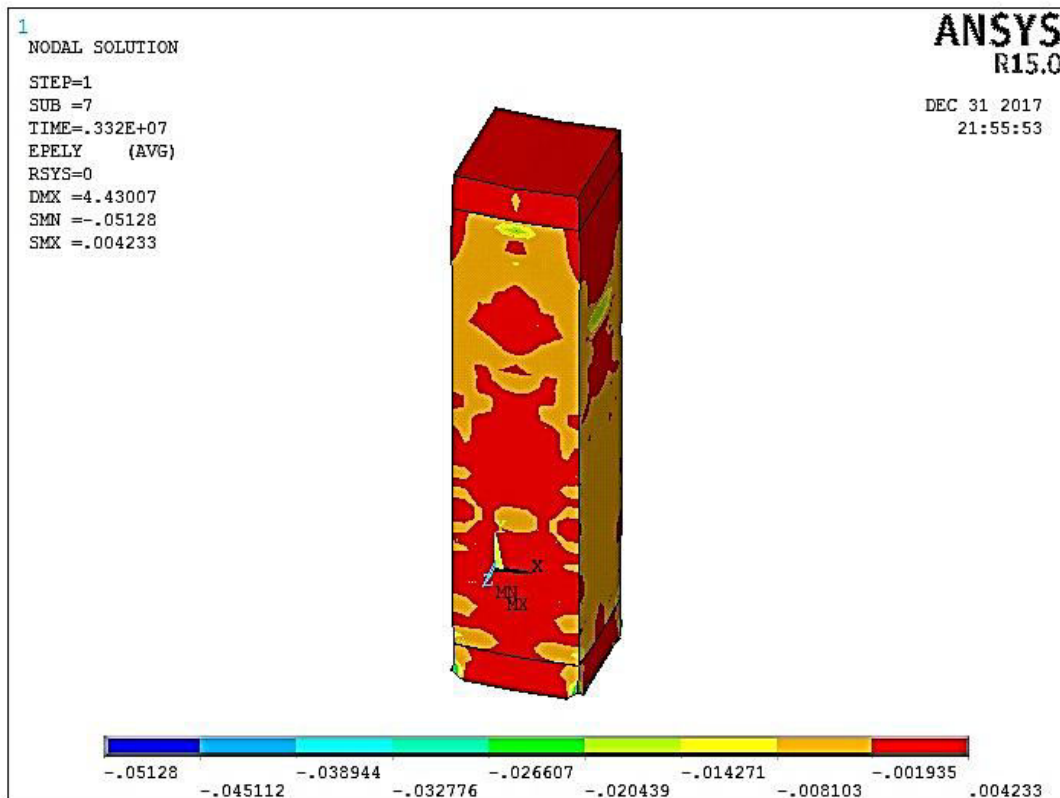


Fig.(4.13): Strains of (1HC0) Model at Ultimate Load.

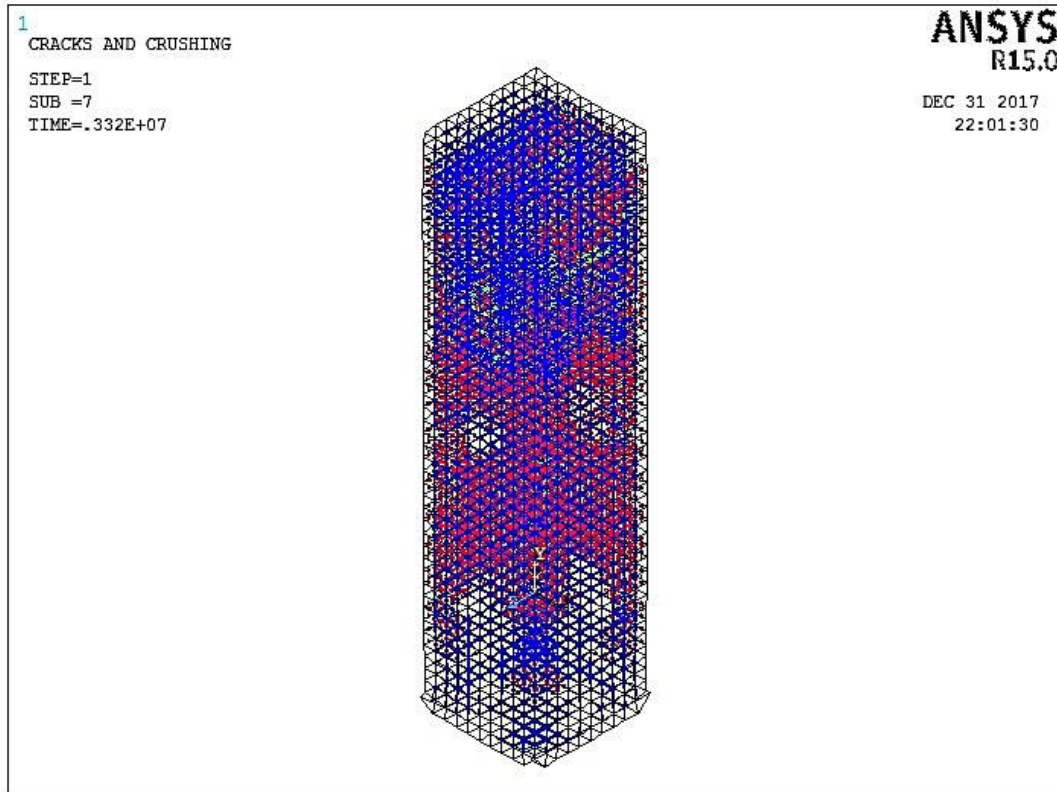


Fig.(4.14): Crack Pattern of (1HC0) Model at Ultimate Load.

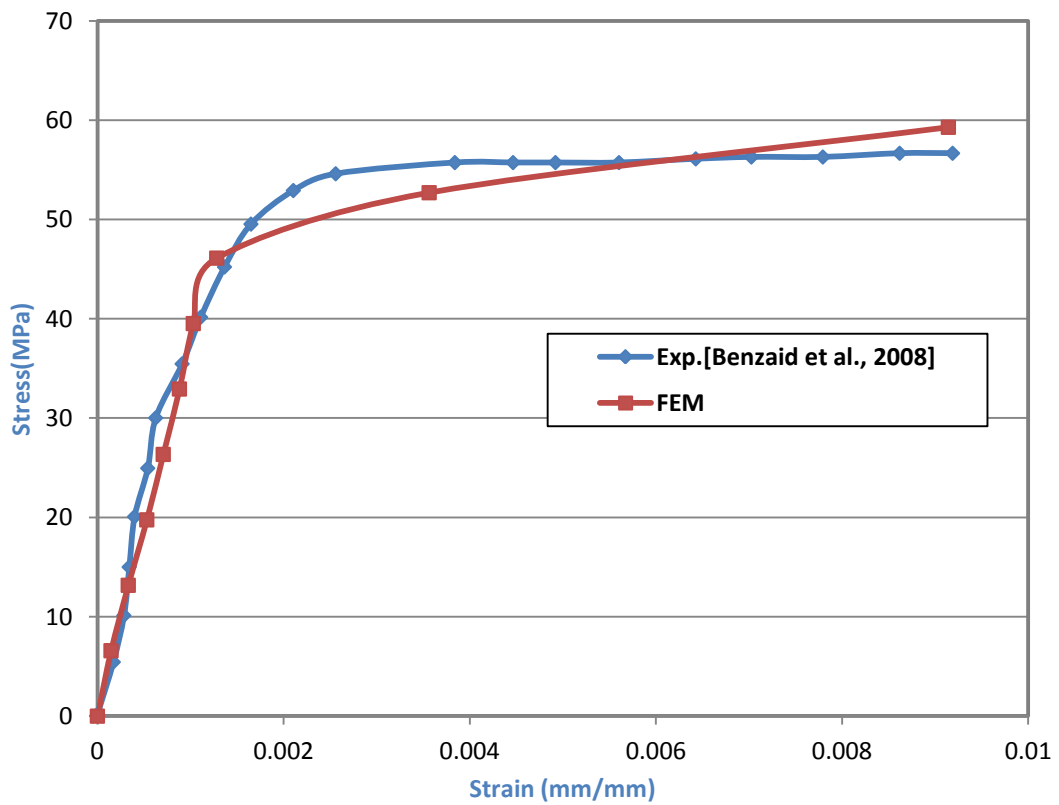


Fig.(4.15): Experimental and Numerical Stress-Strain Curve for (S1R1) Concrete Column.

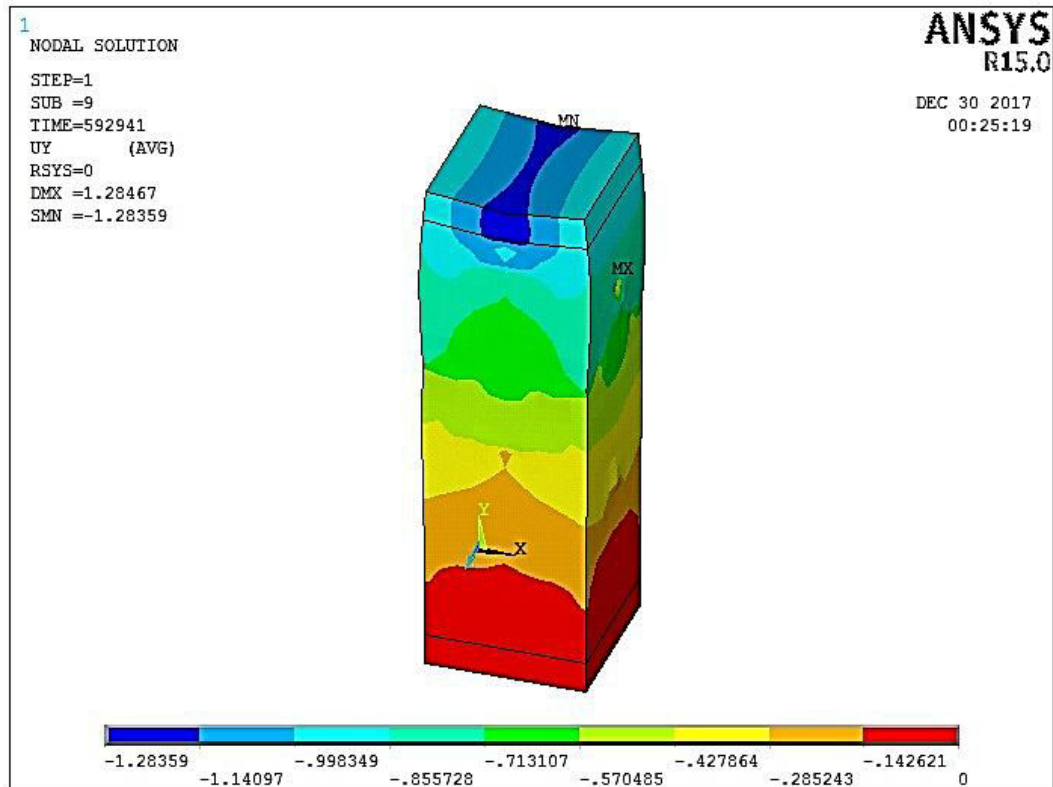


Fig.(4.16): Displacements of (S1R1) Model at Ultimate Load.

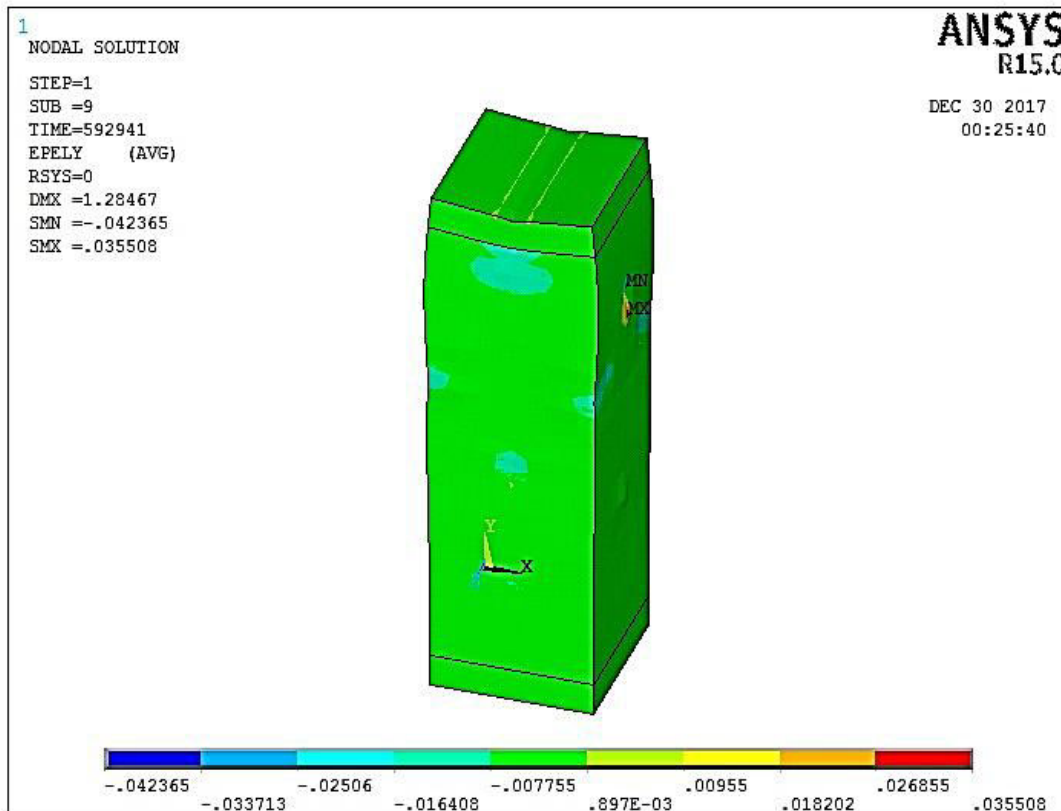


Fig.(4.17): Strains of (Col.05.PI) Model at Ultimate Load.

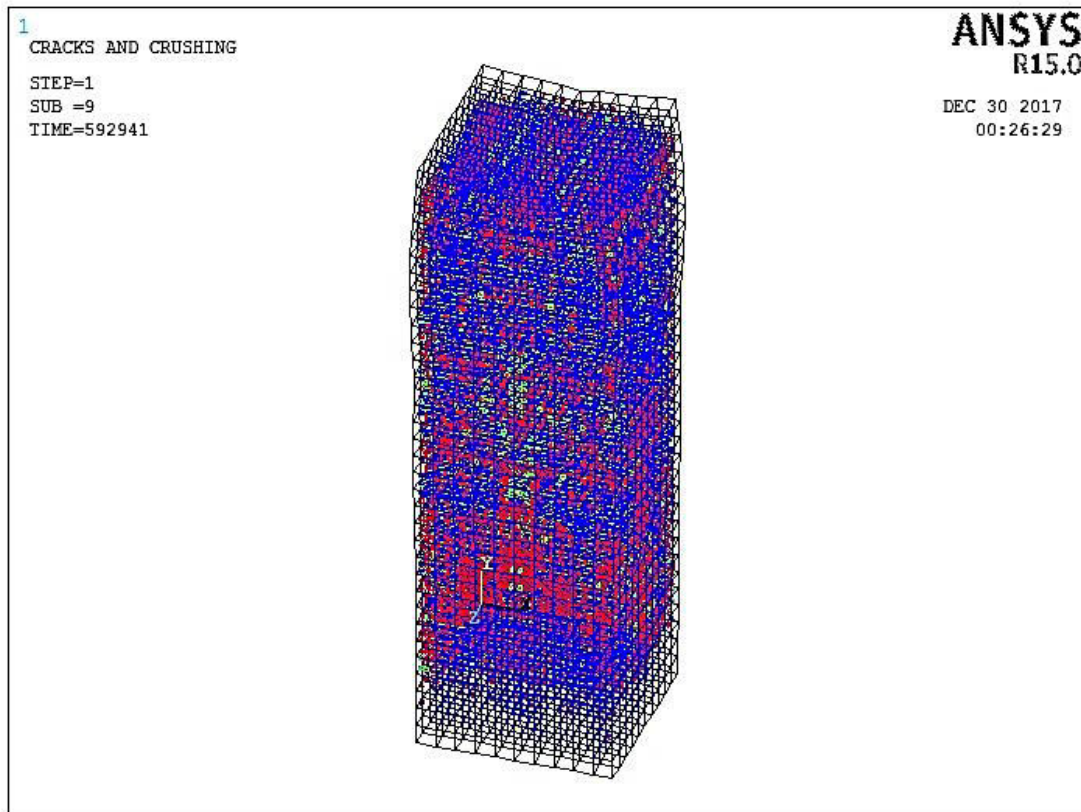


Fig.(4.18): Crack Pattern of (S1R1) Model at Ultimate Load.

4.3 Analysis of Columns Subjected to Long Term Loading:

This section included the analysis of two groups of columns; the first group consists of two un-strengthened reinforced concrete columns (Control Columns) one of these columns was investigated by (*Katoka & Bittencourt, 2014*) and the other was investigated by (*Hamed & Lai, 2016*). The second group consists of three strengthening concrete columns (Jacketed Columns), one of these columns was strengthened by GFRP which was investigated by (*Naguib & Mirmiran, 2002*), the second strengthen by CFRP which investigated by (*Al-Chami, 2006*) and the last was strengthened by AFRP which investigated by (*Wang et al., 2011*).

4.3.1 Control Columns:

4.3.1.1 Katoka and Bittencourt RC Column:

In 2014, Katoka and Bittencourt investigated the effect of creep and shrinkage on the nine RC columns. In this study ANSYS package was used to model one of these specimens by using finite element method, it was designed as F40-1.4-1.

4.3.1.1.1 Description of Test Specimen (F40-1.4-1):

The test specimen was designed to have a square cross section of (150*150) mm with a height of 600mm. The average compressive strength of concrete at 7 days (26.2) MPa while the tensile strength(3.17) MPa and elastic modulus (26.8) GPa. The steel reinforcement that was used in the column was 4Ø10mm in longitudinal reinforcement bar and 6Ø6.3mm in stirrups were distributed @100mm on the mid of the column, the elastic modulus of steel reinforcement for the bar and stirrups was 217.4 GPa and 213.7 GPa respectively, while the yield stress was 635 MPa for bar and 611 MPa for stirrups. Fig.(4.19) shows the details of (F40-1.4-1) column.

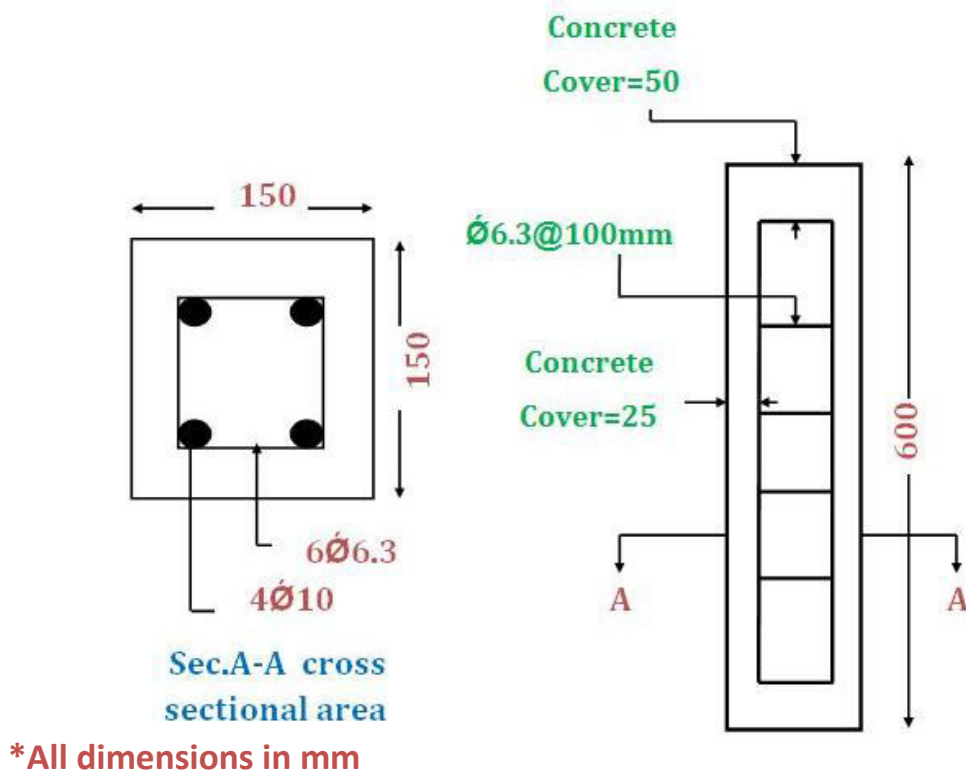


Fig.(4-19): Details of (F40-1.4-1) RC Column (Katoka & Bittencourt, 2014).

4.3.1.1.2 Finite Element Idealization and Material Properties:

In simulation of (F40-1.4-1) RC column used 1040 elements, which include a VISCO89 element for modeling the concrete and LINK8 element for modeling all steel reinforcement. The dimensions of elements in this column were (25*25*25) mm. The properties of concrete mixtures are illustrated in Table (4-5) and Table (4-6) illustrates element types and material properties that were used to simulate (F40-1.4-1) RC column in FEM. In the analysis of this column, four corner nodes at the lower end ($y=0$) and two nodes at (0,0,75) and (150,0,75) coordinates of the column was restrained in all directions, while two nodes at (75,200,0) and (75,200,150) coordinates was restrained in y direction only. The sustained load with value equal to 236.5kN applied at age=7day at the upper end of the column and distributed on the upper nodes. It was stated in Fig.(4-20).

Table(4-5):Properties of Concrete Mix (Katoka & Bittencourt,2014).

τ (day)	λ (%)	h(mm)	S(mm)	Cm(Kg/m3)	ψ (%)	a(%)
7	60	150	132	280	45	3.9

Table (4-6): Element Type and Material Properties of (F40-1.4-1) RC Column (Katoka & Bittencourt, 2014).

Material Type	Element Type	Material Properties
Concrete	VISCO89	$f'_c=26.2\text{MPa}$
		$E_0=24211\text{MPa}^*$
		$G_0=10087.92\text{MPa}^*$
		$K_0=13451\text{MPa}^*$
		$\nu_u= 2.35$
		$\nu=0.2$
Longitudinal steel reinforcement bar	LINK8	$E_s=217400\text{MPa}$
		$\nu=0.3^{**}$
		$f_y=635$
Transverse steel reinforcement bar	LINK8	$E_s=213700\text{MPa}$
		$\nu=0.3^{**}$
		$f_y=611\text{MPa}$

*Calculated according to ACI-318 Equations

**Assumed

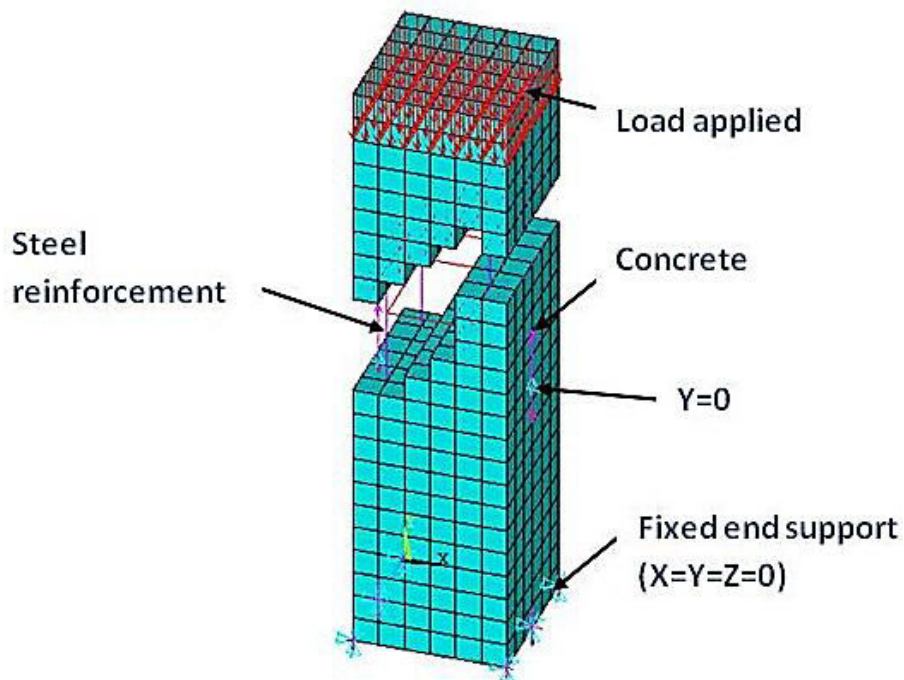


Fig.(4.20):Finite Element Model of (F40-1.4-1)RC Column.

4.3.1.2 Hamed and Lai RC Column:

Hamed and Lai investigate's square RC column to study the effect of creep on RC column. In this study, this column is analyzed by using a nonlinear finite element model also by using ANSYS package. It was designed as E80-C.

4.3.1.2.1 Description of Test Specimen (E80-C):

The column has a square cross section of (400*400) mm and height of 6000mm, the properties of concrete were (32) MPa compressive strength, (30.1) GPa elastic modulus and (3.04) MPa tensile strength. It reinforced with 8Ø24mm longitudinal reinforcement bar and 2Ø6mm ties at the two ends of the column. The yield stress of steel bar was (500) MPa and (240) MPa for ties, while the elastic modulus for all steel reinforcement was 200 GPa. Fig.(4.21) shows the details of (E80-C) RC column.

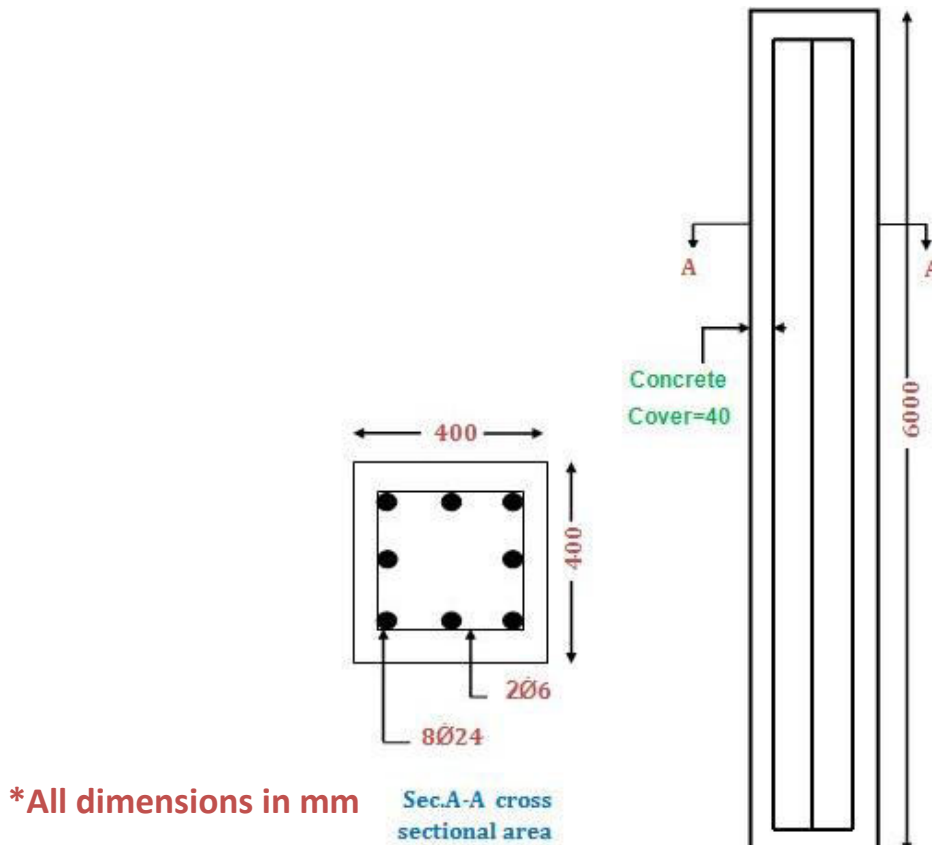


Fig.(4.21): Details of (E80-C) RC Column (Hamed & Lai, 2016).

4.3.1.2.2 Finite Element Idealization and Material Properties:

VISCO89 and LINK8 elements were used for modeling concrete and steel reinforcement respectively. 16248 elements were used in the simulation of (E80-C) RC column. The dimensions of elements were chosen (40*40*40)mm FEM was applied to the selected column (E80-C). Table (4-7) illustrates element types and material properties that were used to simulate (E80-C) RC column in FEM.

Nodes at coordinates (280,0,0), (280,0,200), (280,0,400), (280,20,0), (280,20,200) and (280,20,400) while all nodes at x=0 and y=6000 restrained in x and z directions. The sustained load with value equal to 2000KN was applied with an eccentricity 80 mm from the center of the column at age=28days. It stated in Fig.(4.22).

**Table (4-7): Element Type and Material Properties of (E80-C)
RC Column (Hamed & Lai, 2016).**

Material Type	Element Type	Material Properties
Concrete	VISCO89	$f'_c=32\text{MPa}$
		$E_0=30100\text{MPa}^*$
		$G_0=12541.67\text{MPa}^*$
		$K_0=16722.22\text{MPa}^*$
		$\nu_u= 2.53$
		$\nu=0.2$
Longitudinal steel reinforcement bar	Link8	$E_s=200000\text{MPa}$
		$\nu=0.3^{**}$
		$f_y=500$
Transverse steel reinforcement bar	Link8	$E_s=200000\text{MPa}^{**}$
		$\nu=0.3^{**}$
		$f_y=240\text{MPa}^{**}$

*According to ACI-318 Equations

**Assumed

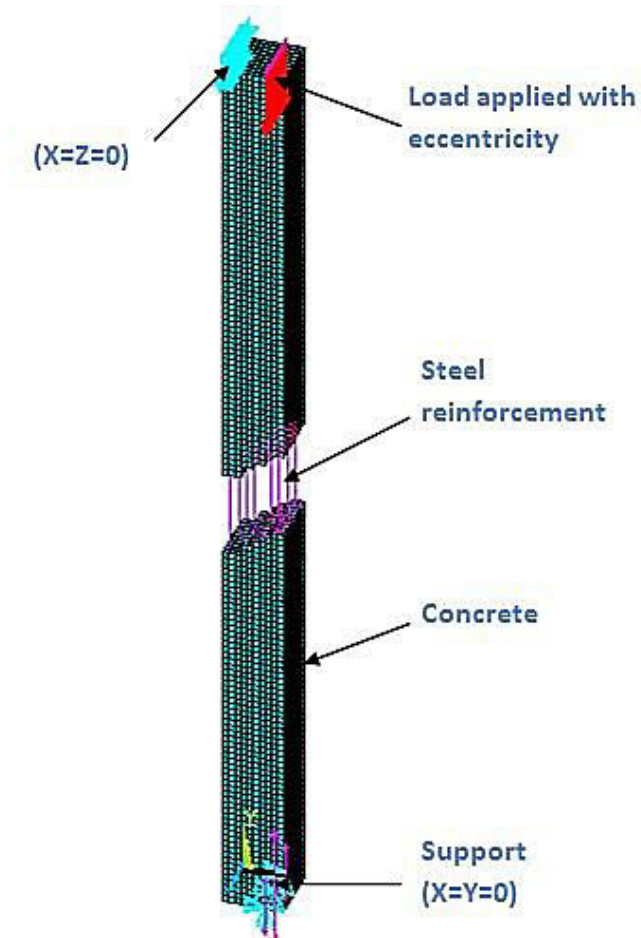


Fig.(4.22):Finite Element Model of (E80-C) RC Column.

4.3.2 Jacketed Columns:

4.3.2.1 Naguib and Mirmiran Column:

Twenty-seven circular concrete columns strengthening with GFRP was investigated by Naguib and Mirmiran in 2002. One of these columns was analyzed with a nonlinear finite element method in this study by using ANSYS package, it was designed as FWCC.

4.3.2.1.1 Description of Test Specimen (FWCC):

A concrete column casting with a circular cross section $d=152\text{mm}$ and a height of 305mm . The average compressive strength is $(29)\text{MPa}$, tensile strength is $(3.34)\text{MPa}$, elastic modulus is $(25.472)\text{GPa}$ and shear modulus is

(10.613)GPa. It strengthens with GFRP layer with a thickness equal to 1mm, tensile strength of GFRP (600)MPa and the ultimate strain is (0.0283). Fig.(4.23) shows the details of (FWCC) column.

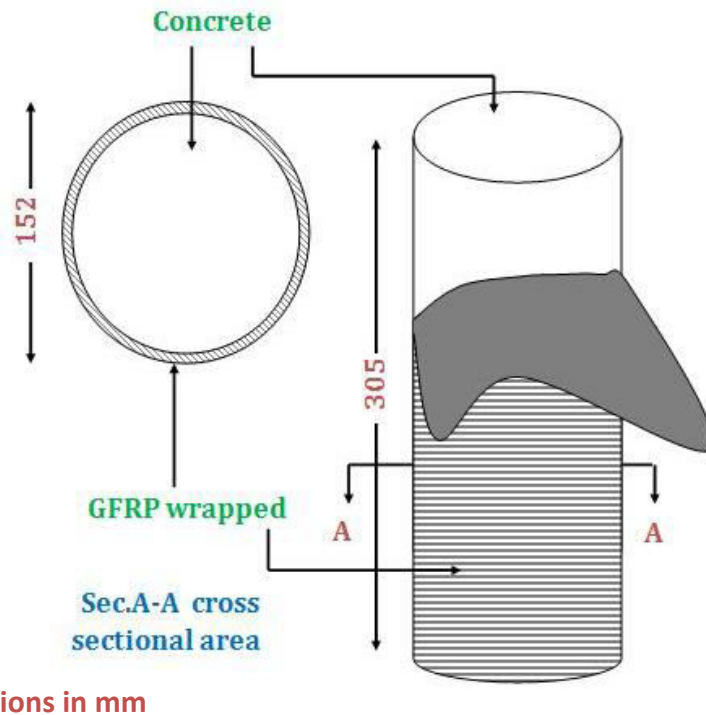


Fig.(4.23): Details of (FWCC) Column (Naguib & Mirmiran, 2002).

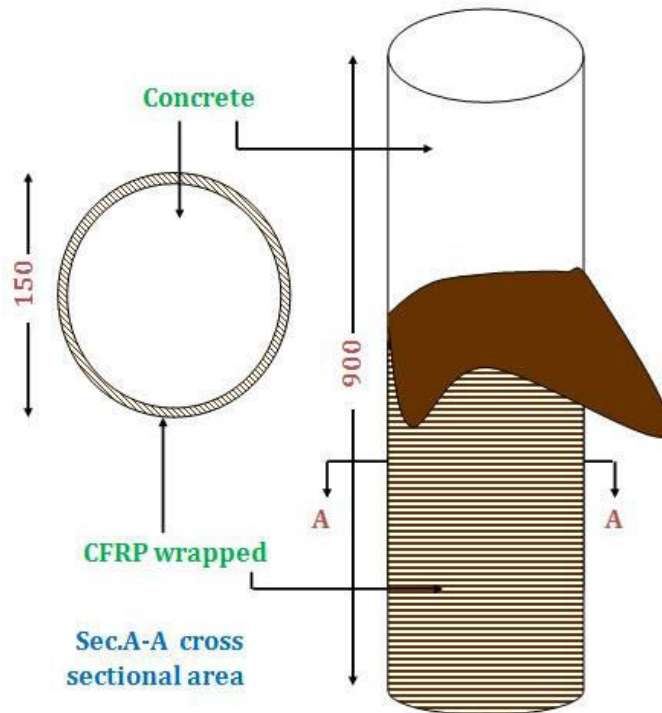
4.3.2.2 Al-Chami Column:

Al-Chami in (2006) tests the effect of creep on the forty-two cylinder concrete (jacketed and non-jacketed), she used CFRP in strengthening concrete columns. In this study, one of jacketed specimens was selected for the analysis using a nonlinear finite element model by using ANSYS package, it was designed as B1C1.

4.3.2.2.1 Description of Test Specimen (B1C1):

The test specimen was designed with 39 MPa average compressive strength and a circular cross section $d=150\text{mm}$ with a height of 900mm. The tensile strength of concrete is (3.87)MPa, elastic modulus is (29.539)GPa and shear modulus is (12.308)GPa.

CFRP layer used in strengthening this column with a 1mm thickness, tensile strength is (760) MPa and ultimate strain is (0.012). Fig.(4.24) shows the details of (B1C1) column.



***All dimensions in mm**

Fig.(4.24): Details of (B1C1) Column (Al-Chami, 2006).

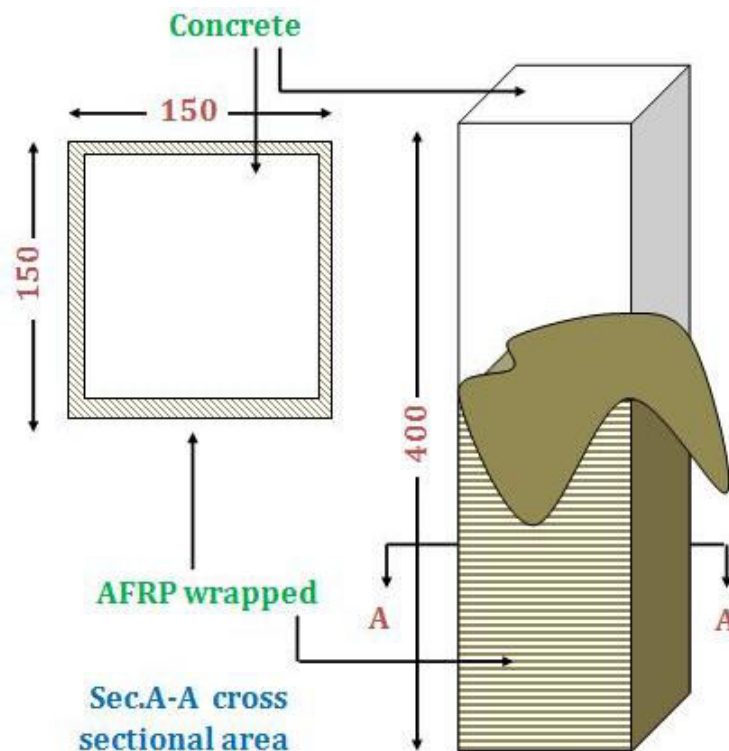
4.3.2.3 Wang et al. Column:

The effect of creep for ten concrete columns (square and circle) strengthening with AFRP was investigated by Wang et al. in 2011. One of strengthening square concrete columns selected in this study for the analysis by using finite element method using by ANSYS package, it was designed as FWCC-A.

4.3.2.3.1 Description of Test Specimen (FWCC-A):

The test column was (150*150) mm cross section and 400mm in height. It was strengthened by a layer of AFRP with 1mm thickness, tensile strength is (3000)MPa and ultimate strain is (0.017). The properties of concrete were compressive strength is (37.84)MPa, tensile strength is (3.81)MPa, elastic

modulus is (29.096)GPa and shear modulus is (12.123)GPa. Fig.(4.25) shows the details of (FWCC-A) column.



***All dimensions in mm**

Fig.(4.25): Details of (FWCC-A) Column (Wang and Liu, 2011).

4.3.2.4 Finite Element Idealization and Material Properties for (FWCC), (B1C1) and (FWCC-A) Models:

The columns were simulated by using a quadratic isoparametric element (VISCO89) and quadratic-order membrane shell element (SHELL41) to model concrete and FRP respectively. (FWCC) model consists of (2352) elements, while (B1C1) consists of (7056) elements and (FWCC-A) consists of (960) elements. Table (4-8) illustrates material properties that were used to simulate these models in FEM.

At a lower plane ($z=0$) for (FWCC) and (B1C1) models and a lower plane ($y=0$) for (FWCC-A) model, all nodes were restrained in all direction, the eight nodes in coordinate (0,76,266.9), (0,76,279.6), (0,76,292.3), (0,76,305), (0,-

76,266.9),(0,-76,279.6),(0,-76,292.3),(0,-76,305) for (FWCC) model restrained in x and z direction, while the sustained load (173.472KN) was applied at age=21 day on the all nodes in an upper plane (z=305), but in the (B1C1) model two nodes in coordinate (75, 0,900), (-75, 0,900) were restrained in x direction and the sustained load with value equal to 605KN applied at age=360day on the all nodes at the upper plane (z=900), and for (FWCC-A) model twelve corner nodes in upper of column restrained in x and direction, while the sustained load with value equal to 213.75KN applied at age=28day on the upper end of the column

The finite element model of (FWCC), (B1C1) and (FWCC-A) columns given in Figs. (4.26) to (4.28).

Table (4-8): Element Type and Material Properties for (FWCC), (B1C1) and (FWCC-A) Models.

Concrete (VISCO89)							
Column	Cross section	f'_c (MPa)	E_0^* (MPa)	G_0^* (MPa)	K_0^* (MPa)	ν_u	ν^{**}
FWCC	Circle	29	25472	10613	14151	0.92	0.2
B1C1	Circle	39	29539	12308	16411	2.34	0.2
FWCC-A	square	37.84	29096	12123	16164	0.8045	0.2
FRP (SHELL41)							
Column	Type of FRP	t (mm)	E (MPa)	G (MPa)	σ_u (MPa)	ϵ_u	ν
FWCC	GFRP***	1	$E_x=21000$ $E_y=7000$ $E_z=7000$	$G_{xy}=1520$ $G_{yz}=2650$ $G_{xz}=1520$	600	0.0283	$\nu_{xy}=0.26$ $\nu_{yz}=0.3$ $\nu_{xz}=0.26$
B1C1	CFRP***	1	$E_x=62000$ $E_y=4800$ $E_z=4800$	$G_{xy}=3270$ $G_{yz}=1860$ $G_{xz}=3270$	760	0.012	$\nu_{xy}=0.22$ $\nu_{yz}=0.3$ $\nu_{xz}=0.22$
FWCC-A	AFRP	1	176470	-	3000	0.017	0.2

*According to ACI-318 Equations

**Assumed

*** From [Kachlakev et al., 2001]

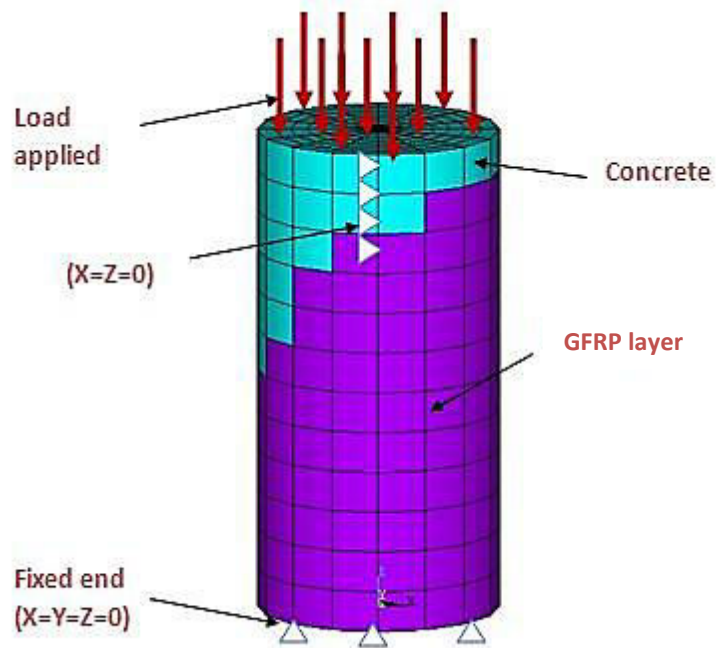


Fig.(4.26): Finite Element Model of (FWCC) Column.

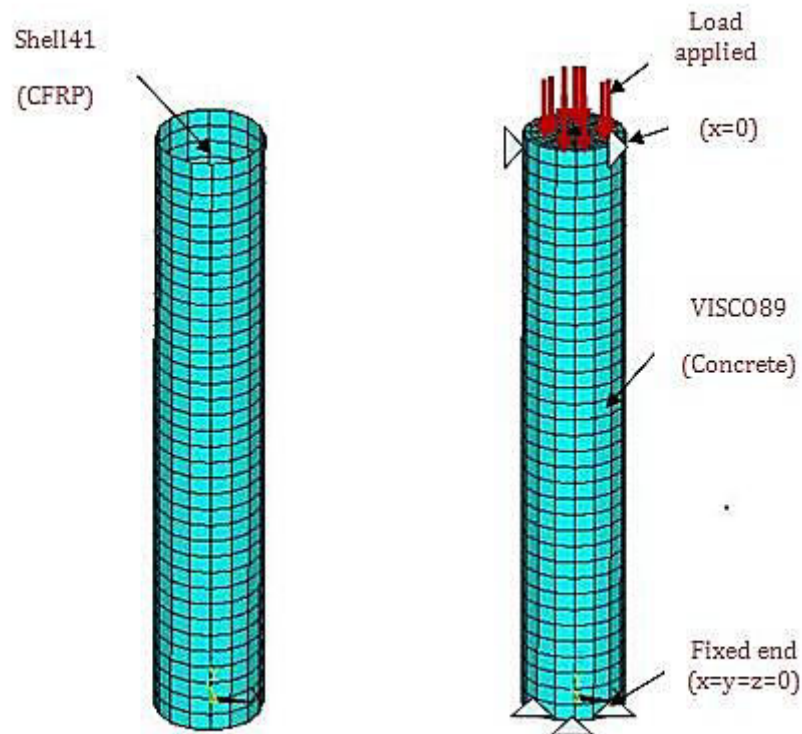


Fig.(4.27): Finite Element Model of (B1C1) Column.

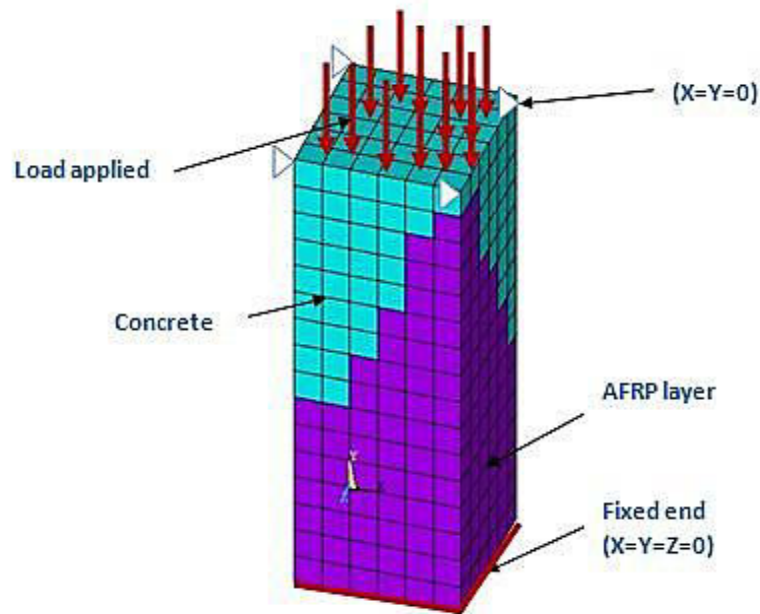


Fig.(4.28): Finite Element Model of (FWCC-A) Column.

4.3.3 Results of Analysis for Columns Under Long-Term Loading:

The analysis of creep for columns under sustained loading needs a function of shear relaxation which obtains from Prony series fitting program that's written in Visual FORTRAN 5.0, these functions were given in Table(4-9). From section (3.5) in chapter three, ANSYS will be needed material characteristics, e.g. initial and final shear modulus, number of Maxwell elements with relaxation modulus and discrete relaxation spectrum for each Maxwell element assuming the constant temperature and stress behavior along age of structure indicated by bulk modulus. From fitting the compliance function from ACI model Eq.(3.33) and from Eq.(4.1) (*Timoshenko & Goodier, 1982*). Using (PSFP) [Prony Series Fitting Program] for Prony series representation of reduction of shear modulus, coding in **Fortran power station 4.0** language, obtain shear relaxation functions

$$G = \frac{E}{2(1+\nu)} \quad \text{and} \quad K = \frac{E}{3(1-2\nu)} \quad \dots(4.1)$$

These functions should be compared with **ACI committee 209R** creep model, according to this comparison, the results give a good agreement with ACI model. The error of these functions do not pass (2.5%) for all the five columns. The comparison of functions, percentage of error, experimental and numerical curves and vibration of displacement, principal stress and strain of five columns are shown in Figs.(4.29) to (4.55), while Table(4-10) shows the results of experimental and finite element of these columns.

Table(4-9): Shear Relaxation Functions for Columns Under Long-Term Loading

Column	Shear Relaxation Function
F40-1.4-1	$G(t) = 4247.606 + 8233.156e^{(-t/5)} - 12627.8e^{(-t/10)} + 10235.02e^{(-t/15)}$
E80-C	$G(t) = 5060.016 + 9951.357e^{(-t/5)} - 14622.5e^{(-t/10)} + 12154.915e^{(-t/15)}$
FWCC	$G(t) = 6549.14 + 5664.833e^{(-t/10)} - 9093.15e^{(-t/20)} + 7478.688e^{(-t/30)}$
B1C1	$G(t) = 4267.857 + 19071.32e^{(-t/30)} - 25886.2e^{(-t/50)} + 14853.71e^{(-t/70)}$
FWCC-A	$G(t) = 7614.764 + 7384.533e^{(-t/15)} - 15906.9e^{(-t/30)} + 13033.52e^{(-t/40)}$

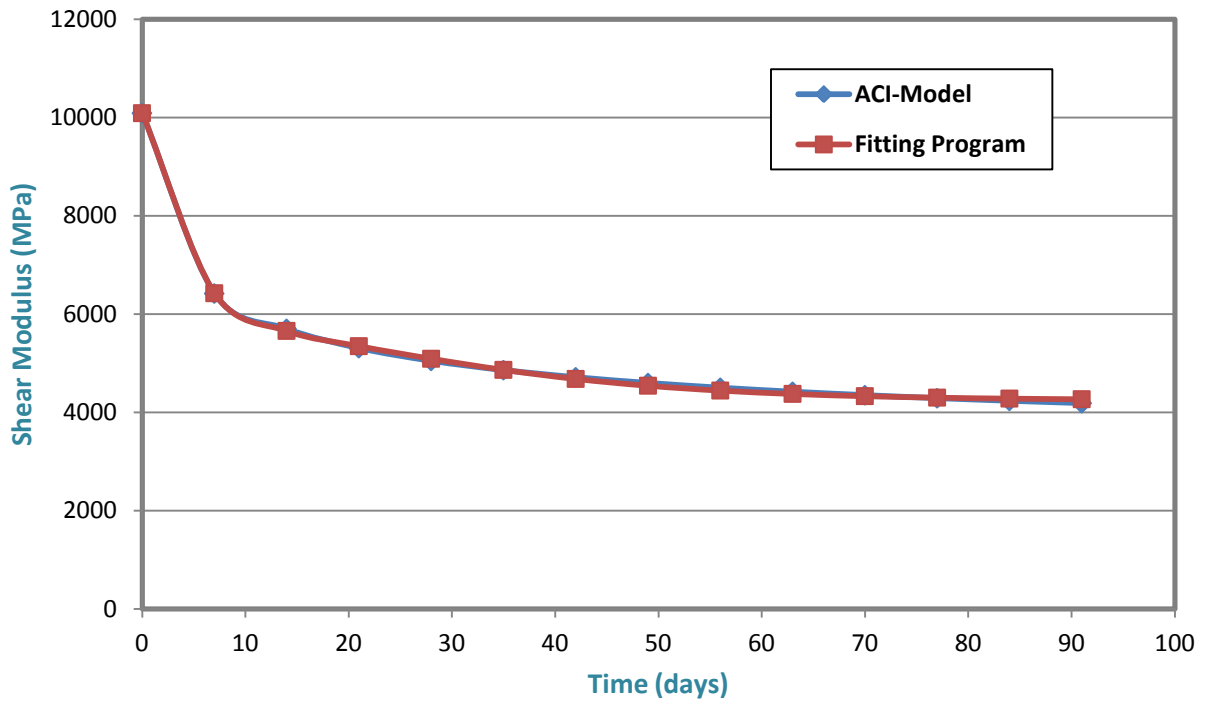


Fig.(4.29): Shear Modulus Relaxation vs Time for (F40-1.4-1) Column.

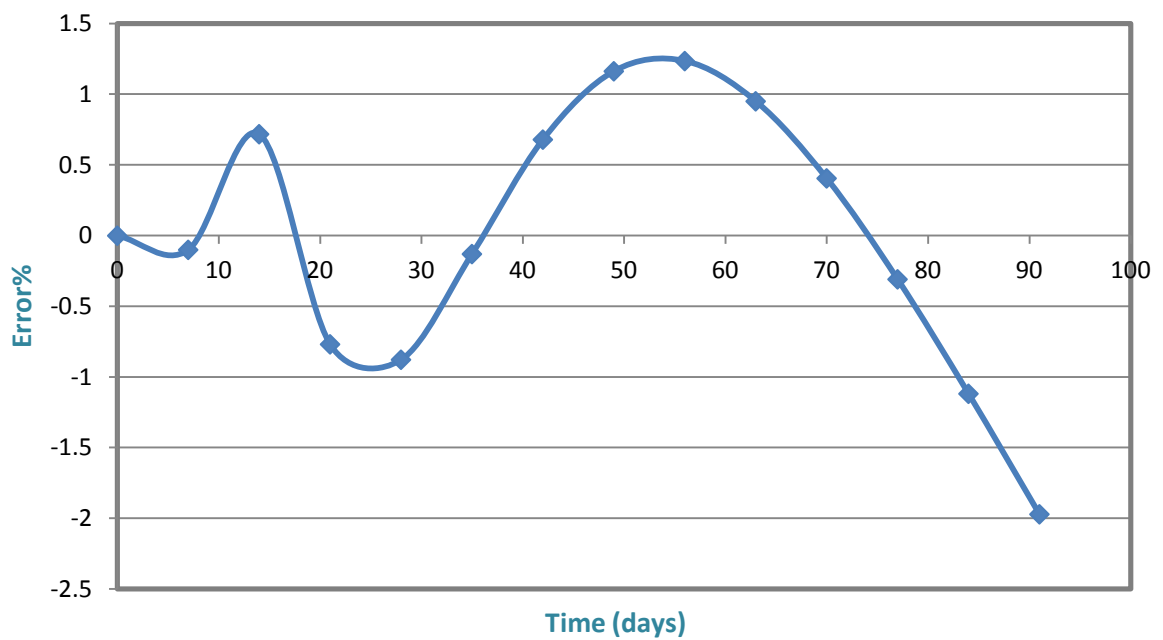


Fig.(4.30):Percent of Error vs Time for (F40-1.4-1) Column.

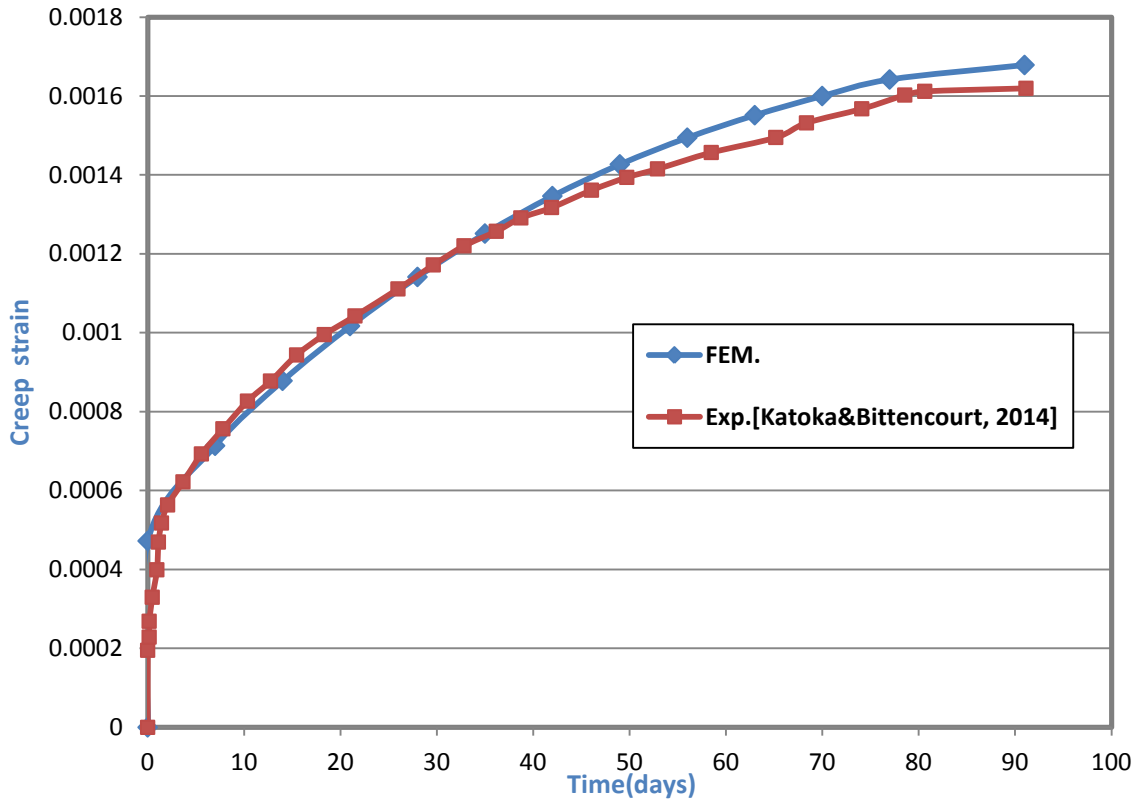


Fig.(4.31): Experimental and Numerical Time-Creep Strain Curve for (F40-1.4-1) Column.

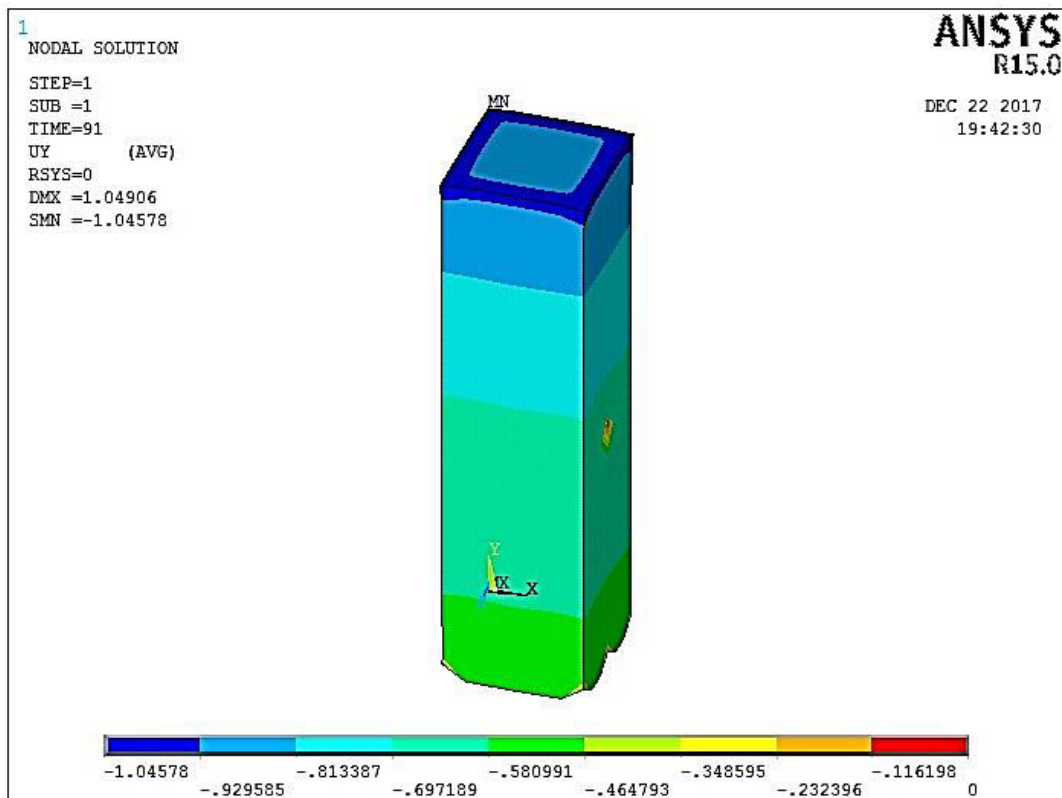


Fig.(4.32): Displacements of (F40-1.4-1) Model in y-direction at 91days.

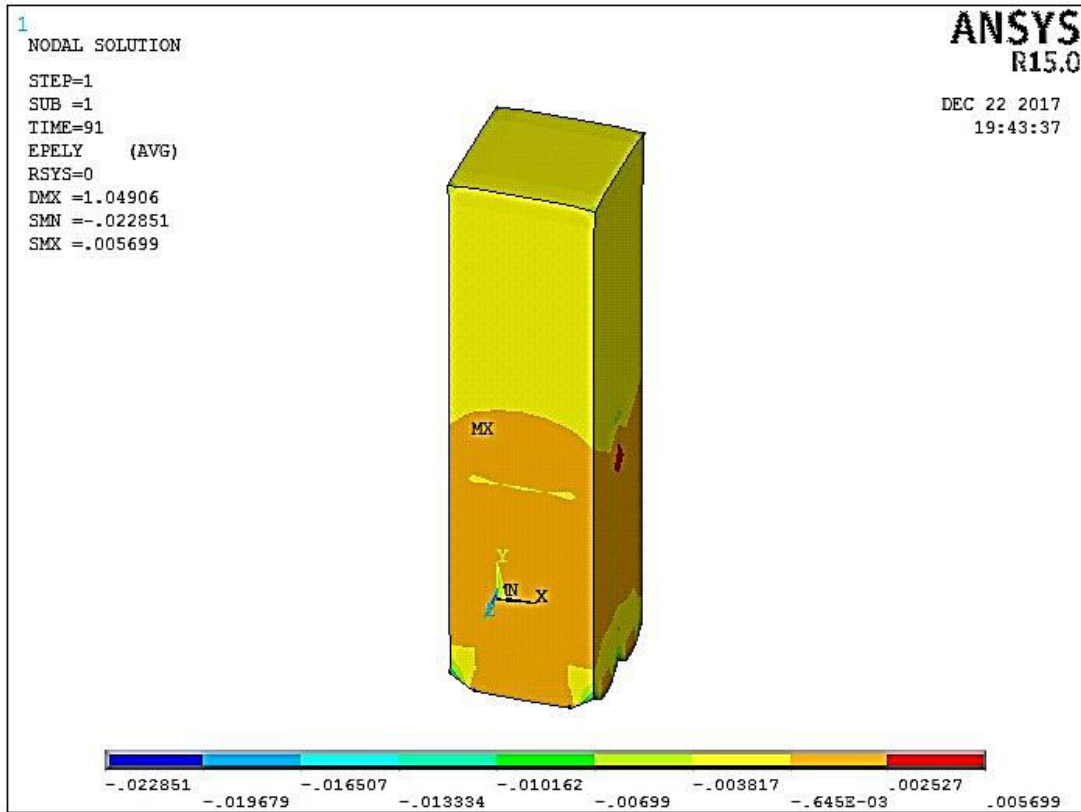


Fig.(4.33): Strains of (F40-1.4-1) Model in y-direction at 91days.

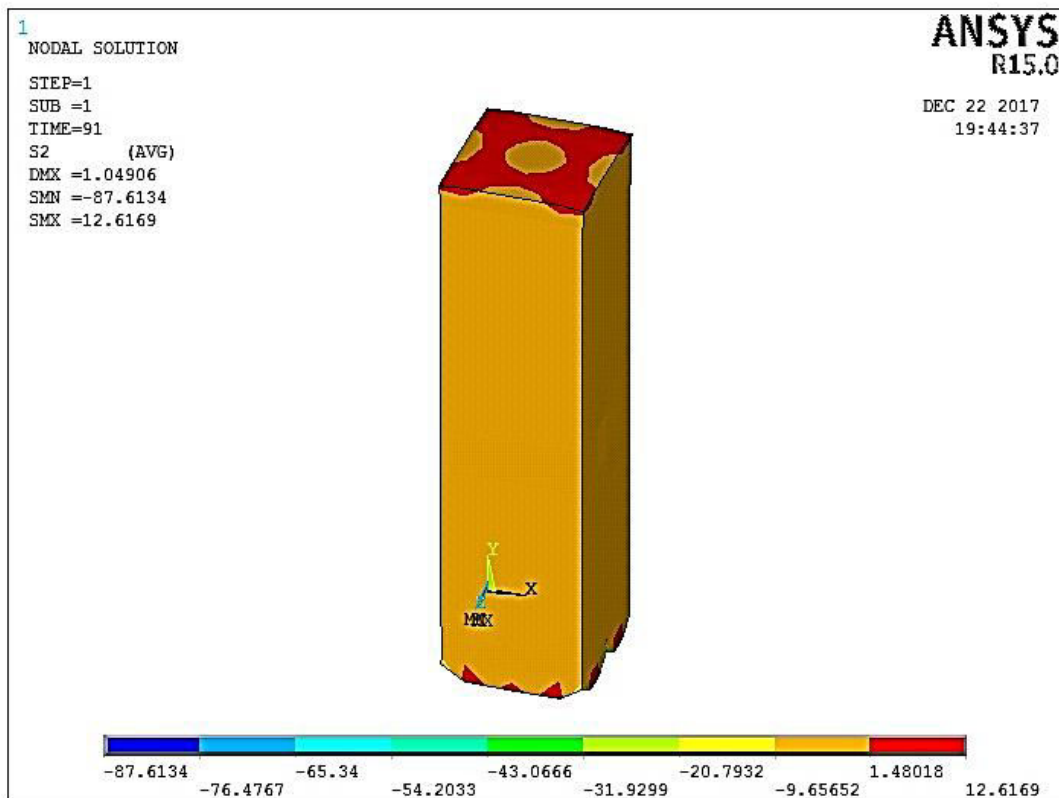


Fig.(4.34): Principal Stresses of (F40-1.4-1) Model in y-direction at 91days.

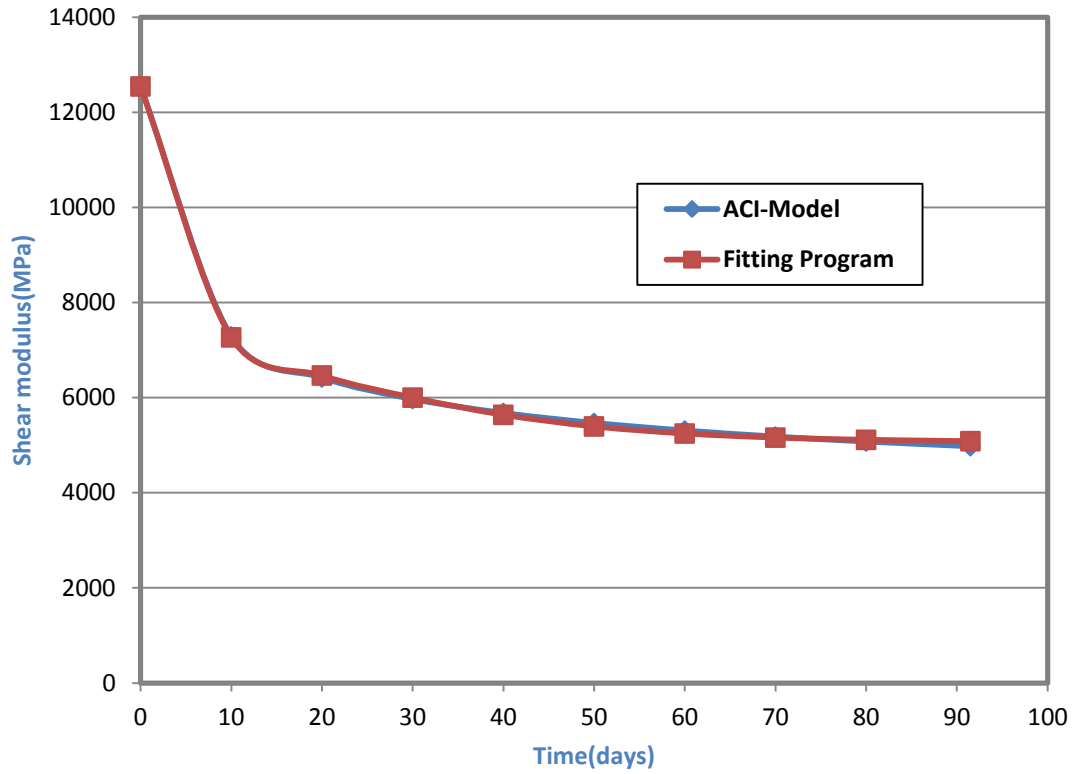


Fig.(4.35): Shear Modulus Relaxation vs Time for (E80-C) Column.

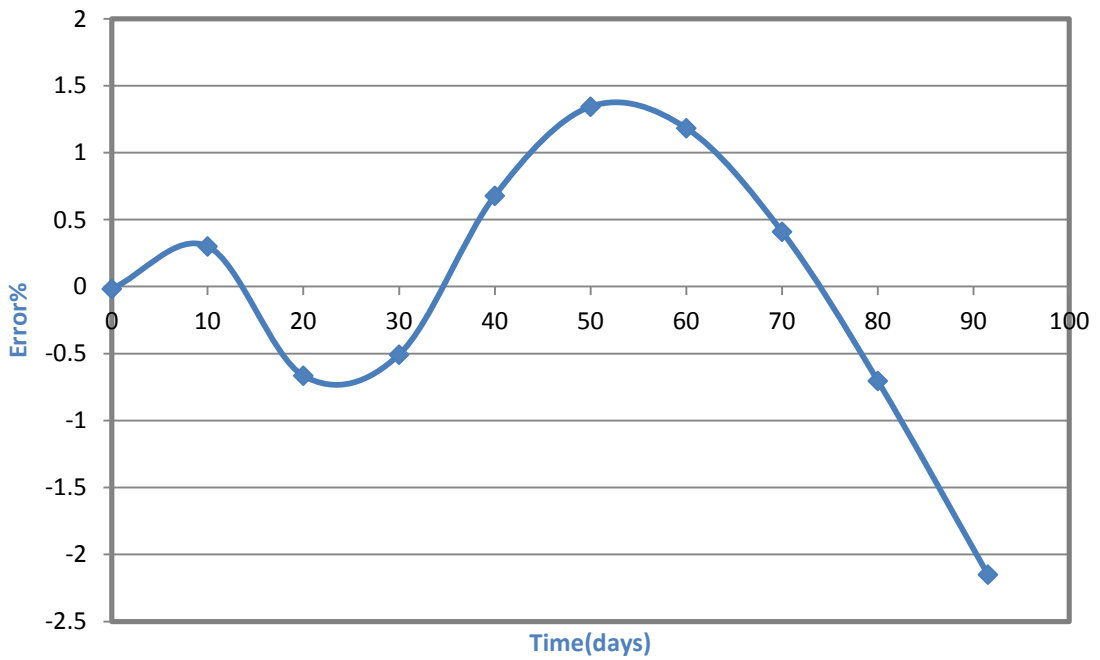


Fig.(4.36):Percent of Error vs Time for (E80-C) Column.

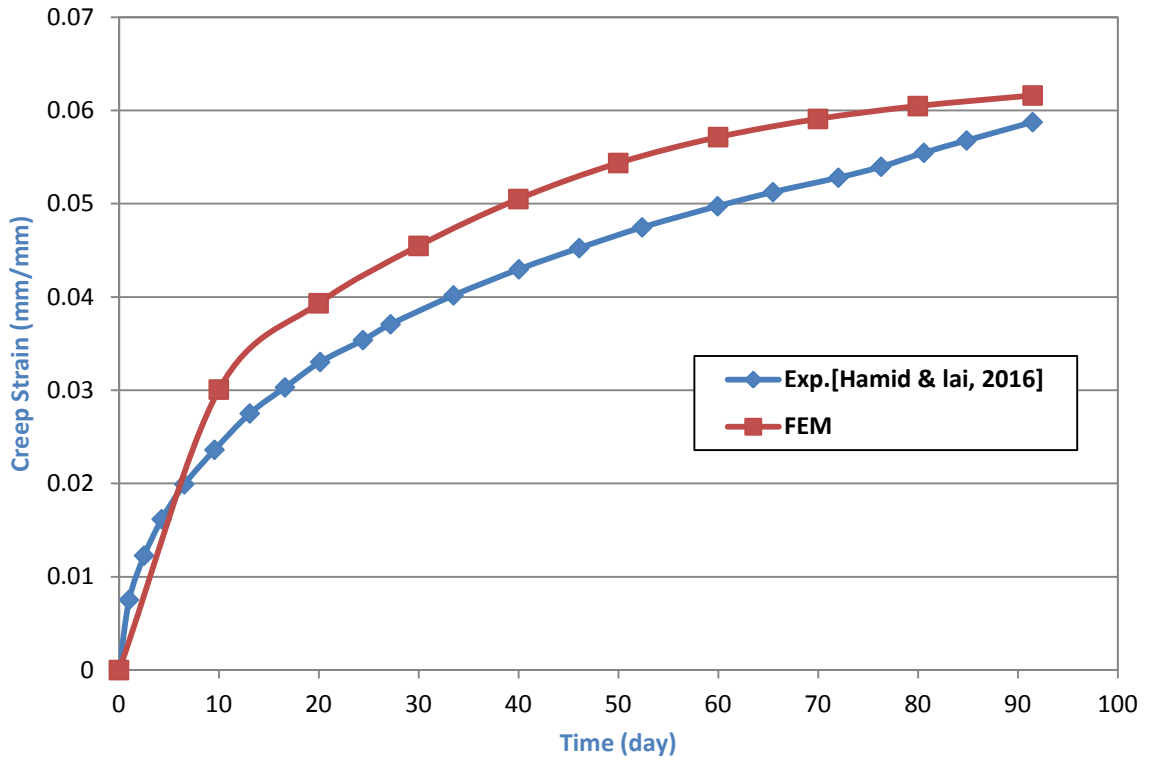


Fig.(4.37): Experimental and Numerical Time-Creep Strain Curve for (E80-C) Column.

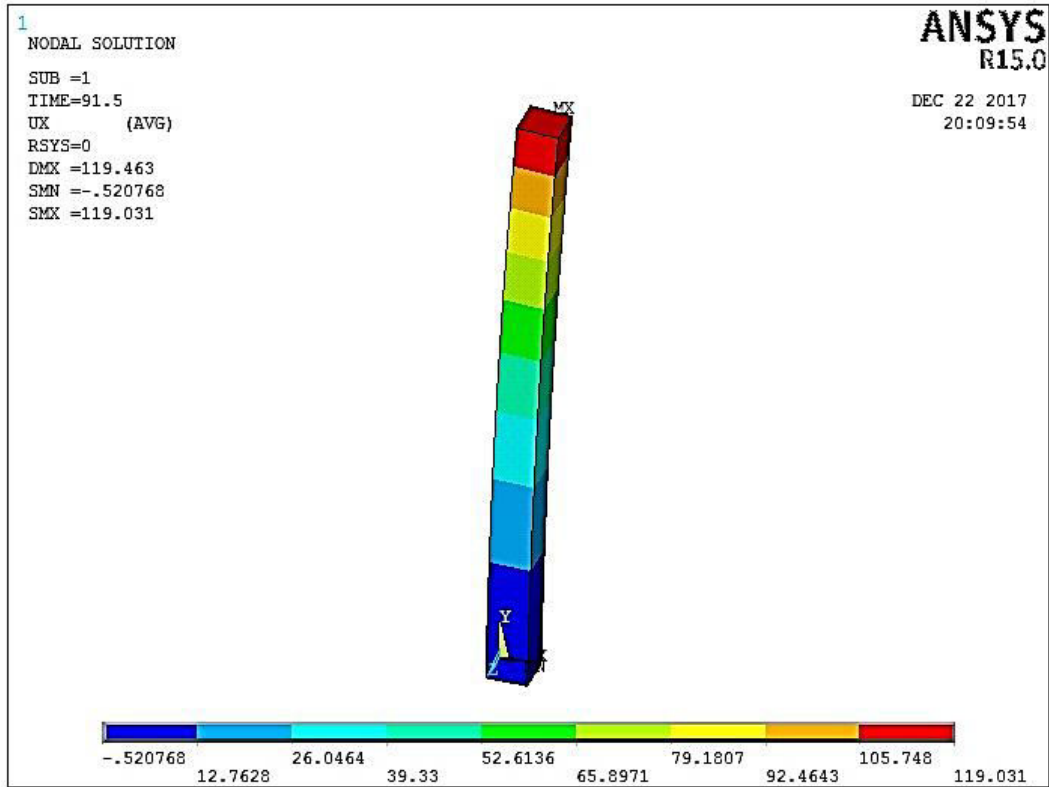


Fig.(4.38): Displacements of (E80-C) Model in x-direction at 91days.

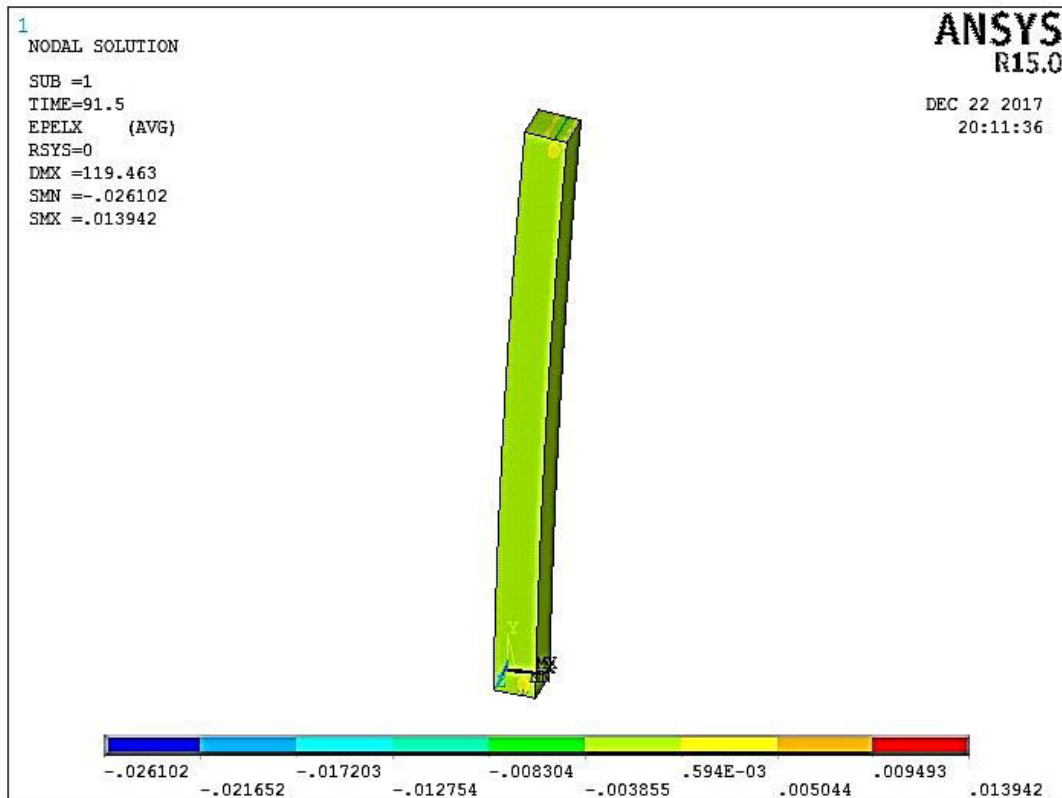


Fig.(4.39): Strains of (E80-C) Model in x-direction at 91days.

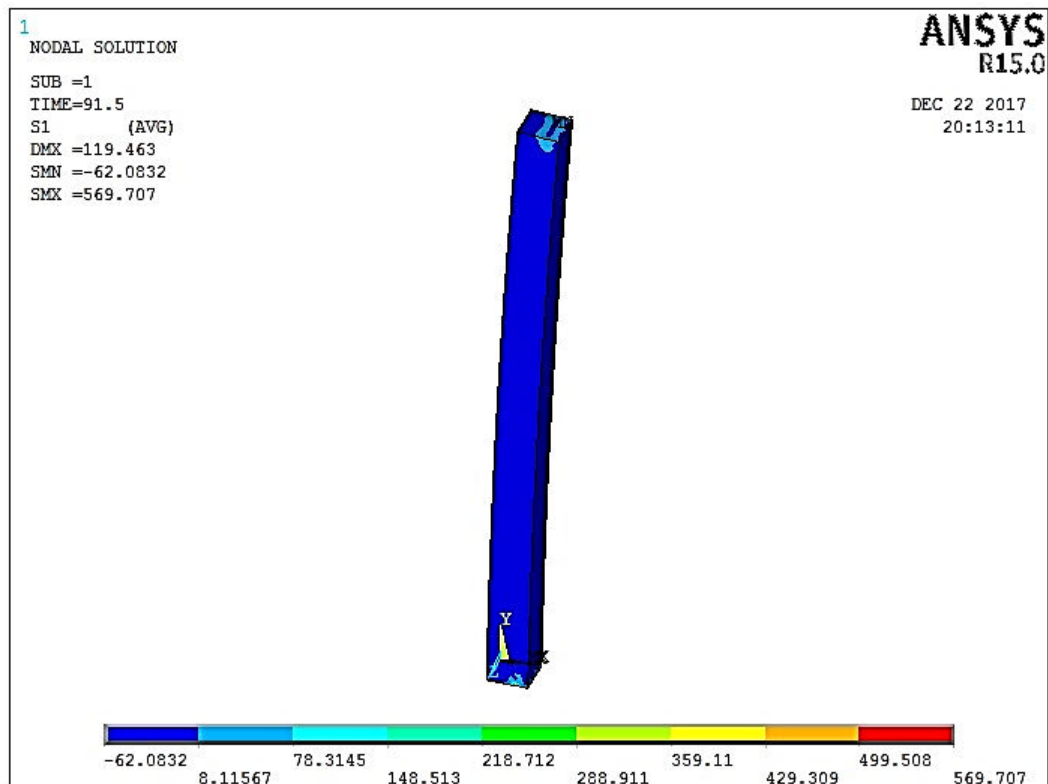


Fig.(4.40): Principal Stresses of (E80-C) Model in x-direction at 91days.

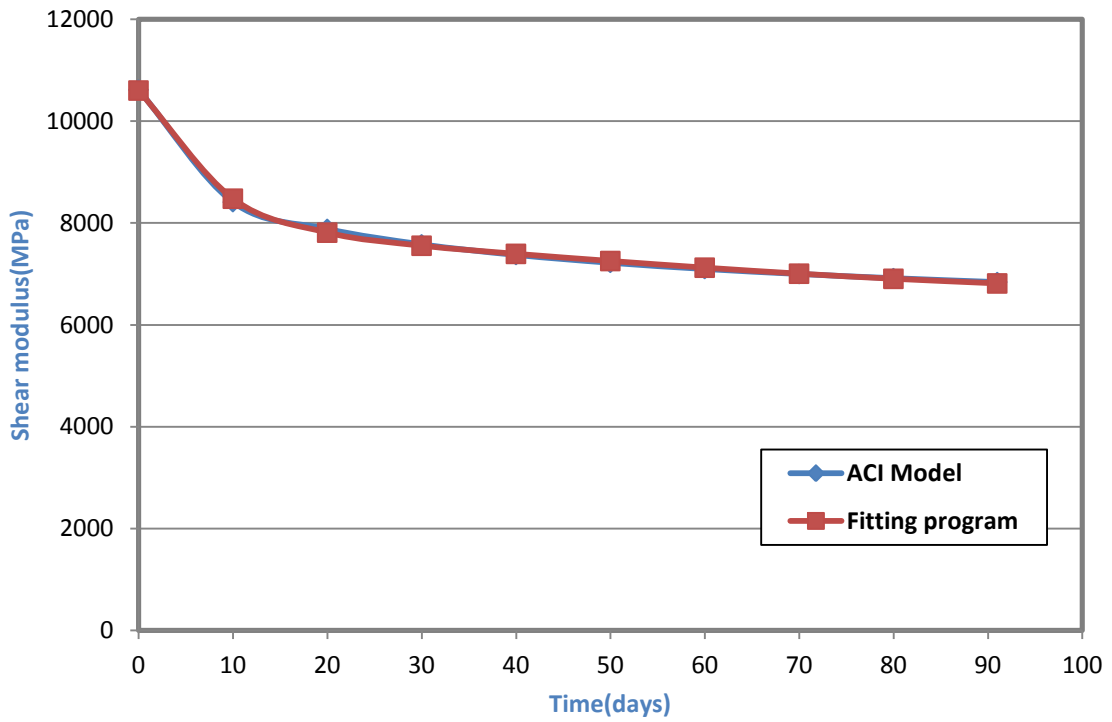


Fig.(4.41): Shear Modulus Relaxation vs Time for (FWCC) Column.

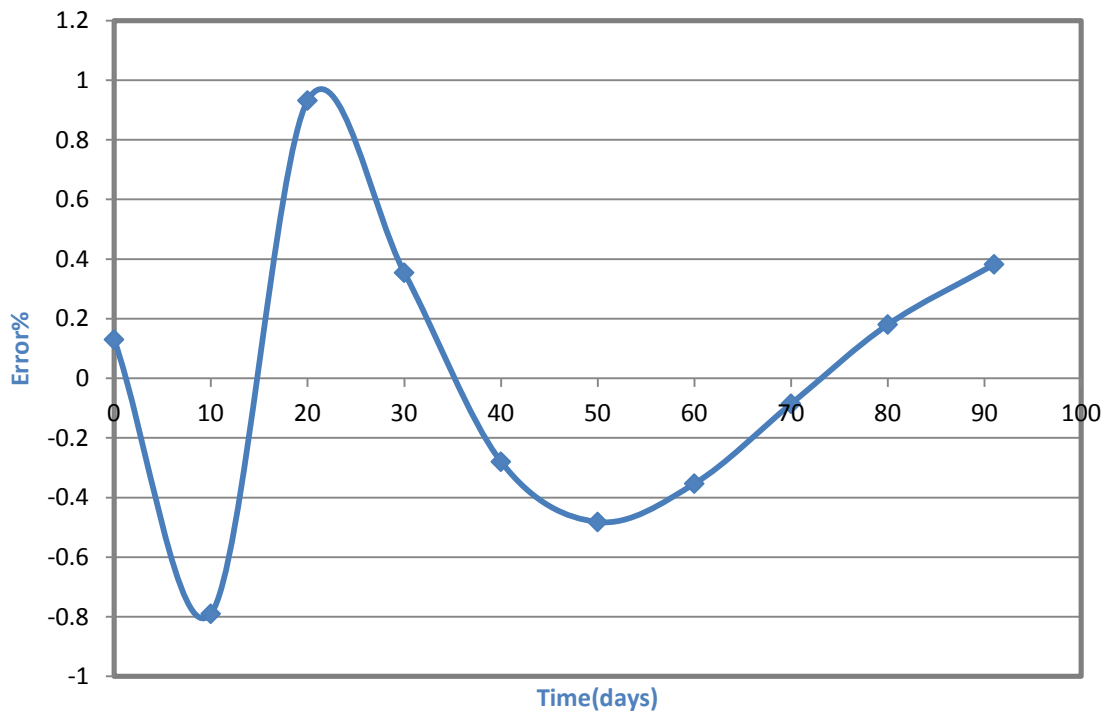


Fig.(4.42):Percent of Error vs Time for (FWCC) Column.

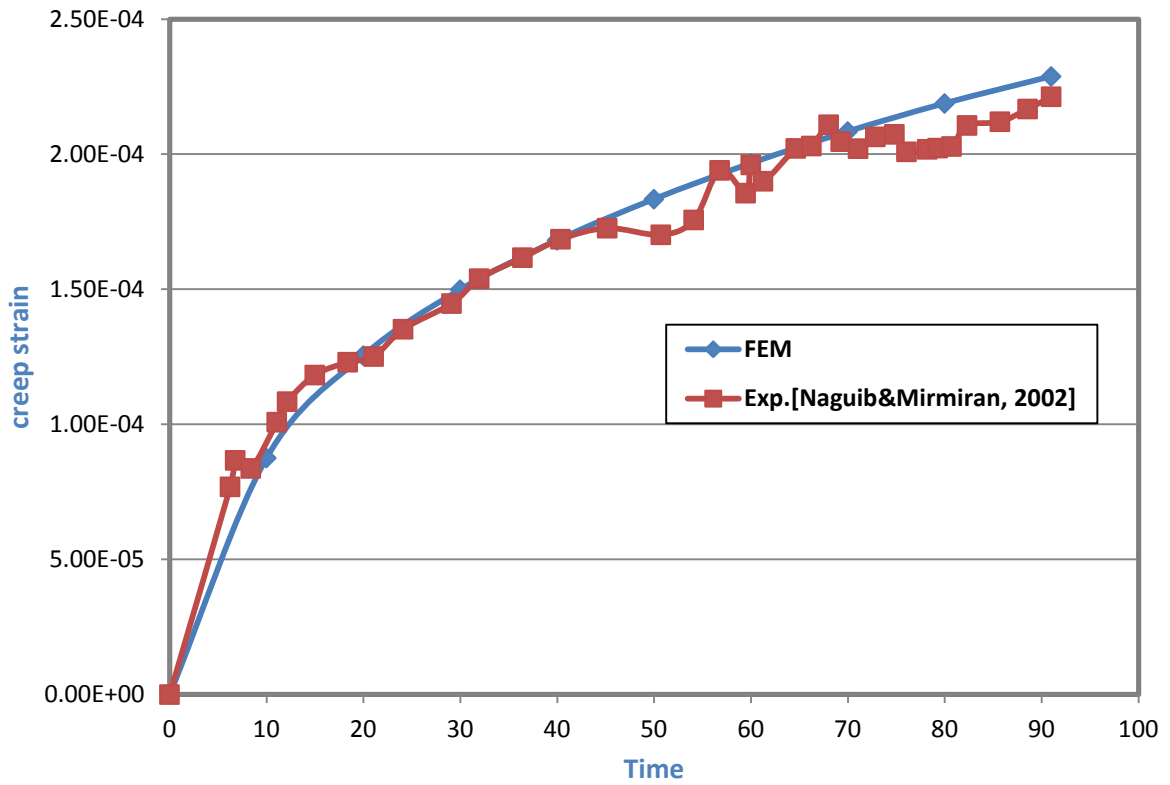


Fig.(4.43): Experimental and Numerical Time-Creep Strain Curve for (FWCC) Column.

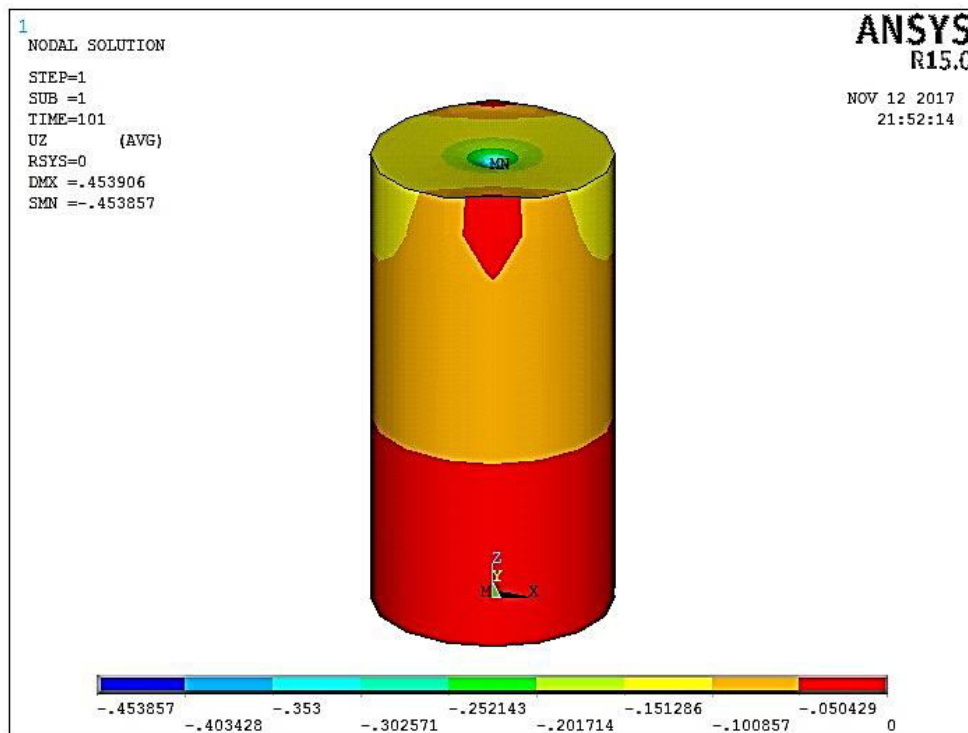


Fig.(4.44): Displacements of (FWCC) Model in z-direction at 91days.

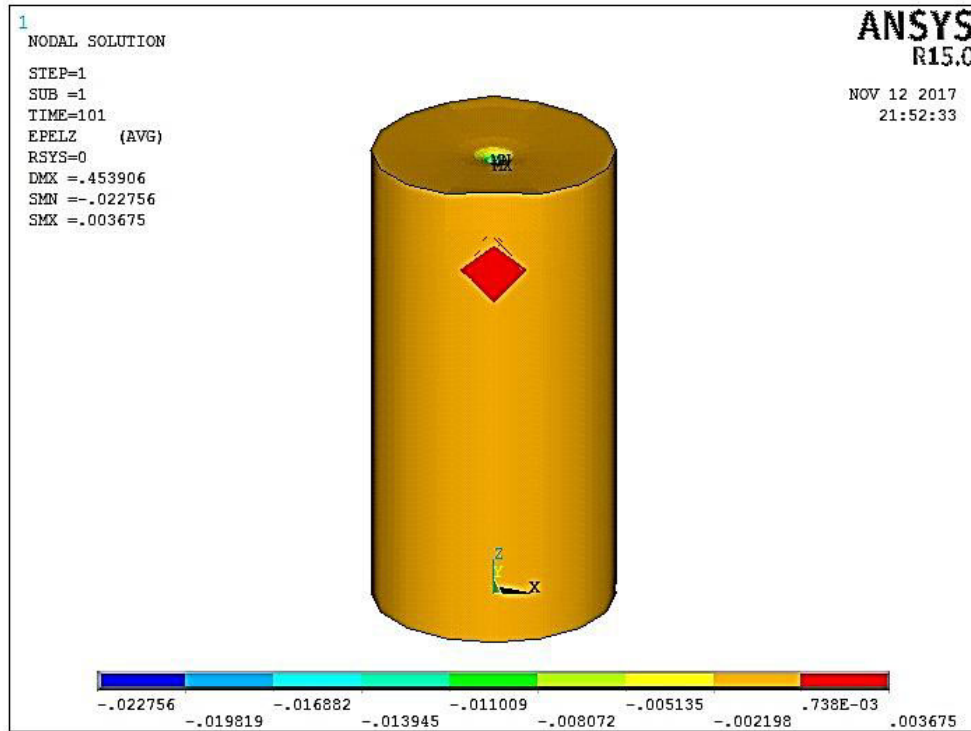


Fig.(4.45): Strains of (FWCC) Model in z-direction at 91days.

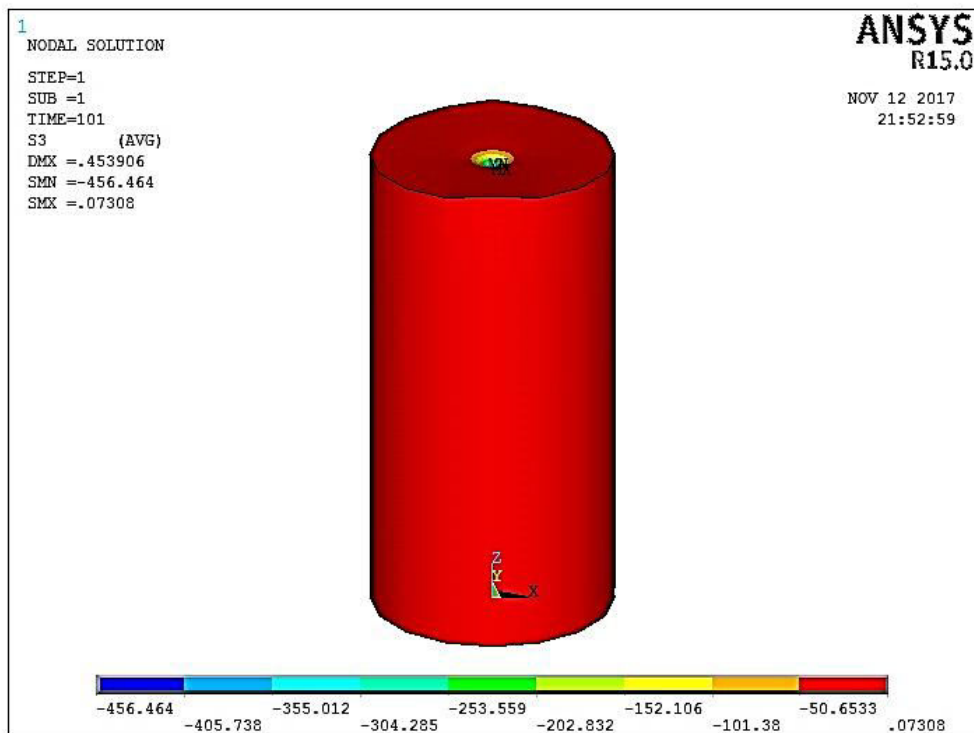


Fig.(4.46): Principal Stresses of (FWCC) Model in z-direction at 91days.

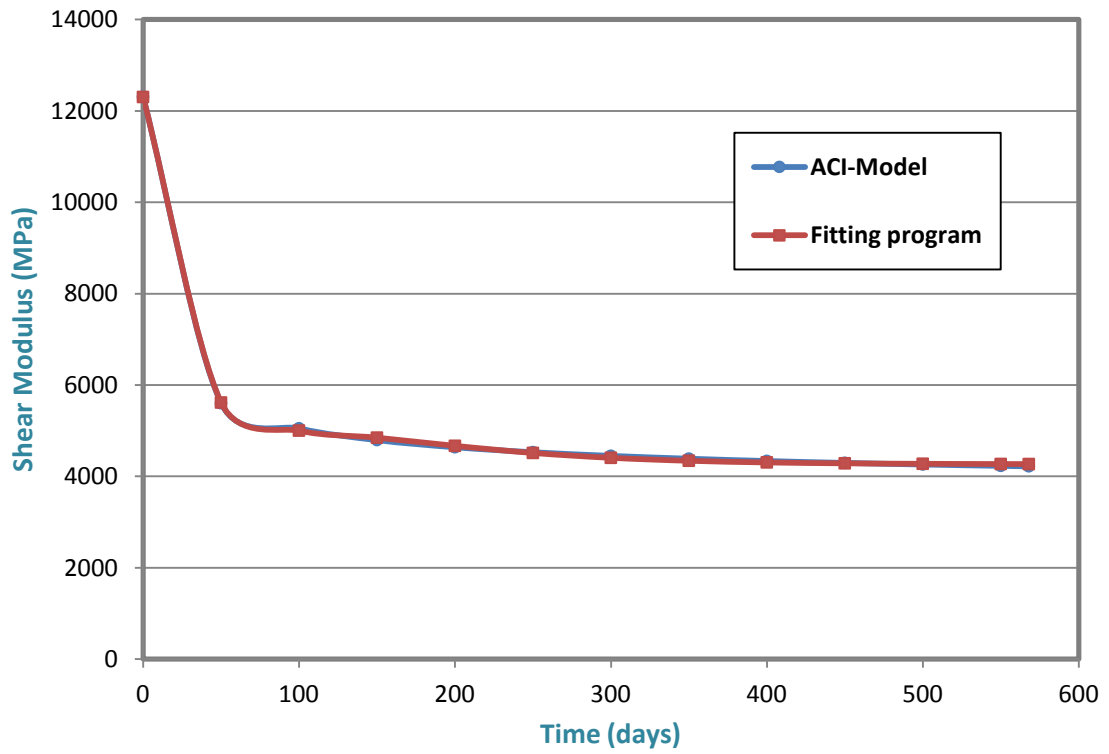


Fig.(4.47): Shear Modulus Relaxation vs Time for (B1C1) Column.

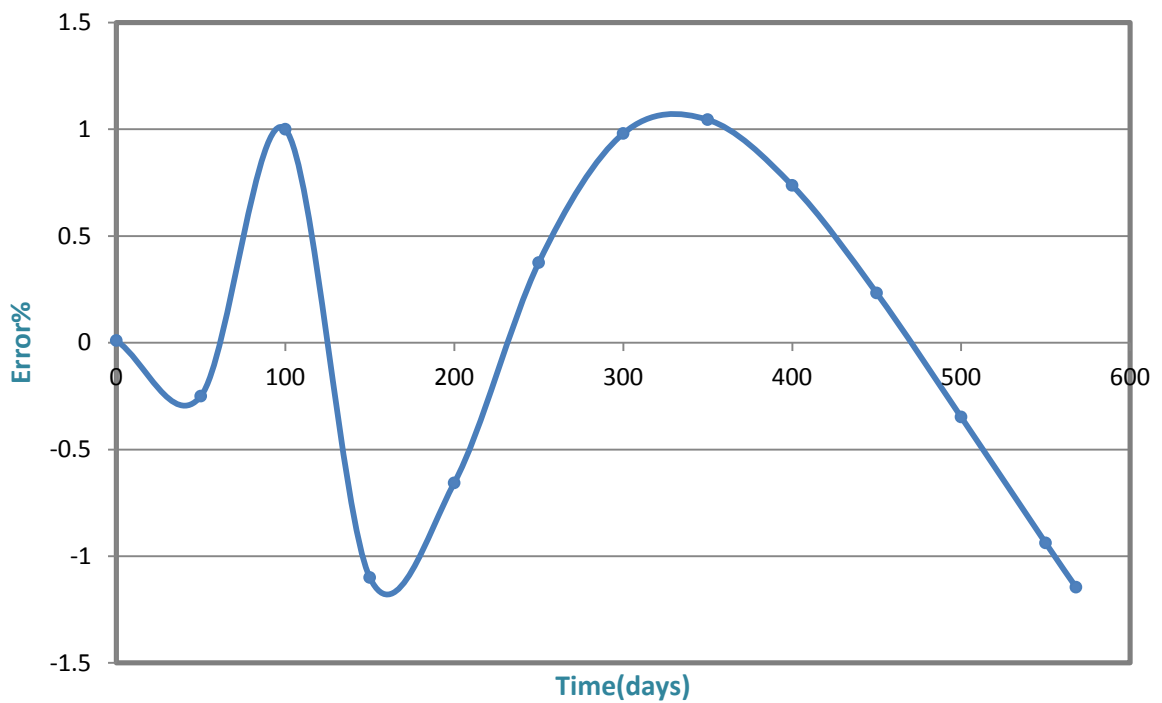


Fig.(4.48):Percent of Error vs Time for (B1C1) Column.

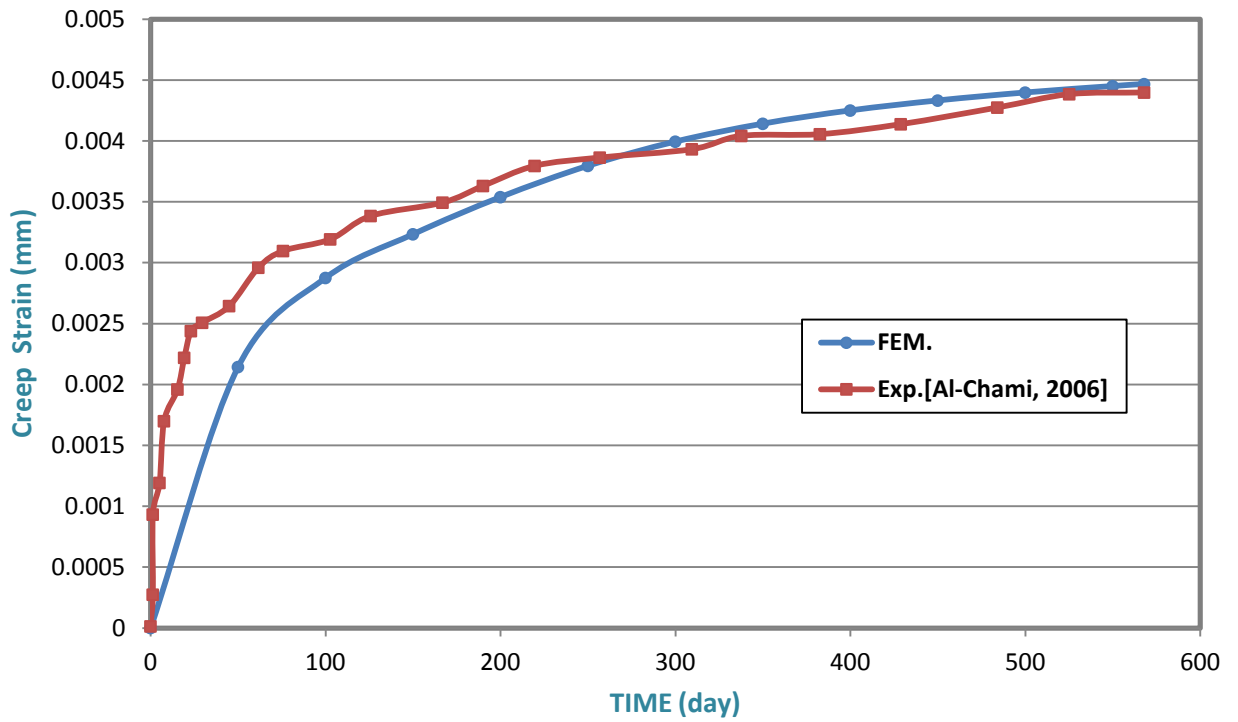


Fig.(4.49): Experimental and Numerical Time-Creep Strain Curve for (B1C1) Column.

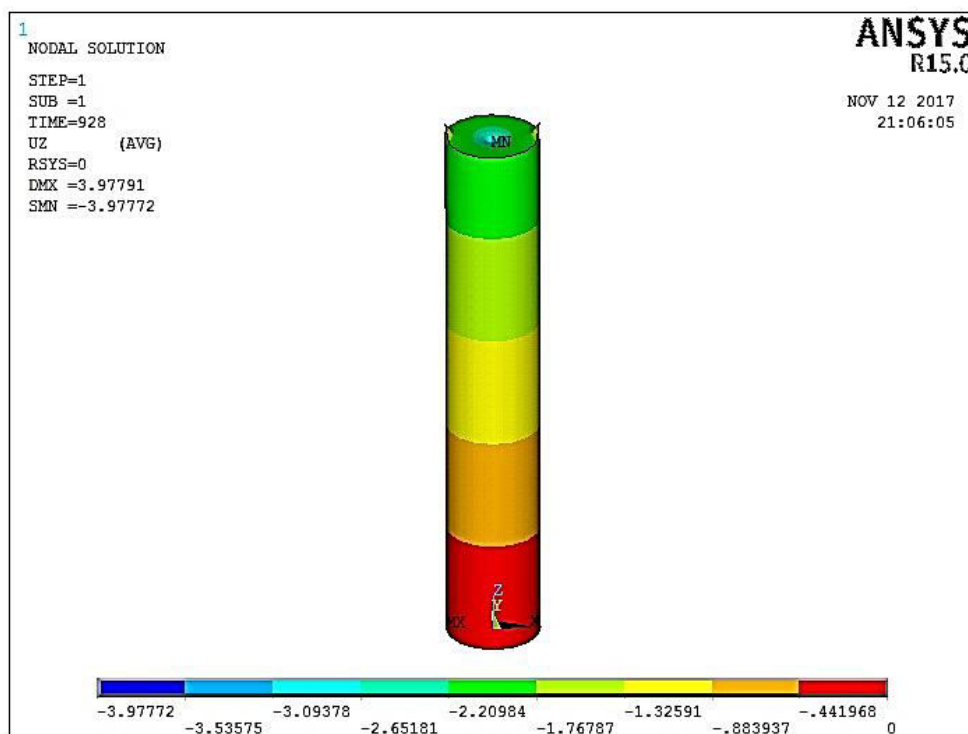


Fig.(4.50): Displacements of (B1C1) Model in z-direction at 568days.

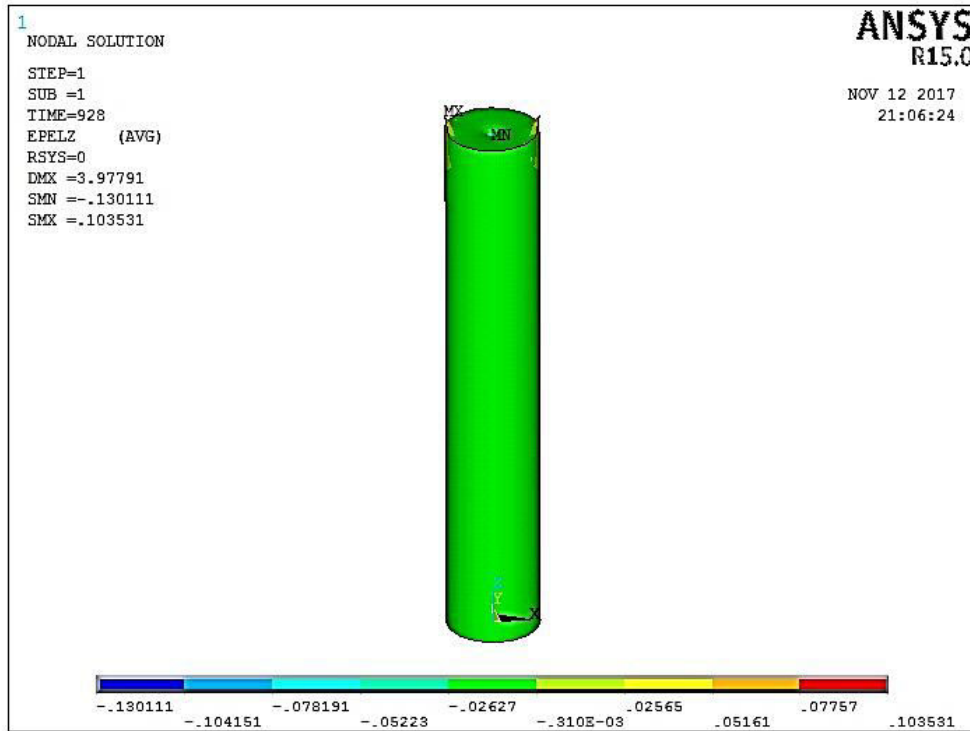


Fig.(4.51): Strains of (B1C1) Model in z-direction at 568days.

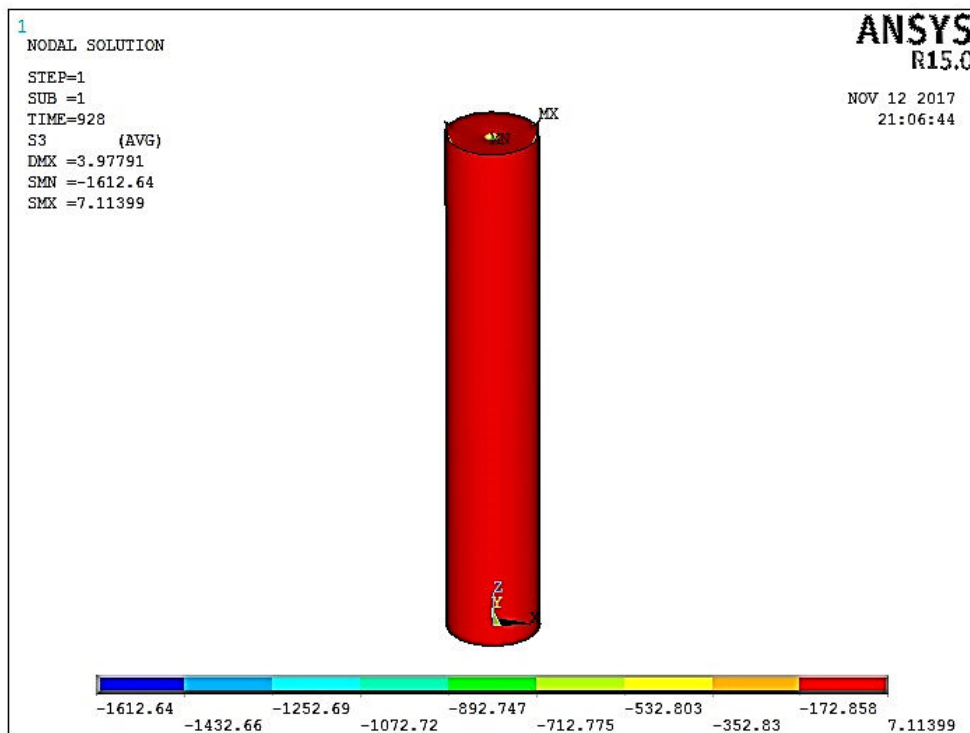


Fig.(4.52): Principal Stresses of (B1C1) Model in z-direction at 568days.

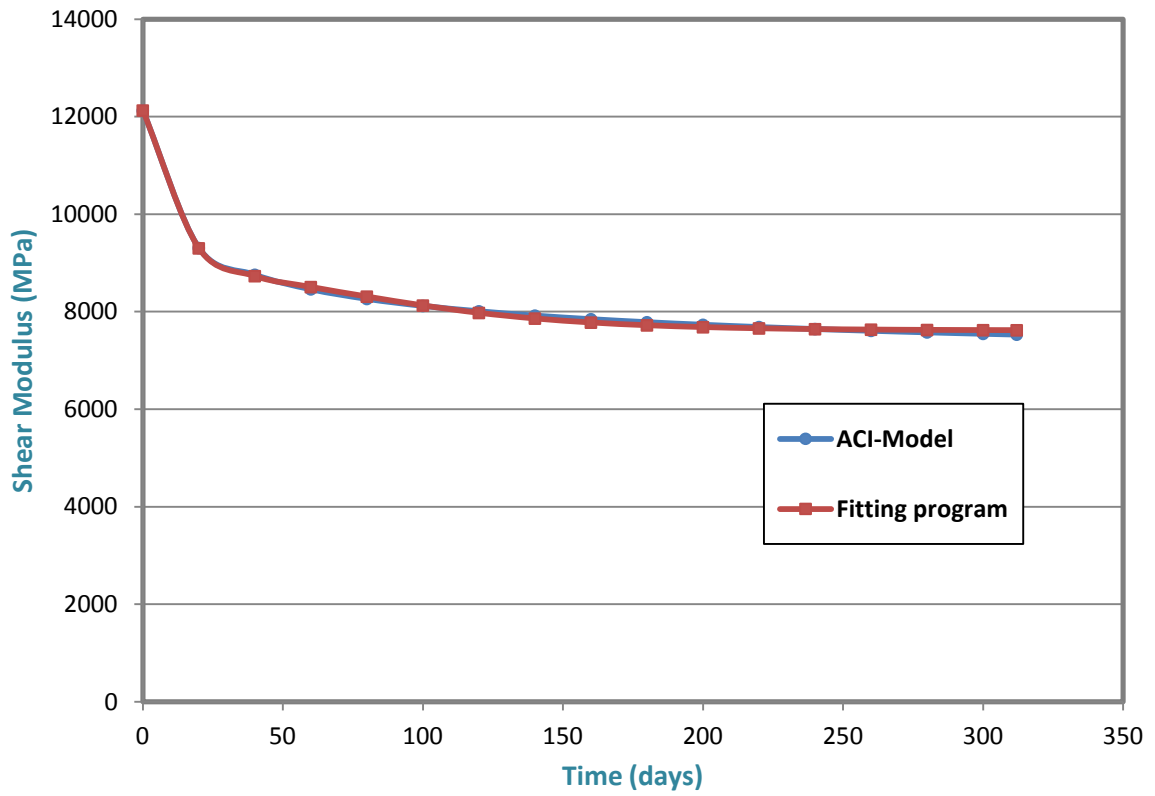


Fig.(4.53): Shear Modulus Relaxation vs Time for (FWCC-A) Column.

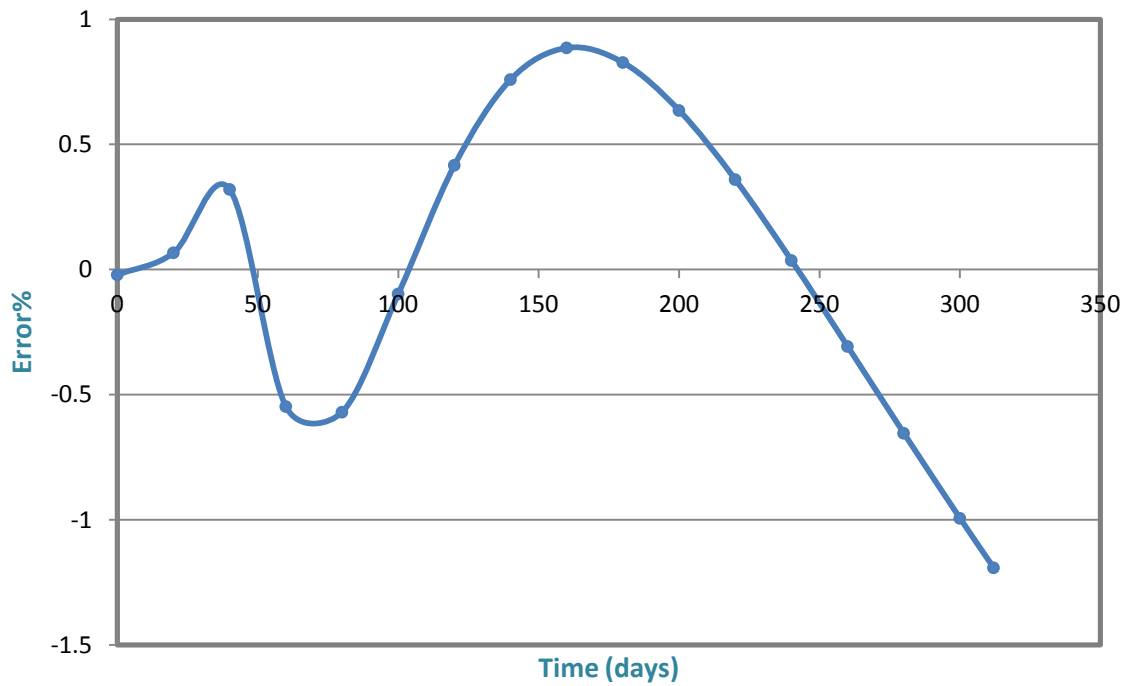


Fig.(4.54):Percent of Error vs Time for (FWCC-A) Column.

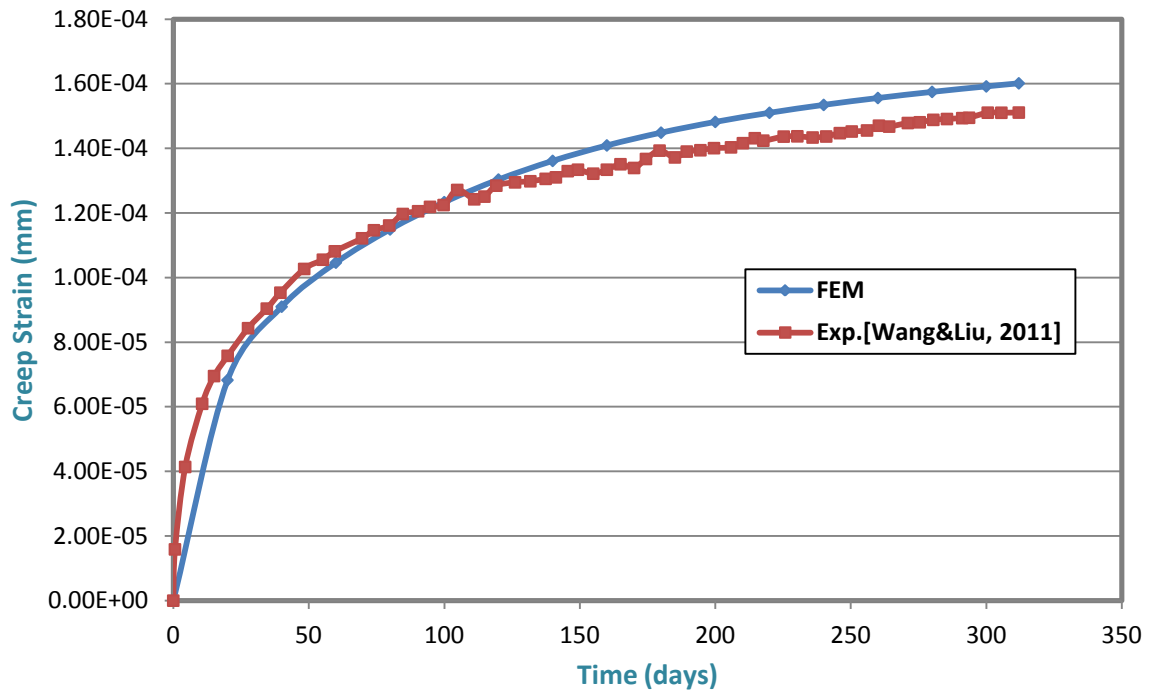


Fig.(4.55): Experimental and Numerical Time-Creep Strain Curve for (FWCC-A) Column.

Table(4-10): The Results of Experimental and Finite Element Method of (F40-1.4-1), (E80-C), (FWCC), (B1C1) and (FWCC-A) Models.

Column	Creep strain (Exp.)	Creep strain (FEM)	$\frac{\text{Creep strain(FEM)}}{\text{Creep strain(Exp.)}}$	Percentage of increase %
F40-1.4-1	0.00162	0.00168	1.037	3.70
E80-C	0.0587	0.0616	1.0494	4.94
FWCC	0.0002213	0.000229	1.0348	3.48
B1C1	0.0044	0.0045	1.0227	2.27
FWCC-A	0.0001511	0.00016	1.0589	5.89

By comparing the results of experimental and finite element method of time-creep strain curves, it achieved a good agreement between finite element and experimental results, whereas Table(4-10) illustrates the percentage of increased for columns and was stated that creep strain of control columns (F40-1.4-1) and (E80-C) higher than creep strain of jacketed columns (FWCC), (B1C1) and (FWCC-A).where the strengthening by FRP layer leads to decrease the creep strain.

Chapter Five

Parametric Study

5.1: General:

This chapter will study the effect of some parameters of the two models (B1C1) of (*Al-Chami, 2006*) and (FWCC) of (*Naguib & Mirmiran, 2002*) that were mentioned in the previous chapter. The parameters studied in this chapter were (Load applied effect, Eccentricity effect, Length effect, Compressive strength effect and FRP type effect).

5.2: Finite Element Idealization and Material Properties:

To investigate the effect of parameters, selected columns (B1C1) and (FWCC) from chapter four and create three models for each one with l/d ratio equal to (8,15 and 30) respectively, each of them was applied to different load with different eccentricity and compressive strength. These models and material properties of the models were stated in Table (5-1), where the material properties were illustrated in Table (5-1), while Fig. (5-1) to (5-3) represent the models of (B1C1) column and Fig. (5-4) to (5-6) represent the models of (FWCC) column.

Table (5-1): Concrete Material Properties.

Column Name	Compressive strength(MPa)	Initial elastic modulus(MPa)	Initial shear modulus(MPa)	Initial bulk modulus(MPa)
B1C1	30	25906	10795	14393
	40	29915	12465	16619
	50	33446	12465	18581
FWCC	30	25906	10795	14393
	40	29915	12465	16619
	50	33446	13936	18581

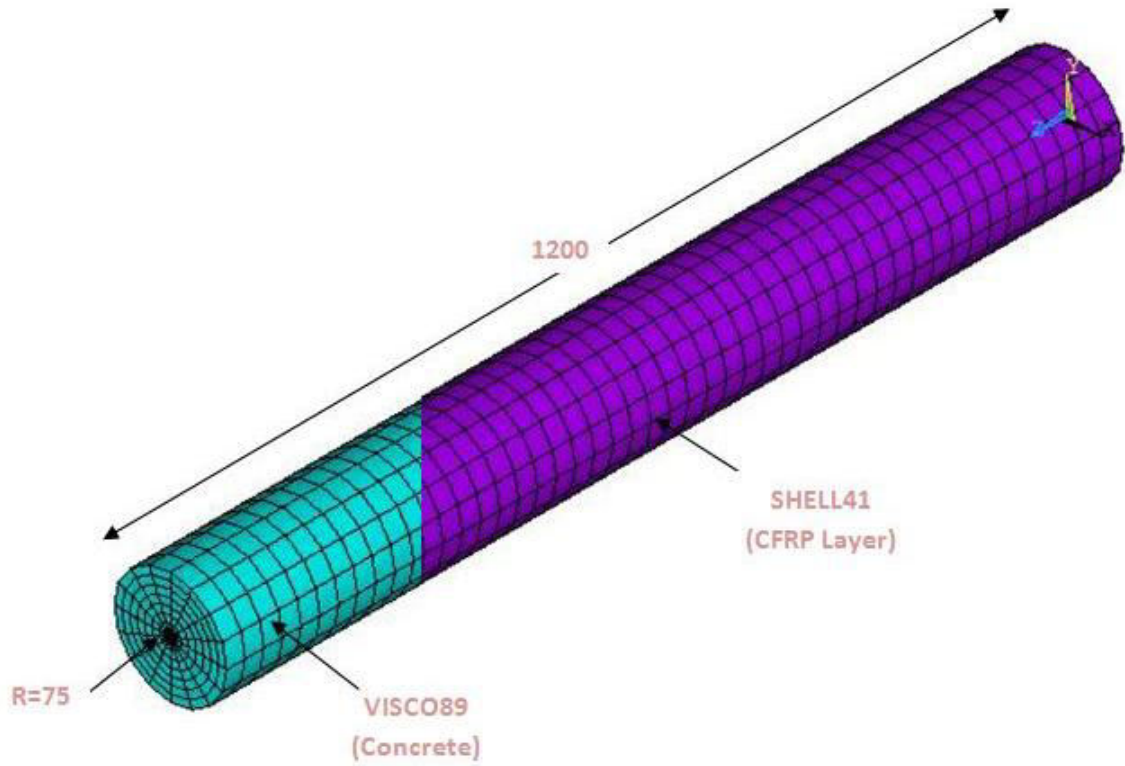


Fig.(5-1): Finite Element Model of (B1C1) with $l/d=8$

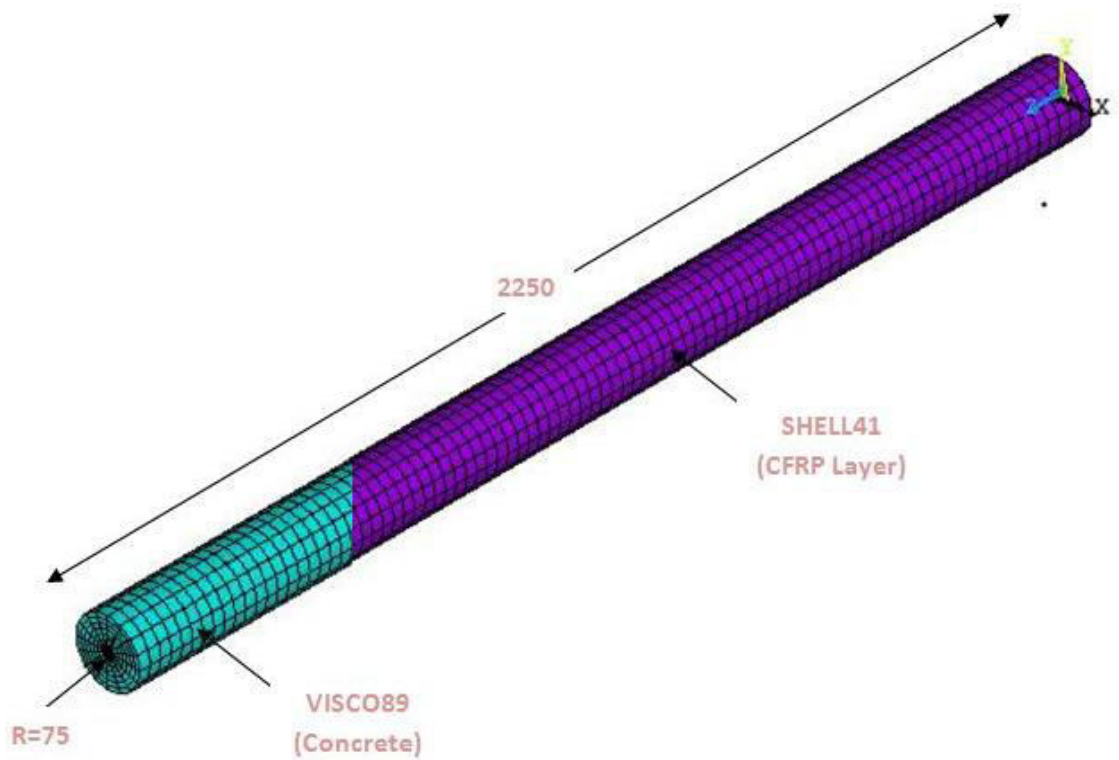


Fig.(5-2) Finite Element Model of (B1C1) with $l/d=15$

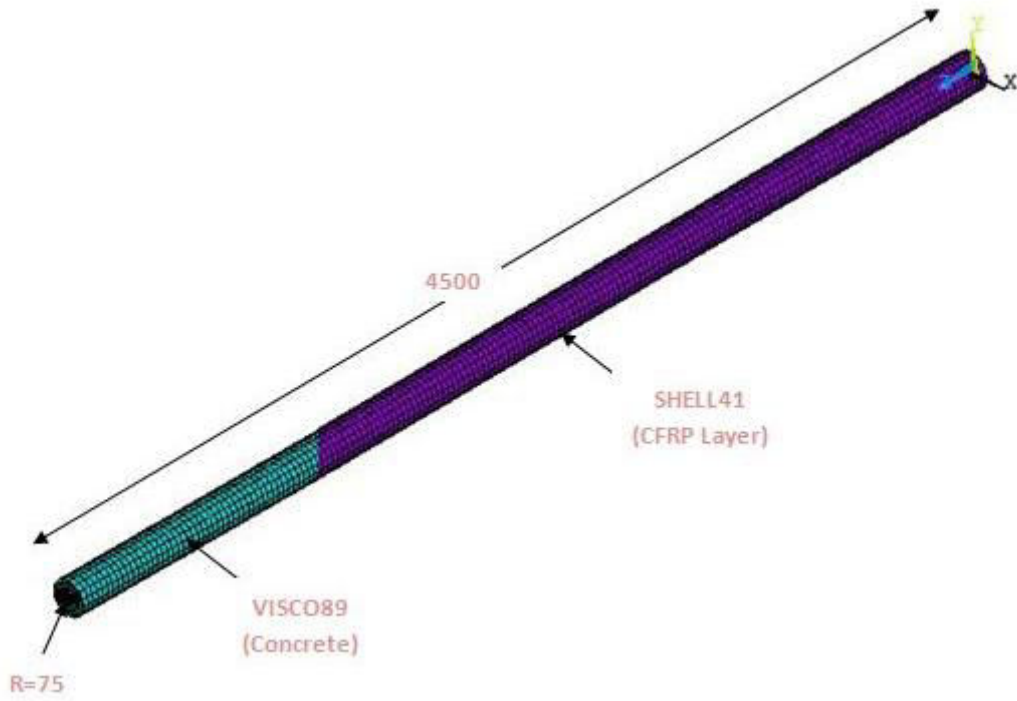


Fig.(5-3) Finite Element Model of (B1C1) with $l/d=30$

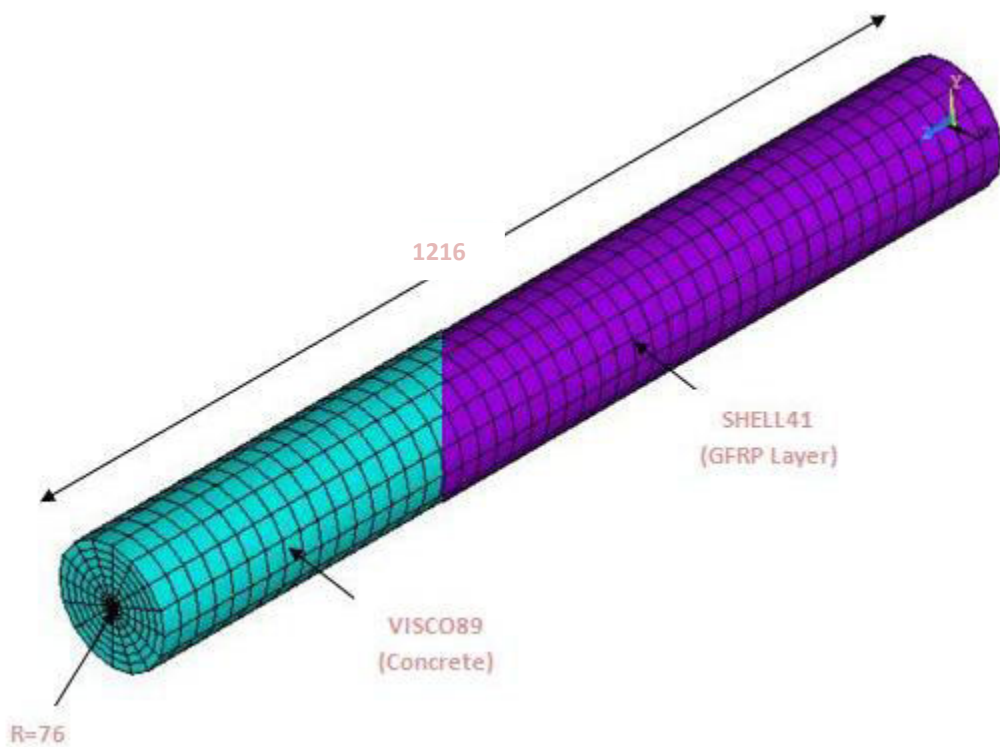


Fig.(5-4) Finite Element Model of (FWCC) with $l/d=8$

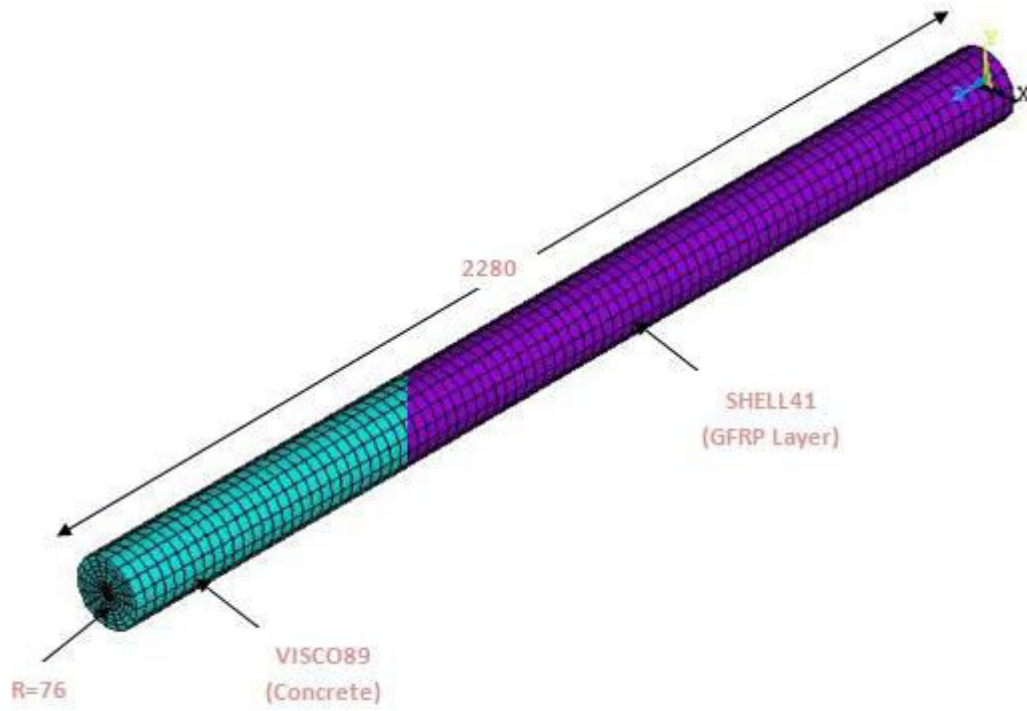


Fig.(5-5) Finite Element Model of (FWCC) with $l/d=15$

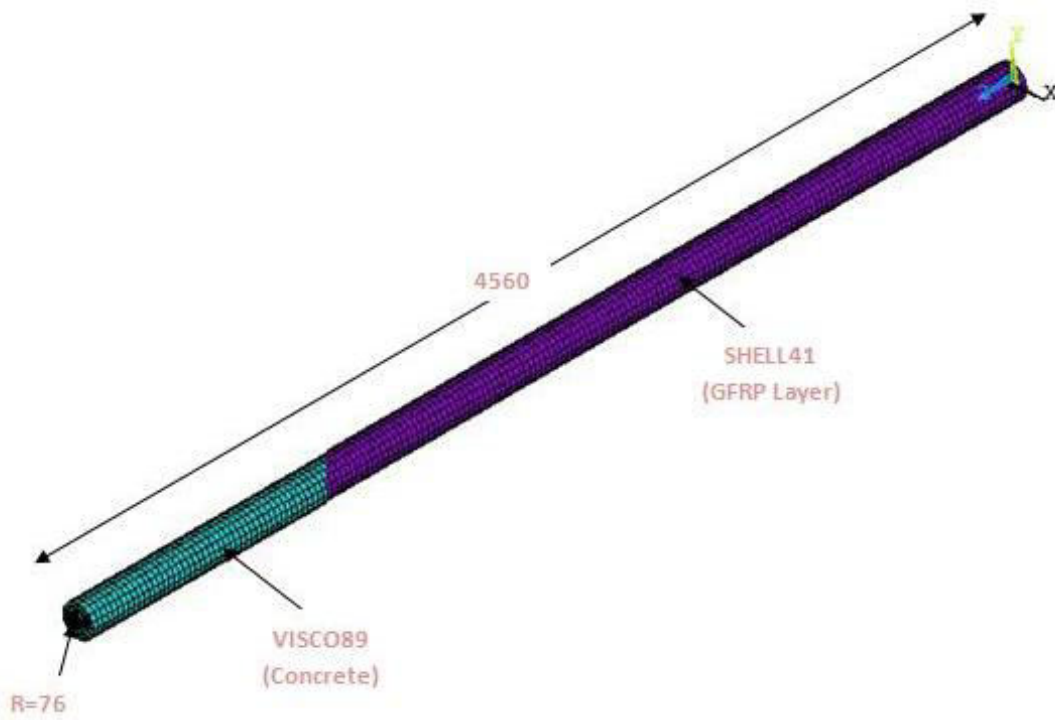
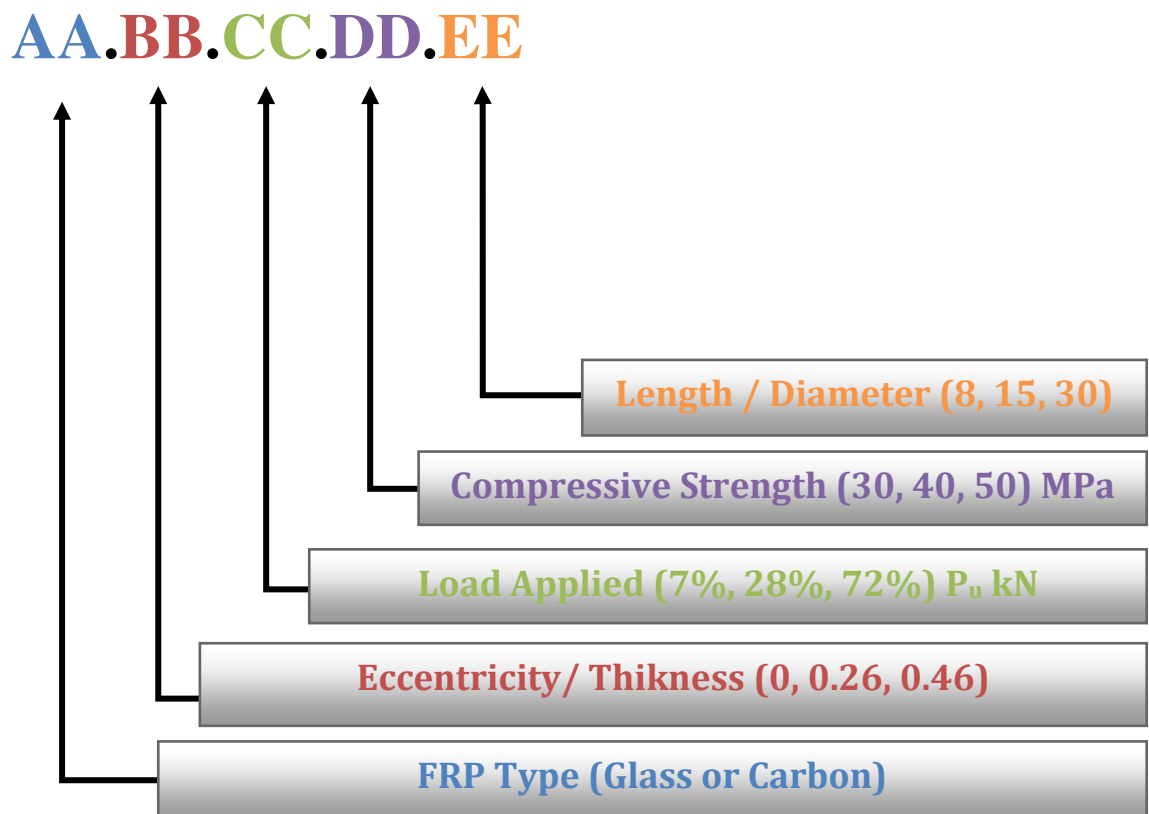


Fig.(5-6) Finite Element Model of (FWCC) with $l/d=30$

5-3: The Parametric:

The current work will study one hundred and sixty-two models with different parameter to predict behavior of strengthening columns when changing the parameter. We should note when studying the effect of one parameter, the other parameter remains constant.

The short name of the model consists of five symbols where



The analysis found that the maximum short –term load value was equal to 2800kN .Thus, the value of the load applied equal to (200, 800, 2000)kN according to the percentage of P_u

For example, the model (**C.0.7% P_u .30.8**) represents a column strengthening with **CFRP** and load applied with **zero** eccentricity with value **7% from maximum short-term load value** and the compressive strength was **30MPa** and l/d ratio **8**.The scheme below illustrates the parametric that is used in this chapter. All results of specimens summarized in Appendix B.

5.3.1: Magnitude of Sustained Load Effect:

The magnitude of sustained load is a major parameter which effects on the creep. To study this effect on the behavior of strengthening column selected two columns were selected (B1C1) of (*Al-Chami, 2006*) and (FWCC) of (*Naguib & Mirmiran, 2002*). For these selected columns, three values of load ($7\%P_u$, $28\%P_u$ and $72\%P_u$) kN, it was observed that increases of load lead to increase the creep strain, whereas increasing the sustained load from ($7\%P_u$ to $28\%P_u$)kN and ($28\%P_u$ to $72\%P_u$)kN causes an increase in creep strain about (3 and 1.5) times respectively. According to (*Mehta & Monterio, 2006; Neville & Brooks, 2010*) the stress applied by 40% of compression strength leads to the fact that the relationship between creep and stress is linear, while increasing the stress by more than 40% of the compression strength, the relationship is nonlinear due to the micro-crack where the micro-crack increases the value of creep strain. Fig. (5-7) to Fig. (5-33) show the effect of load on (*Al-Chami, 2006*) column and Fig.(5-34) to Fig.(5-60) show the effect of load of (*Naguib & Mirmiran, 2002*). Generally, the increasing of applied load leads to reduce the efficiency of strengthening column under long term where it increases creep strain.

*Note that the symbol (#) in figures refers to the variable factor.

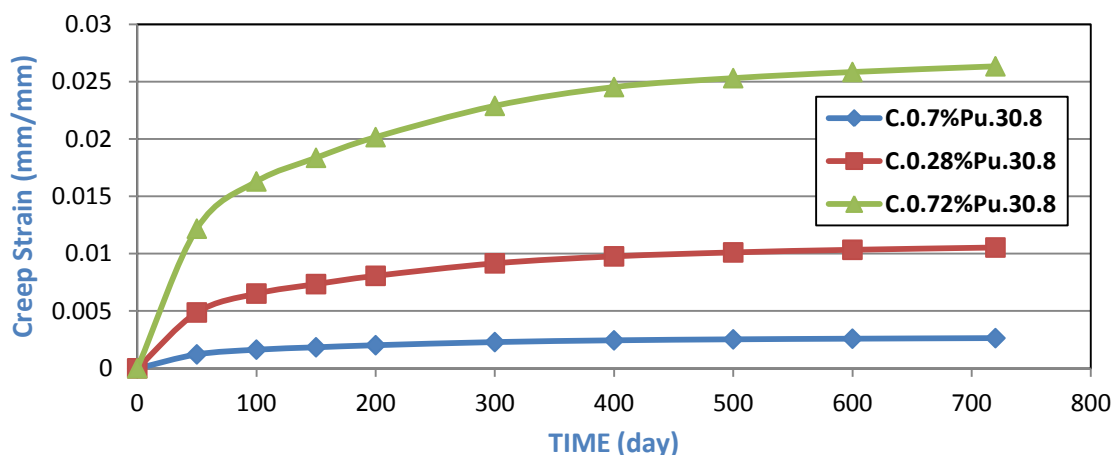


Fig.(5-7):Time vs Creep Strain Behavior for Models(C.0.#.30.8)

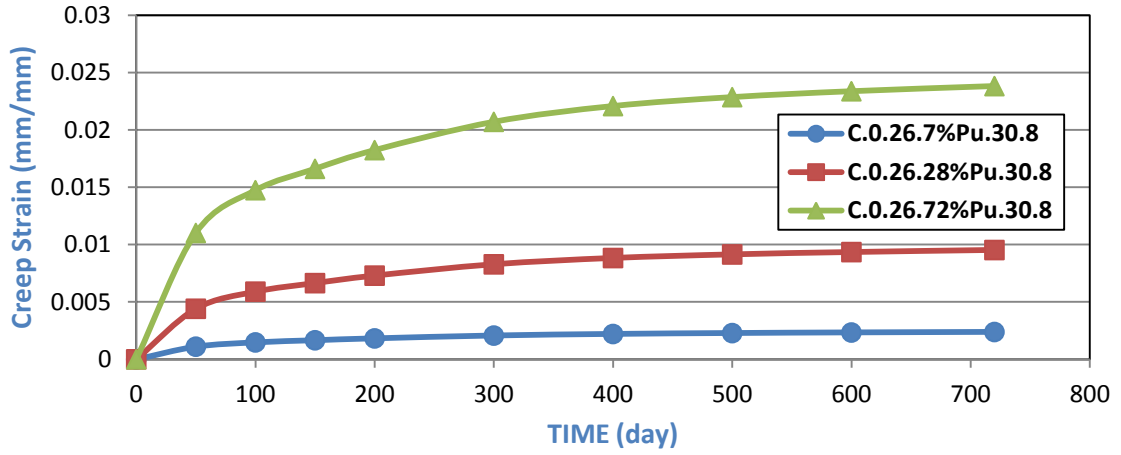


Fig.(5-8):Time vs Creep Strain Behavior for Models(C.0.26.#.30.8)

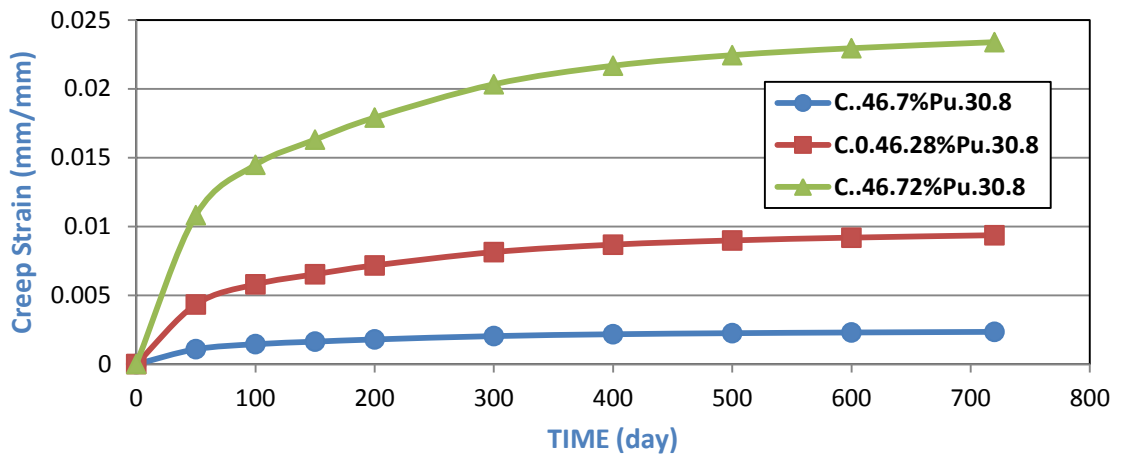


Fig.(5-9): Time vs Creep Strain Behavior for Models(C.0.46.#.30.8)

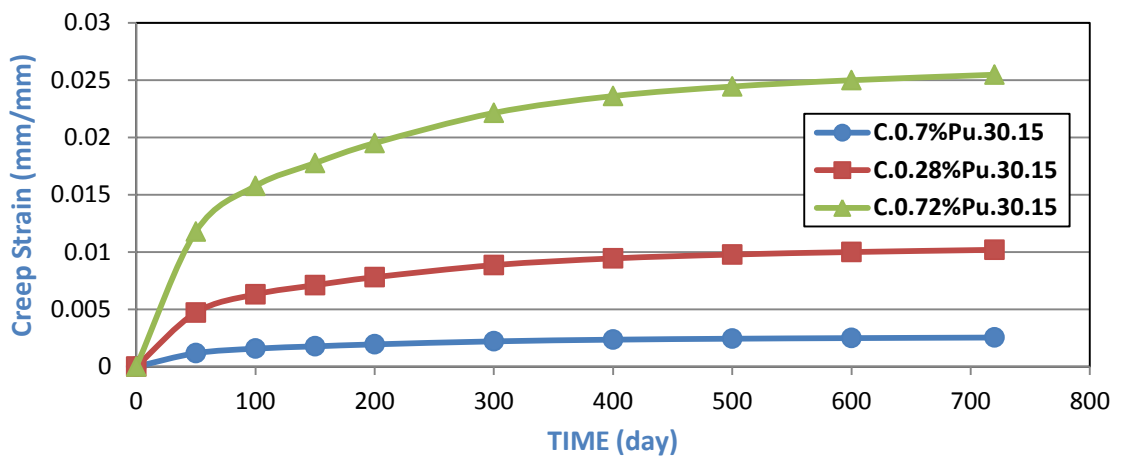


Fig.(5-10):Time vs Creep Strain Behavior for Models(C.0.#.30.15)

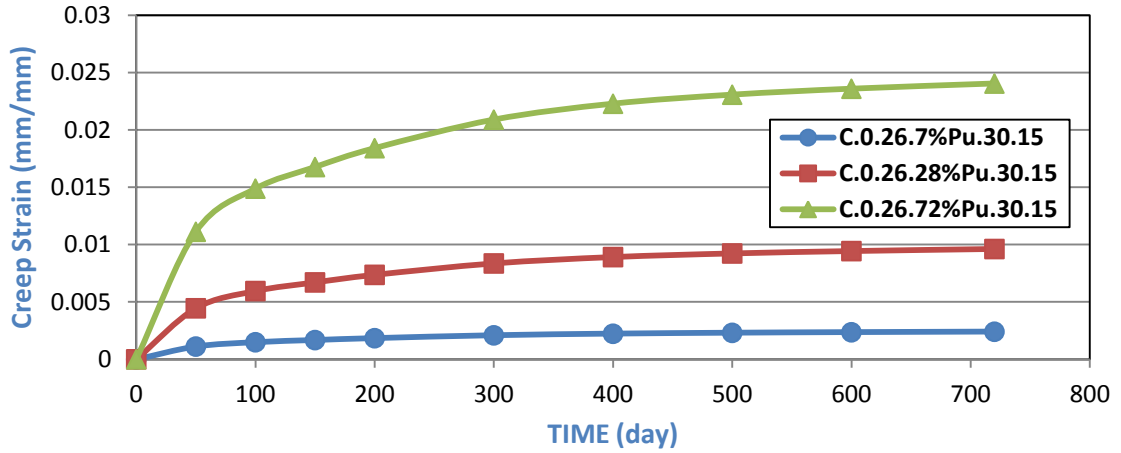


Fig.(5-11) :Time vs Creep Strain Behavior for Models(C.0.26.#.30.15)

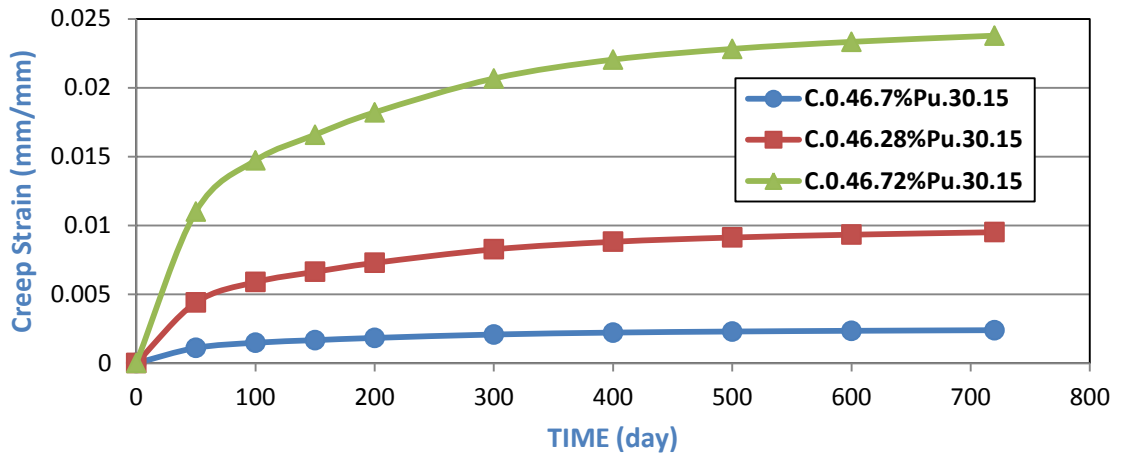


Fig.(5-12) :Time vs Creep Strain Behavior for Models(C.0.46.#.30.15)

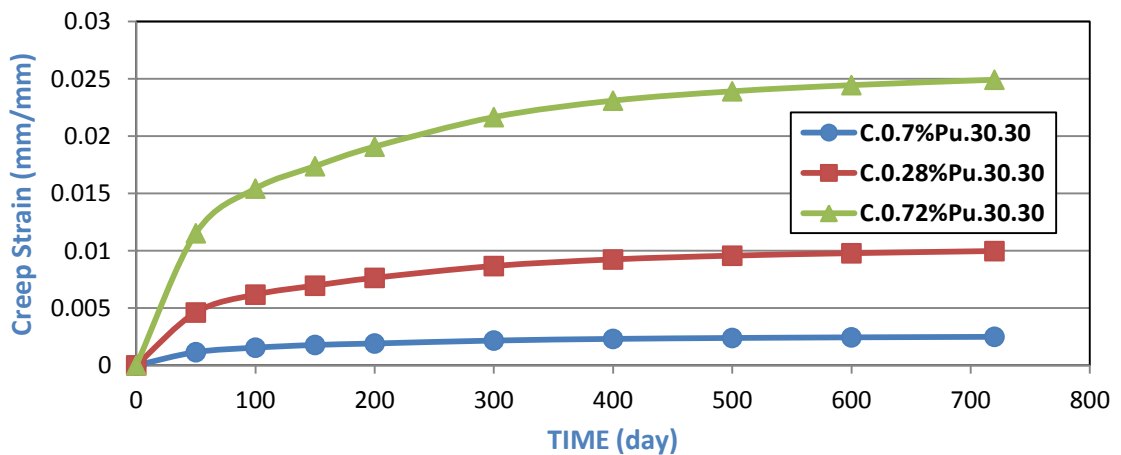


Fig.(5-13) :Time vs Creep Strain Behavior for Models(C.0.#.30.30)

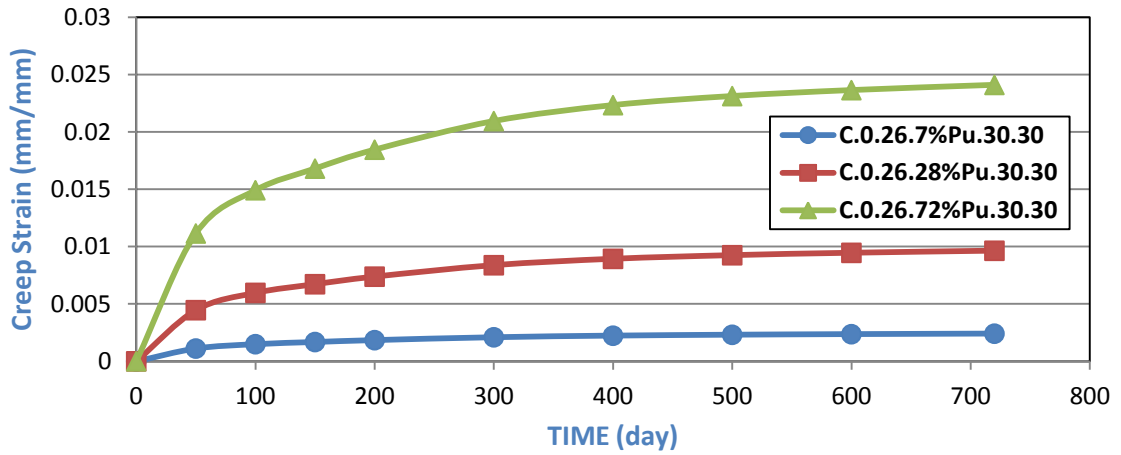


Fig.(5-14) :Time vs Creep Strain Behavior for Models(C.0.26.#.30.30)

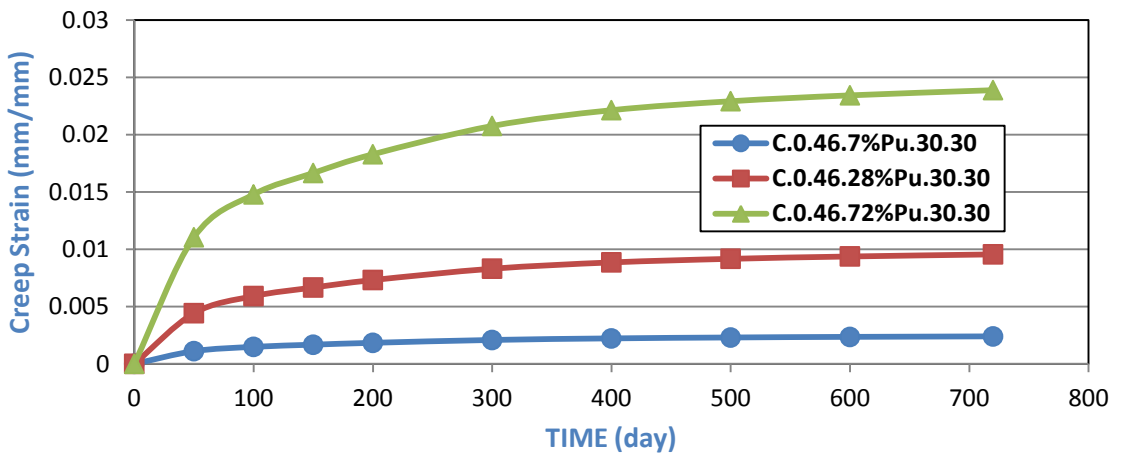


Fig.(5-15) :Time vs Creep Strain Behavior for Models(C.0.46.#.30.30)

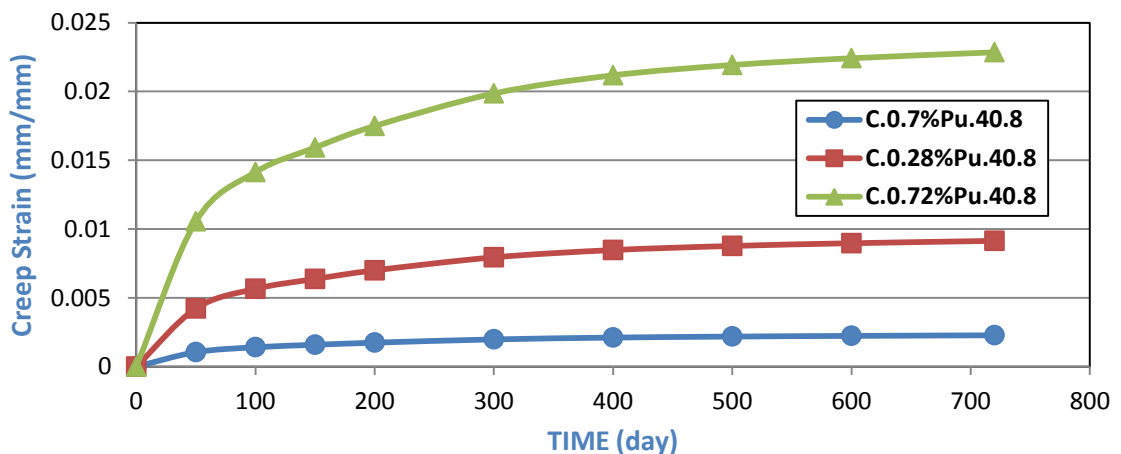


Fig.(5-16) :Time vs Creep Strain Behavior for Models(C.0.#.40.8)

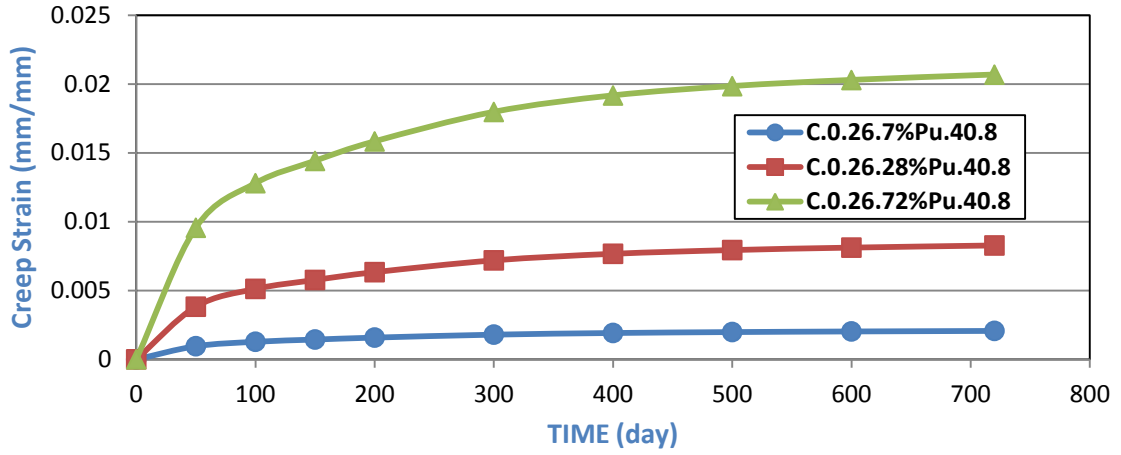


Fig.(5-17) :Time vs Creep Strain Behavior for Models(C.0.26.#.40.8)

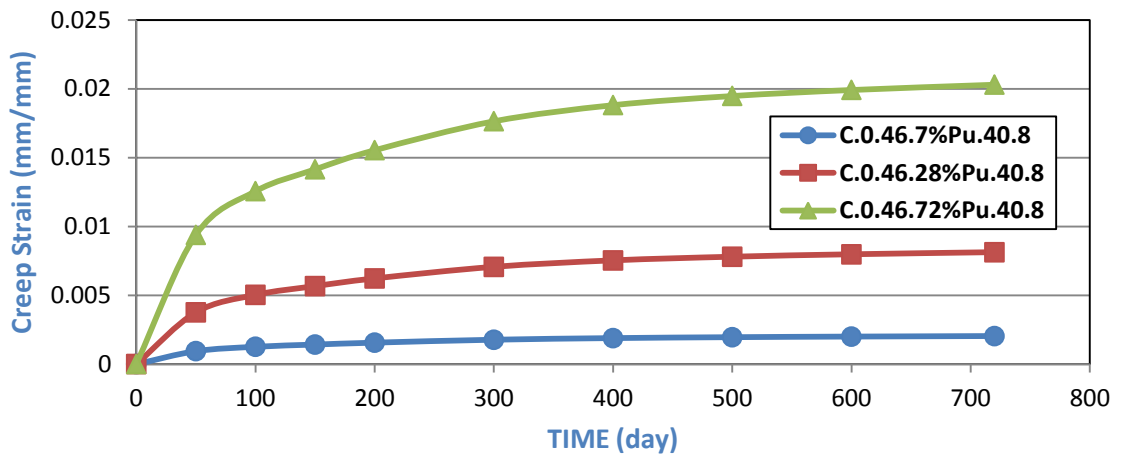


Fig.(5-18) :Time vs Creep Strain Behavior for Models(C.0.46.#.40.8)

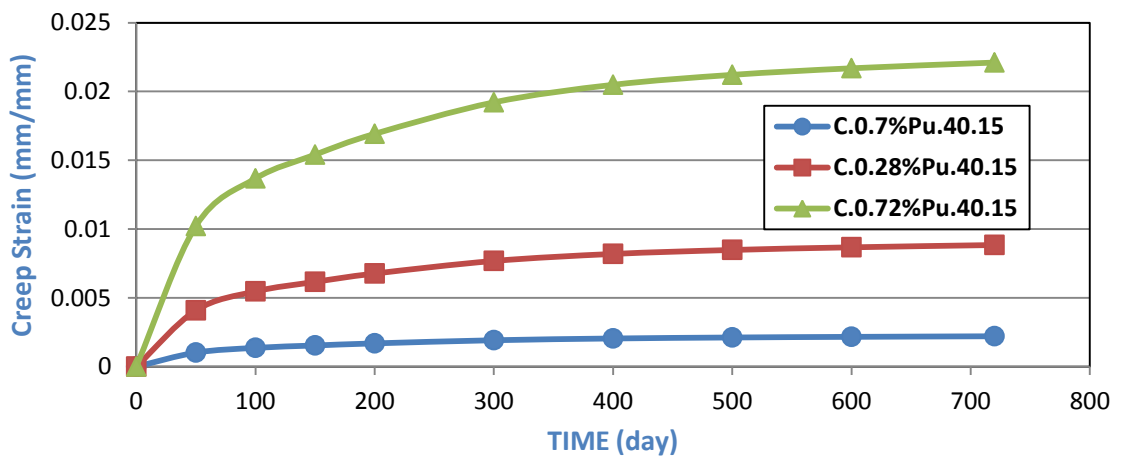


Fig.(5-19) :Time vs Creep Strain Behavior for Models(C.0.#.40.15)

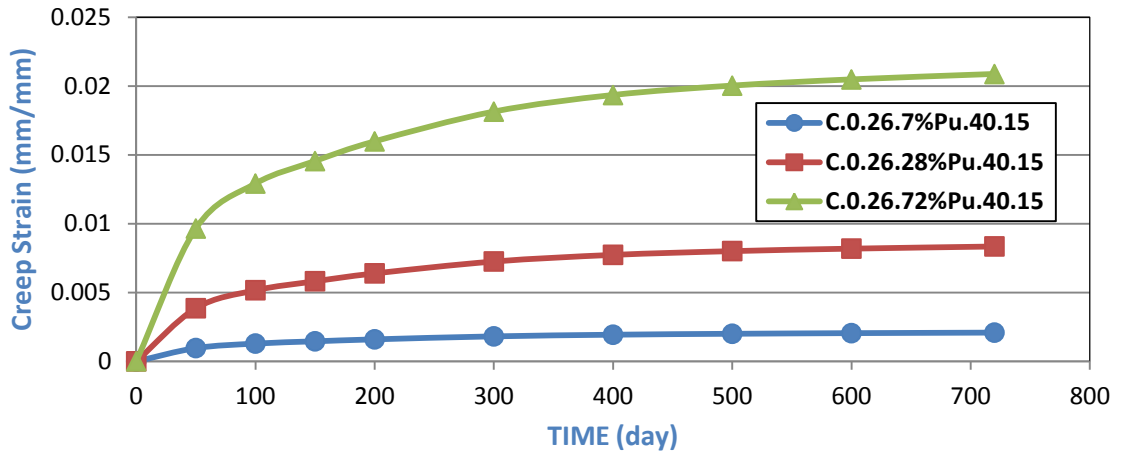


Fig.(5-20) :Time vs Creep Strain Behavior for Models(C.0.26.#.40.15)

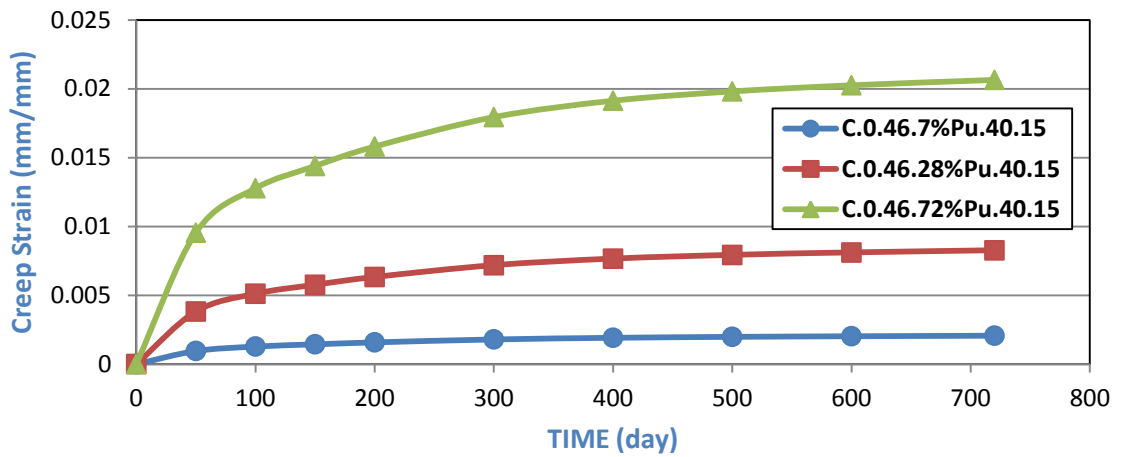


Fig.(5-21) :Time vs Creep Strain Behavior for Models(C.0.46.#.40.15)

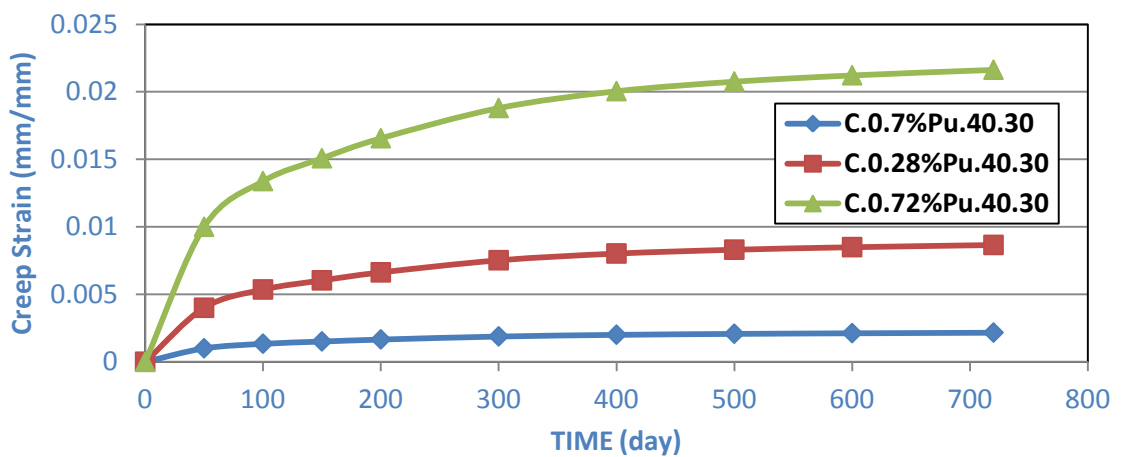


Fig.(5-22) :Time vs Creep Strain Behavior for Models(C.0.#.40.30)

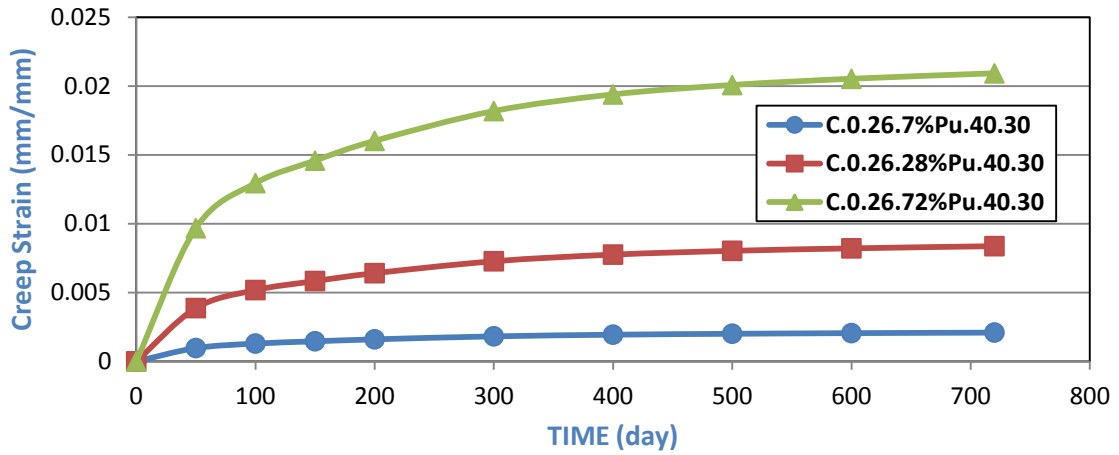


Fig.(5-23) :Time vs Creep Strain Behavior for Models(C.0.26.#.40.30)

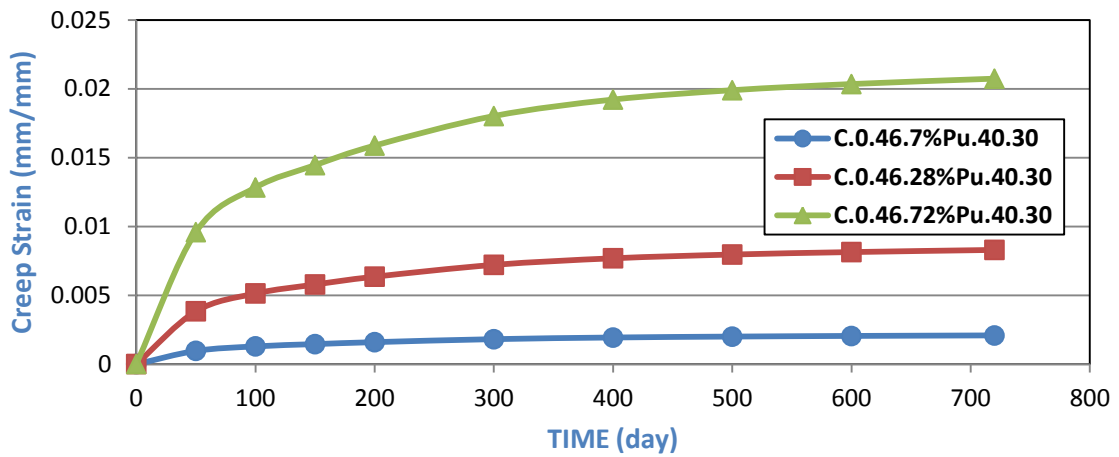


Fig.(5-24) :Time vs Creep strain Behavior for Models(C.0.46.#.40.30)

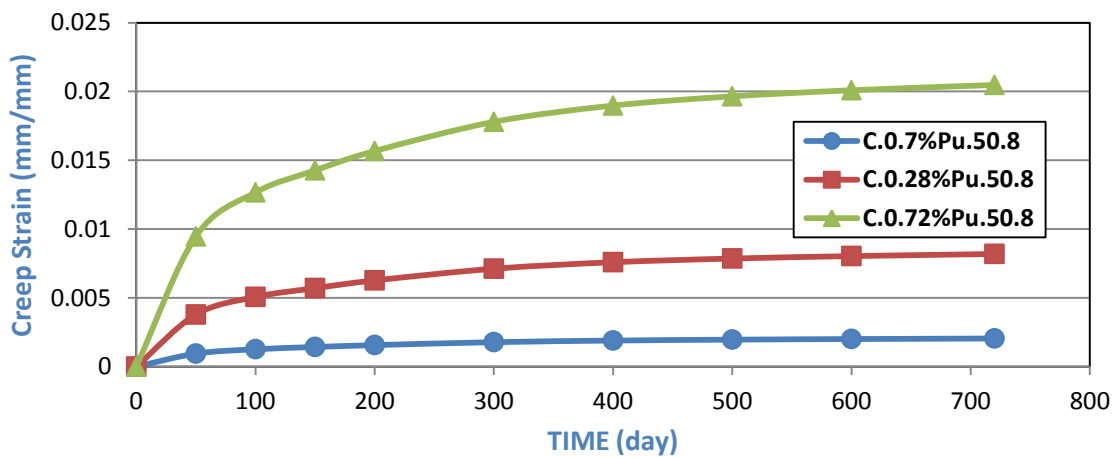


Fig.(5-25) :Time vs Creep Strain Behavior for Models(C.0.#.50.8)

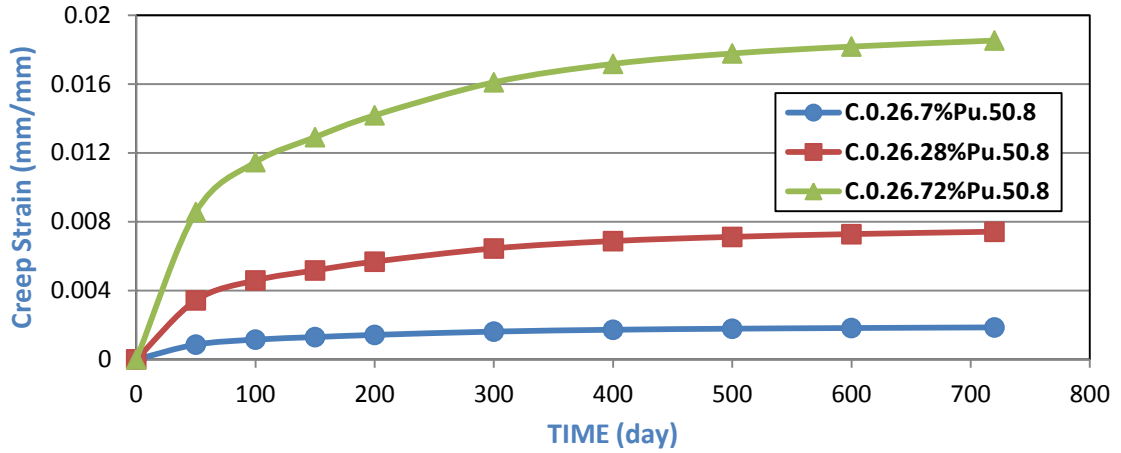


Fig.(5-26) :Time vs Creep Strain Behavior for Models(C.0.26.#.50.8)

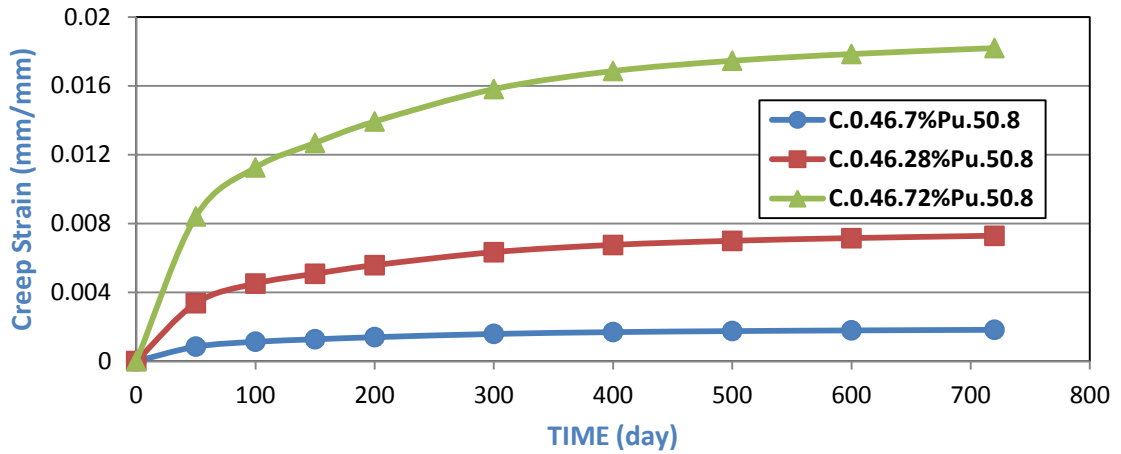


Fig.(5-27) :Time vs Creep Strain Behavior for Models(C.0.46.#.50.8)

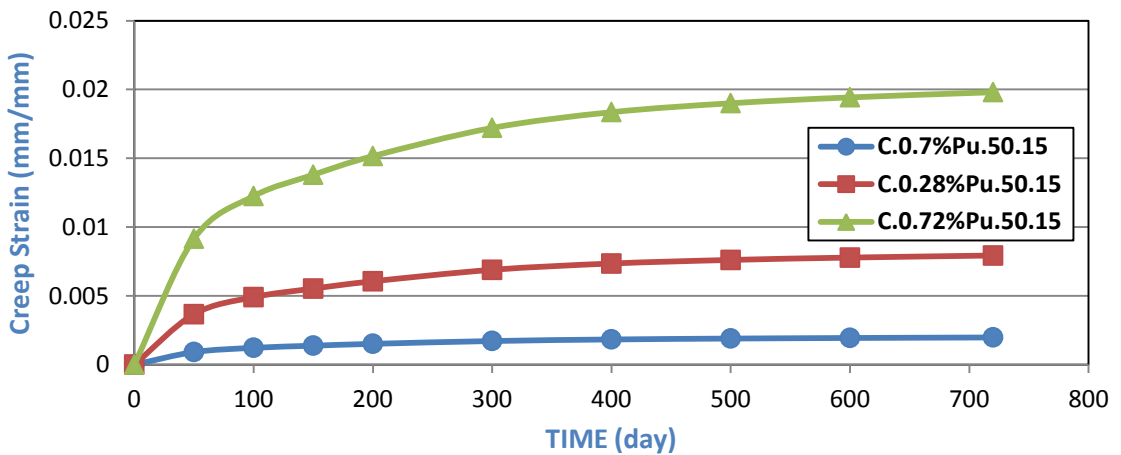


Fig.(5-28) :Time vs Creep Strain Behavior for Models(C.0.#.50.15)

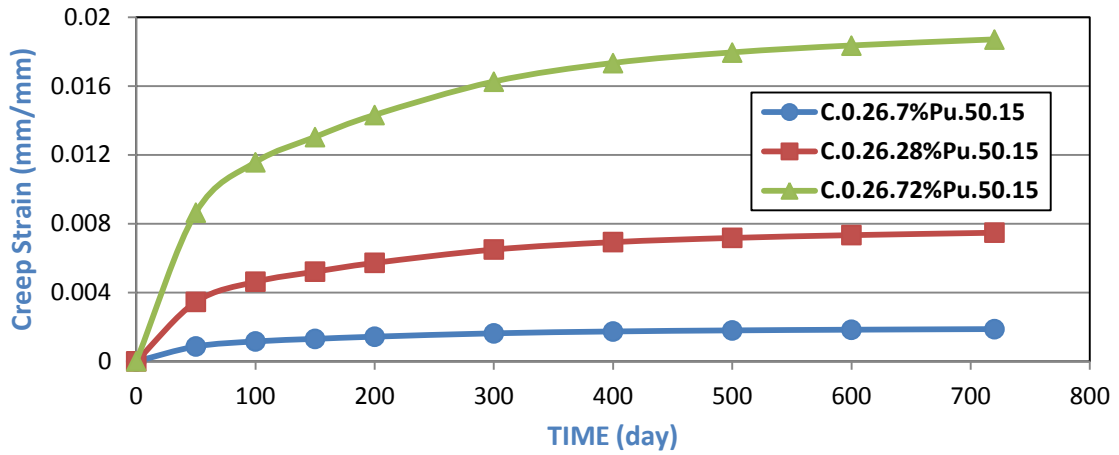


Fig.(5-29) :Time vs Creep Strain Behavior for Models(C.0.26.#.50.15)

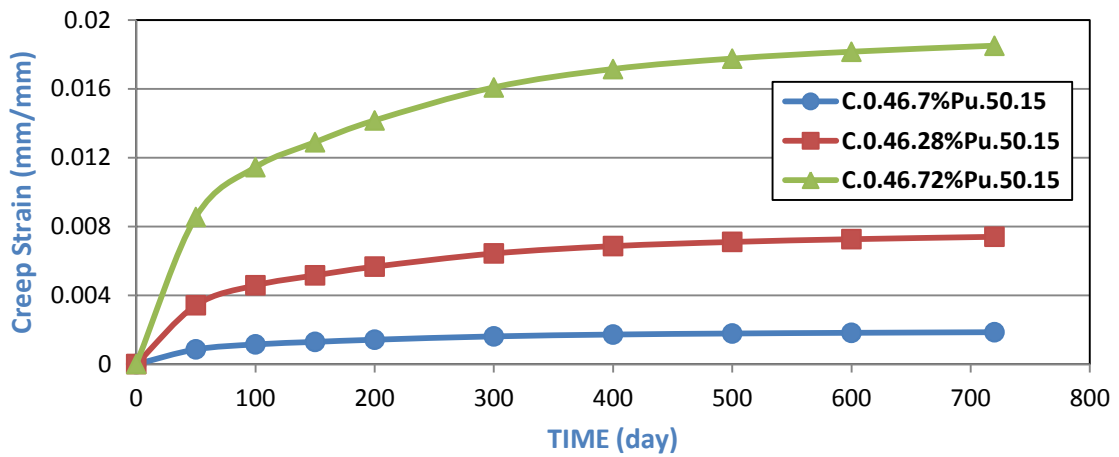


Fig.(5-30) :Time vs Creep Strain Behavior for Models(C.0.46.#.50.15)

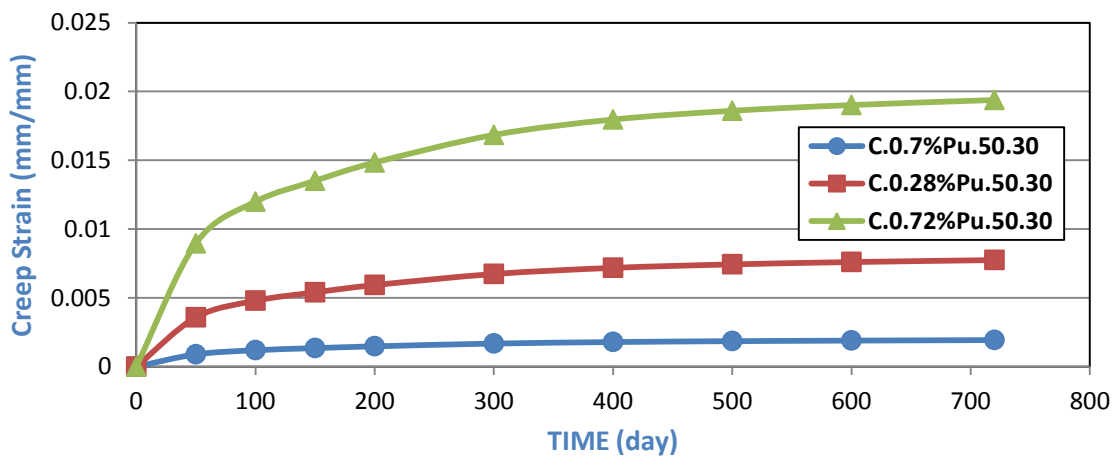


Fig.(5-31) :Time vs Creep Strain Behavior for Models(C.0.#.50.30)

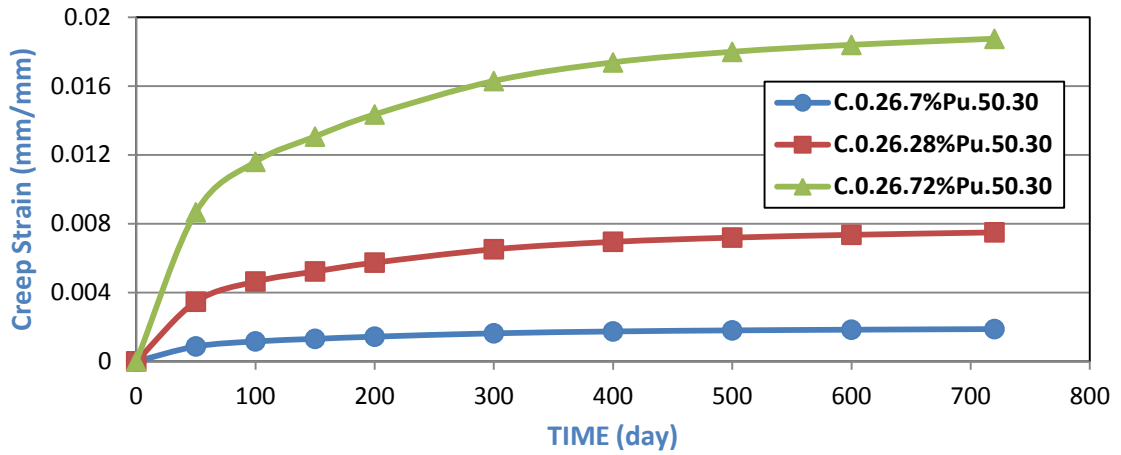


Fig.(5-32) :Time vs Creep Strain Behavior for Models(C.0.26.#.50.30)

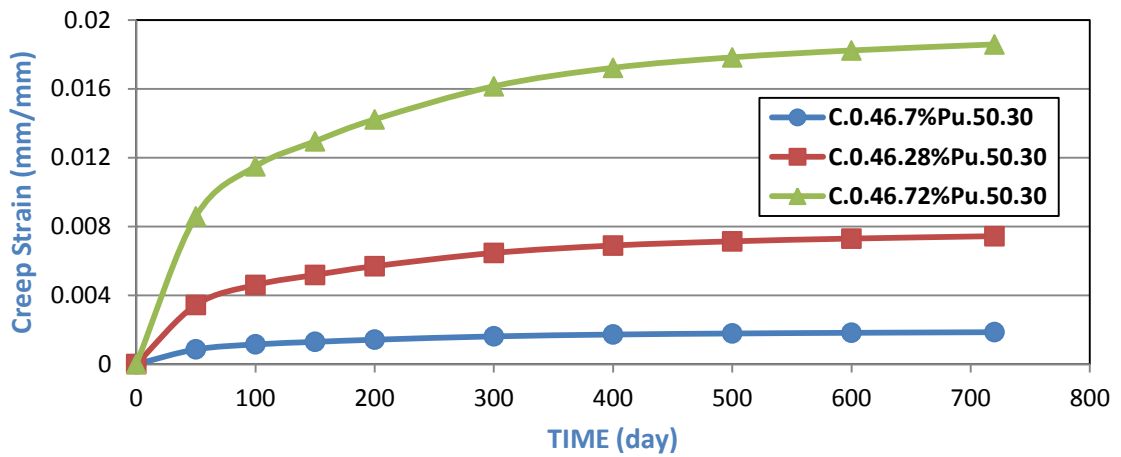


Fig.(5-33) :Time vs Creep Strain Behavior for models(C.0.46.#.50.30)

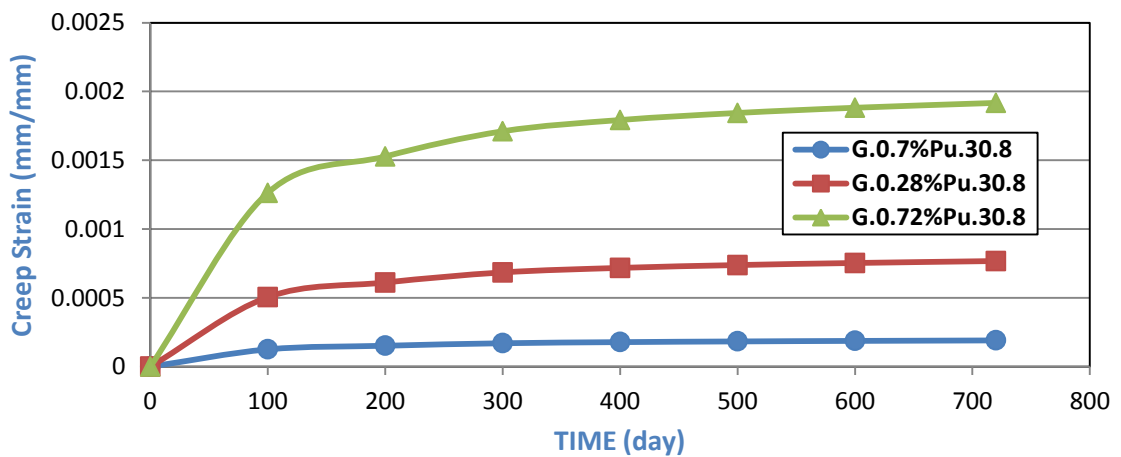


Fig.(5-34) :Time vs Creep Strain Behavior for Models(G.0.#.30.8)

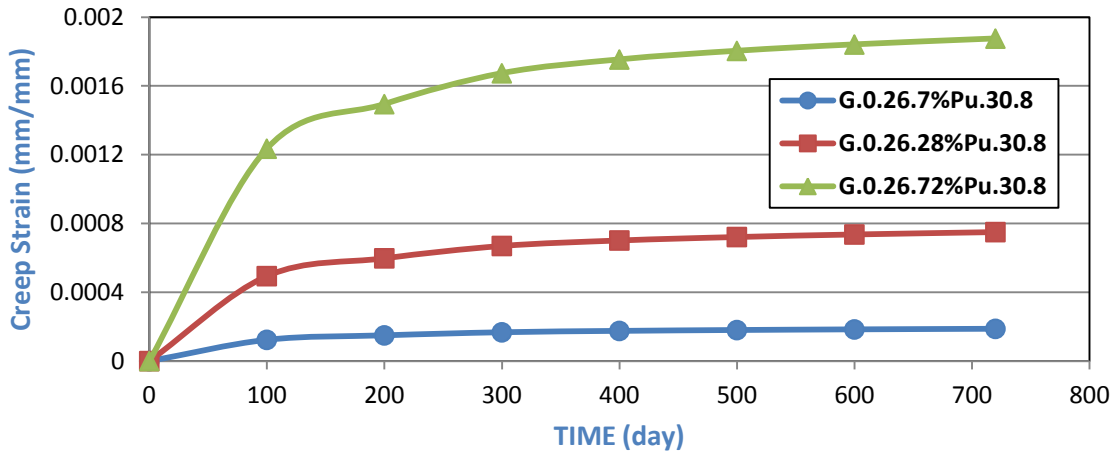


Fig.(5-35) :Time vs Creep Strain Behavior for Models(G.0.26.#.30.8)

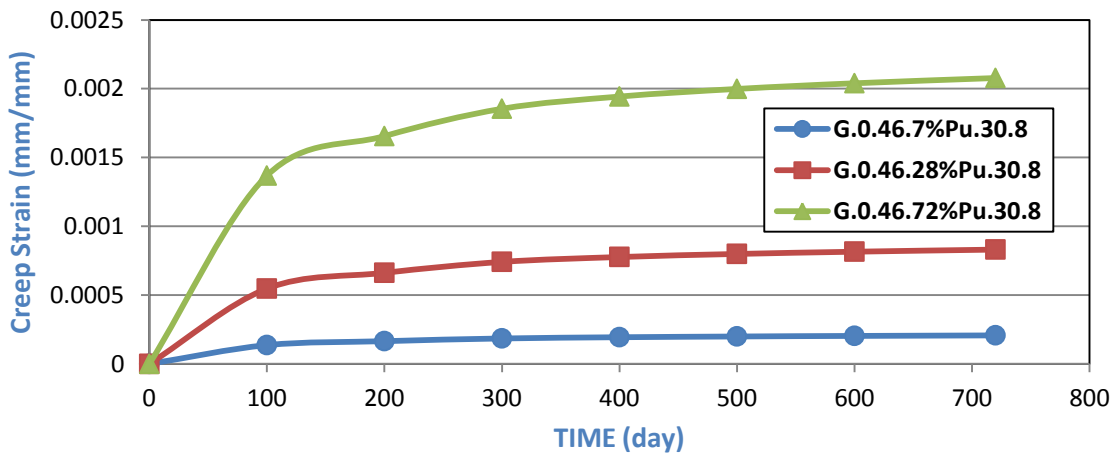


Fig.(5-36) :Time vs Creep Strain Behavior for Models(G.0.46.#.30.8)

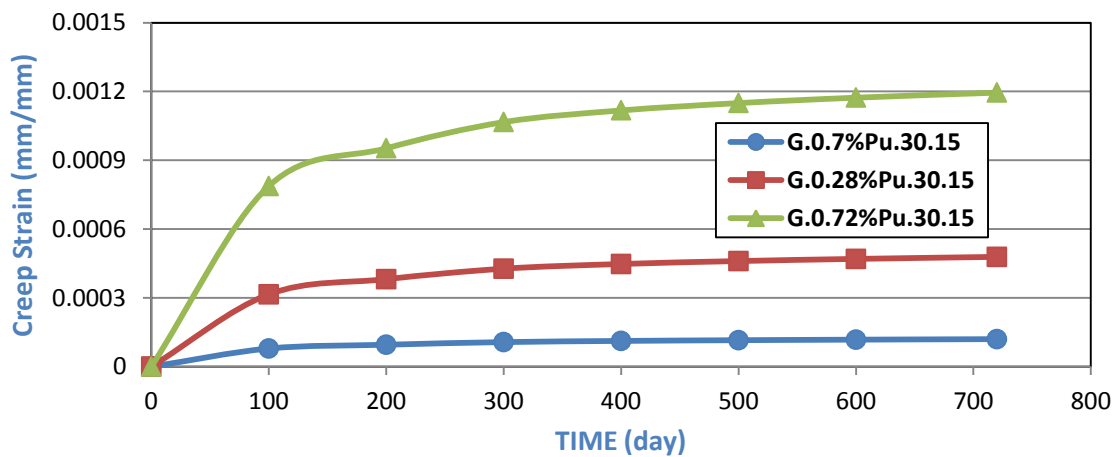


Fig.(5-37) :Time vs Creep Strain Behavior for Models(G.0.#.30.15)

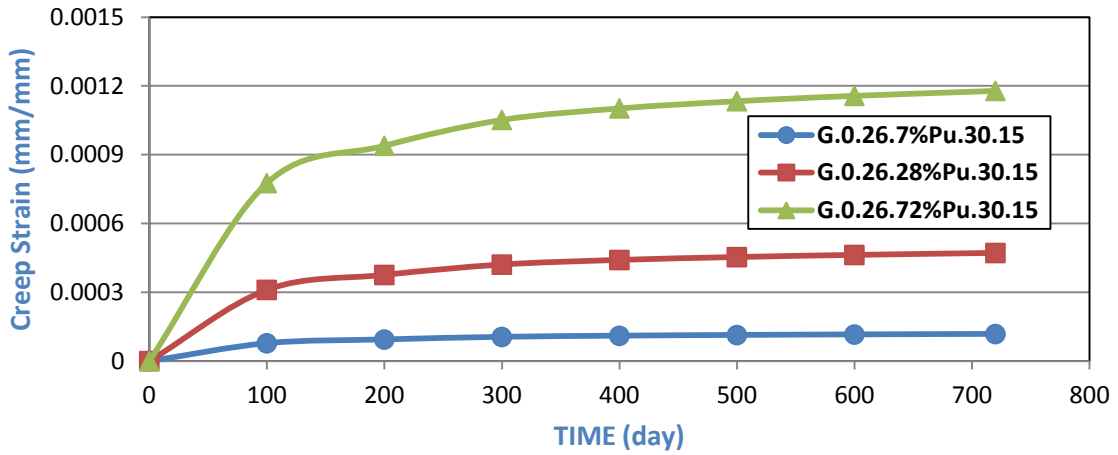


Fig.(5-38) :Time vs Creep strain behavior for models(G.0.26.#.30.15)

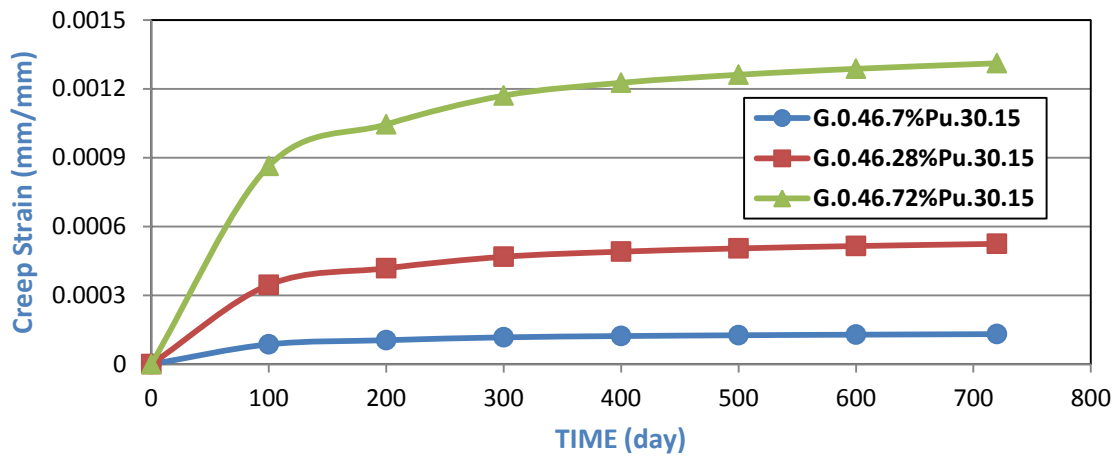


Fig.(5-39) :Time vs Creep Strain Behavior for Models(G.0.46.#.30.15)

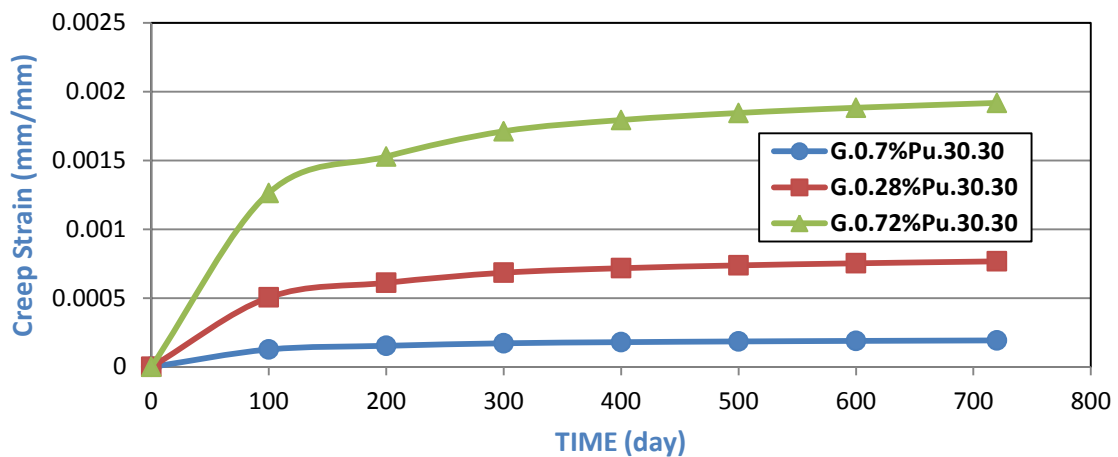


Fig.(5-40) :Time vs Creep Strain Behavior for Models(G.0.#.30.30)

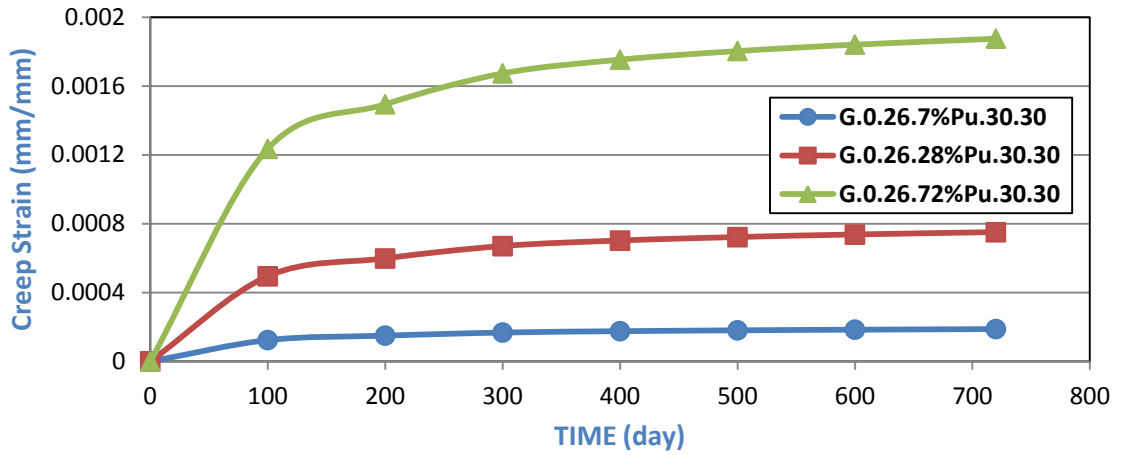


Fig.(5-41) :Time vs Creep Strain Behavior for Models(G.0.26.#.30.30)

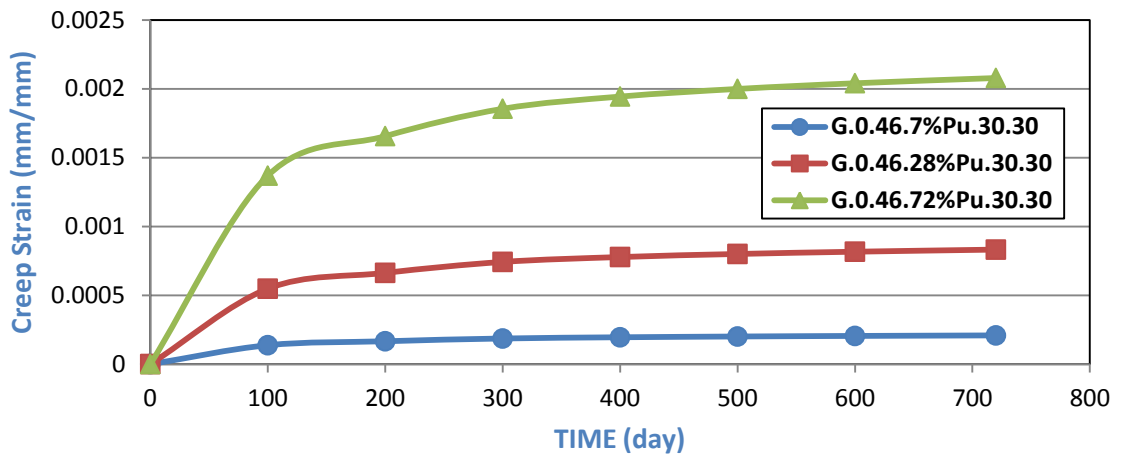


Fig.(5-42) :Time vs Creep Strain Behavior for Models(G.0.46.#.30.30)

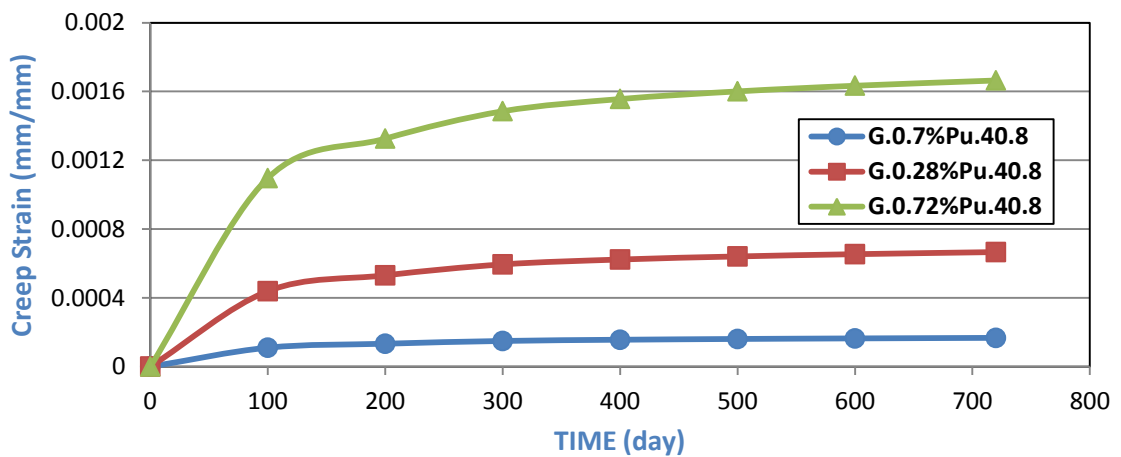


Fig.(5-43) :Time vs Creep Strain Behavior for Models(G.0.#.40.8)

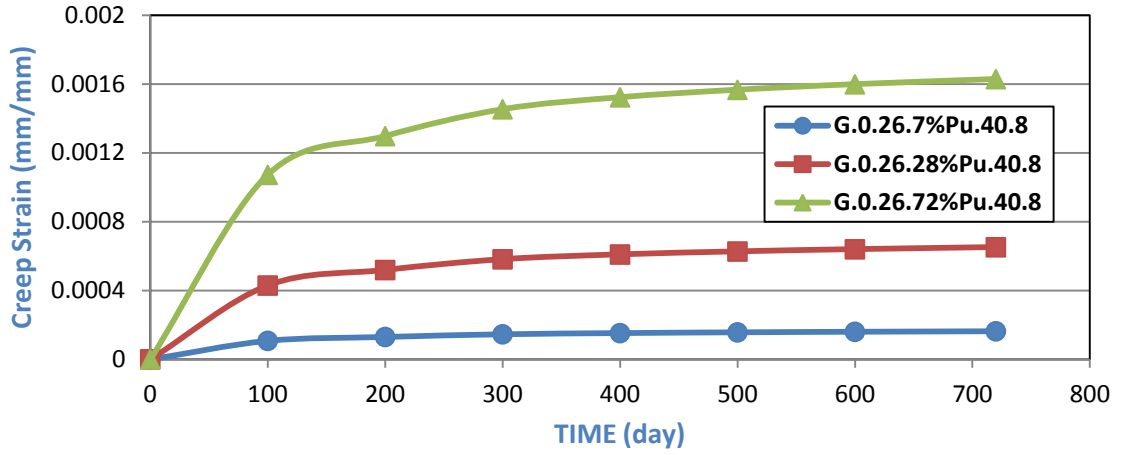


Fig.(5-44) :Time vs Creep Strain Behavior for Models(G.0.26.#.40.8)

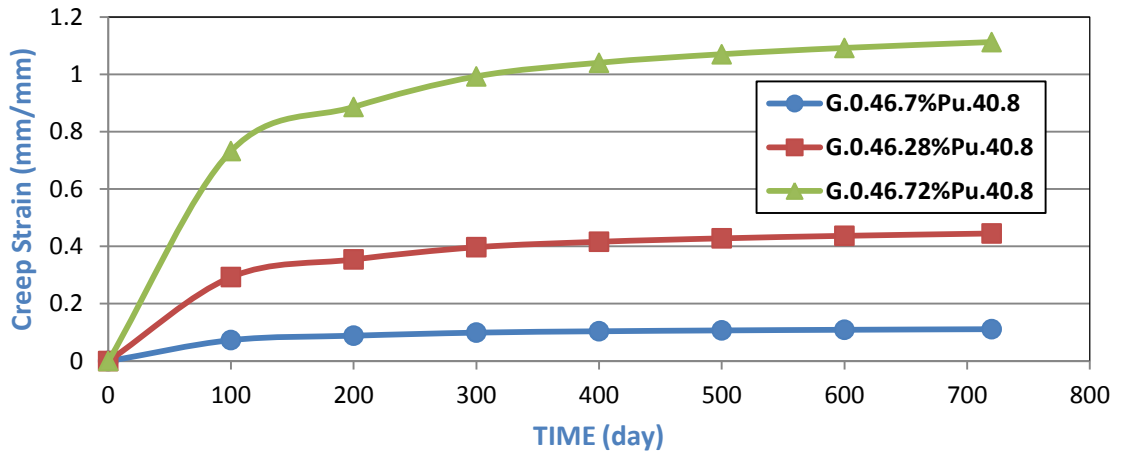


Fig.(5-45) :Time vs Creep Strain Behavior for Models(G.0.46.#.40.8)

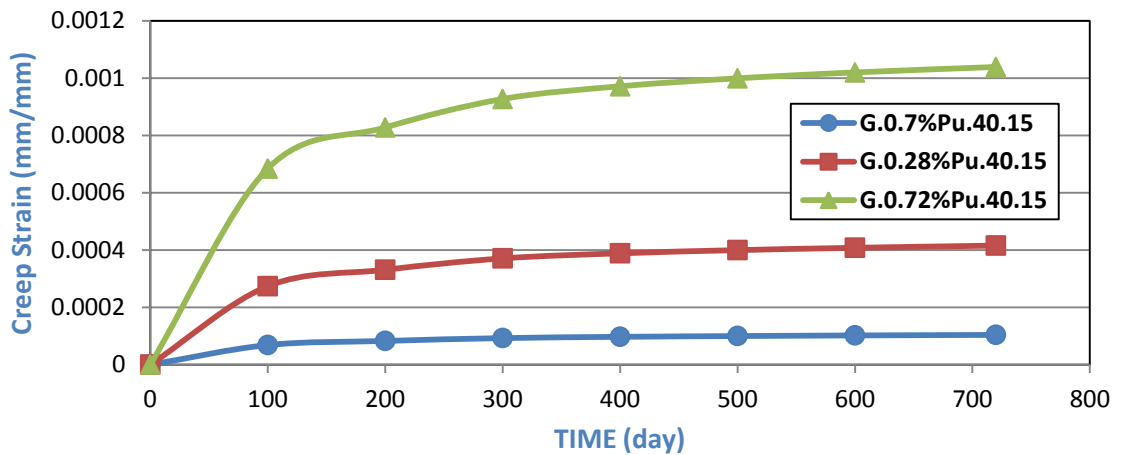


Fig.(5-46) :Time vs Creep Strain Behavior for Models(G.0.#.40.15)

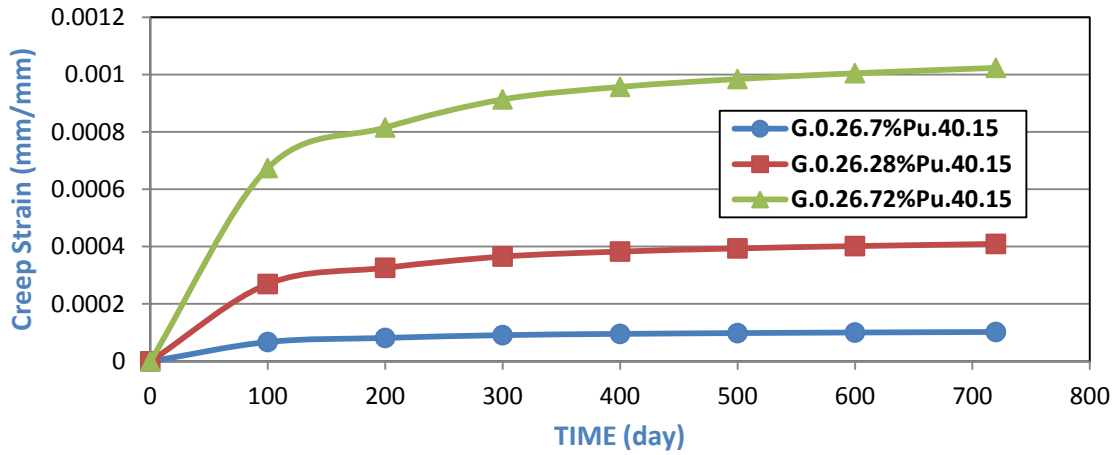


Fig.(5-47) :Time vs Creep Strain Behavior for Models(G.0.26.#.40.15)

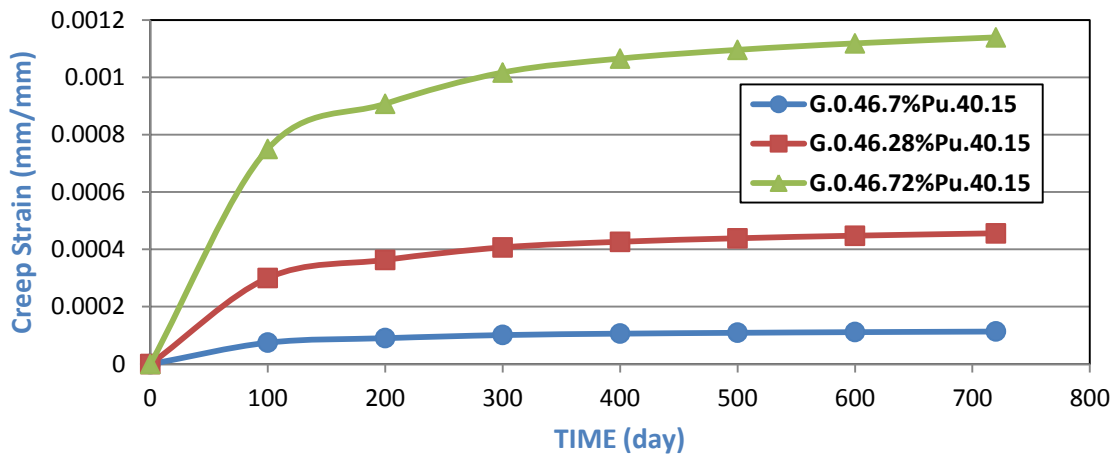


Fig.(5-48) :Time vs Creep Strain Behavior for Models(G.0.46.#.40.15)

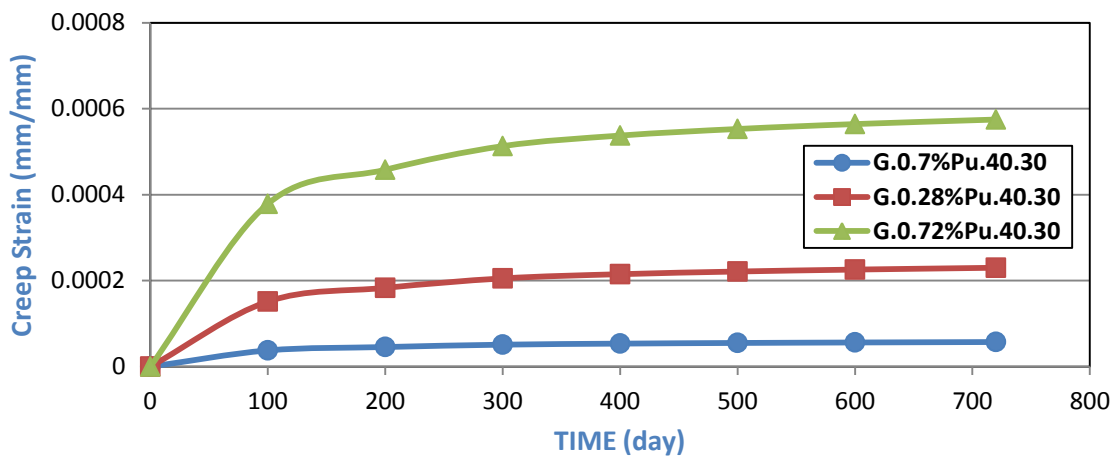


Fig.(5-49) :Time vs Creep Strain Behavior for Models(G.0.#.40.30)

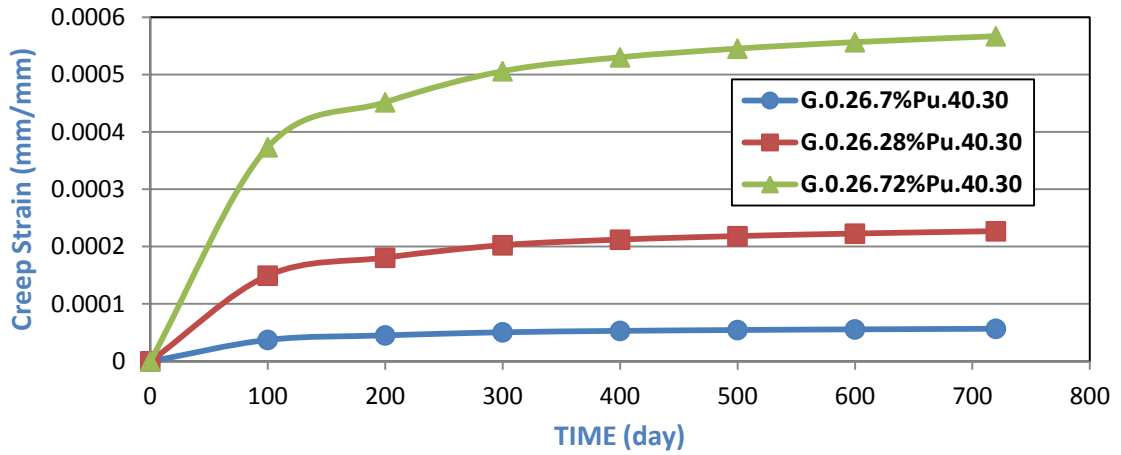


Fig.(5-50) :Time vs Creep Strain Behavior for Models(G.0.26.#.40.30)

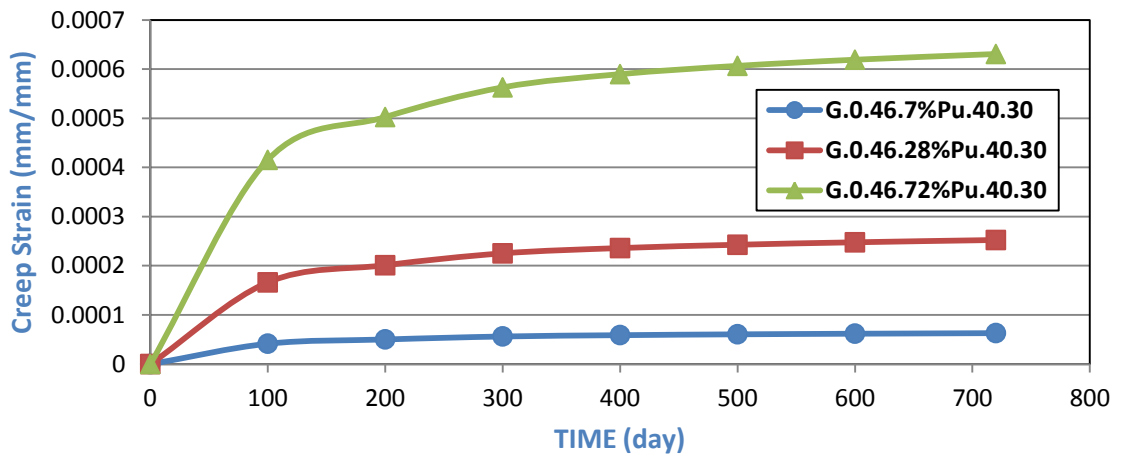


Fig.(5-51) :Time vs Creep Strain Behavior for Models(G.0.46.#.40.30)

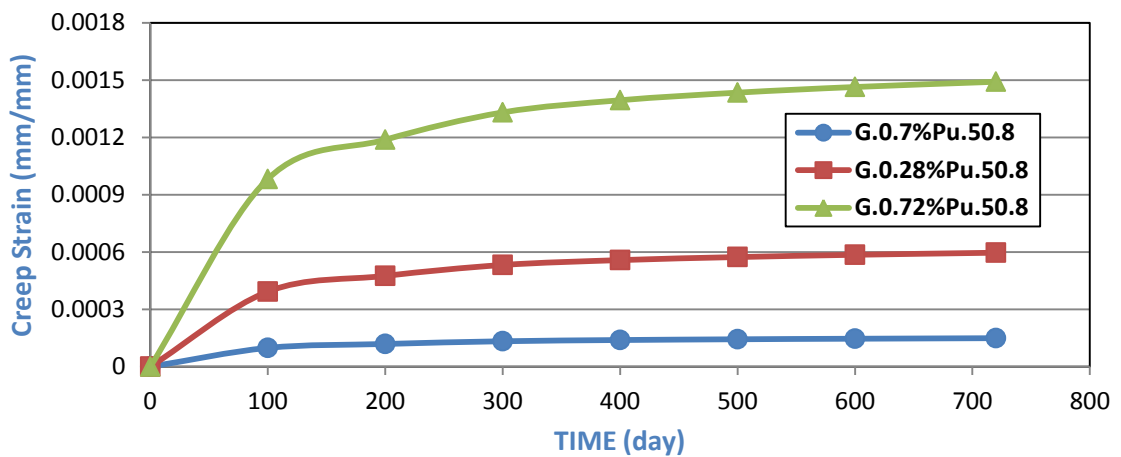


Fig.(5-52) :Time vs Creep Strain Behavior for Models(G.0.#.50.8)

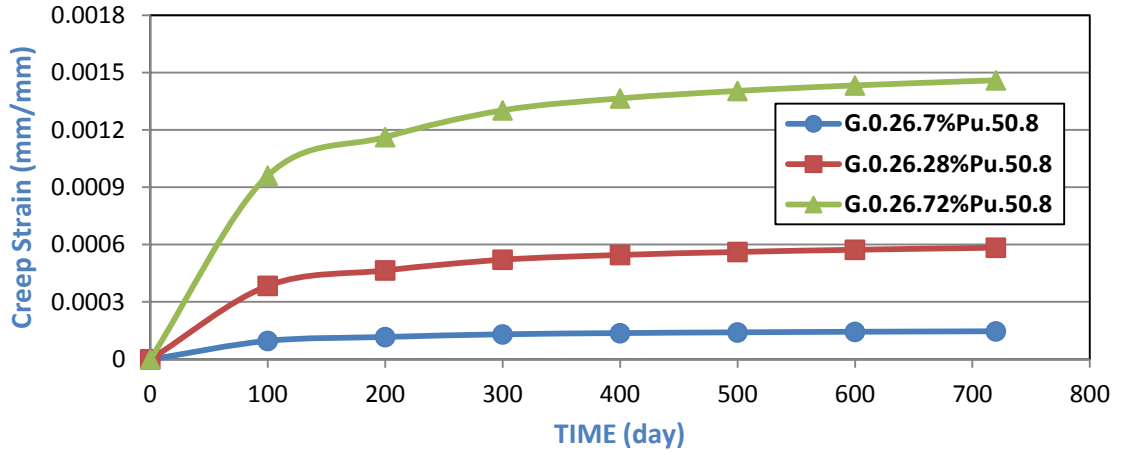


Fig.(5-53) :Time vs Creep Strain Behavior for Models(G.0.26.#.50.8)

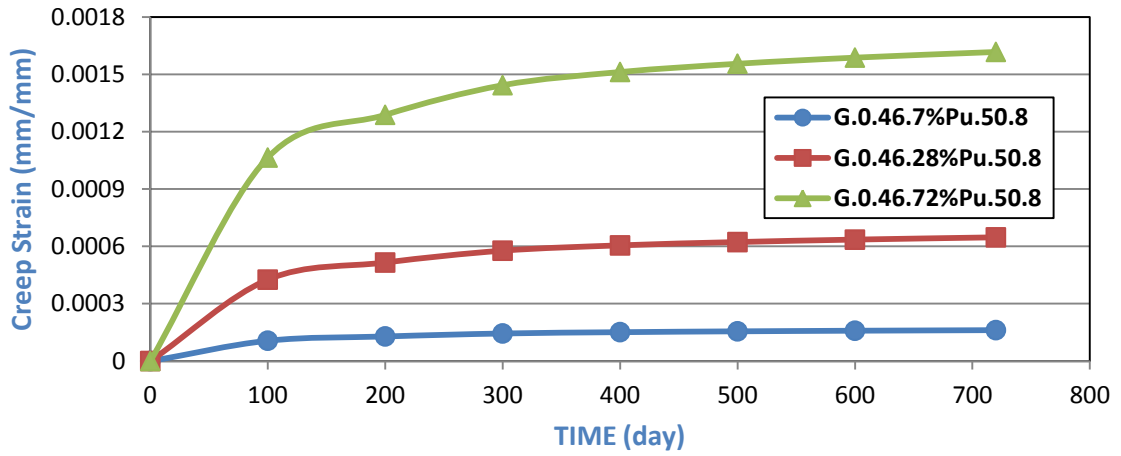


Fig.(5-54) :Time vs Creep Strain Behavior for Models(G.0.46.#.50.8)

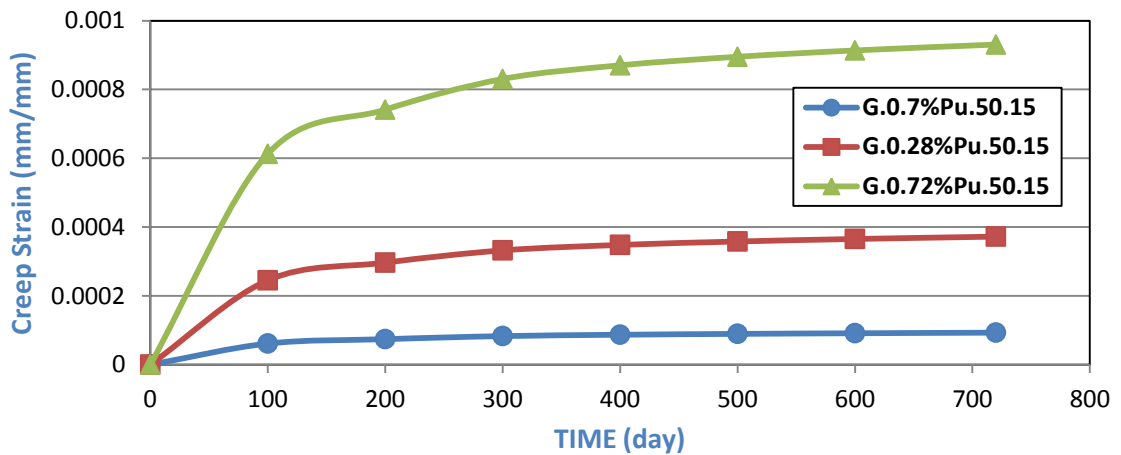


Fig.(5-55) :Time vs Creep Strain Behavior for Models(G.0.#.50.15)

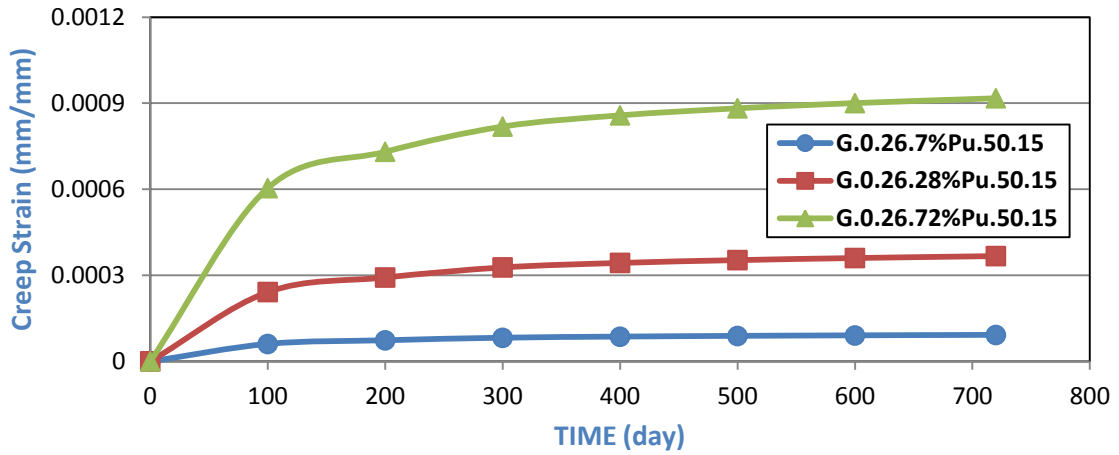


Fig.(5-56) :Time vs Creep Strain Behavior for Models(G.0.26.#.50.15)

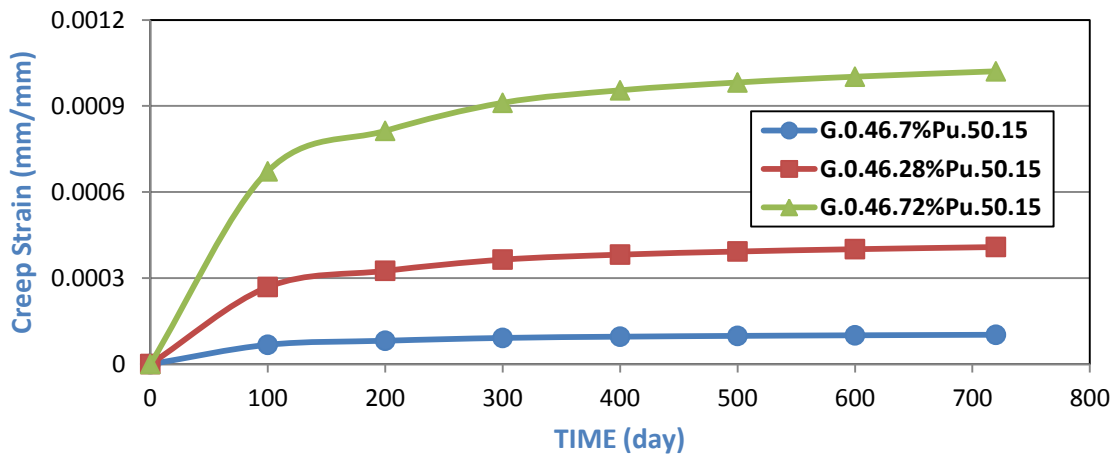


Fig.(5-57) :Time vs Creep Strain Behavior for Models(G.0.46.#.50.15)

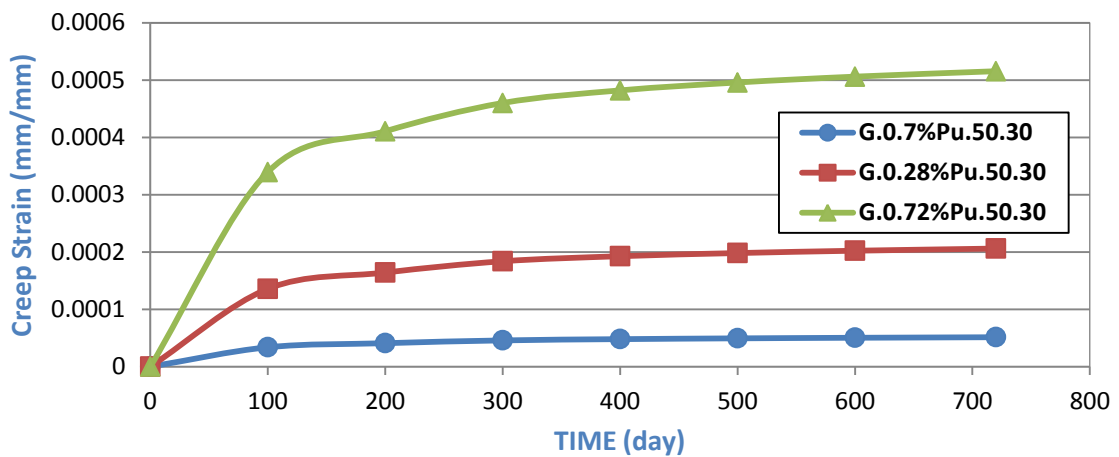


Fig.(5-58) :Time vs Creep Strain Behavior for Models(G. 0.#.50.30)

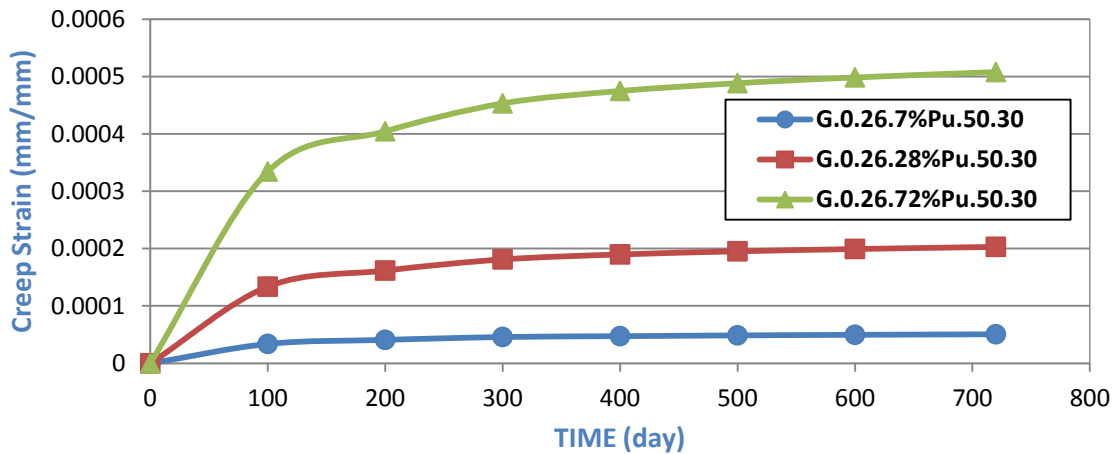


Fig.(5-59) :Time vs Creep Strain Behavior for Models(G. 0.26.#.50.30)

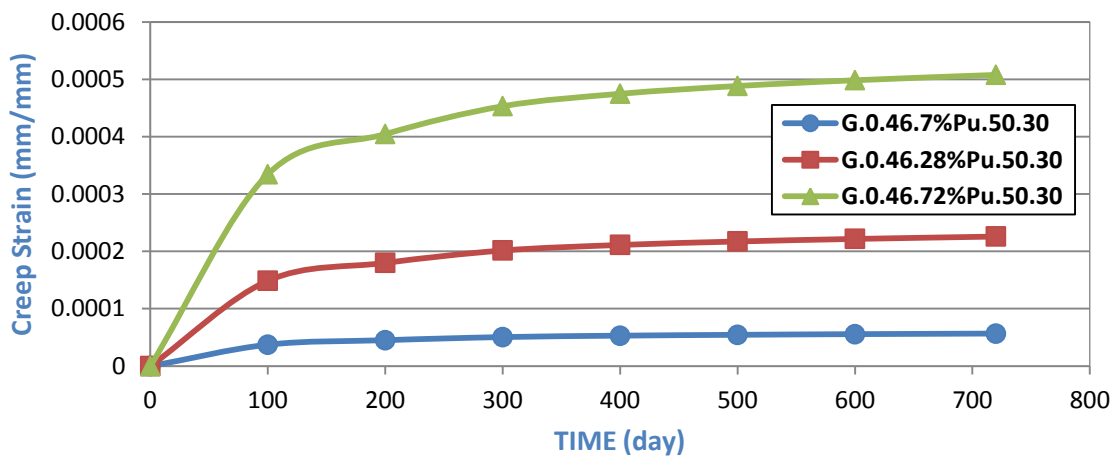


Fig.(5-60) :Time vs Creep Strain Behavior for Models(G. 0.46.#.50.30)

5.3.2: Eccentricity Effect:

To study the effect of the eccentricity on the behavior of strengthening concrete columns, three values of e/h ratio were selected (0, 0.26 and 0.46). For (B1C1). From figures of section B.2 in Appendix B, it was observed that increases of e/h ratio lead to decrease the creep strain, whereas increasing the e/h from (0 to 0.26) and (0.26 to 0.46) leads to decrease creep strain by 9.5% and 1.8%, respectively, while for (FWCC) the increase of e/h ratio from (0 to 0.26) leads to decrease creep strain by 3.2% and increasing the e/h ratio from (0.26 to 0.46) leads to increase the creep strain by 11.3%. Generally, the increasing of e/h ratio leads to enhance the strength of a strengthening concrete column under

long term where it decreases creep strain, due to the generation of tension strains as a result of applied load with eccentricity that reduces the strains of creep.

5.3.3: Length Effect:

This effect was expressed by volume-surface ratio. The member size has an effect on the magnitude of concrete creep due to moisture and temperature gradients between the surfaces and the interior of the member, which is a form of micro-curing. This micro-curing causes a different type of creep through the depth of the member. To study this effect on the behavior of strengthening concrete column three values of the l/d ratio (8, 15 and 30) were selected. From figures reviewed in section B.3 of Appendix B, it was observed that increases of l/d lead to decrease the creep strain, but the effect on the column of (B1C1) was very low, whereas increasing the ratio from (8 to 15) and from (15 to 30) leads to decrease creep strain by 3.3% and 2.17%, respectively, while the effect on the (FWCC) column was very clear, whereas increasing the ratio of (8 to 15) and (15 to 30) leads to decrease creep strain by 37.63% and 44.64% respectively. It has been found that creep decreases with an increase in size of the specimen. The effect of shrinkage and the fact that creep at the surface occurs under drying conditions may explain this phenomenon; it is therefore greater than within the core of the specimen (*Bruegger, 1974*).

5.3.4: Compressive Strength Effect:

To study the effect of the compressive strength of the behavior of strengthening concrete columns, three values of compressive strength (30, 40 and 50)MPa were selected. From Fig. (5-61) to Fig. (5-114), it was observed that increases of compressive strength lead to decrease the creep strain. Whereas increasing compressive strength from (30 to 40)MPa and (40 to 50)MPa leads to decrease creep strain by 13.2% and 10.4% respectively. Generally, the increasing of compressive strength leads to enhance the strength of a

strengthening concrete column under long term where it decreases creep strain. (Paulson *et al.*, 1991) found that the creep coefficient of high strength concrete under sustained axial compression load was significantly less than that of ordinary concrete. The reason for the inverse relationship between concrete compressive strength and creep is that the low aggregate content in low concrete compressive strength as it is the aggregate that restrict creep; therefore, the creep value is low in high concrete compressive strength (Mehta & Monteiro, 2006). In addition, increasing compressive strength means increasing the elastic modulus, leading to a decrease in creep ($D = 1/E$)

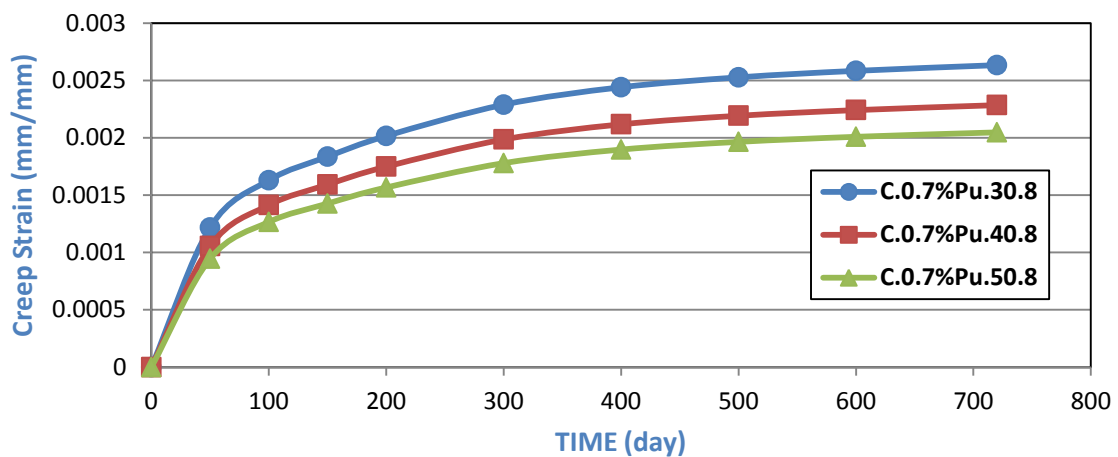


Fig.(5-61) :Time vs Creep Strain Behavior for Models(C.0.7%P_u.#.8)

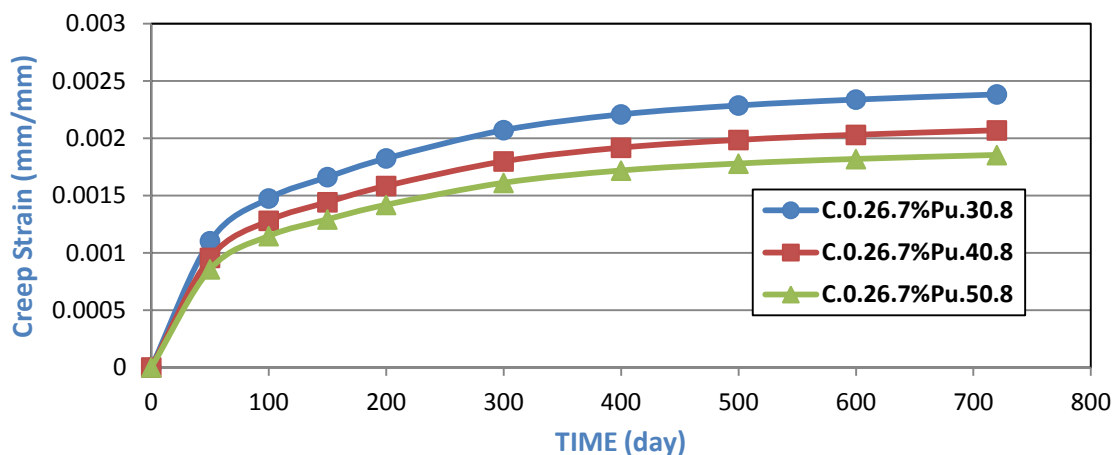


Fig.(5-62) :Time vs Creep Strain Behavior for Models(C.0.26.7%P_u.#.8)

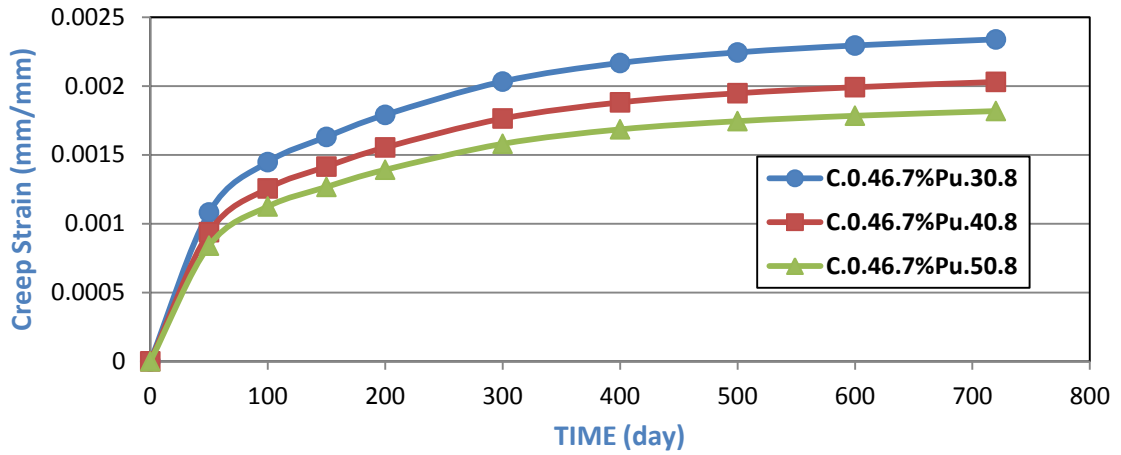


Fig.(5-63):Time vs Creep Strain Behavior for Models(C.0.46.7%Pu.#.8)

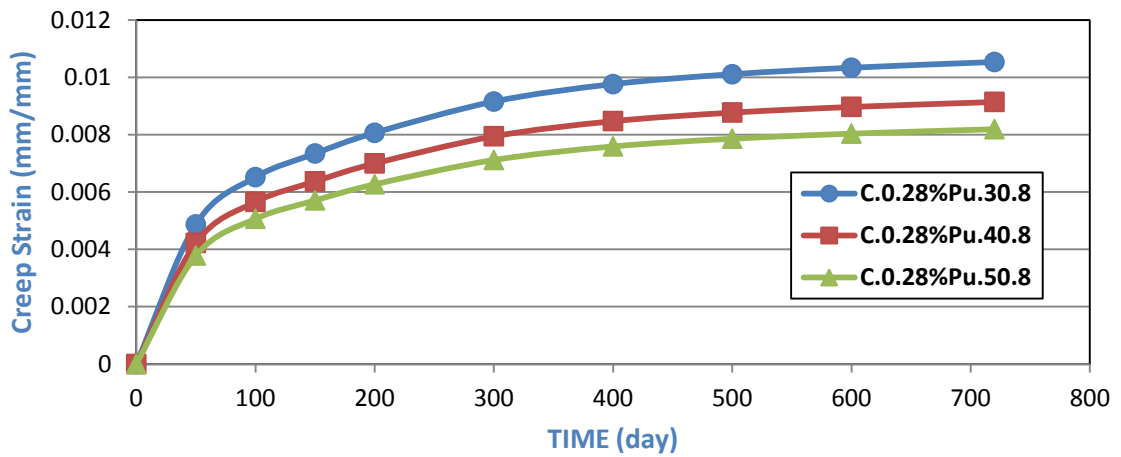


Fig.(5-64):Time vs Creep Strain Behavior for Models(C.0.28%Pu.#.8)

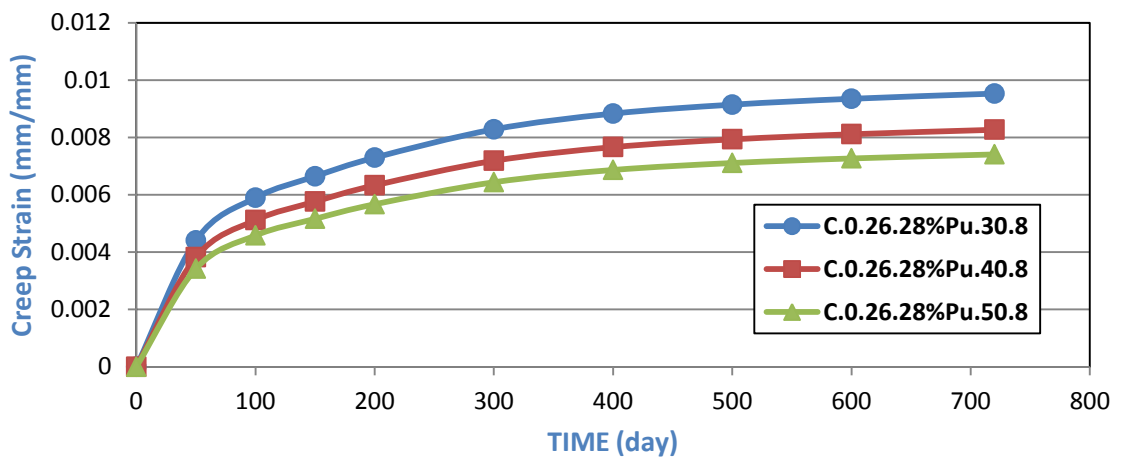


Fig.(5-65) Time vs Creep Strain Behavior for Models(C.0.26.28%Pu.#.8)

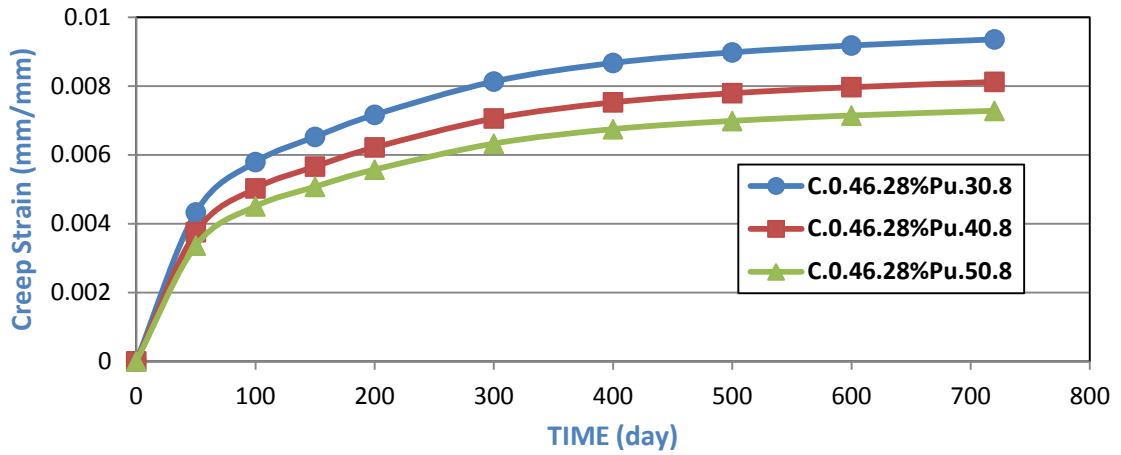


Fig.(5-66) Time vs Creep Strain Behavior for Models(C.0.46.28%Pu.#.8)

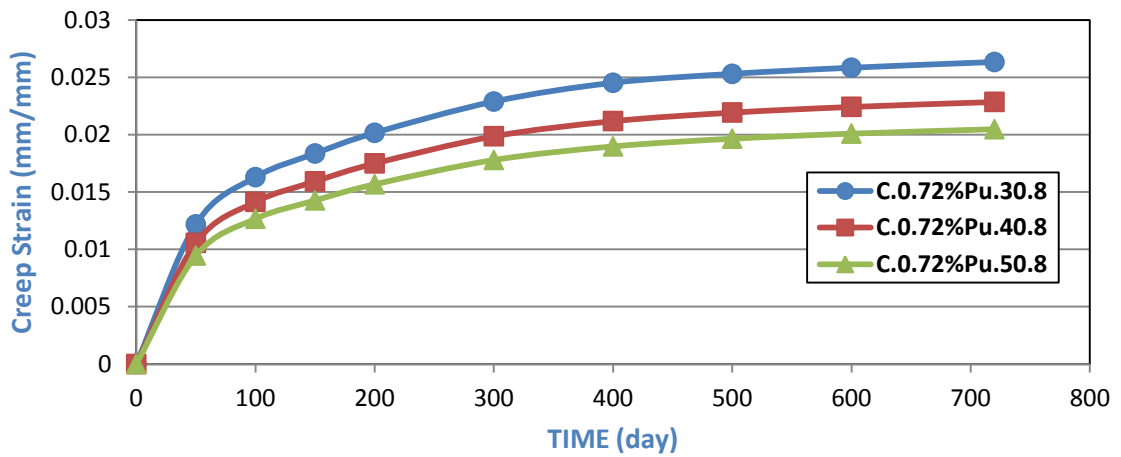


Fig.(5-67) Time vs Creep Strain Behavior for Models(C.0.72%Pu.#.8)

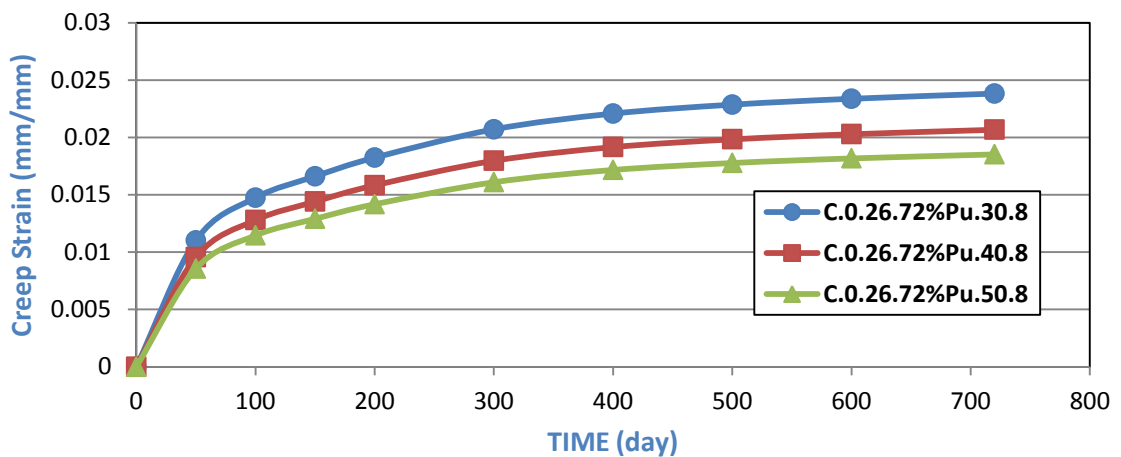


Fig.(5-68) Time vs Creep Strain Behavior for Models(C.0.26.72%Pu.#.8)

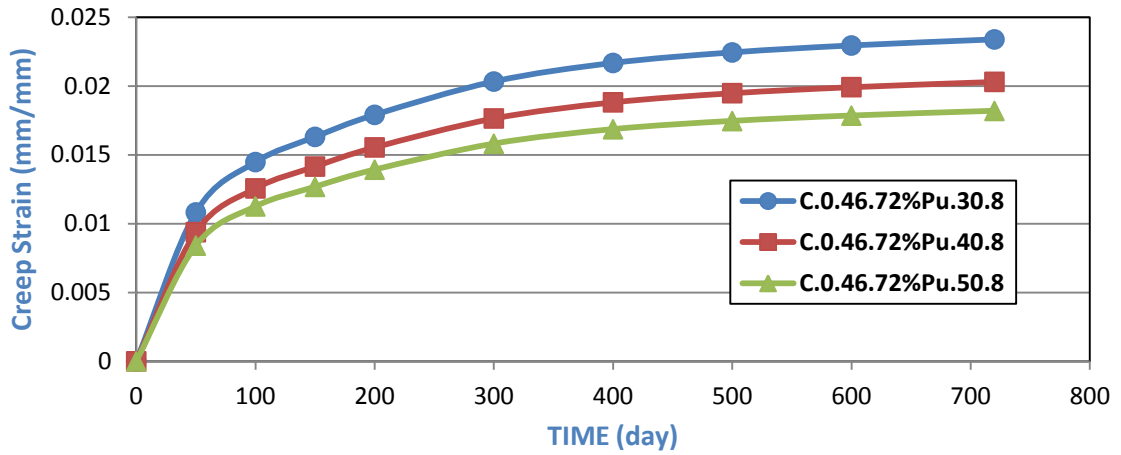


Fig.(5-69) Time vs Creep Strain Behavior for Models(C.0.46.72%Pu.#.8)

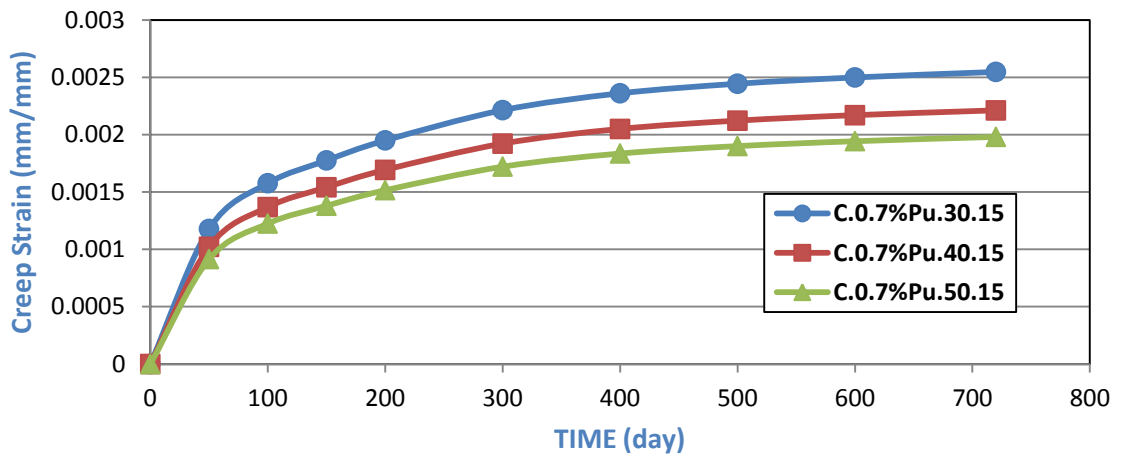


Fig.(5-70) Time vs Creep Strain Behavior for Models(C.0.7%Pu.#.15)

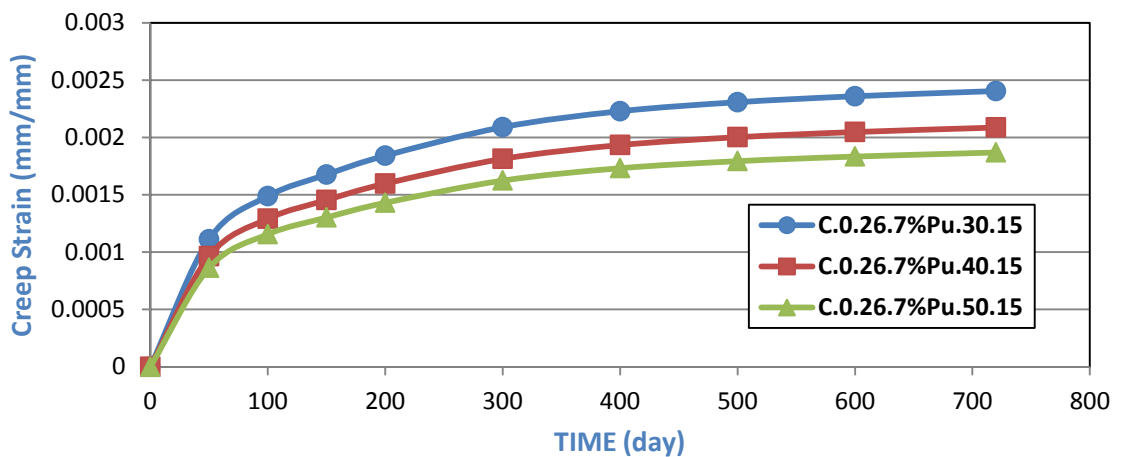


Fig.(5-71) Time vs Creep Strain Behavior for Models(C.0.26.7%Pu.#.15)

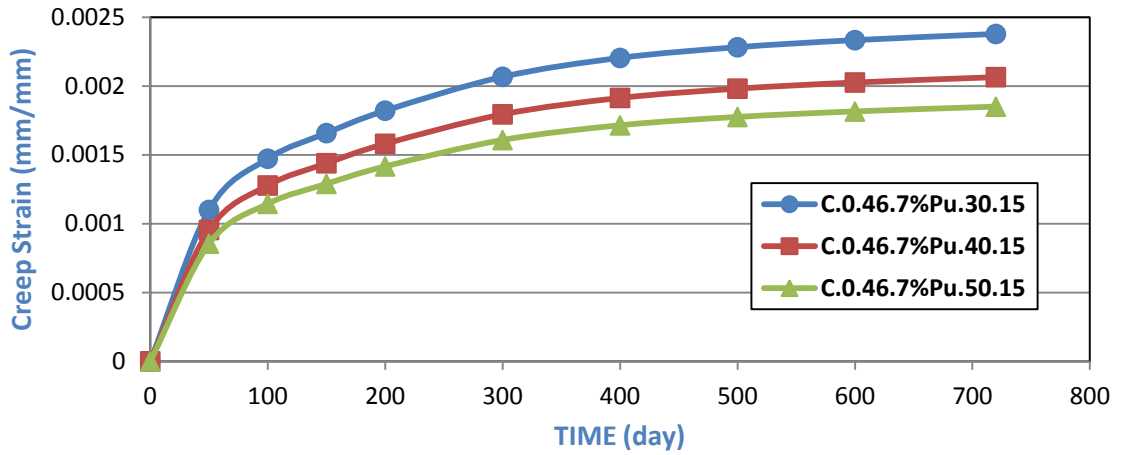


Fig.(5-72) Time vs Creep Strain Behavior for Models(C.0.46.7%Pu.#.15)

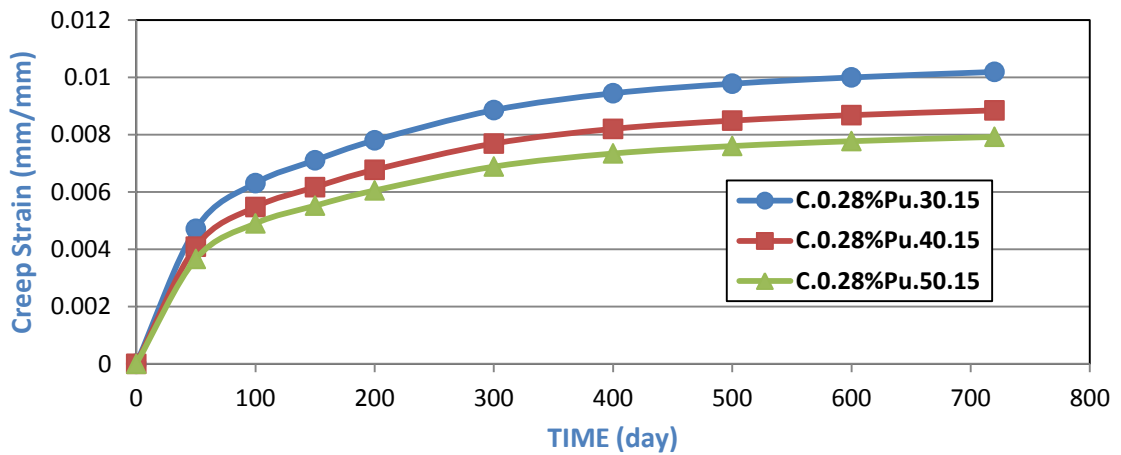


Fig.(5-73) Time vs Creep Strain Behavior for Models(C.0.28%Pu.#.15)

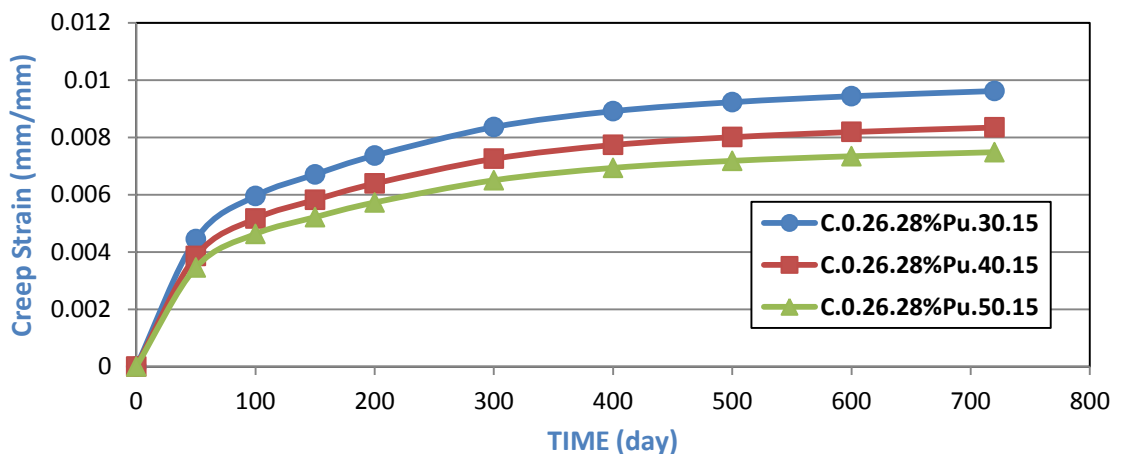


Fig.(5-74) Time vs Creep Strain Behavior for Models(C.0.26.28%Pu.#.15)

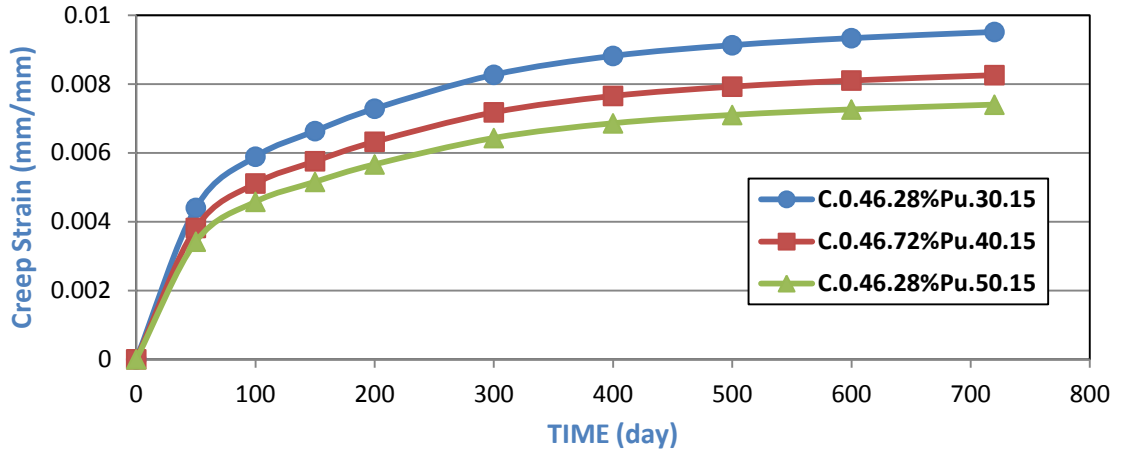


Fig.(5-75) Time vs Creep Strain Behavior for Models(C.0.46.28%Pu.#.15)

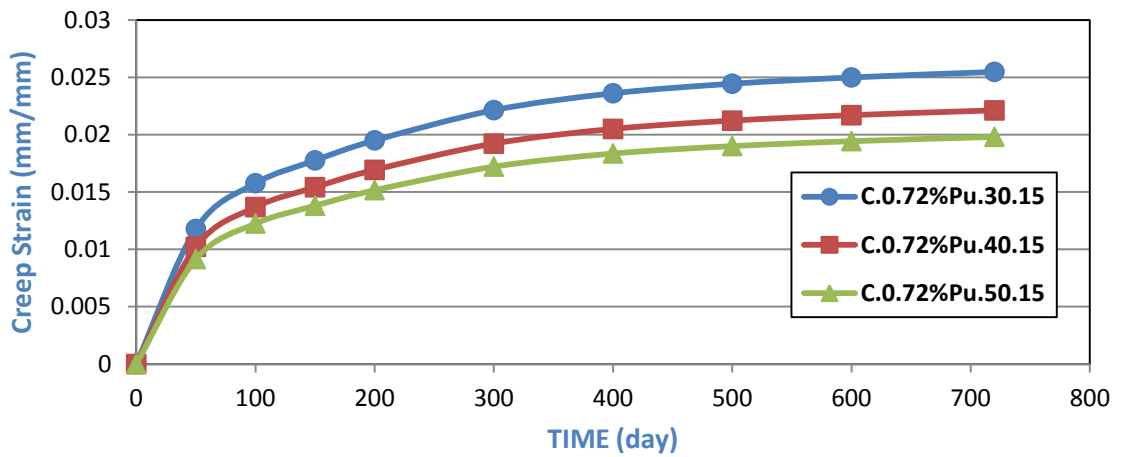


Fig.(5-76) Time vs Creep Strain Behavior for Models(C.0.72%Pu.#.15)

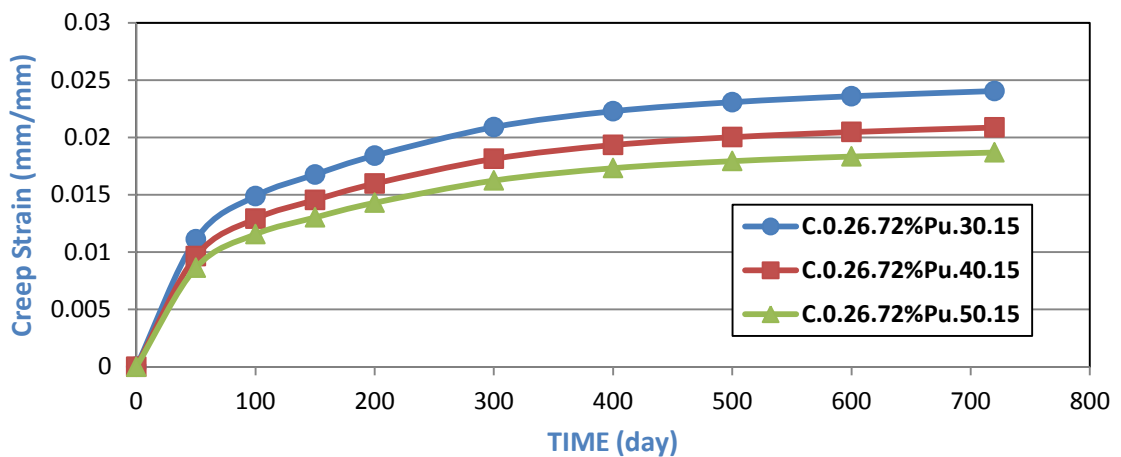


Fig.(5-77) Time vs Creep Strain Behavior for Models(C.0.26.72%Pu.#.15)

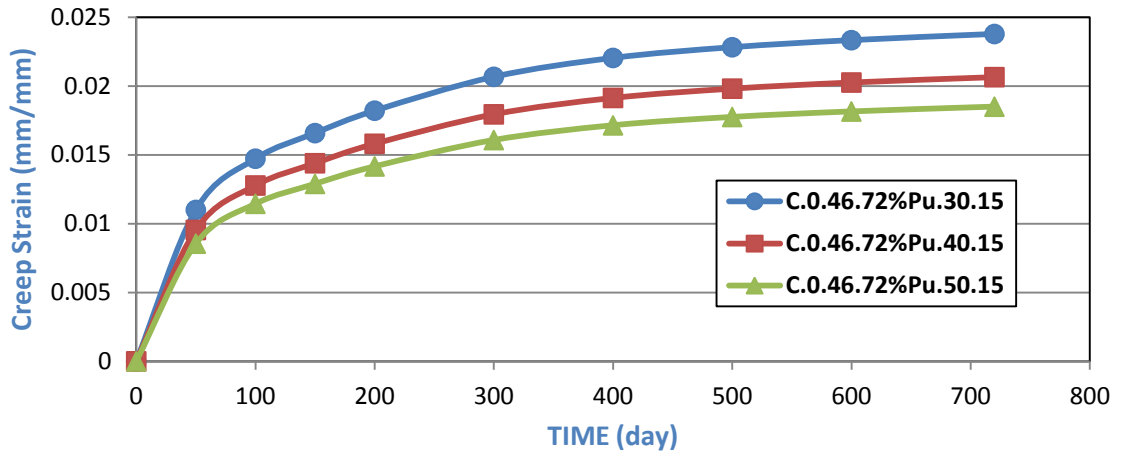


Fig.(5-78) Time vs Creep Strain Behavior for Models(C.0.46.72%Pu.#.15)

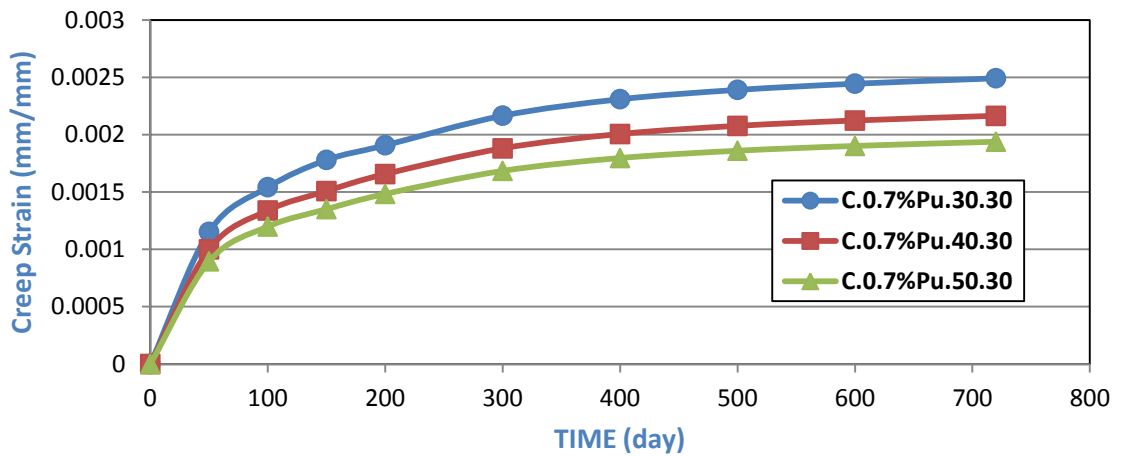


Fig.(5-79) Time vs Creep Strain Behavior for Models(C.0.7%Pu.#.30)

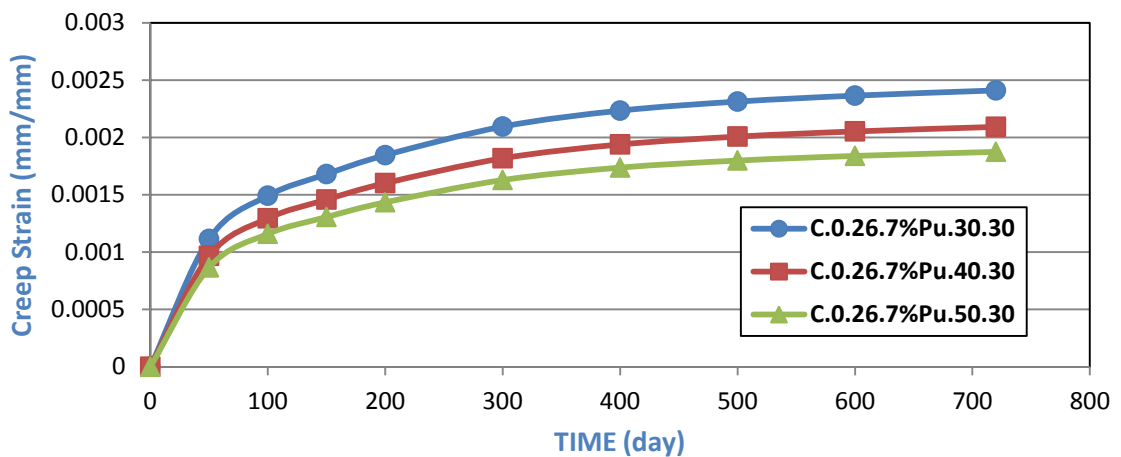


Fig.(5-80) Time vs Creep Strain Behavior for Models(C.0.26.7%Pu.#.30)

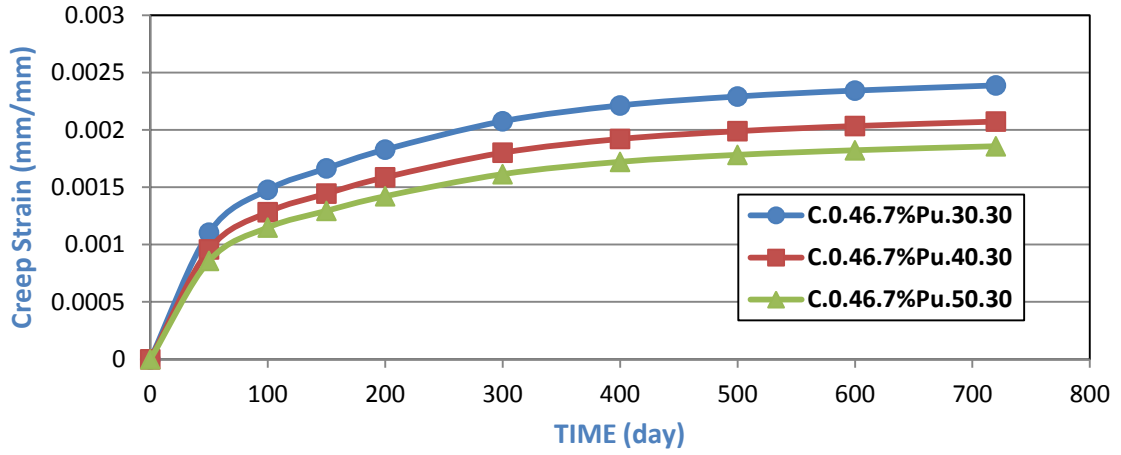


Fig.(5-81) Time vs Creep Strain Behavior for Models(C.0.46.7%Pu.#.30)

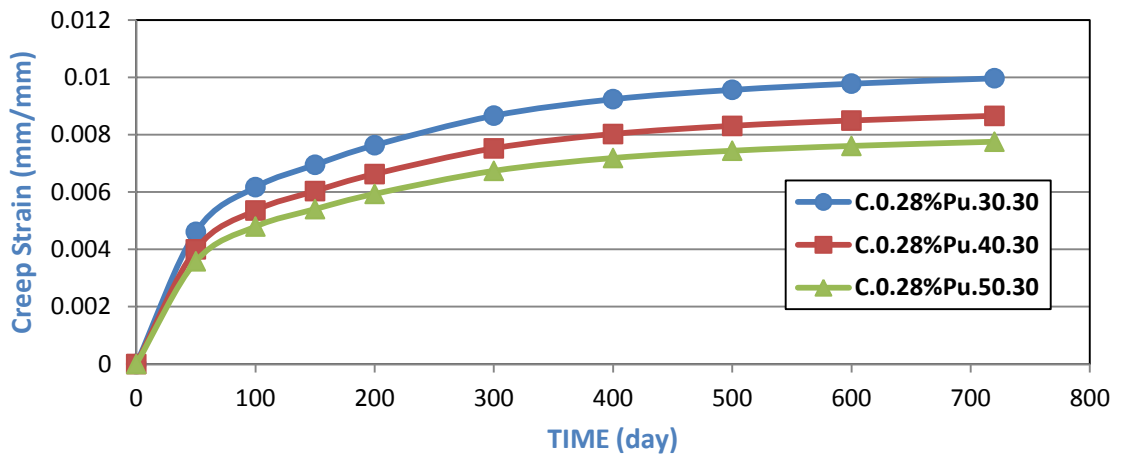


Fig.(5-82) Time vs Creep Strain Behavior for Models(C.0.28%Pu.#.30)

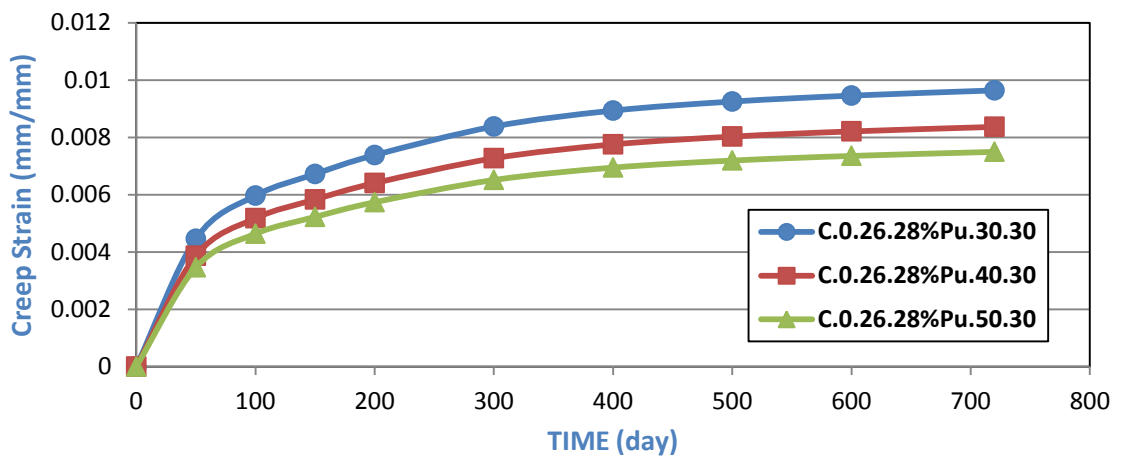


Fig.(5-83) Time vs Creep Strain Behavior for Models(C.0.26.28%Pu.#.30)

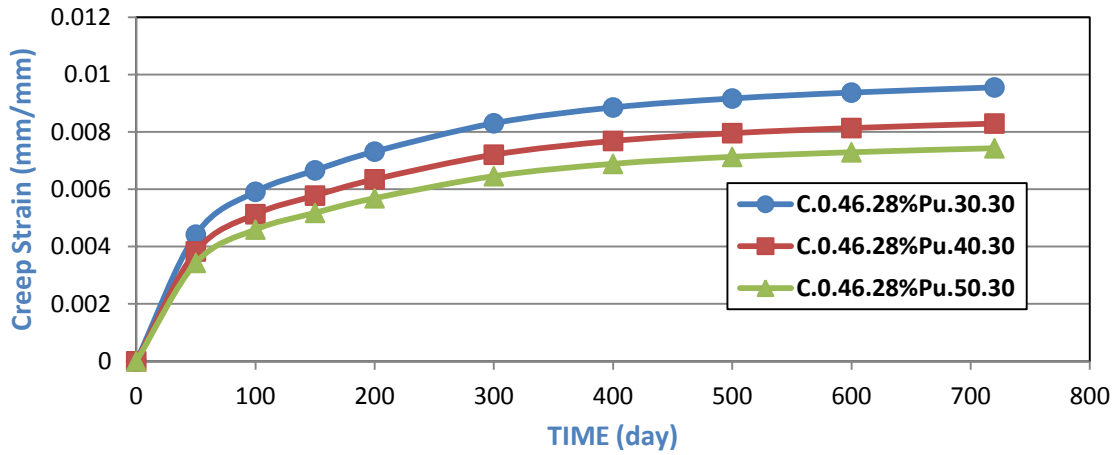


Fig.(5-84) Time vs Creep Strain Behavior for Models(C.0.46.28%Pu.#.30)

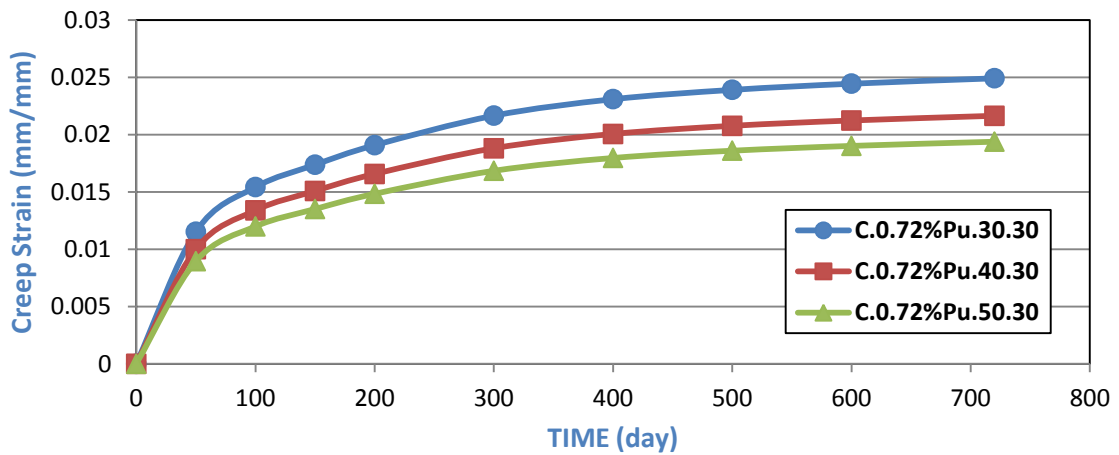


Fig.(5-85) Time vs Creep Strain Behavior for Models(C.0.72%Pu.#.30)

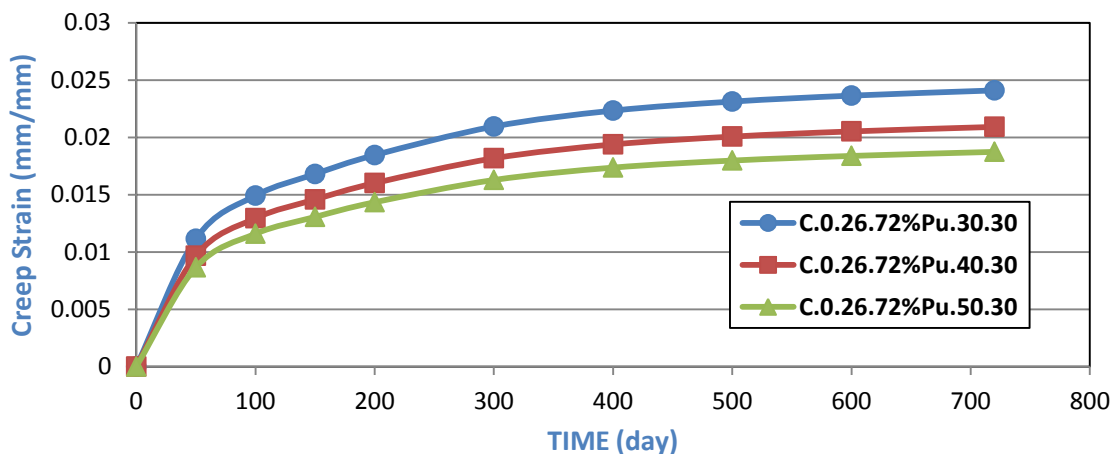


Fig.(5-86) Time vs Creep Strain Behavior for Models(C.0.26.72%Pu.#.30)

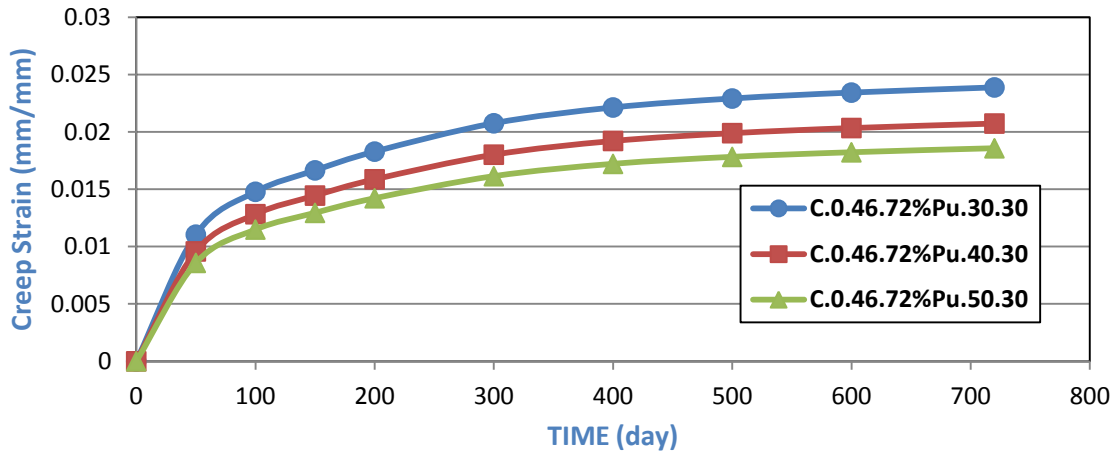


Fig.(5-87) Time vs Creep Strain Behavior for Models(C.0.46.72%Pu.#.30)

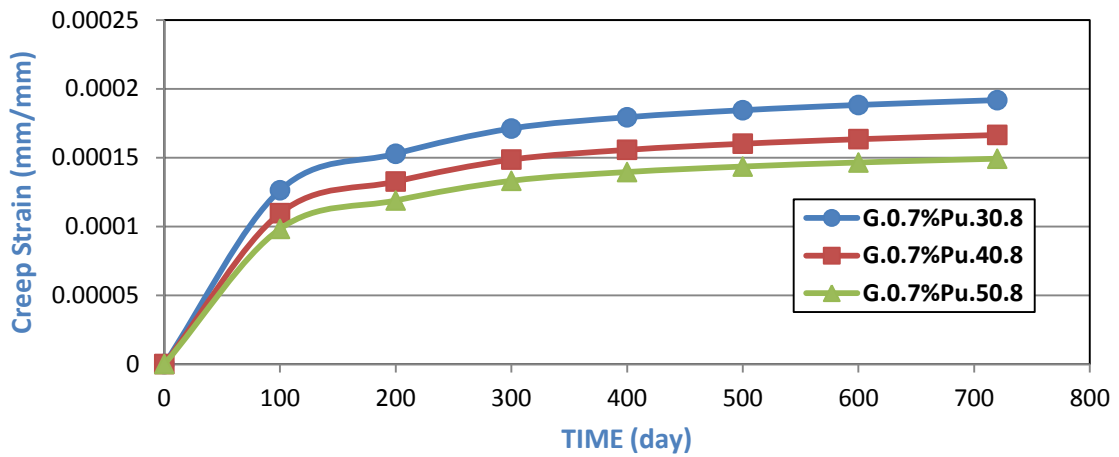


Fig.(5-88) Time vs Creep Strain Behavior for Models(G.0.7%Pu.#.8)

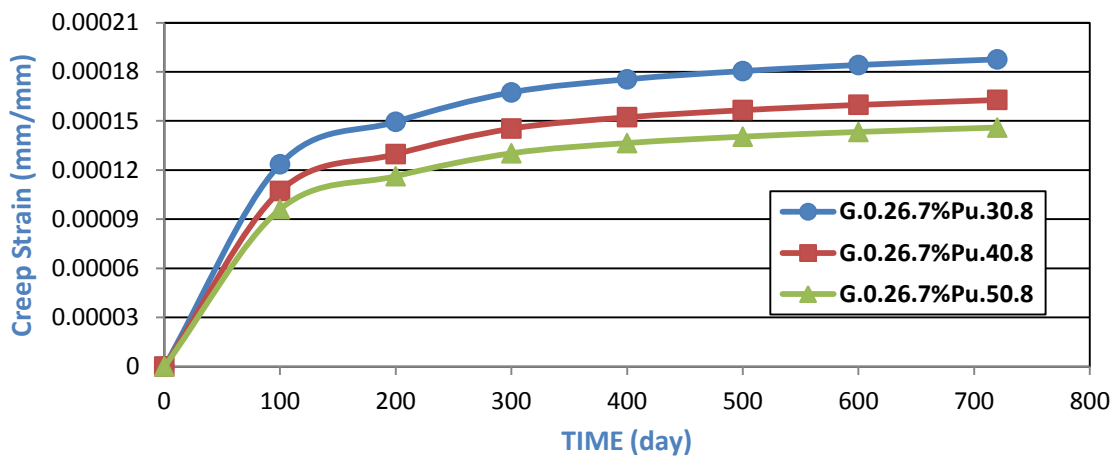


Fig.(5-89) Time vs Creep Strain Behavior for Models(G.0.26.7%Pu.#.8)

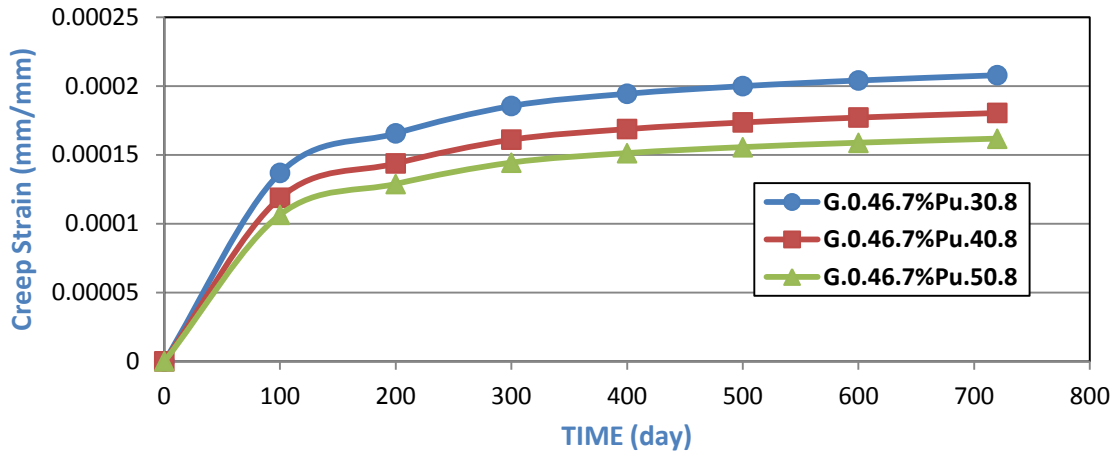


Fig.(5-90) :Time vs Creep Strain Behavior for Models(G.0.46.7%Pu.#.8)

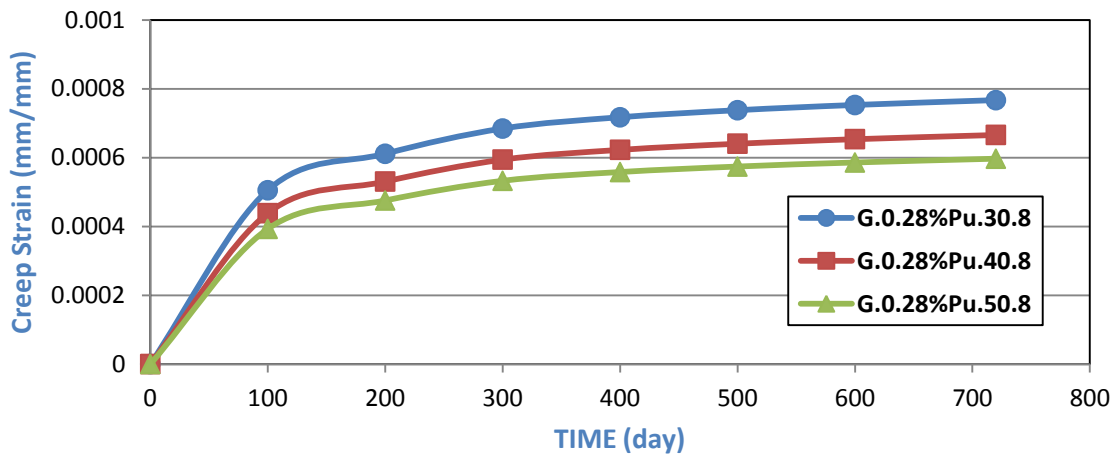


Fig.(5-91) :Time vs Creep Strain Behavior for Models(G.0.28%Pu.#.15)

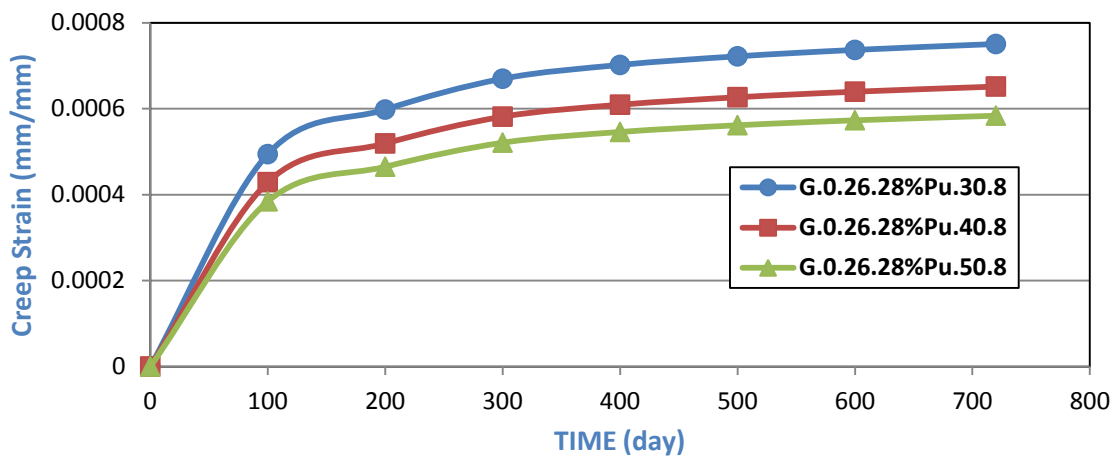


Fig.(5-92) :Time vs Creep Strain Behavior for Models(G.0.26.28%Pu.#.8)

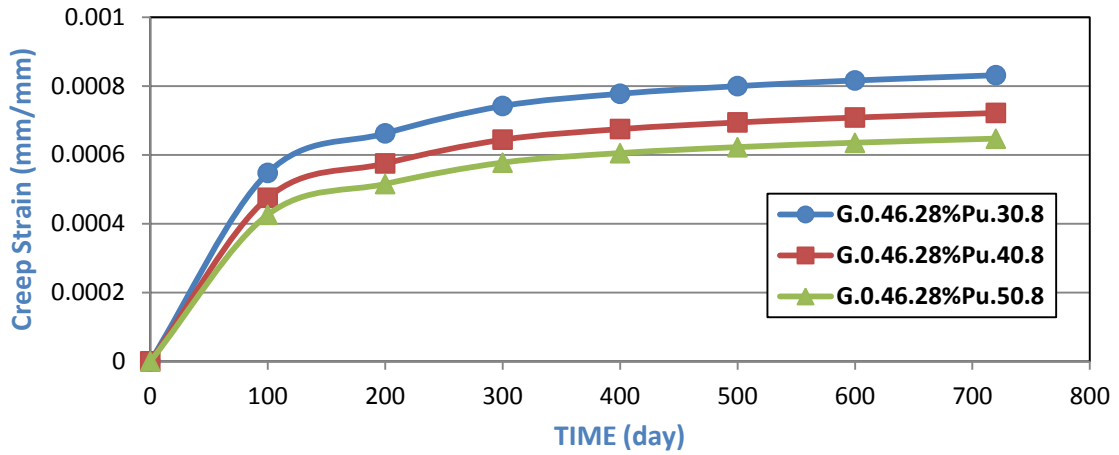


Fig.(5-93) :Time vs Creep Strain Behavior for Models(G.0.46.28%Pu.#.8)

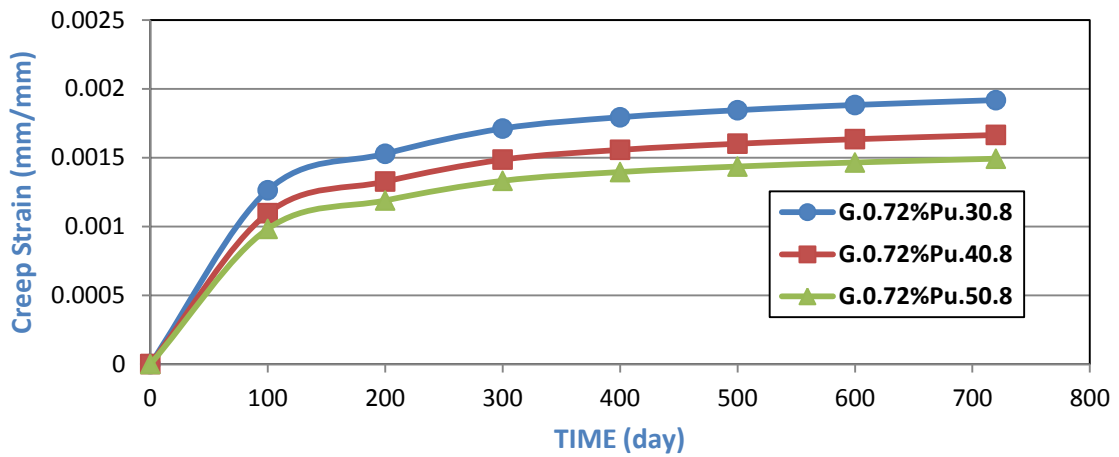


Fig.(5-94) :Time vs Creep Strain Behavior for Models(G.0.72%Pu.#.8)

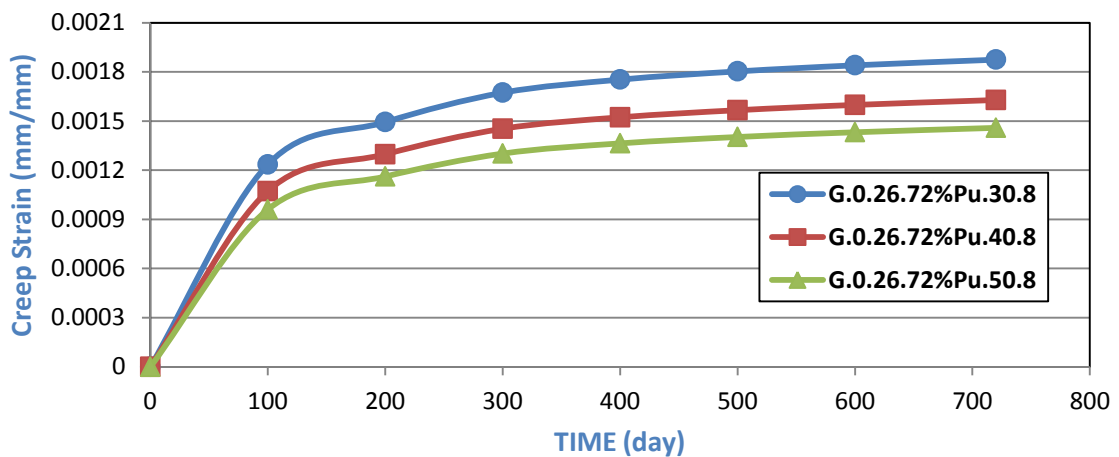


Fig.(5-95) :Time vs Creep Strain Behavior for Models(G.0.26.72%Pu.#.8)

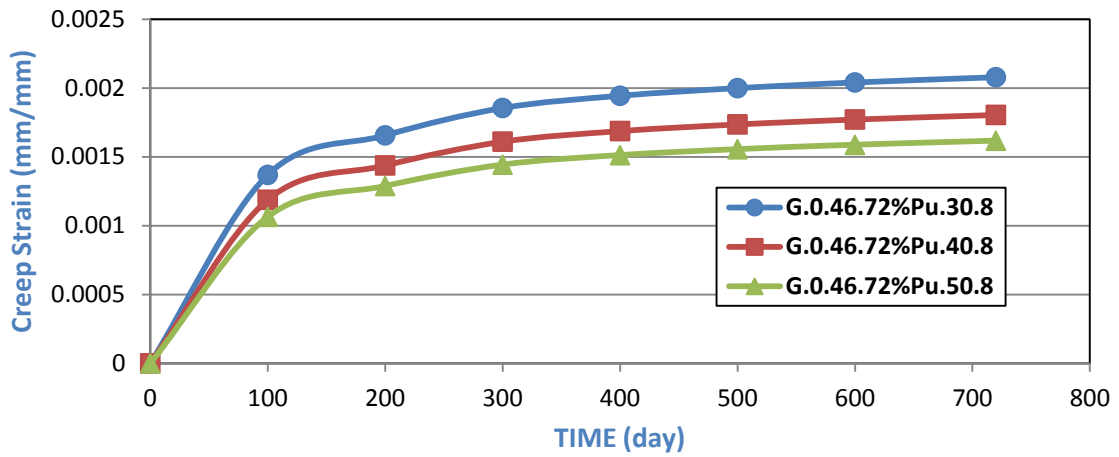


Fig.(5-96) :Time vs Creep Strain Behavior for Models(G.0.46.72%P_u.#.8)

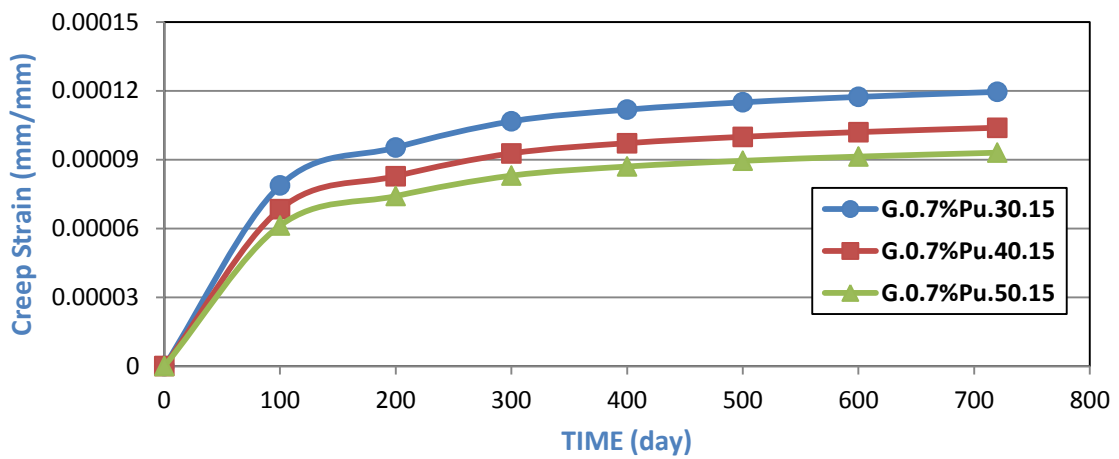


Fig.(5-97) :Time vs Creep Strain Behavior for Models(G.0.7%P_u.#.15)

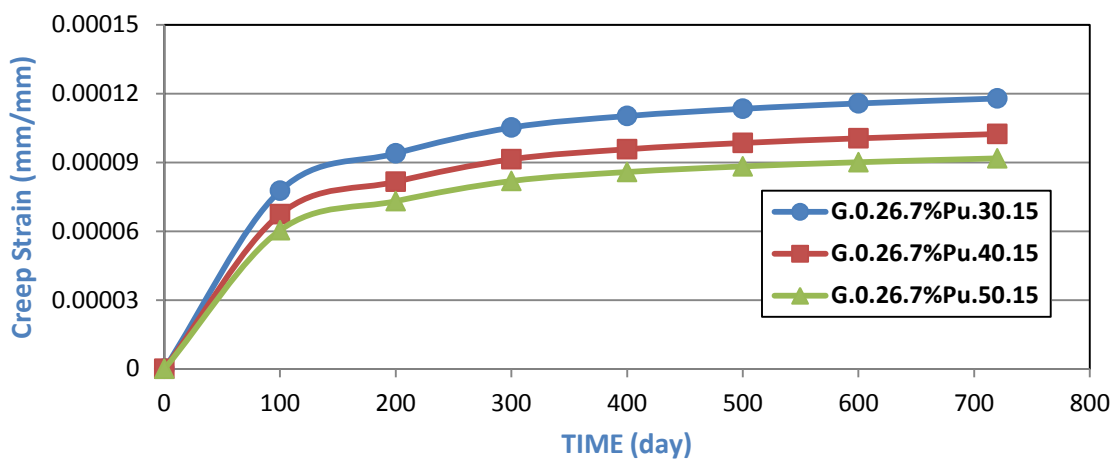


Fig.(5-98) :Time vs Creep Strain Behavior for Models(G.0.26.7%P_u.#.15)

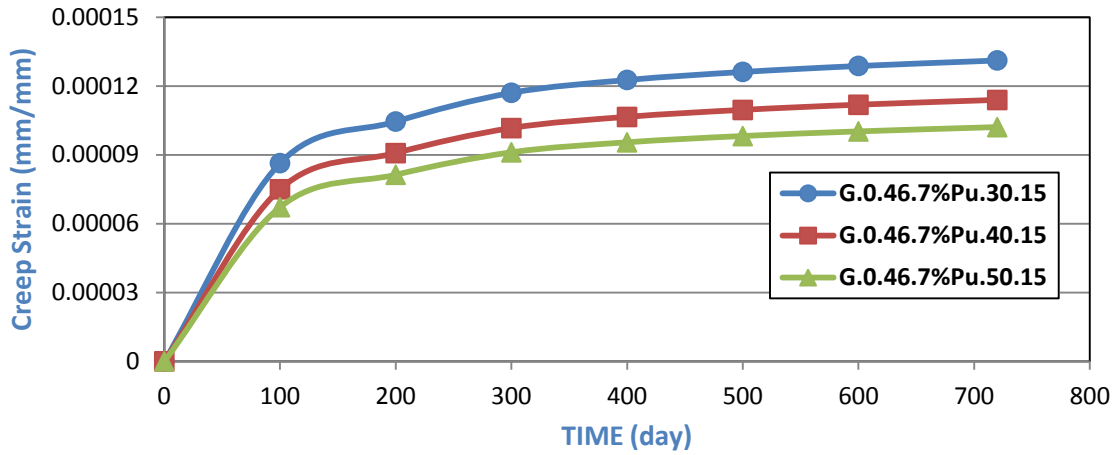


Fig.(5-99) :Time vs Creep Strain Behavior for Models(G.0.46.7%Pu.#.15)

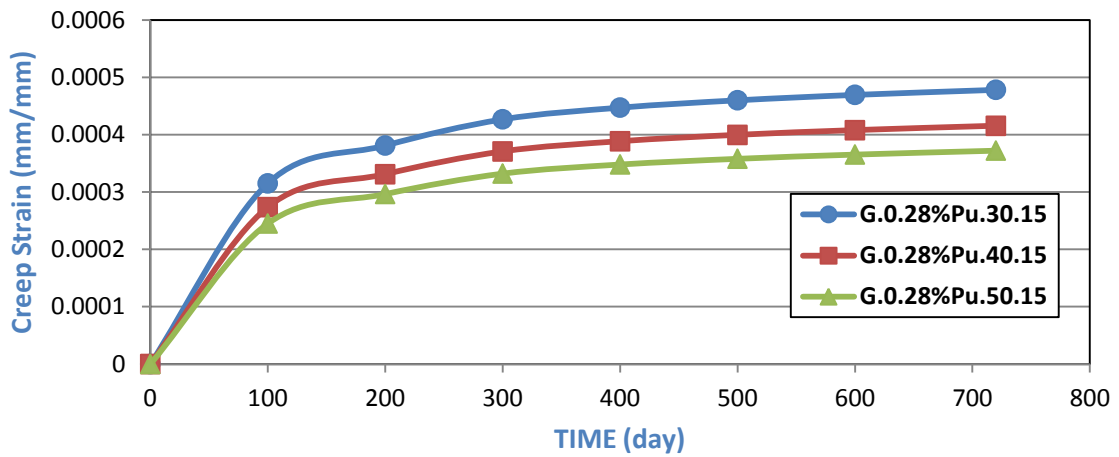


Fig.(5-100) :Time vs Creep Strain Behavior for Models(G.0.28%Pu.#.15)

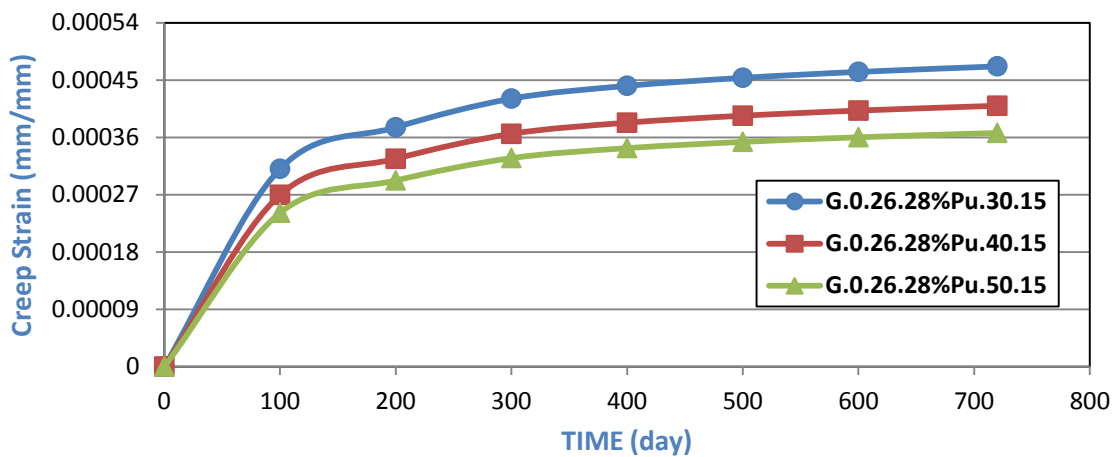


Fig.(5-101) :Time vs Creep Strain Behavior for Models(G.0.26.28%Pu.#.15)

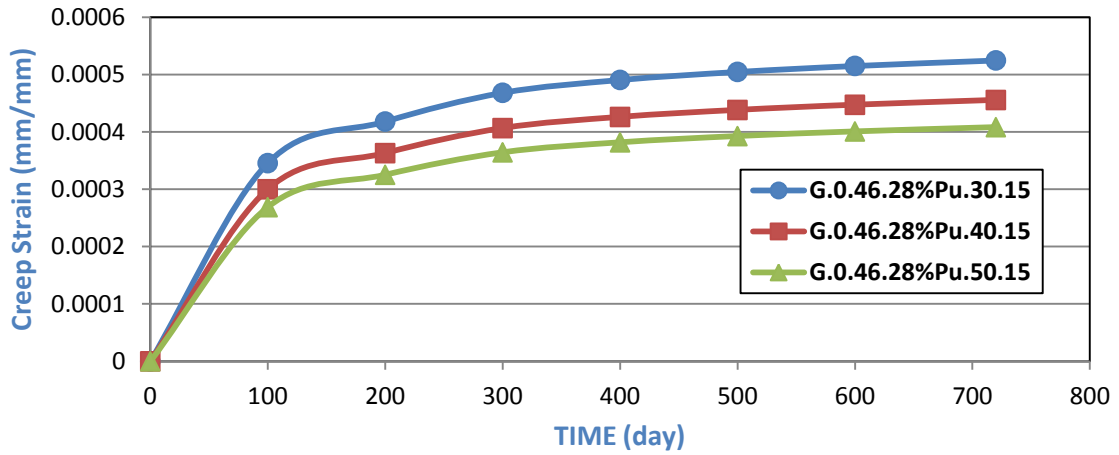


Fig.(5-102) :Time vs Creep Strain Behavior for Models(G.0.46.28%Pu.#.15)

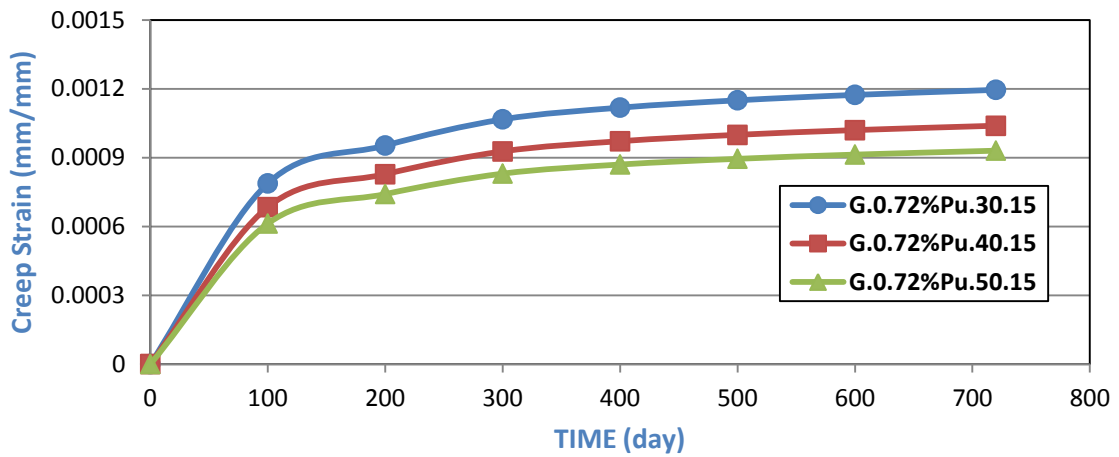


Fig.(5-103) :Time vs Creep Strain Behavior for Models(G.0.72%Pu.#.15)

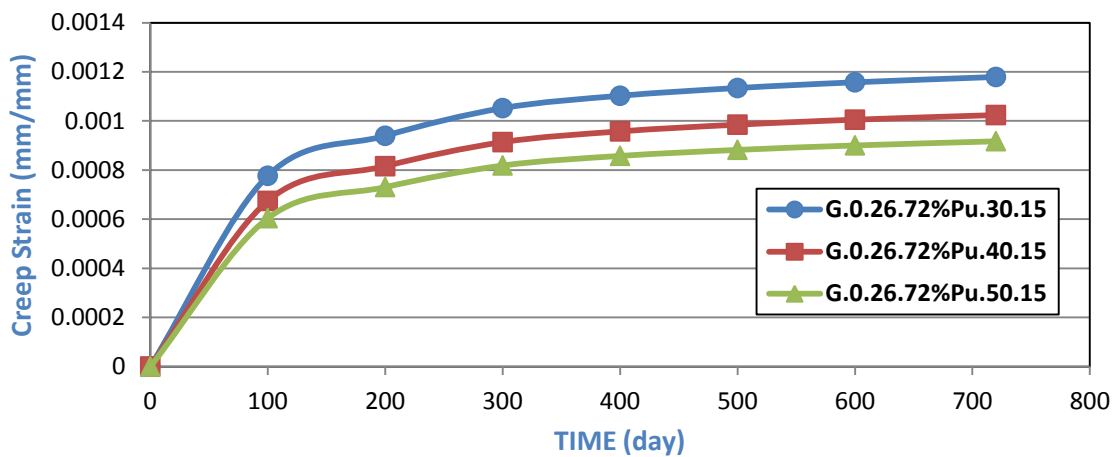


Fig.(5-104) :Time vs Creep Strain Behavior for Models(G.0.26.72%Pu.#.15)

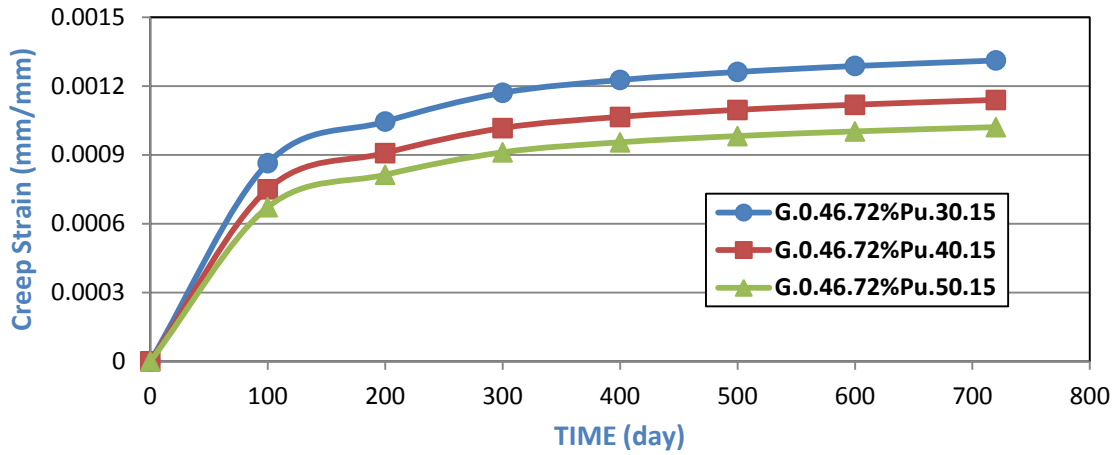


Fig.(5-105) :Time vs Creep Strain Behavior for Models(G.0.46.72%P_u.#.15)

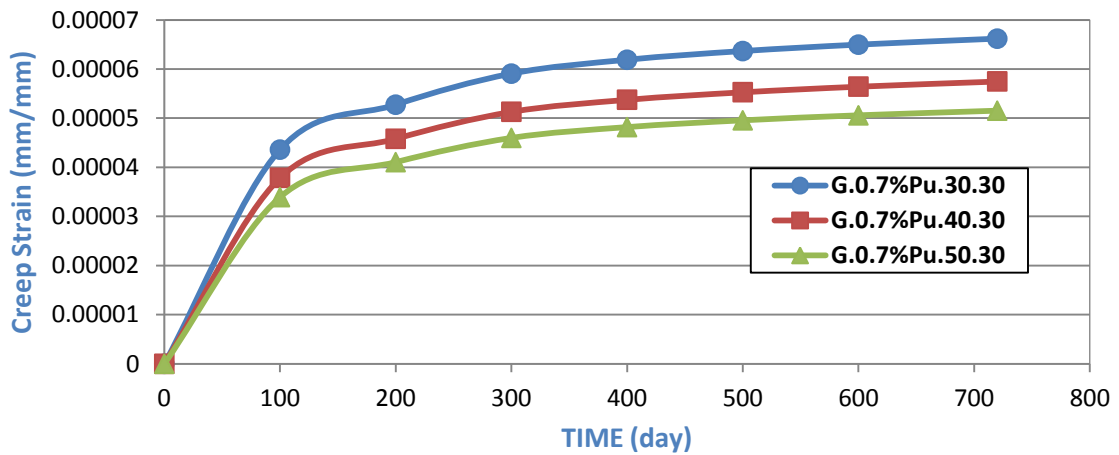


Fig.(5-106) :Time vs Creep Strain Behavior for Models(G.0.7%P_u.#.30)

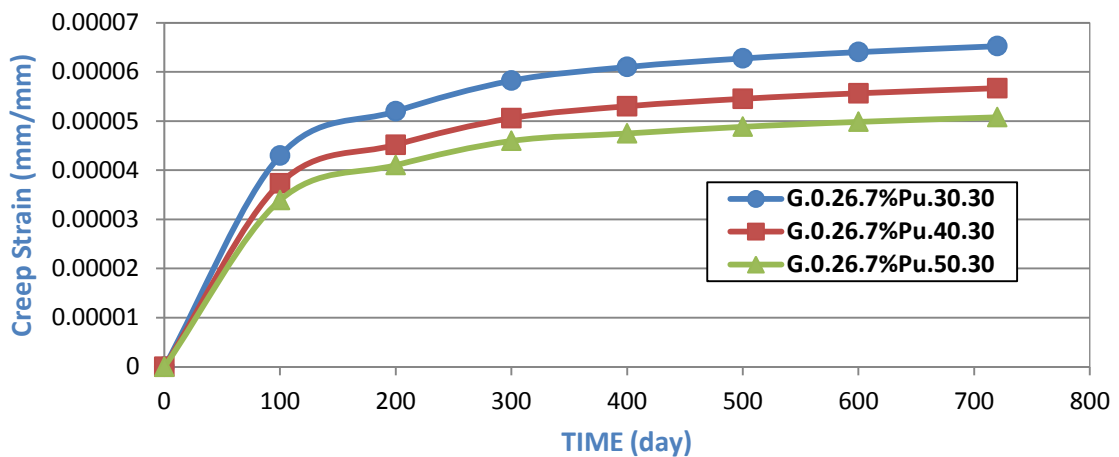


Fig.(5-107) :Time vs Creep Strain Behavior for Models(G.0.26.7%P_u.#.30)

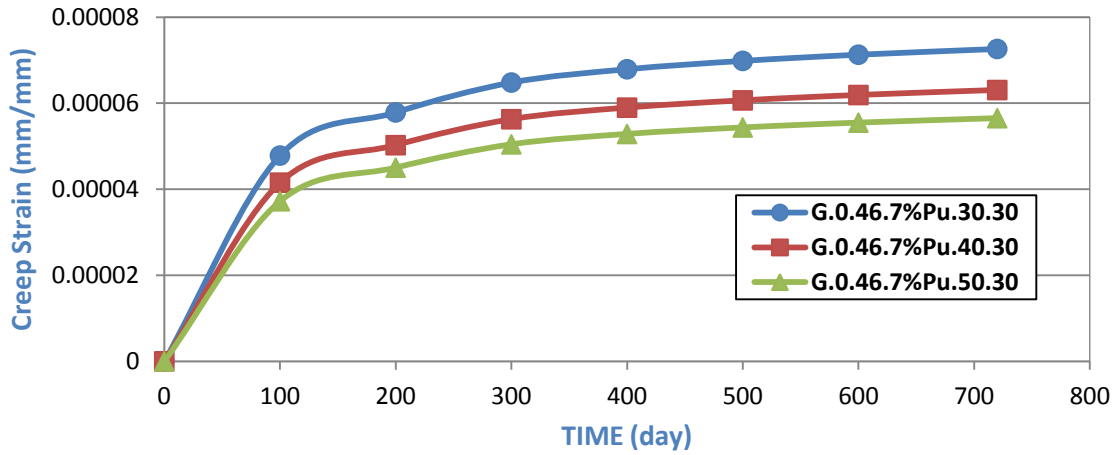


Fig.(5-108) :Time vs Creep Strain Behavior for Models(G.0.46.7%Pu.#.30)

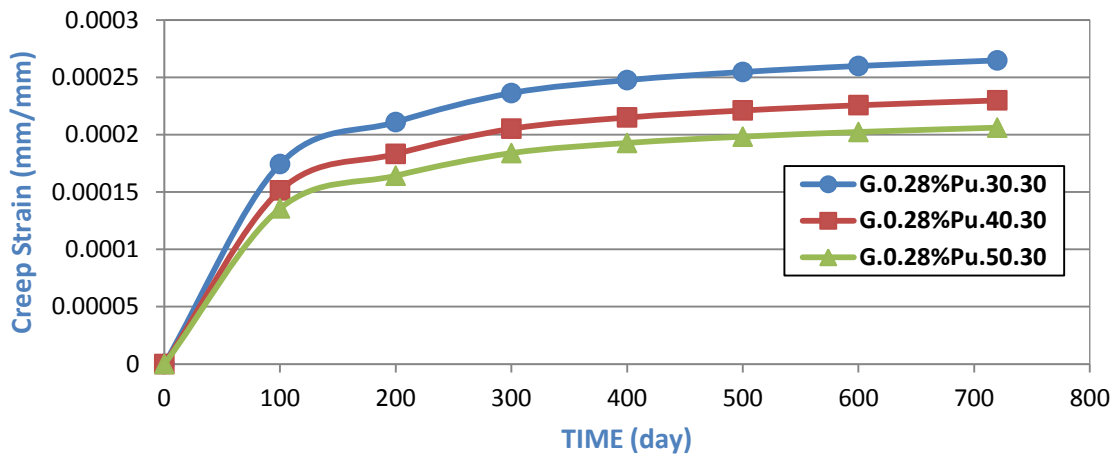


Fig.(5-109) :Time vs Creep Strain Behavior for Models(G.0.28%Pu.#.30)

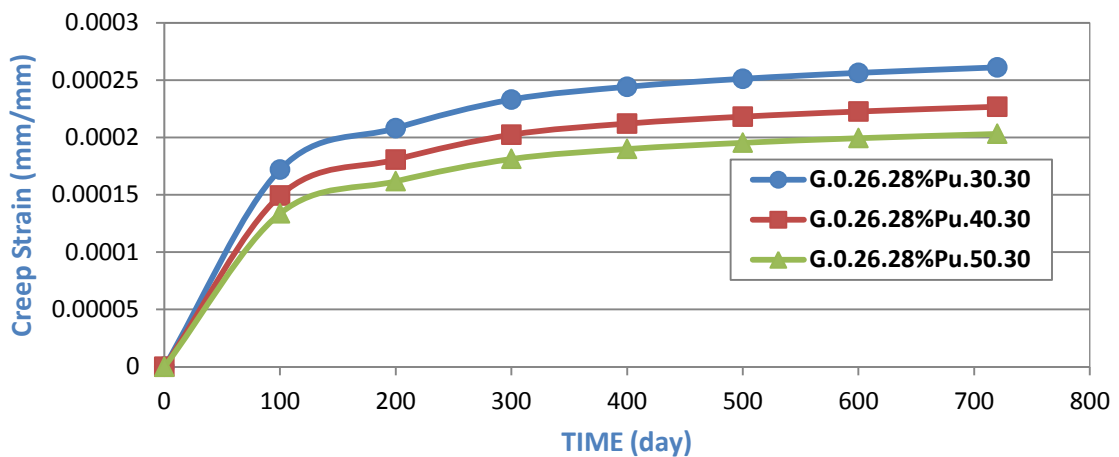


Fig.(5-110) :Time vs Creep Strain Behavior for Models(G.0.26.28%Pu.#.30)

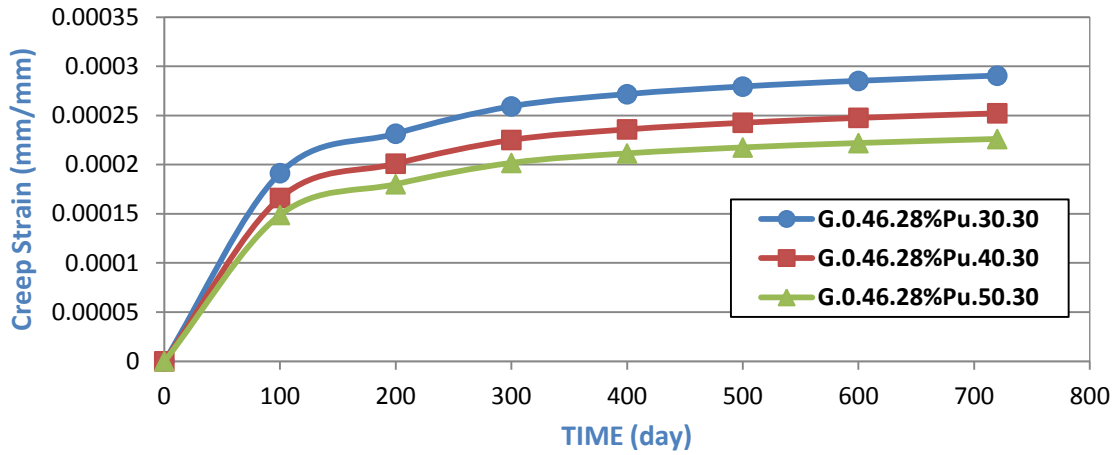


Fig.(5-111) :Time vs Creep Strain Behavior for Models(G.0.46.28%Pu.#.30)

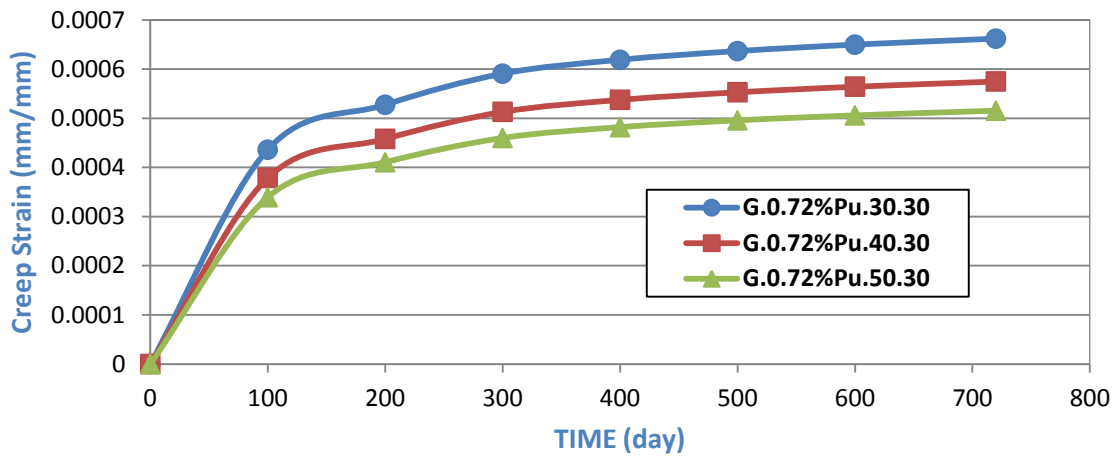


Fig.(5-112) :Time vs Creep Strain Behavior for Models(G.0.72%Pu.#.30)

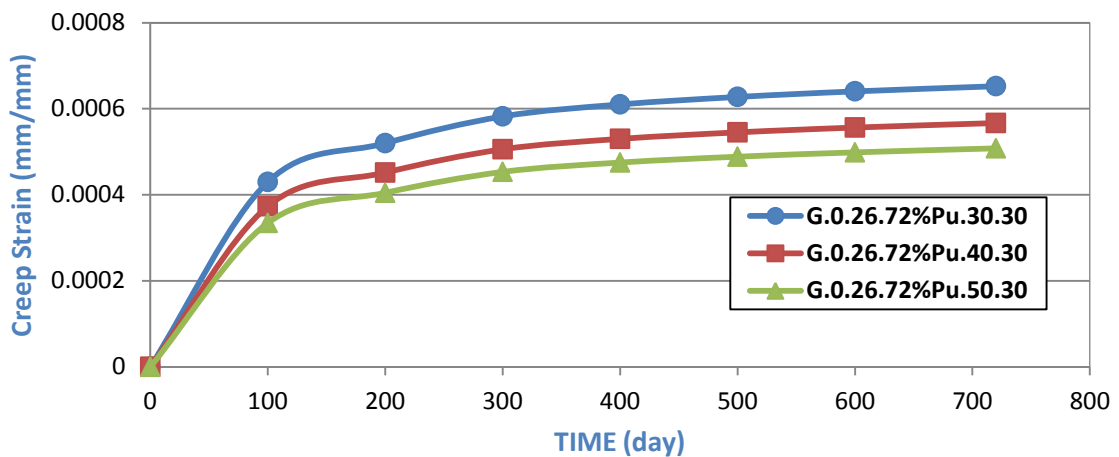


Fig.(5-113) :Time vs Creep Strain Behavior for Models(G.0.26.72%Pu.#.30)

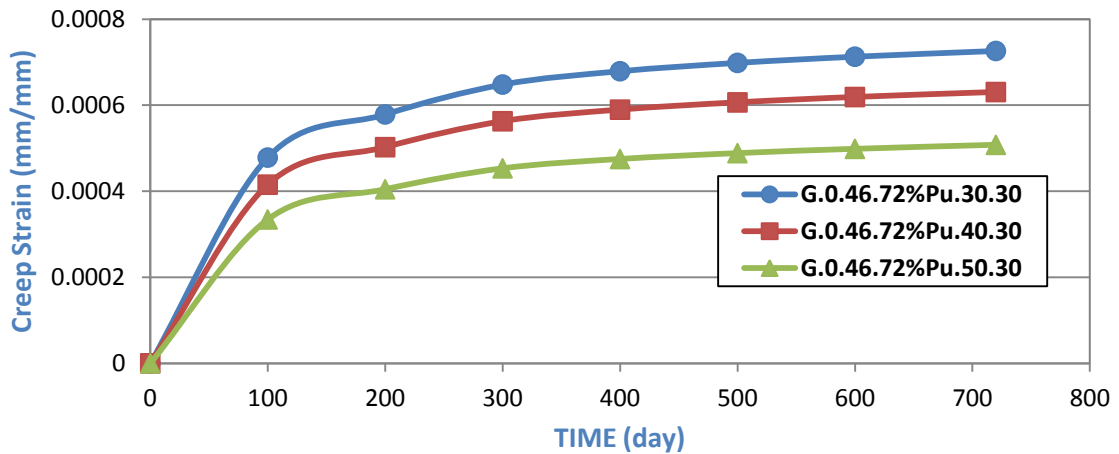


Fig.(5-114) :Time vs Creep Strain Behavior for Models(G.0.46.72%P_u.#.30)

5.3.5: FRP Type Effect:

Studying the effect of FRP type on the behavior of strengthening concrete column compared (B1C1) column, which strengthened with CFRP with (FWCC) column, which strengthened by GFRP has observed that creep strain of (B1C1) column is higher than (FWCC) column by 13 times, the elastic modulus of glass fiber is very close to the elastic modulus of the concrete. Therefore, the creep of the glass fiber is the same as the creep value of the concrete while the elastic modulus of the carbon fiber is much greater than the elastic modulus of the concrete. Therefore, the value of creep of CFRP concrete columns is higher than that of GFRP concrete columns. Fig.(5.115) to Fig. (5-194) show the comparison of these two columns.

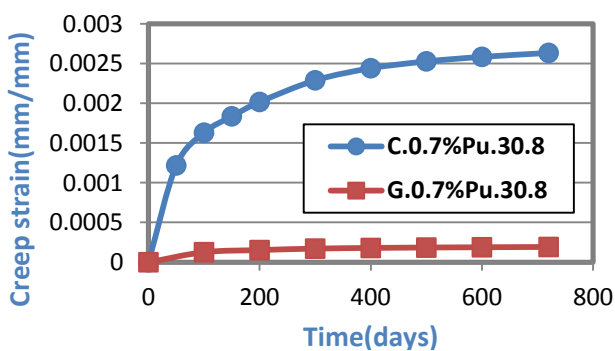


Fig.(5-115): Time vs Creep Strain Behavior for Models(#.0.7%P_u.30.8)

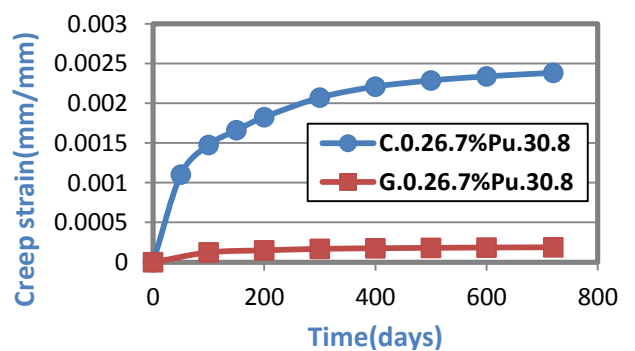


Fig.(5-116): Time vs Creep Strain Behavior for Models(#.0.46.7%P_u.30.8)

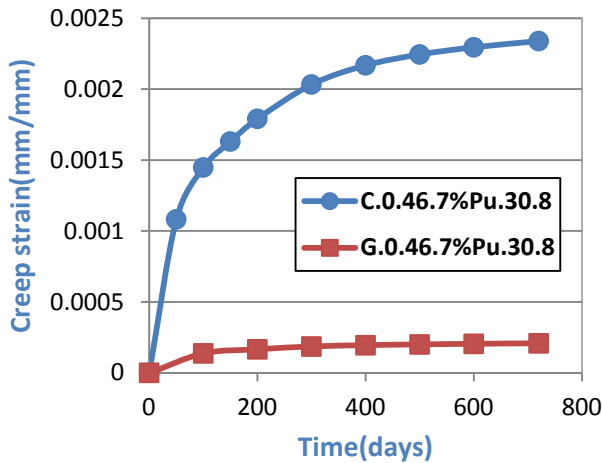


Fig.(5-117): Time vs Creep Strain

Behavior for Models(#.0.46.7%Pu.30.8)

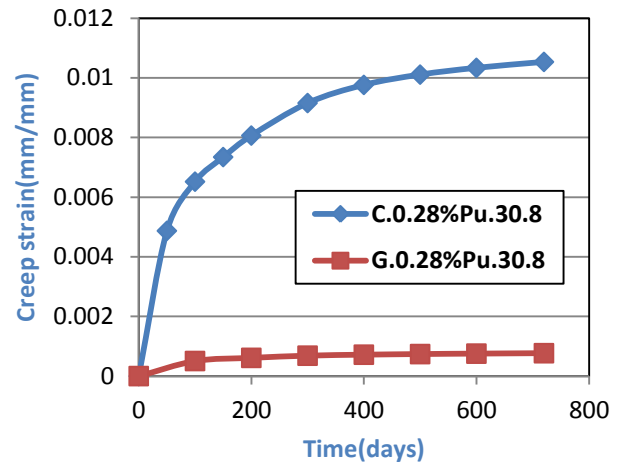


Fig.(5-118): Time vs Creep Strain

Behavior for Models(#.0.28%Pu.30.8)

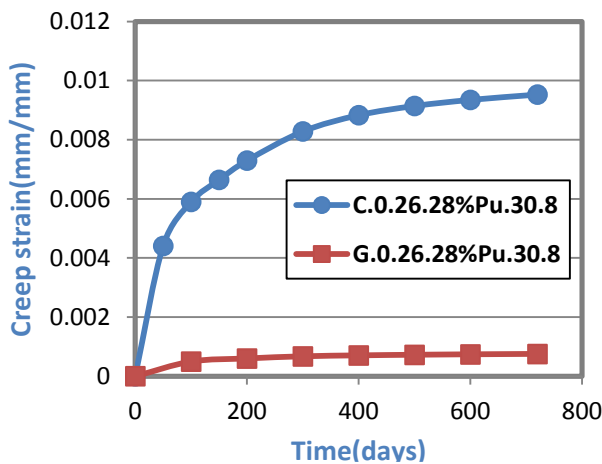


Fig.(5-119): Time vs Creep Strain

Behavior for Models(#.0.26.28%Pu.30.8)

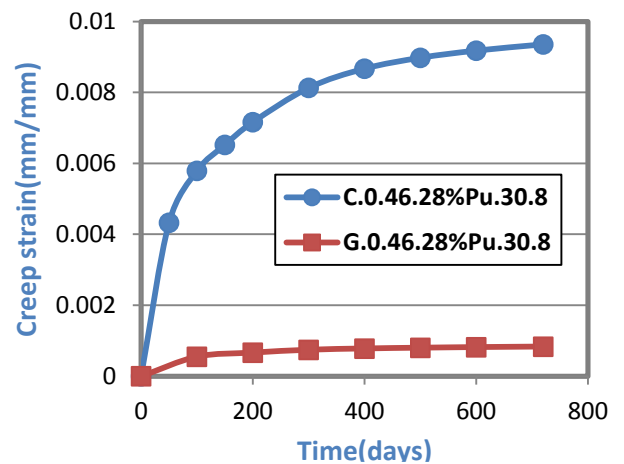


Fig.(5-120): Time vs Creep Strain

Behavior for Models(#.0.46.28%Pu.30.8)

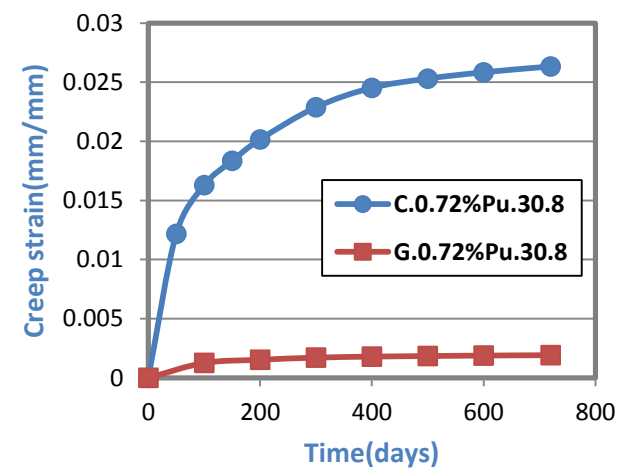


Fig.(5-121): Time vs Creep Strain

Behavior for Models(#.0.72%Pu.30.8)

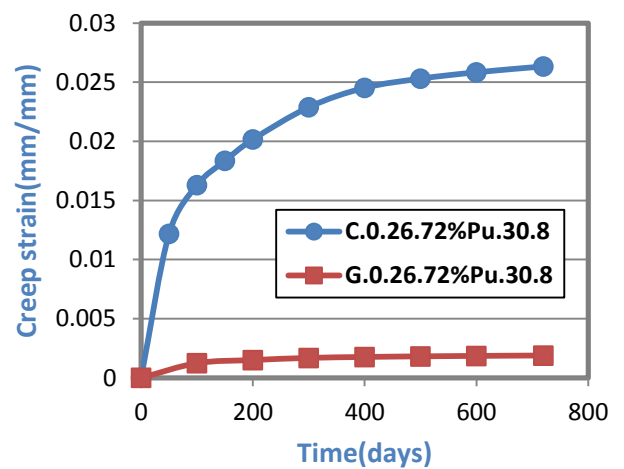


Fig.(5-122): Time vs Creep Strain

Behavior for Models(#.0.26.72%Pu.30.8)

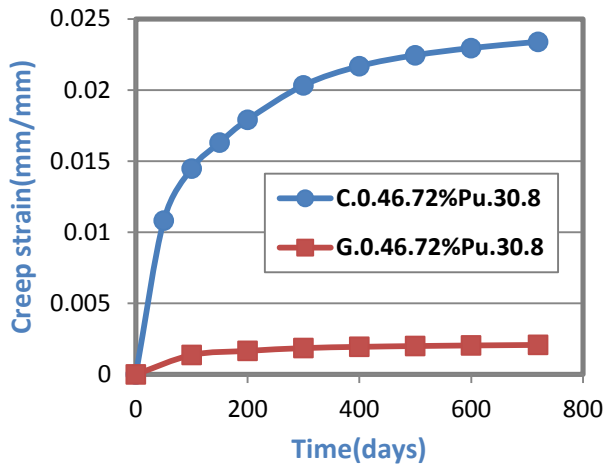


Fig.(5-123): Time vs Creep Strain

Behavior for Models(#.0.46.72%Pu.30.8)

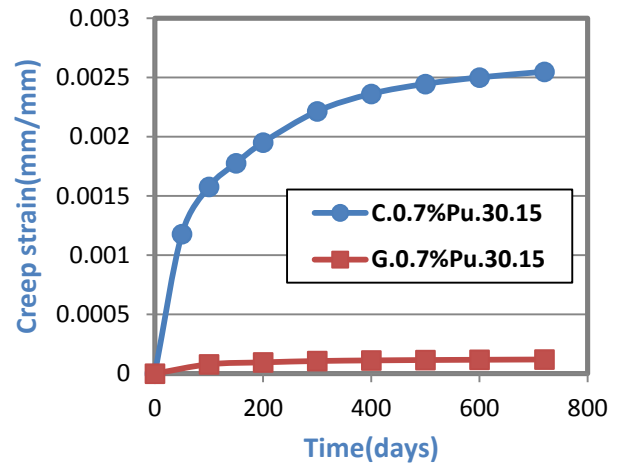


Fig.(5-124): Time vs Creep Strain

Behavior for Models(#.0.7%Pu.30.15)

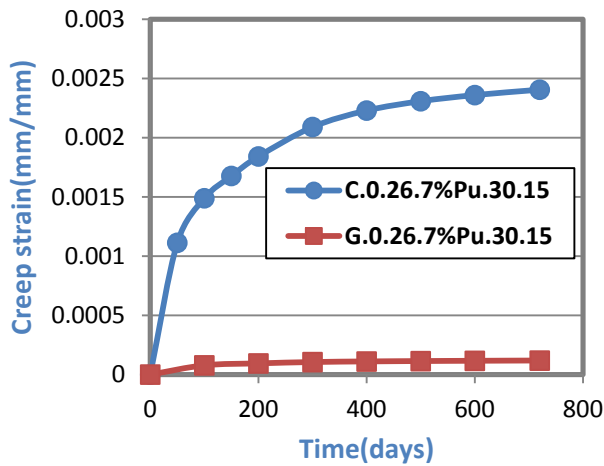


Fig.(5-125): Time vs Creep Strain

Behavior for Models(#.0.26.7%.30.15)

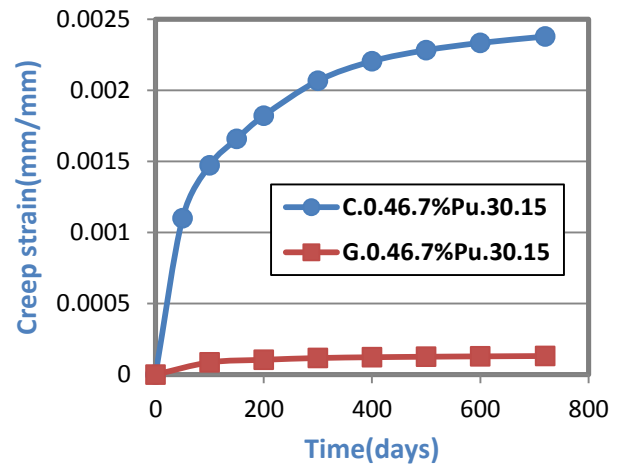


Fig.(5-126): Time vs Creep Strain

Behavior for Models(#.0.46.7%Pu.30.15)

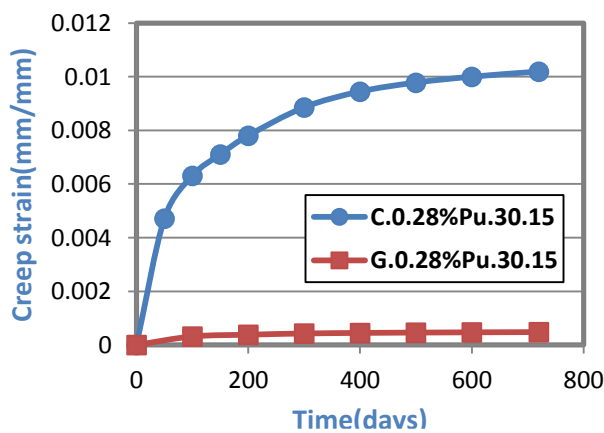


Fig.(5-127): Time vs Creep Strain

Behavior for Models(#.0.28%Pu.30.15)

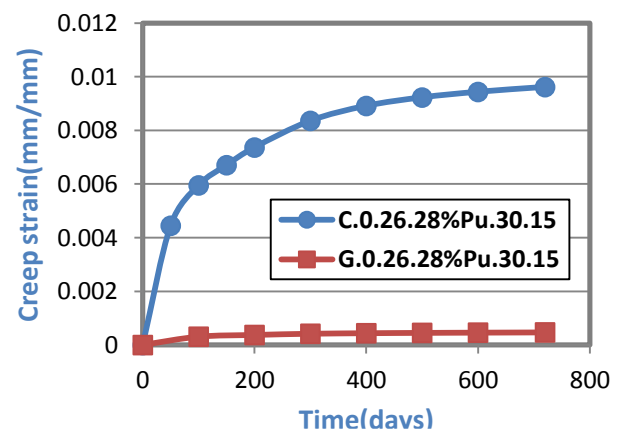


Fig.(5-128): Time vs Creep Strain

Behavior for Models(#.0.26.28%Pu.30.15)

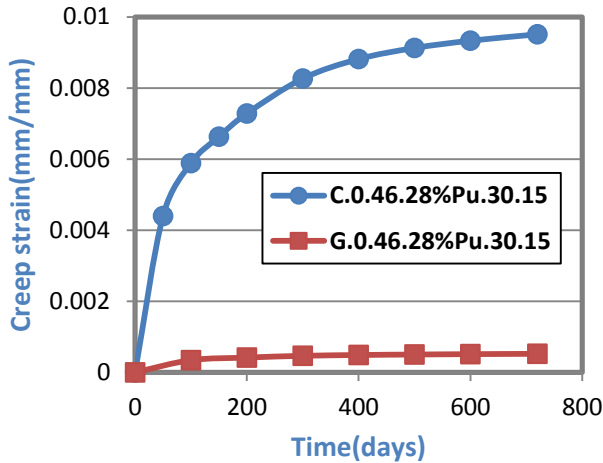


Fig.(5-129): Time vs Creep Strain

Behavior for Models(#.0.46.28%Pu.30.15)

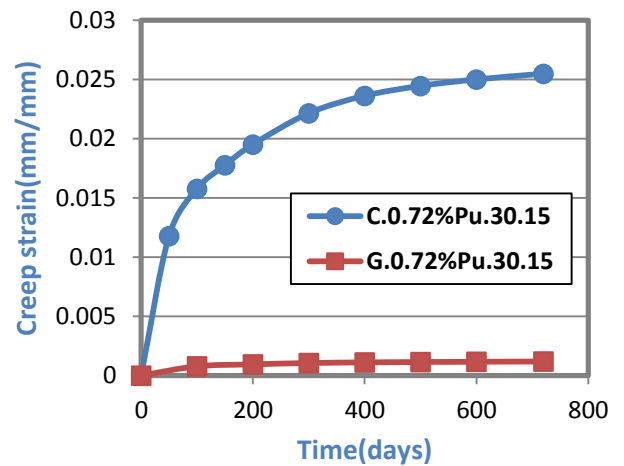


Fig.(5-130): Time vs Creep Strain

Behavior for Models(#.0.72%Pu.30.15)

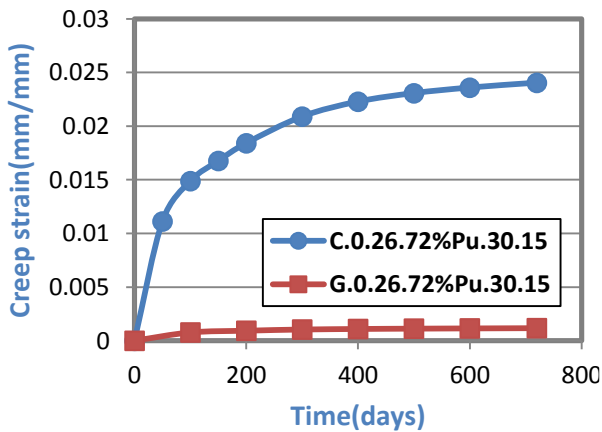


Fig.(5-131): Time vs Creep Strain

Behavior for Models(#.0.26.72%Pu.30.15)

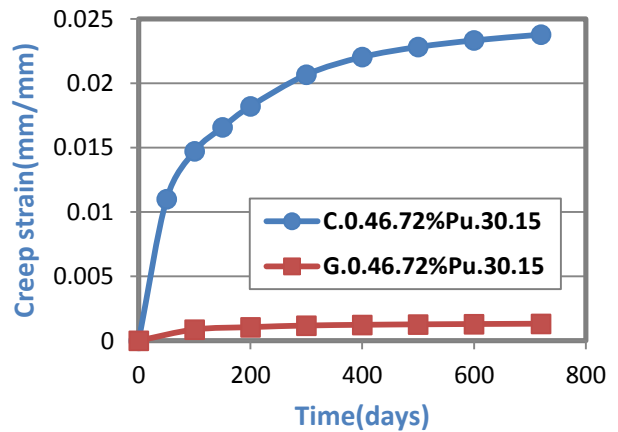


Fig.(5-132): Time vs Creep Strain

Behavior for Models(#.0.46.72%Pu.30.15)

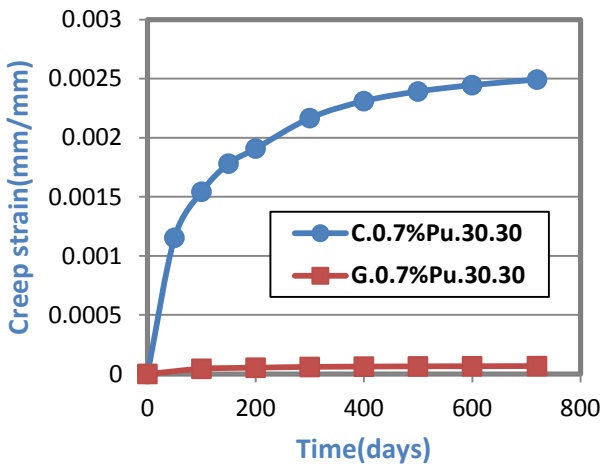


Fig.(5-133): Time vs Creep Strain

Behavior for Models(#.0.7%Pu.30.30)

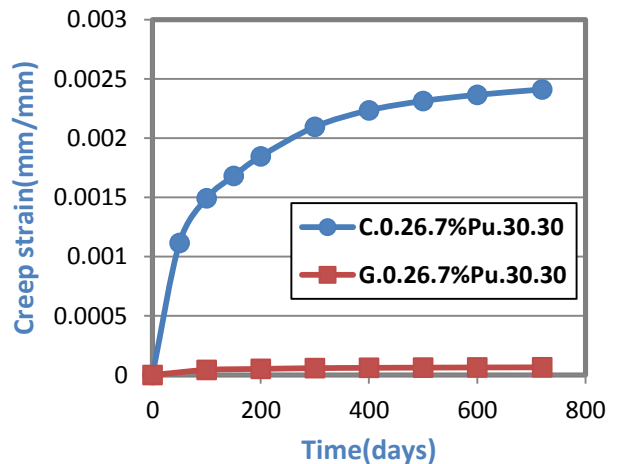


Fig.(5-134): Time vs Creep Strain

Behavior for Models(#.0.26.7%Pu.30.30)

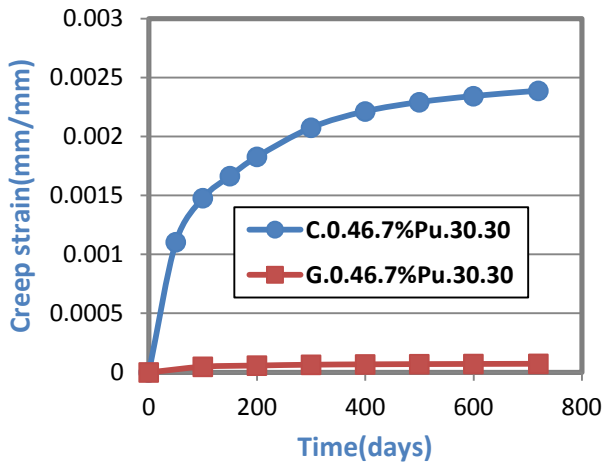


Fig.(5-135): Time vs Creep Strain

Behavior for Models(#.0.46.7%Pu.30.30)

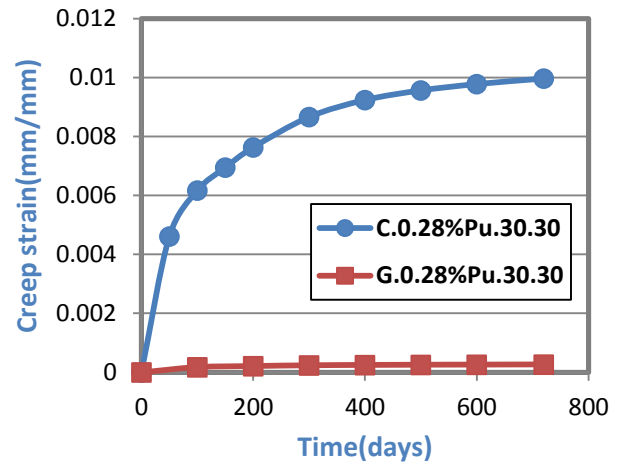


Fig.(5-136): Time vs Creep Strain

Behavior for Models(#.0.28%Pu.30.30)

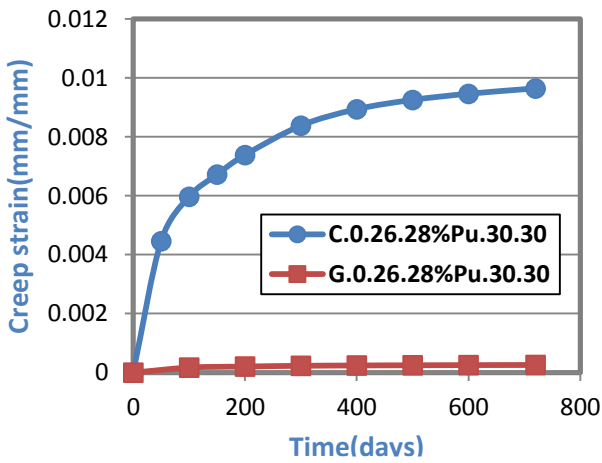


Fig.(5-137): Time vs Creep Strain

Behavior for Models(#.0.26.28%Pu.30.30)

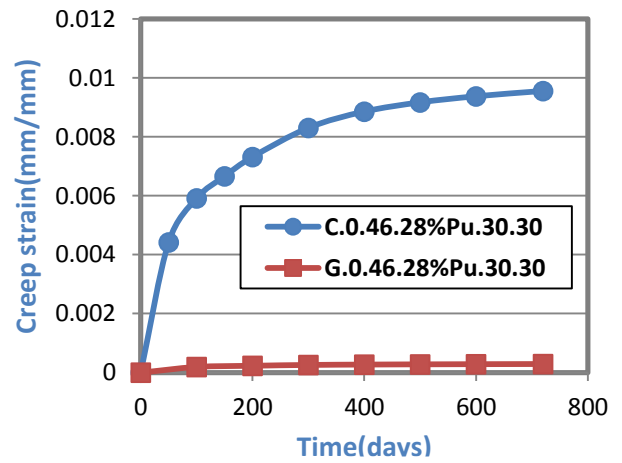


Fig.(5-138): Time vs Creep Strain

Behavior for Models(#.0.46.28%Pu.30.30)

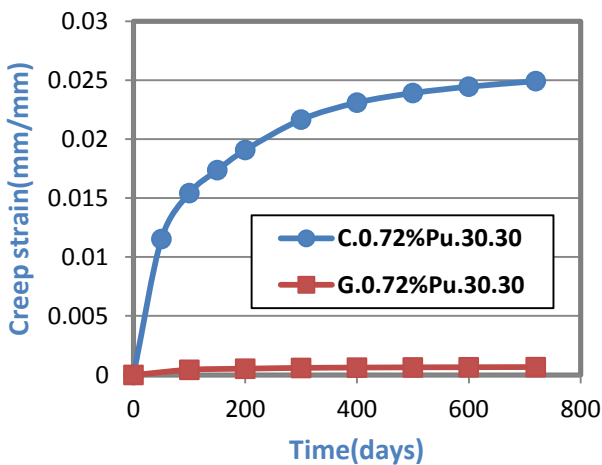


Fig.(5-139): Time vs Creep Strain

Behavior for Models(#.0.72%Pu.30.30)

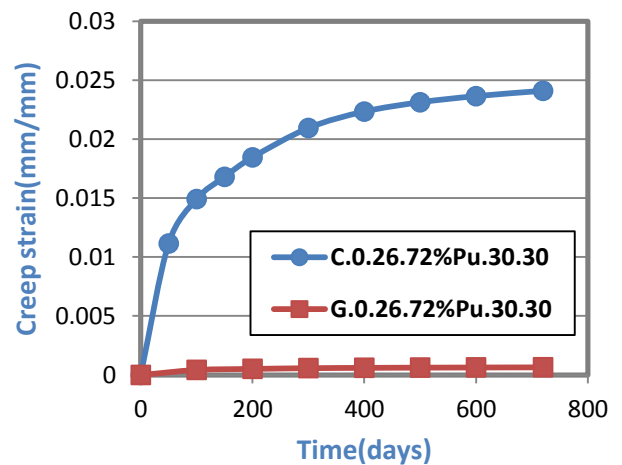


Fig.(5-140): Time vs Creep Strain

Behavior for Models(#.0.26.72%Pu.30.30)

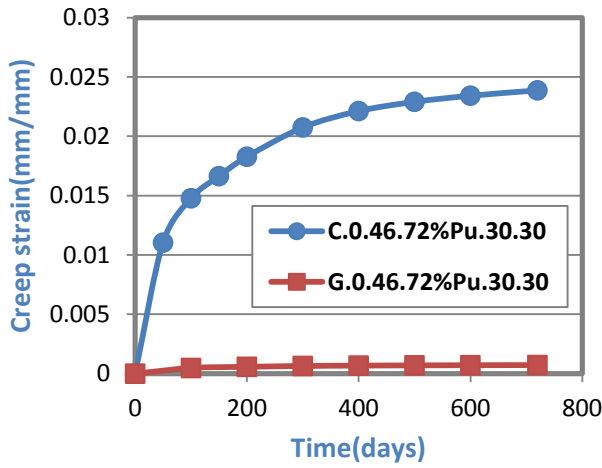


Fig.(5-141): Time vs Creep Strain

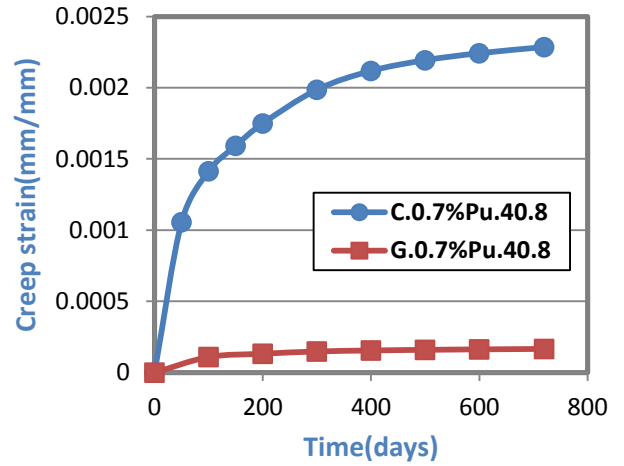


Fig.(5-142): Time vs Creep Strain

Behavior for Models(#.0.64.72%Pu.30.30)

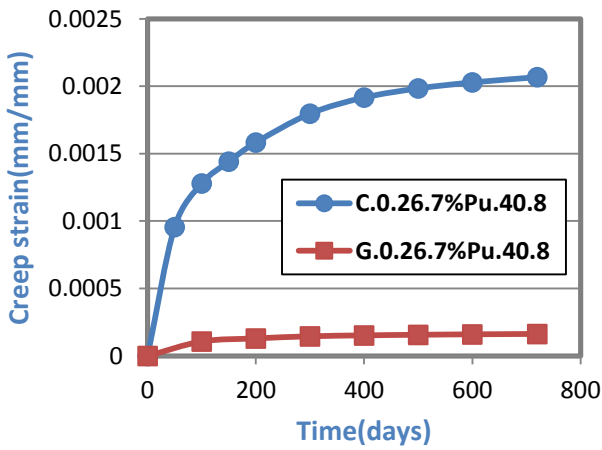


Fig.(5-143): Time vs Creep Strain

Behavior for Models(#.0.7%Pu.40.8)

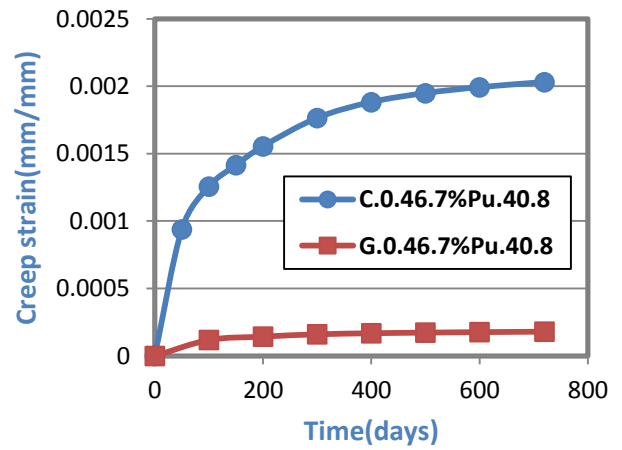


Fig.(5-144): Time vs Creep Strain

Behavior for Models(#.0.26.7%Pu.40.8)

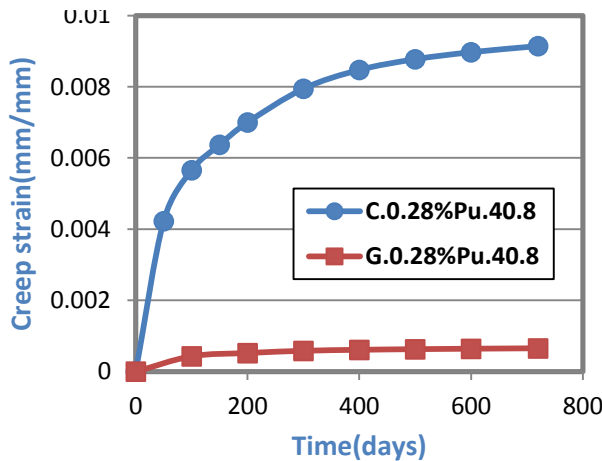


Fig.(5-145): Time vs Creep Strain

Behavior for Models(#.0.64.7%Pu.40.8)

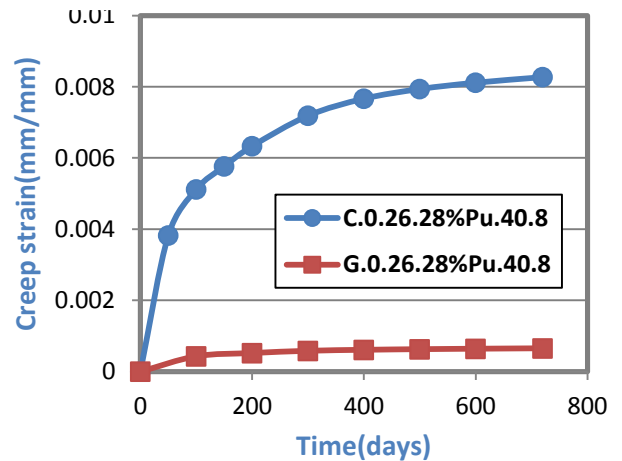


Fig.(5-146): Time vs Creep Strain

Behavior for Models(#.0.28%Pu.40.8)

Behavior for Models(#.0.26.28%Pu.40.8)

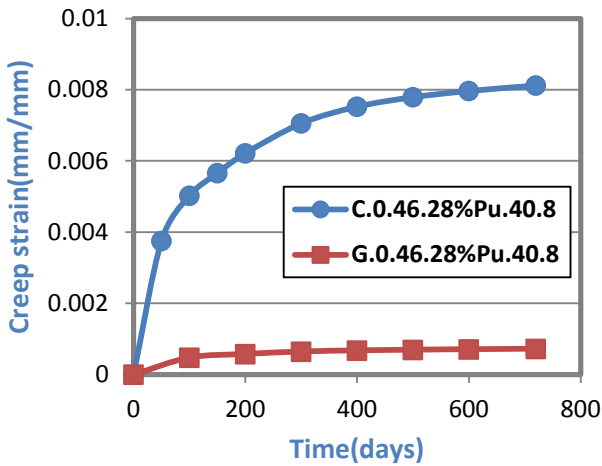


Fig.(5-147): Time vs Creep Strain

Behavior for Models(#.0.46.28%Pu.40.8)

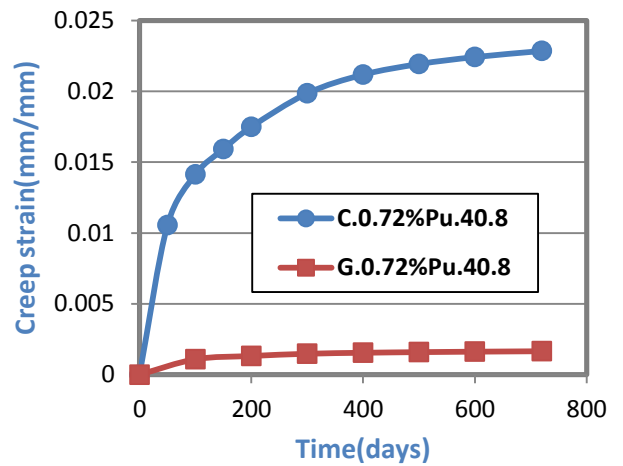


Fig.(5-148): Time vs Creep Strain

Behavior for Models(#.0.72%Pu.40.8)

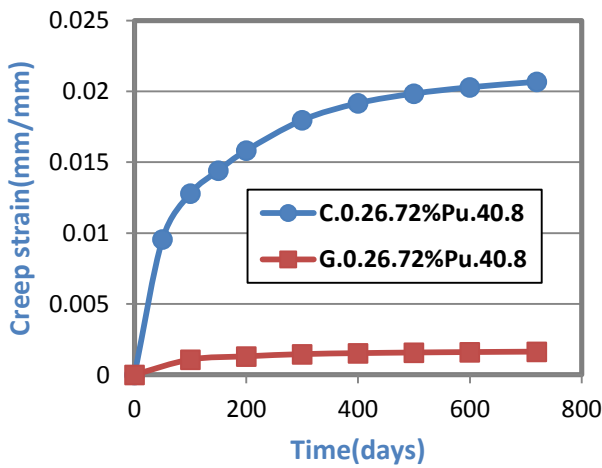


Fig.(5-149): Time vs Creep Strain

Behavior for Models(#.0.26.72%Pu.40.8)

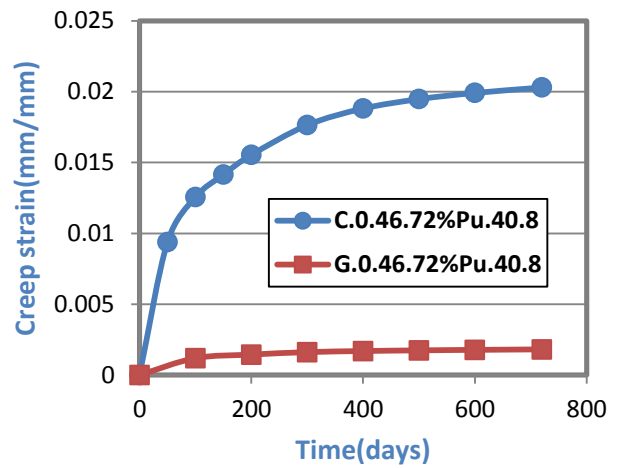


Fig.(5-150): Time vs Creep Strain

Behavior for Models(#.0.46.72%Pu.40.8)

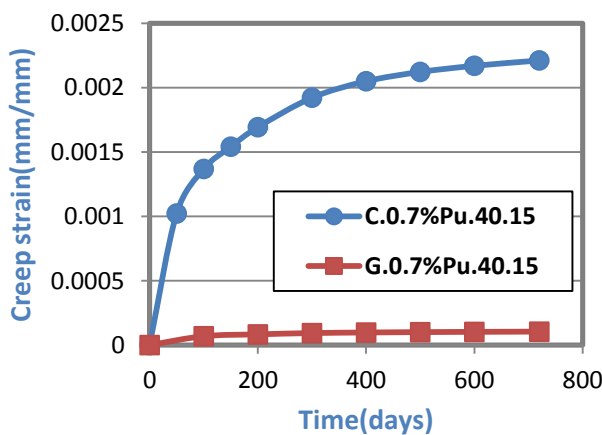


Fig.(5-151): Time vs Creep Strain

Behavior for Models(#.0.7%Pu.40.15)

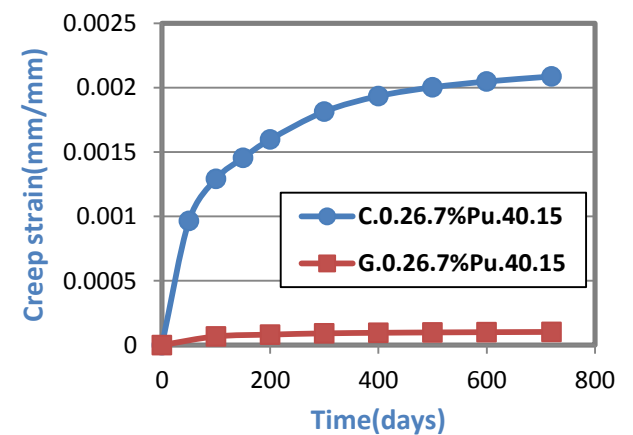


Fig.(5-152): Time vs Creep Strain

Behavior for Models(#.0.26.7%Pu.40.15)

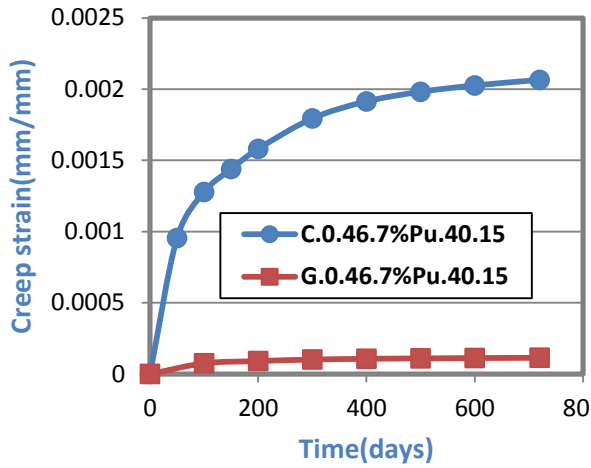


Fig.(5-153): Time vs Creep Strain

Behavior for Models(#.0.46.7%Pu.40.15)

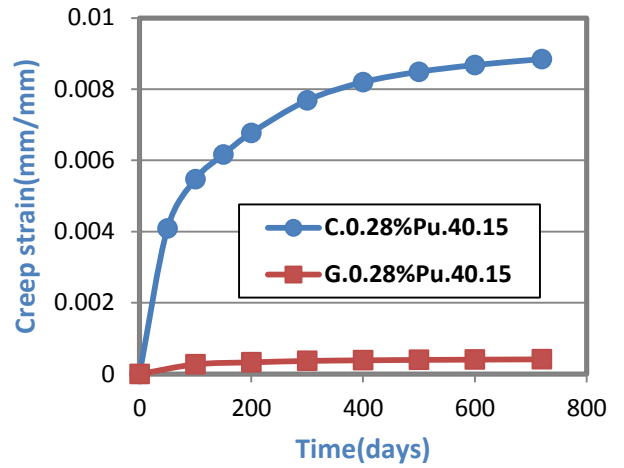


Fig.(5-154): Time vs Creep Strain

Behavior for Models(#.0.28%Pu.40.15)

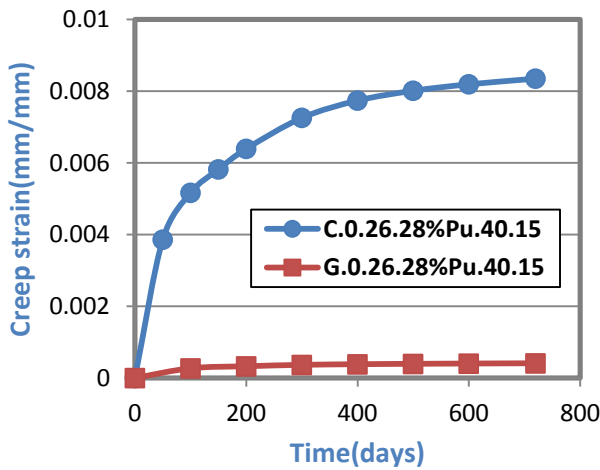


Fig.(5-155): Time vs Creep Strain

Behavior for Models(#.0.26.28%Pu.40.15)

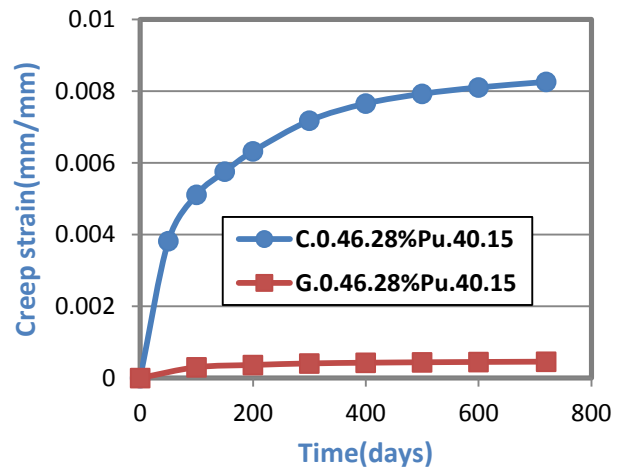


Fig.(5-156): Time vs Creep Strain

Behavior for Models(#.0.46.28%Pu.40.15)

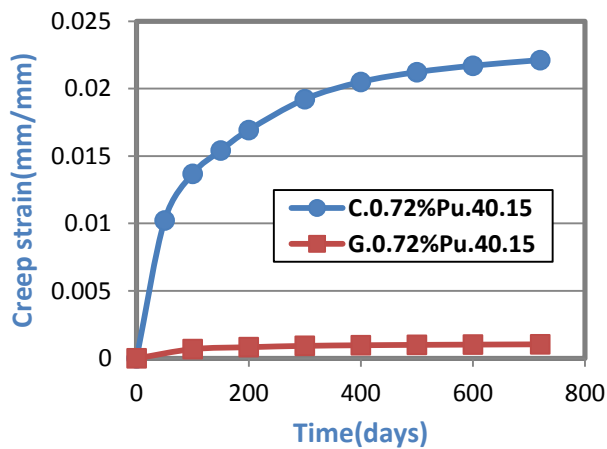


Fig.(5-157): Time vs Creep Strain

Behavior for Models(#.0.72%Pu.40.15)

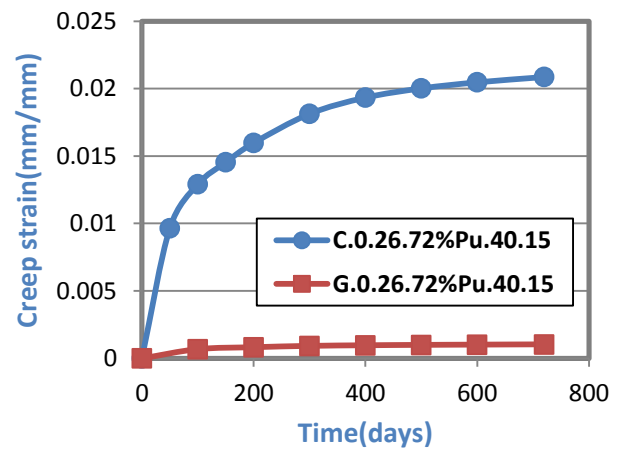


Fig.(5-158): Time vs Creep Strain

Behavior for Models(#.0.26.72%Pu.40.15)

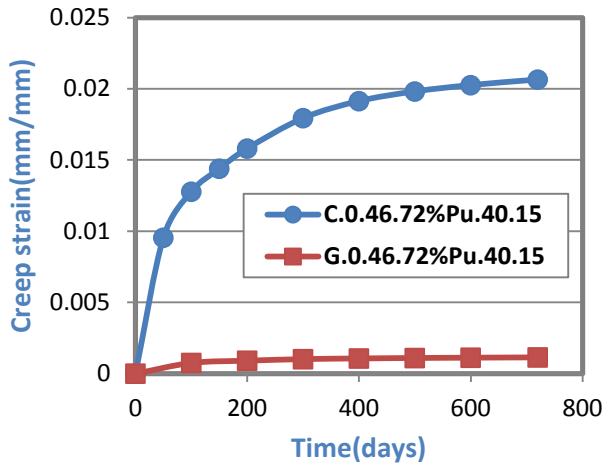


Fig.(5-159): Time vs Creep Strain

Behavior for Models(#.0.46.72% P_u .40.15)

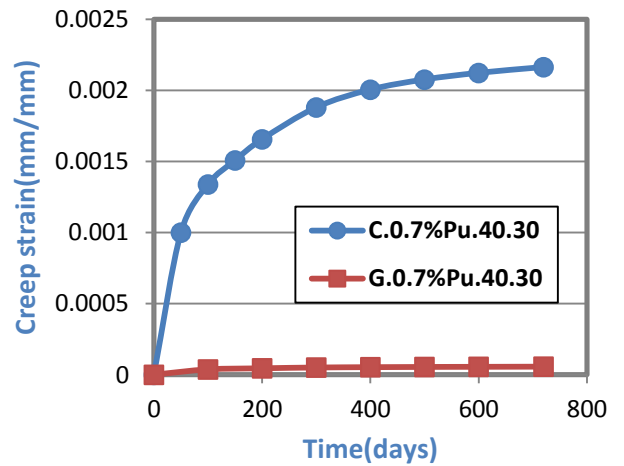


Fig.(5-160): Time vs Creep Strain

Behavior for Models(#.0.7% P_u .40.30)

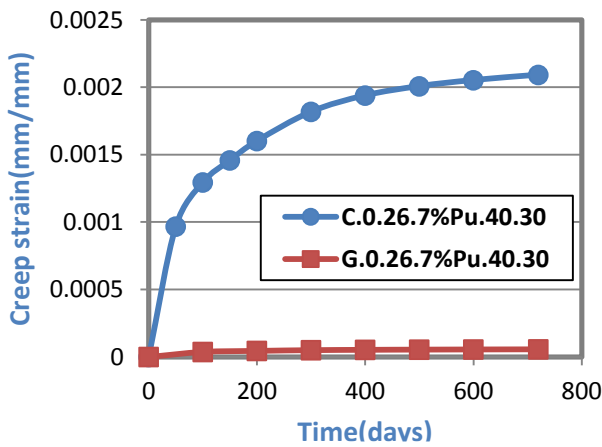


Fig.(5-161): Time vs Creep Strain

Behavior for Models(#.0.26.7% P_u .40.30)

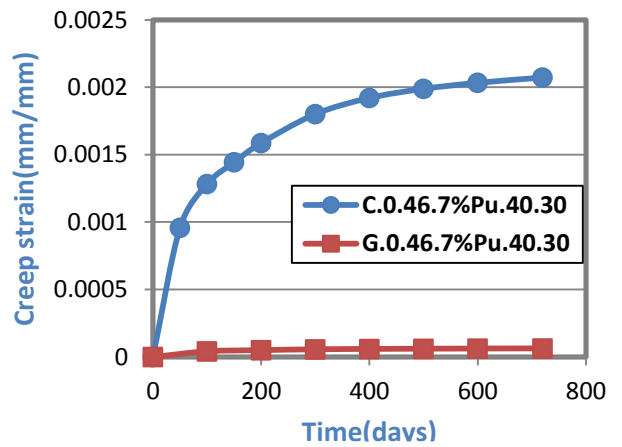


Fig.(5-162): Time vs Creep Strain

Behavior for Models(#.0.26.7% P_u .40.30)

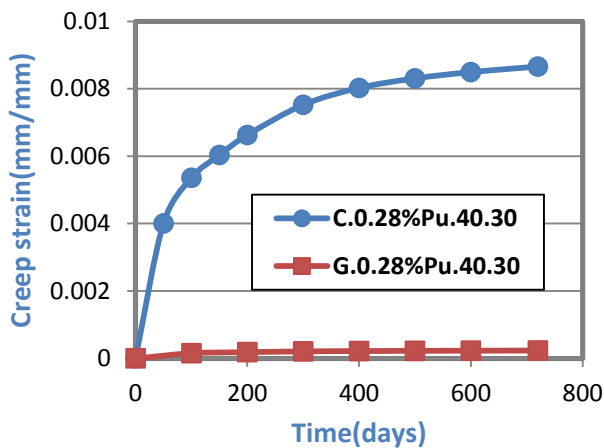


Fig.(5-163): Time vs Creep Strain

Behavior for Models(#.0.28% P_u .40.30)

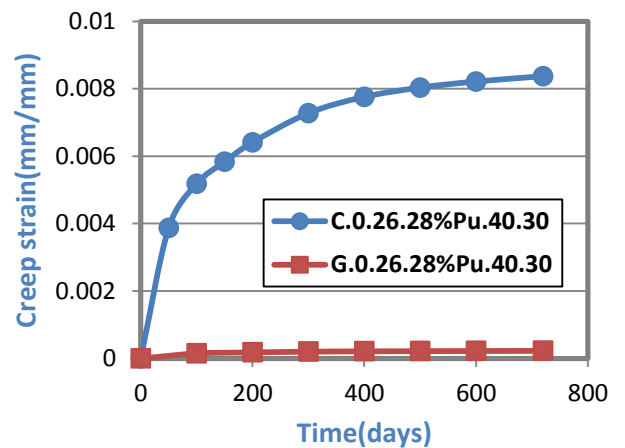


Fig.(5-164): Time vs Creep Strain

Behavior for Models(#.0.26.28% P_u .40.30)

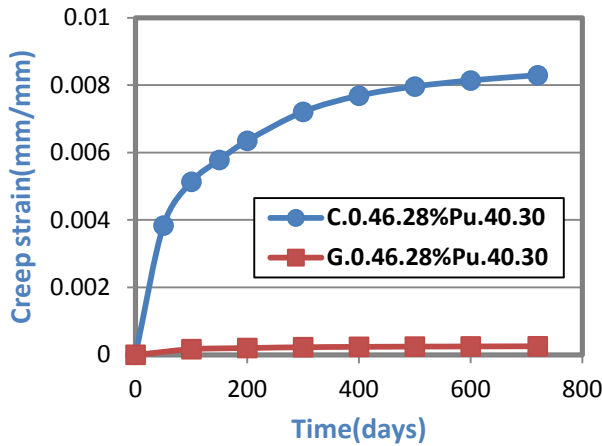


Fig.(5-165): Time vs Creep Strain

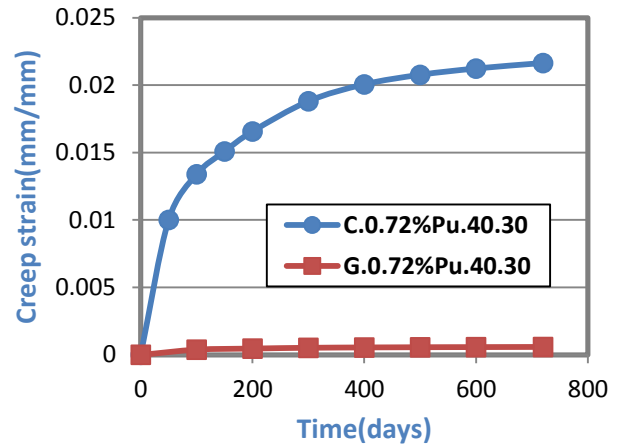


Fig.(5-166): Time vs Creep Strain

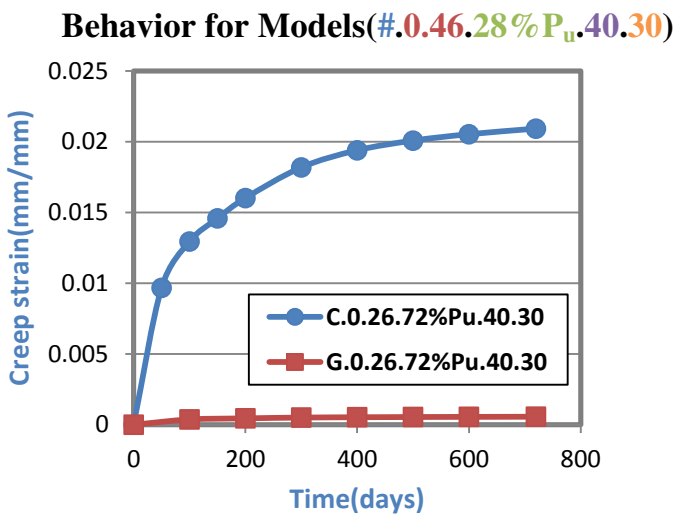


Fig.(5-167): Time vs Creep Strain

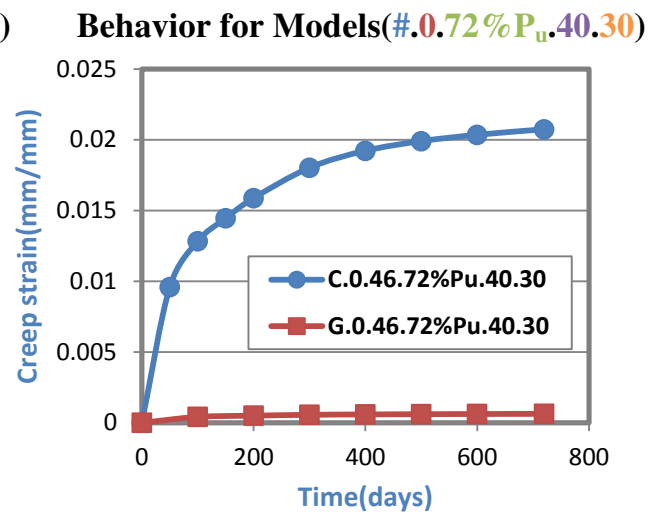


Fig.(5-168): Time vs Creep Strain

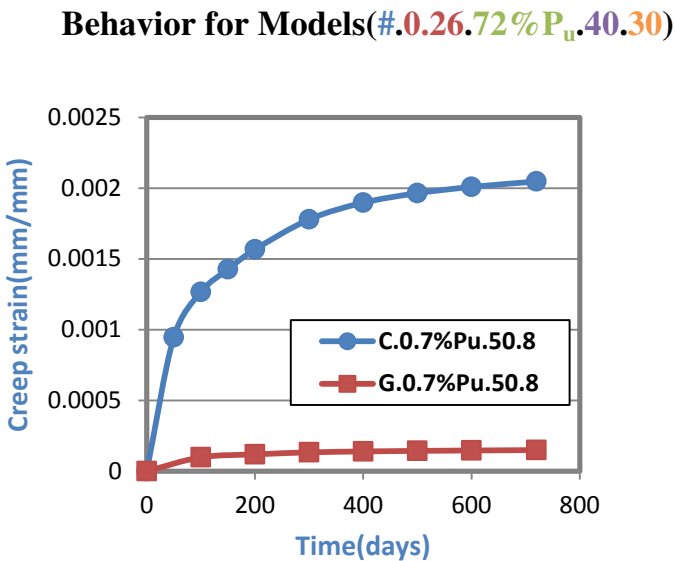


Fig.(5-169): Time vs Creep Strain

Behavior for Models(#.0.7%Pu.50.8)

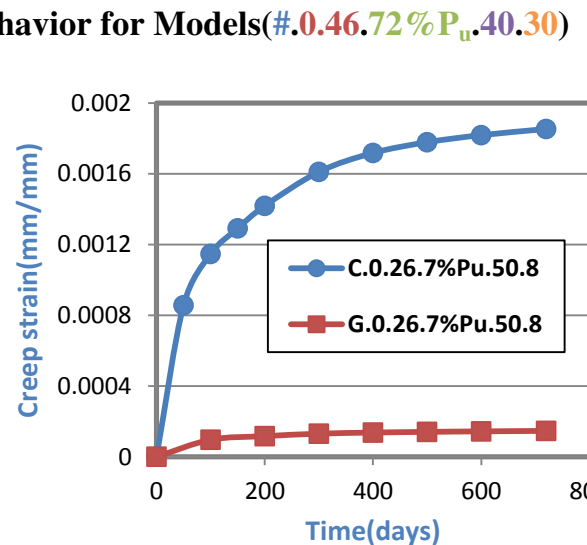


Fig.(5-170): Time vs Creep Strain

Behavior for Models(#.0.26.7%Pu.50.8)

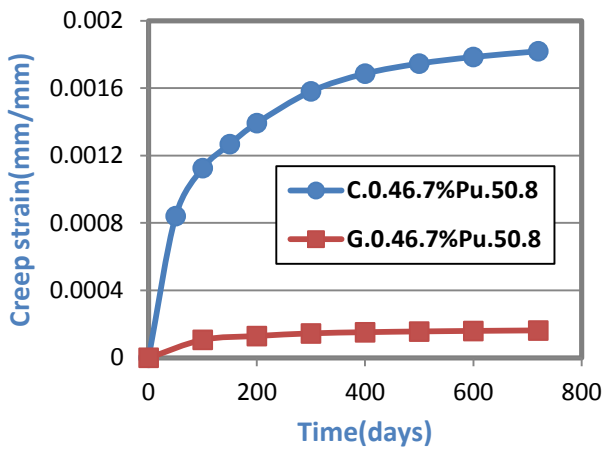


Fig.(5-171): Time vs Creep Strain

Behavior for Models(#.0.46.7%Pu.50.8)

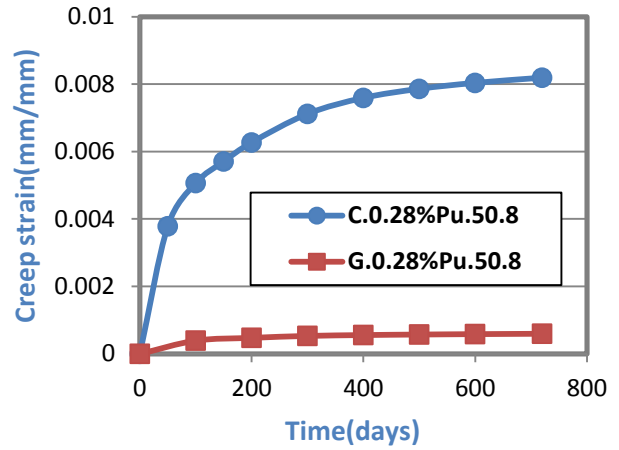


Fig.(5-172): Time vs Creep Strain

Behavior for Models(#.0.28%Pu.50.8)

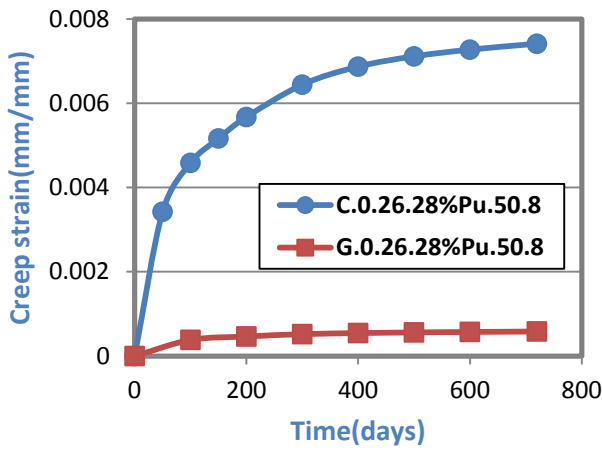


Fig.(5-173): Time vs Creep Strain

Behavior for Models(#.0.26.28%Pu.50.8)

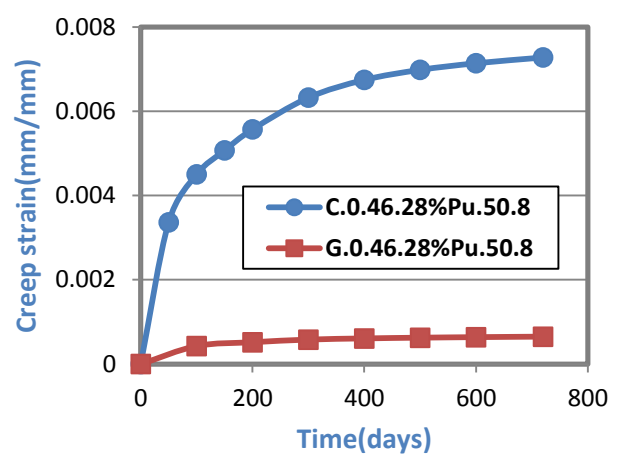


Fig.(5-174): Time vs Creep Strain

Behavior for Models(#.0.46.28%Pu.50.8)

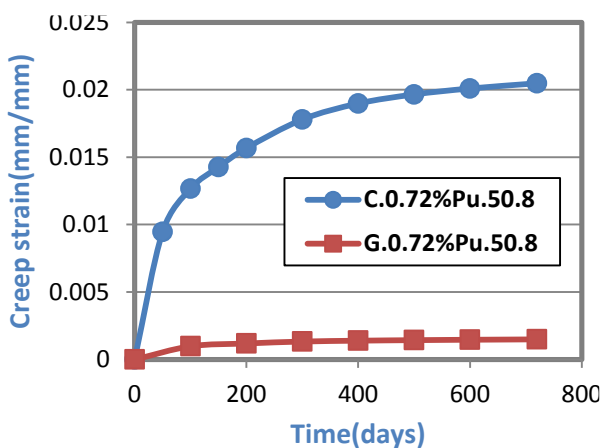


Fig.(5-175): Time vs Creep Strain

Behavior for Models(#.0.72%Pu.50.8)

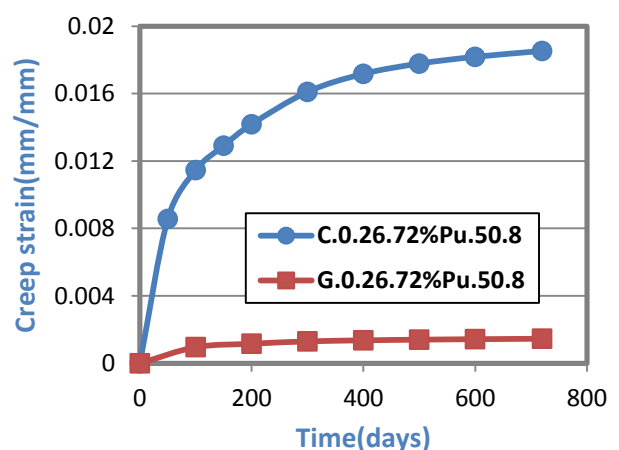


Fig.(5-176): Time vs Creep Strain

Behavior for Models(#.0.26.72%Pu.50.8)

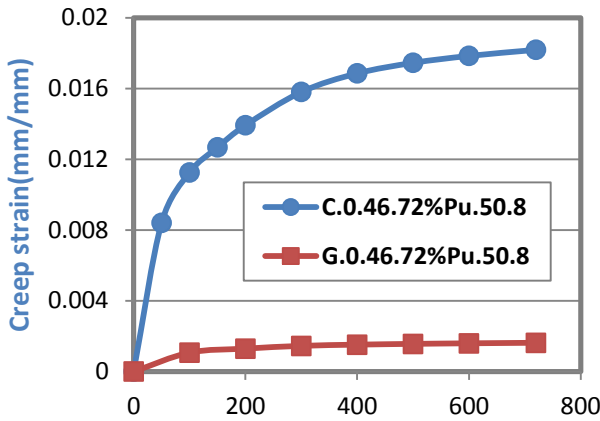


Fig.(5-177): Time vs Creep Strain

Behavior for Models(#.0.46.72%Pu.50.8)

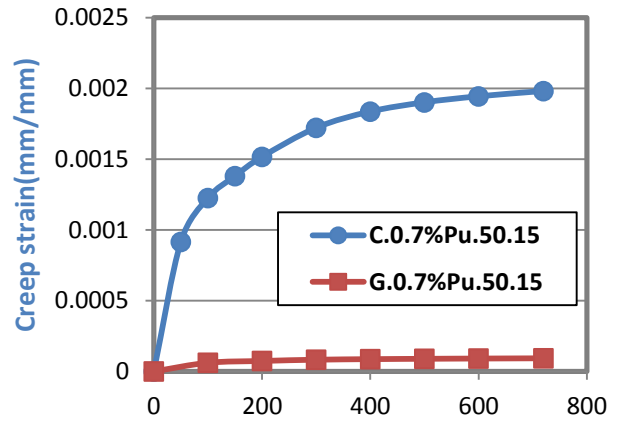


Fig.(5-178): Time vs Creep Strain

Behavior for Models(#.0.7%Pu.50.15)

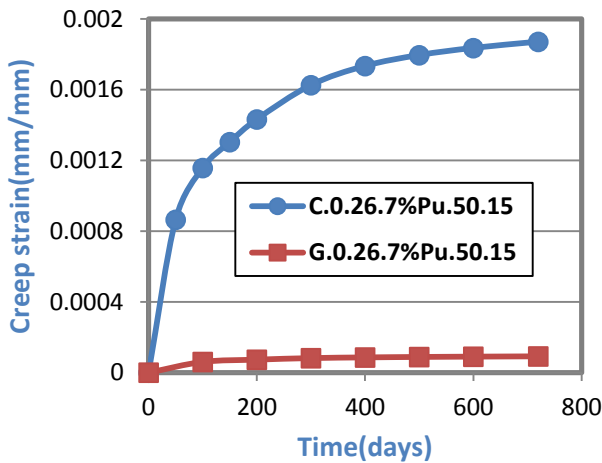


Fig.(5-179): Time vs Creep Strain

Behavior for Models(#.0.26.7%Pu.50.15)

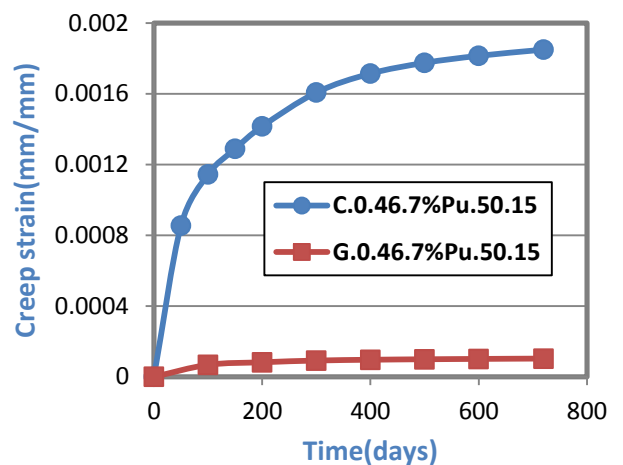


Fig.(5-180): Time vs Creep Strain

Behavior for Models(#.0.46.7%Pu.50.15)

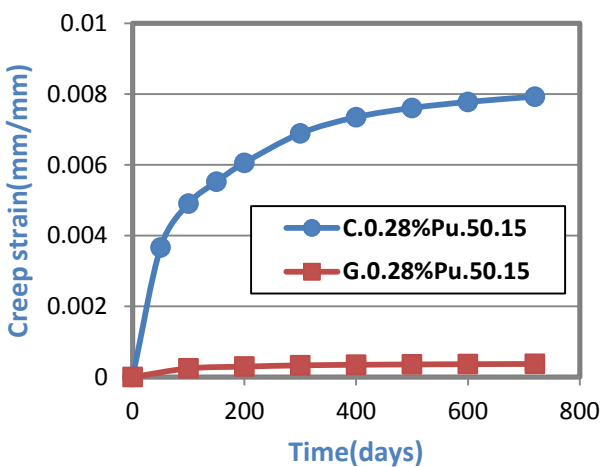


Fig.(5-181): Time vs Creep Strain

Behavior for Models(#.0.28%Pu.50.15)

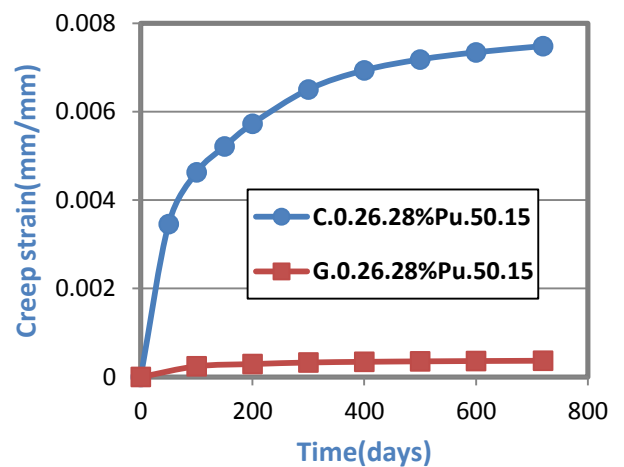


Fig.(5-182): Time vs Creep Strain

Behavior for Models(#.0.26.28%Pu.50.15)

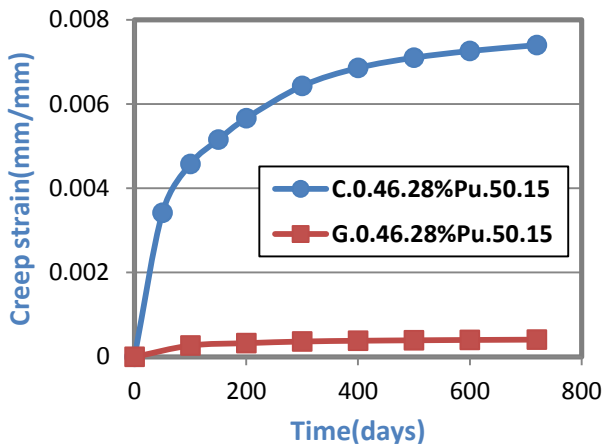


Fig.(5-183): Time vs Creep Strain

Behavior for Models(#.0.46.28%Pu.50.15)

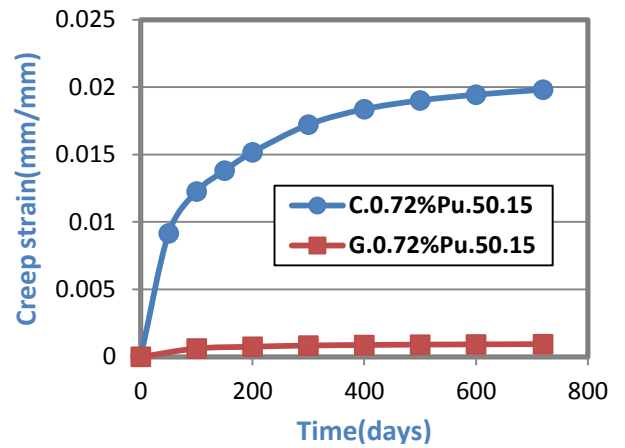


Fig.(5-184): Time vs Creep Strain

Behavior for Models(#.0.72%Pu.50.15)

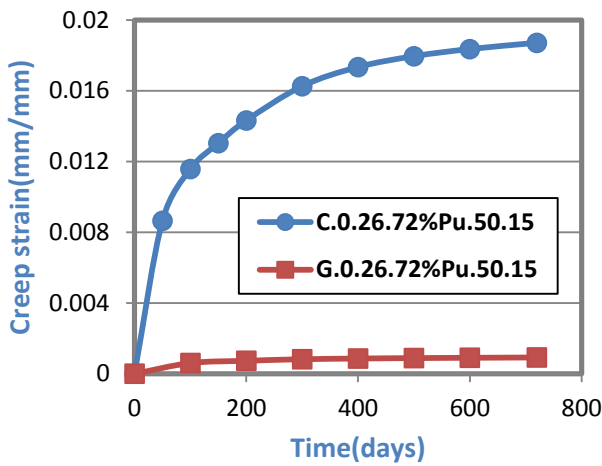


Fig.(5-185): Time vs Creep Strain

Behavior for Models(#.0.26.72%Pu.50.15)

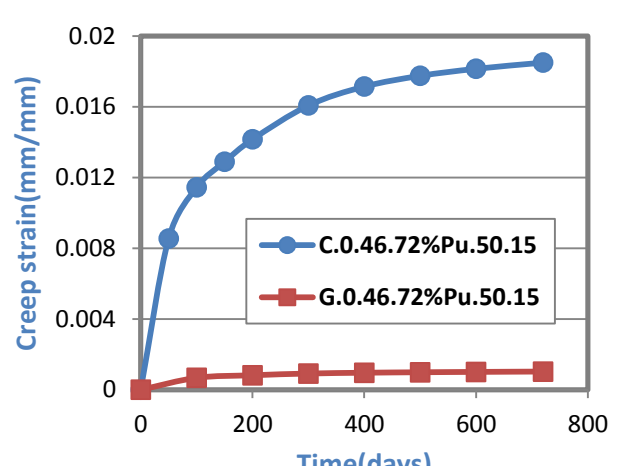


Fig.(5-186): Time vs Creep Strain

Behavior for Models(#.0.46.72%Pu.50.15)

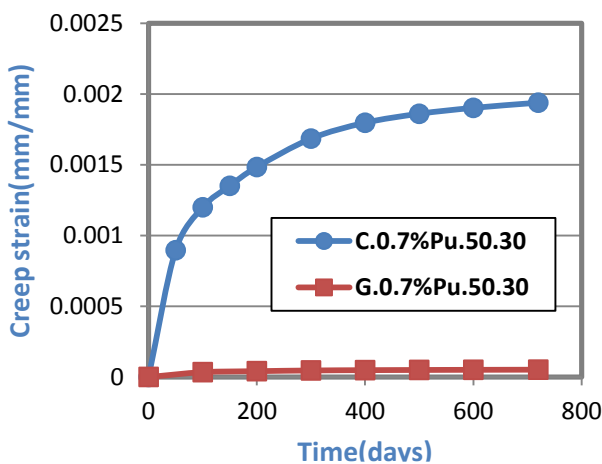


Fig.(5-187): Time vs Creep Strain

Behavior for Models(#.0.7%Pu.50.30)

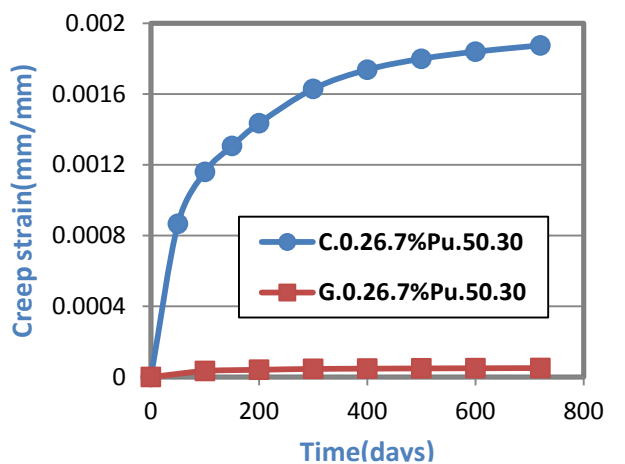


Fig.(5-188): Time vs Creep Strain

Behavior for Models(#.0.26.7%Pu.50.30)

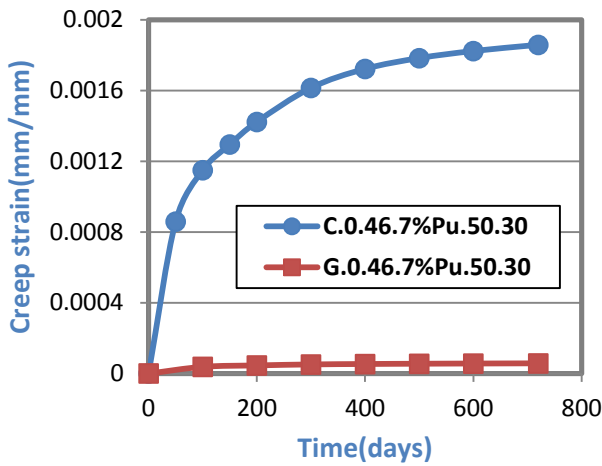


Fig.(5-189): Time vs Creep Strain

Behavior for Models(#.0.46.7%Pu.50.30)

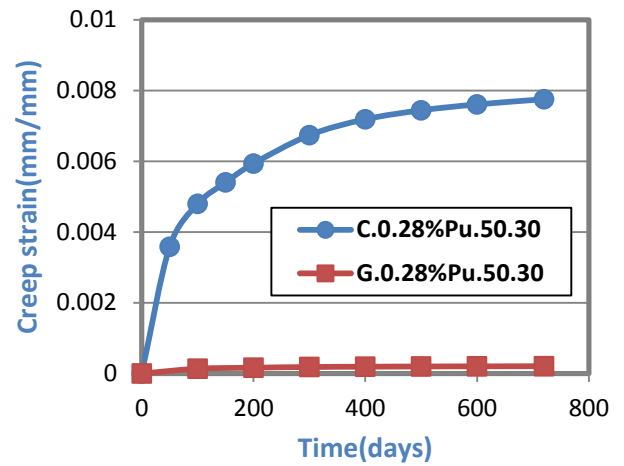


Fig.(5-190): Time vs Creep Strain

Behavior for Models(#.0.28%Pu.50.30)

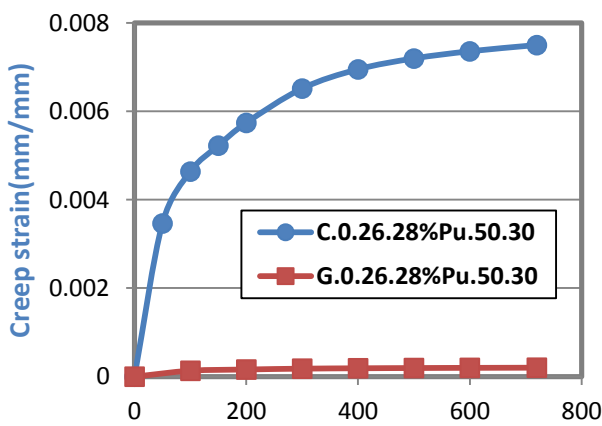


Fig.(5-191): Time vs Creep Strain

Behavior for Models(#.0.26.28%Pu.50.30)

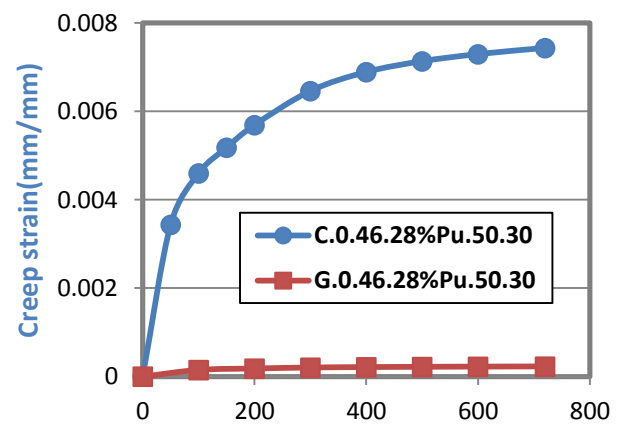


Fig.(5-192): Time vs Creep Strain

Behavior for Models(#.0.46.28%Pu.50.30)

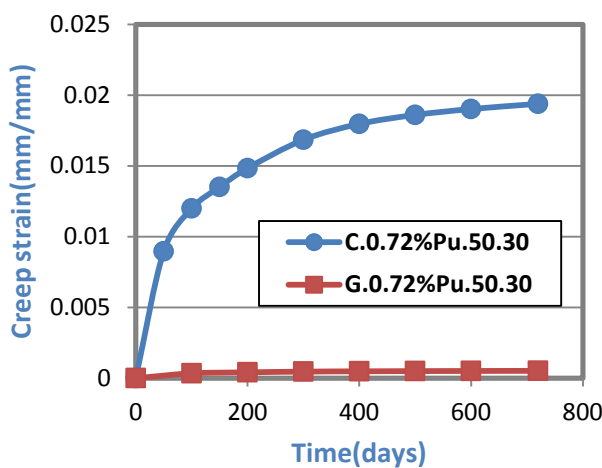


Fig.(5-193): Time vs Creep Strain

Behavior for Models(#.0.72%Pu.50.30)

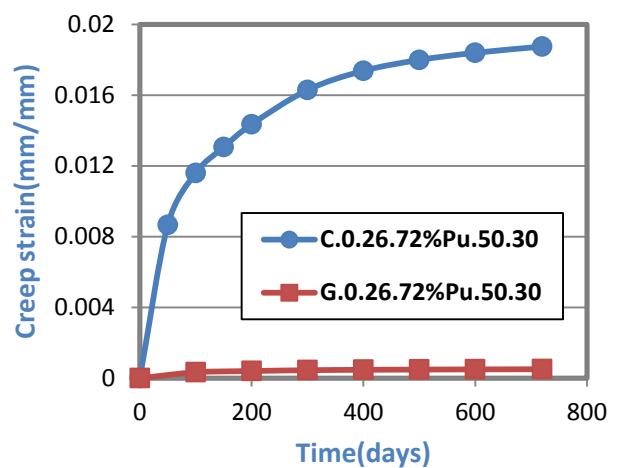


Fig.(5-194): Time vs Creep Strain

Behavior for Models(#.0.26.72%Pu.50.30)

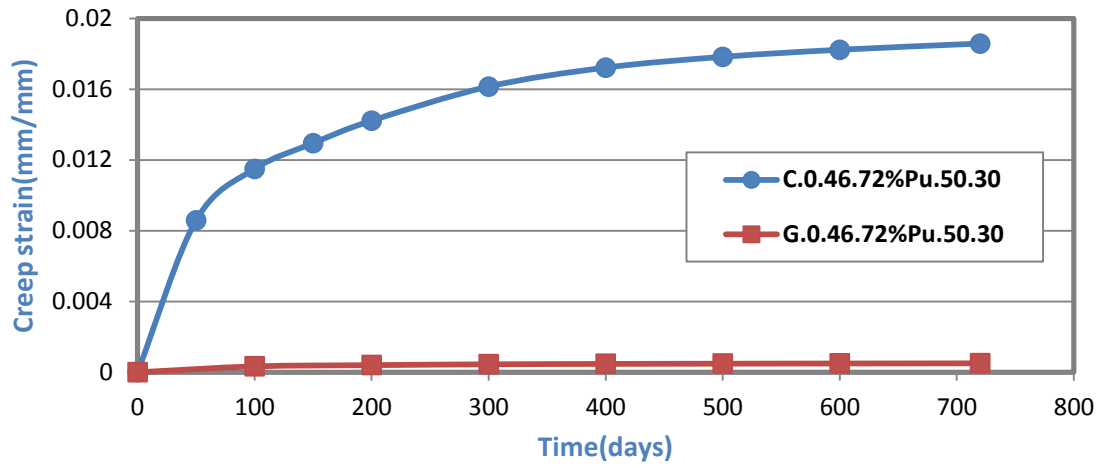


Fig.(5-195): Time vs Creep Strain Behavior for Models(#.0.46.72%Pu.50.30)

Chapter Six

Conclusions and Recommendations for Future Studies

6.1: General:

This chapter presents the conclusion of nonlinear finite element analysis of strengthening reinforced concrete columns, depending on this study. It includes the review of the effect of (magnitude of sustained load, eccentricity magnitude, length-diameter ratio, compressive concrete strength and FRP type). Also, it includes the recommendation and suggestions for future research.

6.2: Conclusions:

An extensive numerical simulation into the long-term behavior of (Carbon-or-Glass) FRP-confined concrete columns were carried out. This study resulted in a number of findings and outcomes as follows:

- 1- Nonlinear finite element with viscoelastic model showed a good agreement when it was compared with experimental results the maximum difference was 5.9%, that's occurred due to this study deals with enhanced the stress relaxation model of concrete material.
- 2- The finite element analysis results showed a significant increase in the axial compressive strength of the FRP-wrapped reinforced concrete columns as compared with the unstrengthened columns about 310.5% for CFRP and 26.6% for GFRP in the short term, whereas, increased about 167.9% and 86.4% in the creep strain of long-term analysis for CFRP and GFRP respectively.
- 3- Strengthening the reinforced concrete columns by bonding a single hooping layer of CFRP to the concrete core of the column increases strength of the

column by 310.5%, whereas it increases about 26.6% of the GFRP hooping layer.

4- The concrete compressive strength has a significant effect on the strength of the columns. Increasing the concrete strength about 33.33% lead to increase the strength of columns about 13.2%. This phenomenon is to be done because the high strength concrete has been less creep strain.

5- Increasing of the sustained axial load of the columns is significantly affecting on creep strain behavior. It was showed, when increased the sustained load about 300% lead to increase the creep strain about 300% for a same column specimen. That occurred due to the residual stresses of concrete have been increased in the same manner.

6- Bond strength target at the interface of the concrete column core and the FRP sheets is low as compared with that of steel and the concrete column surface, but still large enough to counteract, and actually reduce, the creep of the concrete core.

7- The ACI 209 model has a good criteria for calculating the creep of the FRPconfined concrete column. The difference between the ACI 209 model and test results of the of the FRP - specimens, however, is not as significant. The max error of shear strain modulus it was founded less than 2.5%.

8- The eccentricity and length-diameter ratio not significantly effect on the strengthened concrete columns creep strain.

6.3: Recommendations for Future Research:

- 1- It was recommended do a future research for calculating the effect of FRP warping region length.
- 2- Future research needs to focus on creep buckling of CFRP strengthened concrete columns.
- 3- Calculating creep strain of concrete columns using other creep models.
- 4- Studying the behavior of hybrid steel-concrete columns, including time effect.
5. Studying the creep in fired concrete columns.

References:

Abdel-Hay, & Ahmed Shaban., 2014, "***Partial Strengthening of R.C Square Columns Using CFRP***", HBRC Journal, Vol. 10, No. 3, pp. 279-286.

Abdullah, Takiguchi, K., 2003, "***An Investigation into the Behavior and Strength of Reinforced Concrete Columns Strengthened with Ferrocement Jackets***", Cement and Concrete Composites, Vol. 25, No.2, pp. 1-8.

ACI 318-14, American Concrete Institute, 2014, "***Building Code Requirements for Reinforced Concrete***", American Concrete Institute.

ACI Committee 209R, 2010, "***Prediction of Creep, Shrinkage and Temperature Effects on Concrete Structures***", ACI Manual of Concrete Practice, Part 1, pp. 1-47

Al-Ahmad, H., 2011, "***Nonlinear Analysis of Eccentrically Loaded Reinforced Concrete Columns Strengthened with Fiber Reinforced Polymer***", M.Sc. Thesis, Baghdad University, pp. 126.

Al-Chami, G., 2006, "***Creep Behaviour of CFRP Strengthened Concrete Columns and Beams***", Ph.D Thesis, University of Sherbrooke, Canada, pp. 252.

Al-Musawi, A., 2012, "***Experimental Study of Reinforced Concrete Columns Strengthened with CFRP under Eccentric Loading***", M.Sc. Thesis, AI-Mustansiriya University, pp. 120.

Al-Shaarbaf I. A. S., "***Three-Dimensional Nonlinear Finite Element Analysis of Reinforced Concrete Beams in Torsion***", Ph.D. Thesis, University of Bradford, 1990, pp. 323.

Anderson, C. A. , 1982, "***Chapter 8: Numerical Creep Analysis of Structures***", Creep and Shrinkage in Concrete Structures, Bažant, Z.P.and Wittmann, F.H. , John Wiley & Sons , New York , pp.259-304. **As cited in [Mahmood, 2005]**

ANSYS, "***ANSYS Help***", Release 12.0, Copyright 2009.

Bangash, M. Y. H., 1989, "***Concrete and Concrete Structures: Numerical Modeling and Applications***", Elsevier Science Publishers Ltd., London, England.

References

Barbero, E. J., 2014, "*Finite Element Analysis of Composite Materials Using ANSYS*", pp. 314.

Bruegger, J. P., 1974, "*Methods of Analysis of the Effects of Creep in Concrete Structures*", Ph.D thesis, University of Toronto, Toronto.

Bažant, Z. P. ,1972," *Prediction of Concrete Creep Effects Using Age-Adjusted Effective Modulus* " , J. of Am. Concr. Inst., ACI ,Vol. 69, No. 4, pp. 212-217.

Bažant, Z. P. ,1988, "*Mathematical Modeling of Creep and Shrinkage of Concrete*", John Wiley & Sons, Ltd. **As cited in [Mahmood, 2005]**

Bažant, Z. P., "*Creep of Concrete*", Encyclopedia of Material Science and Technology, Vol. 2C, Elsevier, Amsterdam, 2001, pp. 1797-1800. **As cited in [Hassan, 2007]**

Bažant, Z. P., 1982, "*Mathematical Models for Creep and Shrinkage of Concrete*", Creep and Shrinkage in Concrete Structures, Bažant, Z. P. & Wittmann, F. H., John Wiley & Sons, New York, pp. 163-256. **As cited in [Mahmmod, 2005]**

Bažant, Z. P., and Baweja, S., "*Creep and Shrinkage Prediction Model for Analysis and Design of Concrete Structures: Model B3*", ACI, Sp-194, American Concrete Institute, Farmington Hill, Michigan, 2000, pp. 1-83. **As cited in [Mahmmod, 2005]**

Benzaid R., Chikh N. , & Mesbah H., 2008,"*Behaviour of Square Concrete Column Confined with GFRP Composite Warp*", Journal of Civil Engineering and Management, Vol. 14, No. 2, pp. 115-120.

Bradford, M. A., 2005, " *Shrinkage and creep response of slender reinforced concrete columns under moment gradient: theory and test results*", Magazine of Concrete Research, Vol. 57, No. 4, pp. 235-246.

Carlion, A., 2003, "*Carbon Fiber Reinforced Polymers for Strengthening of Structural Elements*", Lulea University of Technology, Sweden, pp. 13-16.

CEB-FIP, CEB-FIP Model Code 1990,"*Design Code Comite Euro-International Du Buton*", ASCE (Editor & Publisher), January 1993, pp. 1-462. **As cited in [Hassan, 2007]**

Christensen, R. M. , 1982, "*Chapter 1: Theory of Viscoelasticity*",

References

Viscoelastic Stress Strain Constitutive Relations, New York , pp.1-30.

Claeson, C. and Gylltoft, K., 2000, "*Slender Concrete Columns Subjected to Sustained and Short-Term Eccentric Loading*", *ACI Structural Journal*, Vol. 97, No. 1, pp. 45-53.

Dave, A., Nagar, P. & Parmar, J., 2014, "*Comparative Study of Gfrp Laminated RC Column Using Experimental Results and Isis-Canada*", *International Journal of Research in Engineering and Technology*, Vol. 3, No. 4, pp. 700-704.

Dong, C., Yu, L. & Ru, Y., 2005, "*Three-Dimensional Nonlinear Analysis of Creep in Concrete-Filled Steel Tube Columns*", *Journal of Zhejiang University Science*, Vol. 6A, No. 8, pp. 826-835.

El Maaddawy T., 2009, "*Strengthening of Eccentrically Loaded Reinforced Concrete Columns with Fiber-Reinforced Polymer Wrapping System: Experimental Investigation and Analytical Modeling*", *Journal of Composites for Construction*, ASCE, Vol. 13, No. 1, pp. 13-24, as cited in [Al-Ahmad, 2011]

Fahmi, H. M. and Karim, A, 2016, "*Creep Analysis of Axially Loaded Frp Concrete Columns*", *Al-Mansour Journal*, No. 6, pp. 1-28.

Findley, W. N., Lai, J. S. and Onaran, K., 1976, "*Creep and Relaxation of Nonlinear Viscoelastic Materials*", North-Holland Publishing Company.

Gilbert, R. & Ranzi, G., 2011, "*Time-Dependent Behaviour of Concrete Structures*", pp. 423.

Grestle, K. H., 1980, "*Behavior of Concrete under Multiaxial Stress State*", *Journal of the Engineering Mechanics Division*, ASCE, Vol. 106, No. EM6, pp. 1383-1403.

Hamed, E & Lai, C., 2016, "*Geometrically and Materially Nonlinear Creep Behaviour of Reinforced Concrete Columns*", *Structures*, Vol. 5, pp. 1-12.

Han, L. H., Tao, Z., & Liu, W., 2004, "*Effects of Sustained Load on Concrete-Filled Hollow Structural Steel Columns*", *Journal of Structural Engineering*, ASCE, Vol. 130, No. 9, pp. 1392-1404.

Hassan, D., 2007, "*Time-Dependent Behavior of Concrete-Filled Steel Tube Columns*", M.Sc. Thesis, Al-Nahrain University, pp. 102.

References

Hutton, D., 2004, "*Fundamentals of Finite Element Analysis*"

Hollaway, L. & Teng, J., 2008, "*Strengthening and Rehabilitation of Civil Infrastructures Using Fiber-Reinforced Polymers(FRP) composites*", Woodhead Publishing in Materials, pp. 385.

Ichinose, L. H., Watanabe, E., & Nakai, H., 2001, "*An Experimental Study on Creep of Concrete-Filled Steel Pipes*", Journal of Constructional Steel Research, Vol. 57, pp. 453-466.

Kabashi, Naser, Violeta Nushi, & Ridvan Aliu.,2015,"*Strengthening the Concrete Columns With the Carbon Polymer Fibres and Behaviour Under Centric Loads*",Vol. 2,No. 9,pp. 1-8.

Kachlakev, D., Miller, T. and Chansawat, K. ,2001, "*Finite Element Modeling of Reinforced Concrete Structures Strengthened with FRP Laminates*" Final Report, SPR 316, Oregon Department of Transportation Research Group and Federal Highway Administration, Washington DC.

Kaish, A. B. M. A., M. Jamil, S. N. Raman, & M. F. M. Zain., 2015, "*Axial Behavior of Ferrocement Confined Cylindrical Concrete Specimens with Different Sizes*", Construction and Building Materials, Vol.78, pp. 50–59.

Kaish, a. B. M. a., M. Jamil, S. N. Raman, M. F. M. Zain, & M. R. Alam., 2015, "*An Approach to Improve Conventional Square Ferrocement Jacket for Strengthening Application of Short Square RC Column*", Materials and Structures,.

Kaish, A. B. M., M. R. Alam, M. Jamil, & M. A. Wahed., 2013, "*Ferrocement Jacketing for Restrengthening of Square Reinforced Concrete Column under Concentric Compressive Load*", Procedia Engineering, Vol.54, pp. 720–728.

Katoka, L. T., 2010, " *ANÁLISE DA DEFORMABILIDADE POR FLUÊNCIA E RETRAÇÃO E SUA UTILIZAÇÃO NA MONITORAÇÃO DE PILARES DE CONCRETO*", Ph.D. Thesis, pp.204.

Katoka, L. & Bittencourt, T., 2014, "*Numerical and experimental analysis of time-dependent load transfer in reinforced concrete columns*", IBRACON Structures and Materials Journal, Vol.7, No. 5, pp. 747-774.

Kaw, A. K., 1997, "*Mechanics of Composite Materials*", CRC Press LLC, Boca Raton, Florida.

References

- Kown, S., Kim, T., Kim, Y. & Kim, J., 2007, "*Long-Term Behaviour of Square Concrete-Filled Steel Tubular Columns Under Axial Service Loads*", Magazine of Concrete Research, Vol. 59, No. 1, pp. 53-68.
- Kupfer, H. B, Hilsdorf, H. K. and Rusch, H., 1969, "*Behaviour of Concrete under Biaxial Stresses*", Journal of ACI, Vol. 66, No. 8, pp. 656-666.
- Logan, D. L. et al., 2007, "*A First Course in the Finite Element Method*", Fourth Edition
- Ma, Y. S. and Wang, Y. F., 2012, "*Creep of high strength concrete filled steel tube columns*", Thin Walled Structures, Vol. 53, pp. 91-98.
- MacGregor, J. G., 1992, "*Reinforced Concrete Mechanics and Design*", Prentice-Hall, Inc., Englewood Cliffs, NJ.
- Madureira, E., Siqueira, T. & Rodrigues, E., 2013, "*Creep strains on reinforced concrete columns*", IBRACON Structures and Materials Journal, Vol.6, No. 4, pp. 537-560.
- Maheswari, V. & Soman, M., 2015, "*Strengthening of RC Short Square Columns Using Improved Ferrocement Jacketing*", Vol.5, No.7, pp. 555-560.
- Mahmood, A. S., 2005, "*Analysis of Folded Plates Including Time Effects Using Finite Strip Method*", M.Sc. Thesis, University of Al-Mustansiriya, Department of Civil Engineering, pp. 140.
- Marqus, S. P. C. & Creus, G. J., 2012, "*Chapter Two: Rheological Models Integral and Differential Representations*"
- Masud, M., & Kumar, A., 2016, "*Strengthening of Circular RC Column Through External Confinement Using Ferrocement*", Indian Journal of Science and Technology, Vol. 9, No. 30, pp. 1-5.
- Mehta, P. K & Monteiro, P. J. M., 2006, "*Chapter 4: Concrete Microstructure, Properties and Materials*", Dimensional Stability, New York, pp. 85-120.
- Moshiri, Niloufar, Ardalan Hosseini, & Davood Mostofinejad, 2015, "*Strengthening of RC Columns by Longitudinal CFRP Sheets: Effect of Strengthening Technique*", Construction and Building Materials, Vol. 79, pp. 318-325.

References

- Mourad, S., & Shannag, M., 2012, "**Repair and Strengthening of Reinforced Concrete Square Columns Using Ferrocement Jackets**", Cement and Concrete Composites, Vol.34, No.2, pp. 288-294.
- Moaveni, S., 1999, "**Finite Element Analysis - Theory and Appln. With ANSYS**", Prentice Hall.
- Murray, A. L. & Gilbert, R. I. , 2015, "**Effects of Creep on The Strength of Eccentrically-Loaded Slender Reinforced Concrete Columns**", Australian Journal of Structural Engineering, Vol. 16, No. 2, pp. 129-136.
- Nabil, A., Heiza, K., Meleka, N. , & Tayel, M., 2014, "**Strengthening of Axially Loaded Circular Concrete Columns Using Externally Bonded GFRP Lateral Confinement and Near Surface Mounting Technique**", Sixth International Conference on NANO-Techonology in Construction, pp. 1-21.
- Naguib, W. & Mirmeran, A., 2002, "**Time-Dependent Behavior of Fiber Reinforced Polymer-Confined Concrete Columns under Axial Loads**", ACI Structural Journal, pp. 142-148.
- Naguib, W., & Mirmiran, A., 2003, "**Creep Modeling for Concrete-Filled Steel Tubes**", Journal of Constructional Steel Research, Vol. 59, pp. 1327-1344.
- Nasrin, S., 2013, "**Nonlinear Finite Element Analysis of Concrete Columns Confined by Fiber- Reinforced Polymers**", M.Sc. Thesis, Bangladesh University of Engineering and Technology, pp. 85.
- Neville, A. M. & Brooks, J. J., 2010, "**Chapter 12: Concrete Technology**", Elasticity and Creep, British, pp. 206-231.
- Olivova, K. & J. Bilcik., 2009, "**Strengthening of Concrete Columns With CFRP**", Slovak Journal of Civil Engineering, Vol. 1, pp. 1-9.
- Owen, D. R. J. and Hinton, E. , 1980, "**Finite element in Plasticity, Theory and Practice**" , Pineridge Press Limited, Swansea, U. K., 594p.
- Paulson, K. A., Nilson, A. H. and Hover, K. C., 1991, "**Long-Term Deflection of High-Strength Concrete Beams**", ACI Material Journal, Vol. 88, No. 2, pp.197-206.
- Phillips, D. V. and Zienkiewics, O. C., "**Finite Element Nonlinear Analysis of Concrete Structures**", Journal of Structural Division, ASCE Proceedings,

References

Part 2, Vol. 61, 1976, pp. 59-88.

Raval, R. & Dave, U., 2013, "*Behavior of GFRP Wrapped RC Columns of Different Shapes*", Procedia Engineering, Vol. 51, pp. 240-249.

Rolli, Yuvaraj & K. V. Mahesh Chandra, 2015, "*An Experimental Study on Strengthening of Rc Square Columns By Circularizing and Wrapping With Frp*", pp. 210-13.

Sadaoui, A. and Khennane, A., 2009, "*Effect of transient creep on the behaviour of reinforced concrete columns in fire*", Engineering Structures, Vol. 31, pp. 2203-2208.

Seffo, M. & M. Hamcho., 2012, "*Strength of Concrete Cylinder Confined by Composite Materials (CFRP)*", Energy Procedia, Vol. 19, pp. 276-285.

Shafeeq, S., 2016, "*Strengthening and Retrofitting of Reinforced Concrete Hollow Columns using Ultra-High Strength Ferro-Cement Fibers Composites*", M.Sc. Thesis, University of Anbar, pp. 103.

Silva, M. A. G., 2011, "*Behavior of Square and Circular Columns Strengthened with Aramidic or Carbon Fibers*", Construction and Building Materials, Vol. 25, No. 8, pp. 3222-3228.

Sirimontree, Sayan., 2015, "*Strengthening of Reinforced Concrete Column via Ferrocement Jacketing*", American Transactions on Engineering and Applied Sciences, Vol. 4, No. 1, pp. 39-47.

Sousa, P. C., Silva, H. N. & Soares, J. B., 2008, "*Prony Series Study for Viscoelastic Characterization of Asphalt Mixtures*". In: *19° Encontro de Asfalto, Instituto Brasileiro de Petróleo, Gás e Biocombustíveis – IBP*, Rio de Janeiro, Brazil.

Taghia, P. & Abu Bakar, S., 2013, "*Mechanical Behaviour of Confined Reinforced Concrete-CFRP Short Column- Based on Finite Element Analysis*", Civil Engineering, Vol. 24, No. 7, pp. 960–970.

Tarkhan, Mohamed A., 2015, "*Strengthening of Loaded Reinforced Concrete Columns Using Ferrocement Jackets*", International Journal of Innovative Research in Science Engineering and Technology, Vol.4, No.12, pp. 12154–12161.

Timoshenko, S. P., and Goodier, J. N. , 1982, "*Theory of Elasticity*", International Student Edition ,McGraw-Hill Book Co. ,Singapore.

References

- Toutanji, H. and Saafi, M., 2001, "*Stress-Strain Behavior of Concrete Columns Confined with Hybrid Composite Materials*", *Materials and Structures*, Vol. 35, pp. 338-347.
- Toutanji, H. and Saafi, M., 2001, "*Durability Studies on Concrete Columns Encased in PVC-FRP composite tubes*", *Composite Structures*, Vol. 54, pp. 27-35.
- Toutanji, H. and Deng, Y., 2002, "*Strength and Durability Performance of Concrete Axially Loaded Members Confined with AFRP Composite Sheets*", *Composites*, Vol. 33, pp. 255-261.
- Turgay, T., Z. Polat, H. O. Koksall, B. Doran, & C. Karakoç., 2010, "*Compressive Behavior of Large-Scale Square Reinforced Concrete Columns Confined with Carbon Fiber Reinforced Polymer Jackets*", *Materials and Design*, Vol. 31, No. 1, pp. 357–364.
- Turner, M. C., Martin, R. H. and Topp, L., 1956, "*Stiffness and Deflection Analysis of Complex Structures*", *Journal of Aeronautical Sciences*, Vol. 23, No. 9, pp. 805-823.
- Uy, B. & Das, S., 1997, "*Time Effects in Concrete-Filled Steel Box Columns in Tall Buildings*", *The Structural Design of Tall Buildings*, Vol. 6, pp. 1-22.
- Wang, J., 2013, "*Behaviour of ferrocement columns under static and cyclic loading*", Ph.D Thesis, University of Manchester, pp. 234.
- Wang, Y., Ma, Y., Han, B & Liu, M., 2011, "*Creep of Fully or Partially FRP-Confined Square or Circular Concrete Columns*", 18th International Conference on Composite Materials.
- Wang, Y. and Zhang, D., 2009, "*Creep-Effect on Mechanical Behavior of Concrete Confined by FRP under Axial Compression*", *Journal of Engineering Mechanics*, Vol. 135, No. 11, pp. 1315-1322.
- Wang, Y., Ma, Y. & Zhou, L., 2011, "*Creep of FRP-Wrapped Concrete Columns with or Without Fly Ash Under Axial Load*", *Construction and Building Materials*.
- Widiarsa, Ida Bagus Rai & Muhammad N. S. Hadi, 2013, "*Performance of CFRP Wrapped Square Reinforced Concrete Columns Subjected to Eccentric Loading*", *Procedia Engineering*, Vol. 54, pp. 365-376.

References

- William, K. J. and Warnke, E. P., 1975, "***Constitutive Model for the Triaxial Behavior of Concrete***", Proceedings, International Association for Bridge and Structural Engineering, Vol. 19, ISMES, Bergamo, Italy, pp. 174.
- Winter, G. and Nilson, A.H., 1979 "***Design of Concrete Structures***", Ninth Edition, McGraw-Hill, New York, pp. 646.
- Wu, H. L., Wang, Y. F., Yu, L. and Li, X. R., 2009, "***Experimental and Computational Studies on High-Strength Concrete Circular Columns Confined by Aramid Fiber-Reinforced Polymer Sheets***", Journal of Composites for Construction, Vol. 13, No. 2, pp. 125-134.
- Wu, Yu Fei and You Yi Wei., 2010, "***Effect of Cross-Sectional Aspect Ratio on the Strength of CFRP-Confined Rectangular Concrete Columns***", Engineering Structures, Vol. 32, No. 1, pp. 32-45.
- Yehia, S., 2015, "***Behavior of Low Compressive Strength Short Columns Strengthened With External GFRP Strips/Jacket Techniques Behavior Of Low Compressive Strength Short Columns Strengthened With External GFRP Strips/Jacket Techniques***", International Journal of Technology Enhancements and Emerging Engineering Research, Vol. 3, No. 4, pp. 1-5.
- Youssf, O., Elgawady, M. A., Mills, J. and Ma, X., 2014, "***Finite element modelling and dilation of FRP-confined concrete columns***", Engineering Structures, Vol.79, pp. 70-85.
- Zhang, D. G., Wang, Y. F. and Ma, Y. S., 2010, "***Compressive behaviour of FRP-confined square concrete columns after creep***", Engineering Structures, Vol.32, pp. 1957-1963.
- Zhang, D. G., Ma, Y. S. and Wang, Y., 2015, "***Compressive behavior of concrete filled steel tubular columns subjected to long-term loading***", Thin Walled Structures, Vol.89, pp. 205-211.
- Zienkiewicz, O. C., Watson, M., and King, I. P., 1968, "***A Numerical Method of Visco-Elastic Creep Analysis***", International journal of Mechanical Science, Vol.10, pp.807-827 .
- Zienkiewicz, O. C., Watson, M., and King, I. P., 1988, "***A Numerical Method of Visco-Elastic Stress Analysis***", International Journal of Mechanical Science, Vol.10, pp.807-827.
- Zeinkiwicz, O. C. ,1977, "***The Finite Element Method***" Third Edition, McGraw-Hill, London.

References

Appendix A

Finite Element Formulation and Material Modeling

A.1: General:

The finite element technique has been used for linear and nonlinear analysis of reinforced concrete structures. Attention, at early stages of use, was focused on two dimensional and axisymmetric models, but it was soon extended to include plate, shell and beam systems under general states of loading. Despite, the fact that two-dimensional analysis gives an adequate and computational efficient in many problems, it is necessary to represent the behavior of strengthening reinforced concrete columns using three-dimensional models. Therefore, it is believed that the use of three-dimensional analysis provides better representation of material nonlinearity of reinforced concrete members (*Zeinkiewicz 1977; Owen and Hinton 1980*). In the present work, (*ANSYS 2011*) software, a powerful FEM package is used for the model analysis.

In this chapter, the finite element formulation, material idealization, material behavior, nonlinear solution technique and convergence criteria are briefly reviewed.

A.2: Finite Element Formulation:

In general, applying the finite element method for any problem leads to a set of algebraic equations leading to the stiffness matrix [k] for a particular element in the following form:

$$[k] = \int_{\Omega} [B]^T [D] [B] d\Omega \quad \dots(A-1)$$

where [D] is the **Material stiffness matrix** and [B] is the **Geometry matrix** which [D] matrix is a stress-strain relationships may be written as (*Logan et al. 2007; Moaveni S. 1999; Hutton 2004*).

$$\{\varepsilon\} = \begin{Bmatrix} \varepsilon_x \\ \varepsilon_y \\ \varepsilon_z \\ \gamma_{xy} \\ \gamma_{yz} \\ \gamma_{xz} \end{Bmatrix} = \begin{Bmatrix} \frac{\partial u}{\partial x} \\ \frac{\partial v}{\partial y} \\ \frac{\partial w}{\partial z} \\ \frac{\partial u}{\partial y} + \frac{\partial v}{\partial x} \\ \frac{\partial v}{\partial z} + \frac{\partial w}{\partial y} \\ \frac{\partial u}{\partial z} + \frac{\partial w}{\partial x} \end{Bmatrix} \quad \text{..... (A-2)}$$

where u , v , and w are the displacements in x , y and z directions respectively. The corresponding vector of stress is given by:

$$\{\sigma\} = [\sigma_x \ \sigma_y \ \sigma_z \ \tau_{xy} \ \tau_{yz} \ \tau_{xz}]^T \quad \text{.....(A-3)}$$

And can be written the above relations as:

$$\{\sigma\} = [D] \cdot \{\varepsilon\} \quad \text{.....(A-4)}$$

[B] Matrix is a relationship between strain and displacement may be written as:

$$\{\varepsilon\} = [B] \cdot \{U\} \quad \text{.....(A-5)}$$

When $\{U\} = [N] \cdot \{a\}$ and $[B] = [J][N]$

$\{U\}$ is a vector of displacement, $[N]$ is the matrix of shape function, $\{a\}$ is a nodal displacement vector and $[J]$ is Jacobian matrix.

A.3:Material Idealization:

A.3.1:Concrete Brick Element:

Concrete is represented by the SOLID65 isoparametric brick element shown in Fig. (A.1). This element has been successfully used in three dimensional nonlinear R.C. analyses. This element has eight nodes with three degrees of freedom at each node (translations u , v and w in the nodal x , y and z directions

Appendix A: Finite Element Formulation and Material Modeling

respectively). This element is capable of plastic deformation, cracking in three orthogonal directions and crushing.

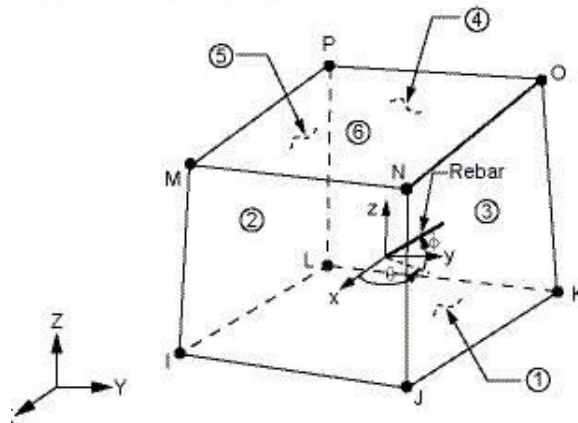


Fig.(A.1):Brick Element with 8-Node(Solid65)(ANSYS 2011).

A.3.2:Concrete As Viscoelastic Material:

Concrete is represented by the VISCO89 is a quadratic isoparametric element shown in Fig. (A.2). This element defined by 20 nodes having three degrees of freedom at each node (translations u , v and w in the nodal x , y and z directions respectively). This element has viscoelastic and stress stiffening.

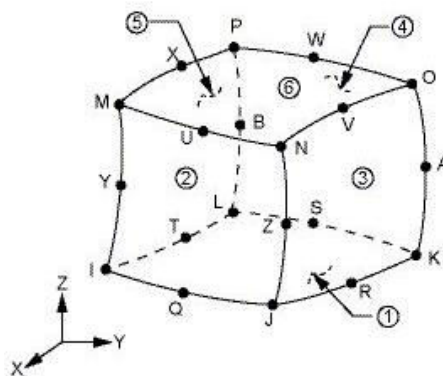


Fig.(A.2):Brick Element with 20-Node(VISCO89)(ANSYS 2011).

A.3.3: Steel Plate Element:

An eight-node solid element, SOLID 45, is used for the steel plates at the support in the Reinforced concrete column models. The element has eight nodes that have three degrees of freedom at each node-translation in the nodal x , y , and z directions. The geometry and locations of the node of this element type shown in Fig. (A.3).

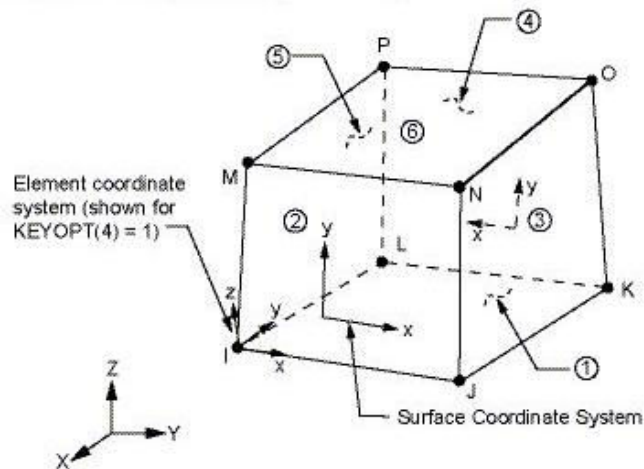


Fig.(A.3):Brick Element with 8-Node(Solid45)(ANSYS 2011).

The element has plasticity; swelling, creep, large deflection, large strain and stress stiffen abilities.

A.3.4: FRP Representation:

The 4-node quadratic-order membrane shell element (SHELL41) shown in Fig. (A.4) is used in the present work to model the FRP. This element has three degrees of freedom u , v and w in the x , y and z direction respectively at each node.

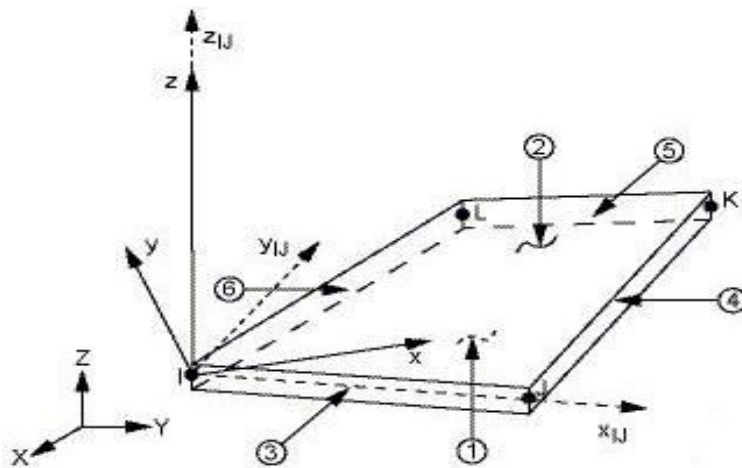


Fig.(A.4):Shell Element with 4-Node(SHELL41)(ANSYS 2011).

A.3.5:Steel Reinforcement Representation:

Analysis of RC structures using the FEM requires a simple, yet accurate way of representing the reinforcement. Three alternative representations have been usually used to simulate the reinforcement in this type of analysis, which are:

- i) Embedded representation.
- ii) Smearred representation.
- iii) Discrete representation.

The embedded representation (*Phillips and Zeinkiewicz, 1976*) assumes that the reinforcing bar as an axial member is built into the isoparametric element whose displacements are consistent with those of the element. The bars are restricted to lie parallel to the local coordinate axes of the basic element and perfect bond must be assumed between concrete and the reinforcement.

For the smearred representation, the steel bars are assumed to be distributed into an equivalent layer within the concrete with axial properties in the direction of the bars only. A composite concrete-reinforcement constitutive relationship is used in this case and perfect bond is assumed between concrete and steel bars.

Appendix A: Finite Element Formulation and Material Modeling

A discrete representation of the reinforcement using one-dimensional element is the most widely used. For two dimensional analysis axial bar members with two degrees of freedom at each node are usually employed. A one dimensional flexural element with three degrees of freedom per node has also been adopted. A significant advantage of the discrete representation, in addition to its simplicity can account for possible displacement of reinforcement with respect to the surrounding concrete. Their disadvantages are to restrict the mesh and increase the total number of elements(*Al-Shaarbaf, 1990*). In the present study, the discrete representation is used for the analysis of RC columns.

LINK8 which has been used to model the reinforcement is a bar (or truss) element which may be used in a variety of engineering applications. This 3-D spar element is a uniaxial tension-compression element with three degrees of freedom at each node. The geometry, node locations, and the coordinate system for the element are shown in Fig.(A.5).

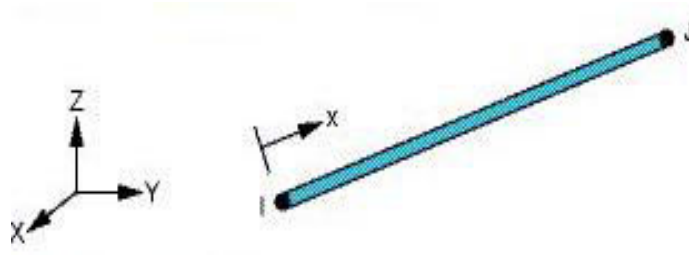


Fig.(A.5):3D-Spar Element (LINK8).

In translation in the nodal x , y and z directions, as in a pin-jointed structure, no bending of the element is considered. This element is used in the present study to simulate the behavior of reinforcing bars which work as stirrups in resisting the vertical shear in concrete and main steel reinforcement in resisting the flexural stresses.

A.4: Materials Behavior:

Depending on the nature and the level of the applied stresses, concrete may behave as either a linear or nonlinear material. Under a low level of stresses, linear elastic behavior is observed, while concrete exhibits a highly nonlinear response at higher stress levels (*Al-Shaarbaf,1990*).

A.4.1:Concrete

Development of a model for the behavior of concrete is a challenging task. Concrete is a quasi-brittle material and has a different behavior in compression and tension. The tensile strength of concrete is typically 8-15% of the compressive strength (*Shah, et al. 1995*). Fig.(A.6) shows a typical stress-strain curve for normal weight concrete (*Bangash 1989*).

In compression, the stress-strain curve for concrete is linearly elastic up to about 30 percent of the maximum compressive strength. Above this point, the stress increases gradually up to the maximum compressive strength. After it reaches the maximum compressive strength σ_{cu} , the curve descends into a softening region, and eventually crushing failure occurs at an ultimate strain ϵ_{cu} . In tension, the stress-strain curve for concrete is approximately linearly elastic up to the maximum tensile strength. After this point, the concrete cracks and the strength decrease gradually to zero (*Bangash 1989*).

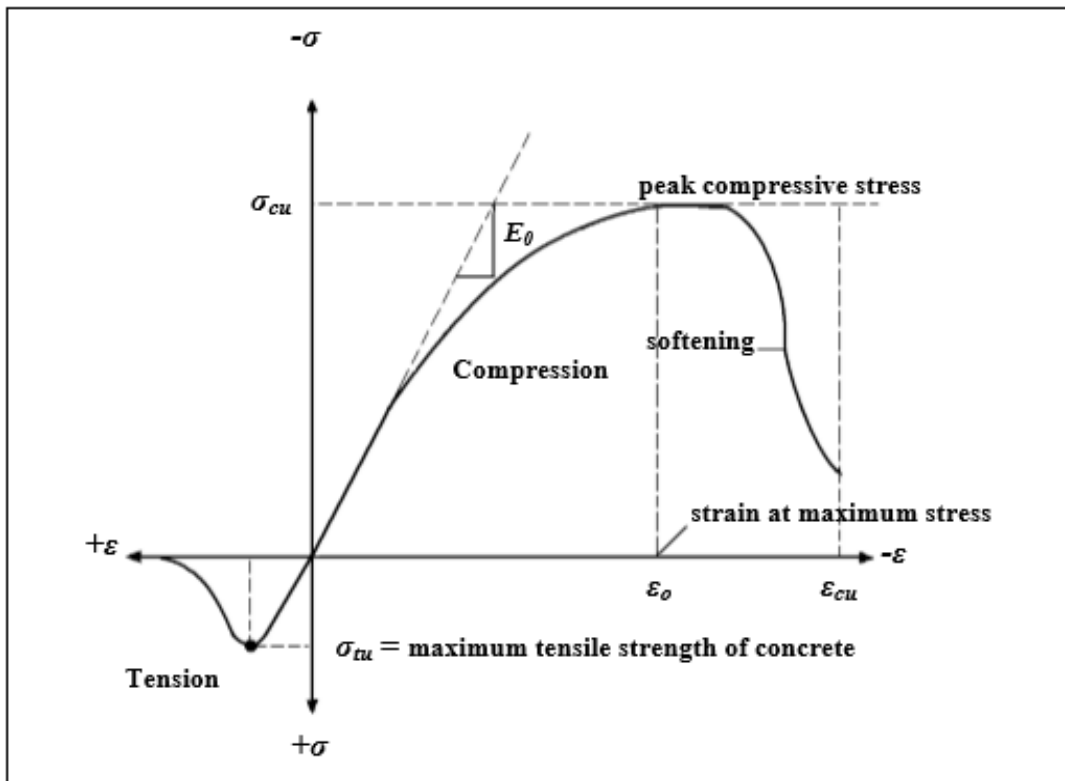


Fig.(A.6): Typical Uniaxial Compressive and Tensile Stress-Strain Curve for Concrete(Bangash,1989).

For concrete, ANSYS requires input data for material properties as follows: Elastic modulus (E_c), Ultimate uniaxial compressive strength (f'_c), Ultimate uniaxial tensile strength (modulus of rupture, f_r), Poisson's ratio (ν) and Shear transfer coefficient (β_t).

where $E_c = 4730\sqrt{f'_c}$ and $f_r = 0.62\sqrt{f'_c}$ recommended by by (ACI 318, 2014) Poisson's ratio of concrete has been observed to remain approximately constant and ranges from about 0.15 to 0.22 up to a stress level of 80 percent of f'_c (Grestle, 1980). The shear transfer coefficient, β_t , represents conditions of the crack face. The value of β_t ranges from 0.0 to 1.0, with 0.0 representing a smooth crack (complete loss of shear transfer) and 1.0 representing a rough crack (no loss of shear transfer) (ANSYS 2011).

A.4.4.1 Compressive Uniaxial Stress-Strain Relationship for Concrete:

The ANSYS program requires the uniaxial stress-strain relationship for concrete in compression. In the present model, a multilinear stress-strain curve was used for the uniaxial stress-strain relationship beyond the limit of elasticity, $0.3 f'_c$. This parabolic curve represents the work-hardening stage of behavior. When the peak compressive stress was reached, a perfectly plastic response was assumed to occur. Compressive stress-strain relationship of the concrete model was obtained by using the following equations to compute the multilinear isotropic stress-strain curve for the concrete (*MacGregor, 1992*).

$$f = \frac{E_c \varepsilon}{1 + \left(\frac{\varepsilon}{\varepsilon_o}\right)^2} \quad \text{.....(A-6)}$$

$$\varepsilon_o = \frac{2 f'_c}{E_c} \quad \text{.....(A-7)}$$

$$E = \frac{f}{\varepsilon} \quad \text{.....(A-8)}$$

Where:

f : Stress at any strain, ε

ε : Strain of concrete

ε_o : Strain at ultimate compressive strength f'_c

E : Tangent modulus of elasticity

Fig.(A.7) shows the simplified compressive uniaxial stress-strain relationship that was used in this study. The simplified stress-strain curve for each beam model is constructed from six points connected by straight lines. The curve

Appendix A: Finite Element Formulation and Material Modeling

starts at zero stress and strain. Point No.1, at $0.3f'_c$, is calculated for the stress-strain relationship of the concrete in the linear range Eq(A-8). Point Nos. 2, 3, and 4 are obtained from Eq(A-6), in which ε_0 is calculated from Eq(A-7). Point No. 5 is at ε_0 and f'_c .

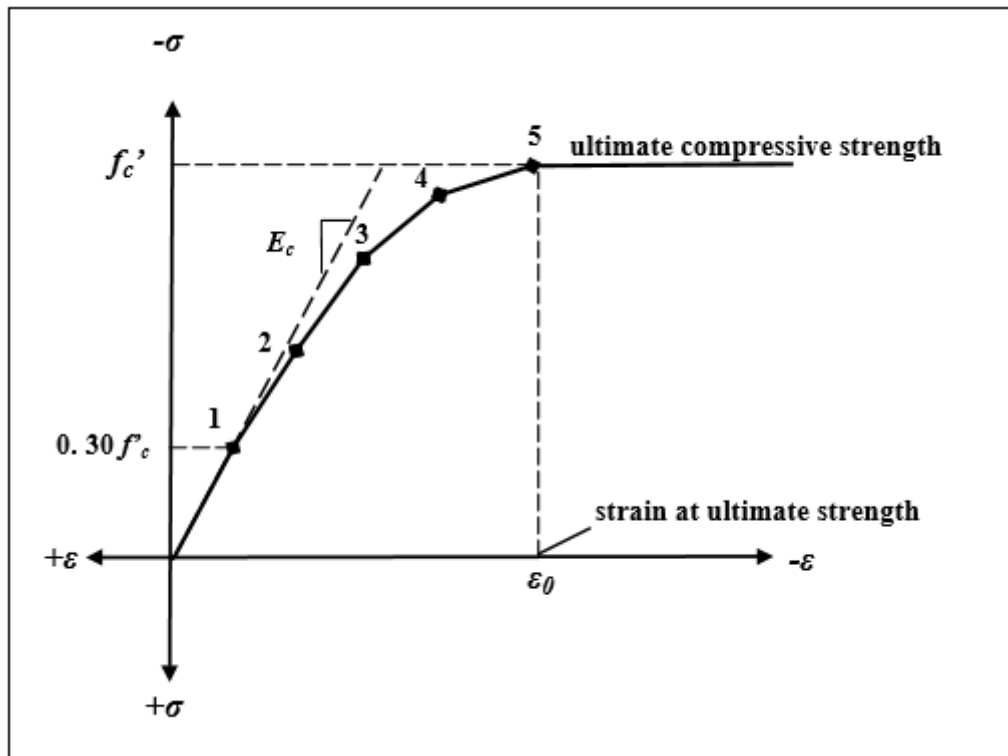


Fig.(A.7): Simplified Compressive Uniaxial Stress-Strain Curve for Concrete (Kachlakev, 2000).

A.4.1.2 : Biaxial Behavior of Concrete:

The strength and stress-strain behavior of concrete under combined biaxial or triaxial compressive stresses are somewhat different from those of uniaxial behavior. The maximum compressive strength increases for a biaxial compressive strength of approximately 25%, which is achieved at a stress ratio of lateral stress/axial stress of 0.5. For equal biaxial compressive stresses, the increase in the compressive strength is about 16%. Under biaxial compression, tension state of stress, the compressive strength decreases almost linearly as the

applied tensile stress is increased. Under biaxial tensile stresses, the tensile strength is almost the same as that of uniaxial tensile strength (*Kupfer, 1969*).

A.4.1.3: Behavior of Concrete in Tension:

Linear elastic model prior to cracking is usually used to simulate the behavior of concrete in tension. In general, the cracking criterion of concrete is expressed in terms of principal tensile stresses or strains. In the (*ANSYS 11*), the onset of cracking is controlled by a maximum principal stress criterion. A smeared crack model with fixed orthogonal cracks was adopted to represent the fractured concrete.

A.4.1.3.1 :Post-Cracking Model (Tension-Stiffening Model):

The tensile stresses normal to the cracked plane are gradually released, and are usually represented by an average stress-strain curve. To obtain such a relationship, either the tension-stiffening or strain-softening concepts may be used(*Al-Shaarbaf, 1990*). This has been achieved in (*ANSYS 11*) by assuming gradual release of the concrete stress component normal to the cracked plane. The normal stress that was carried by cracked concrete can be obtained from Fig. (A.8).

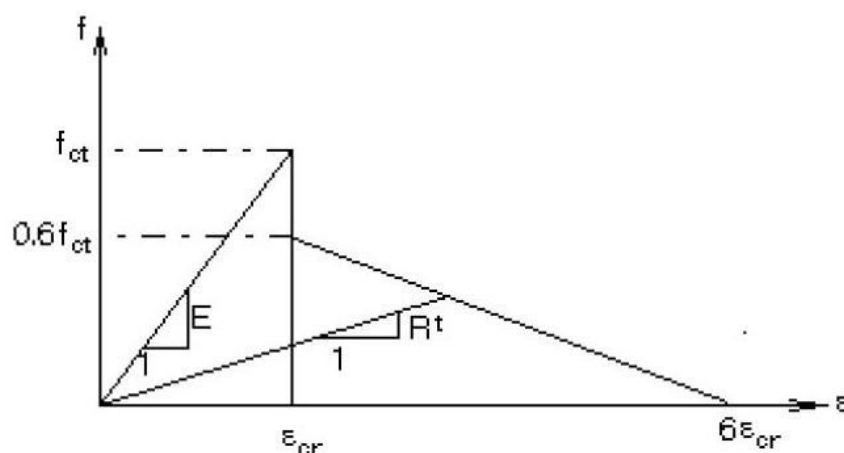


Fig.(A.8): Post Cracking Stress-Strain Response of Concrete(*ANSYS 11*)

Appendix A: Finite Element Formulation and Material Modeling

where:

ε_{cr} is the cracking strain

f_t is the uniaxial tensile cracking stress.

T_c is the multiplier for amount of tensile stress (default in ANSYS 2011 = 0.6).

All effects of the shear transfer coefficients for an open crack β_o and the shear transfer coefficients for a closed crack β_l on the stress-strain relations are stated below.

The shear transfer coefficient β_o represents a strength reduction factor subsequent loads which induce sliding (shear) across the crack face. The stress-strain relations for a material that has cracked in one direction only become:

$$[D^{ck}] = \frac{E}{(1+\nu)} \begin{bmatrix} \frac{R^t(1+\nu)}{E} & 0 & 0 & 0 & 0 & 0 \\ 0 & \frac{1}{1-\nu} & \frac{\nu}{1-\nu} & 0 & 0 & 0 \\ 0 & \frac{\nu}{1-\nu} & \frac{1}{1-\nu} & 0 & 0 & 0 \\ 0 & 0 & 0 & \beta_o & 0 & 0 \\ 0 & 0 & 0 & 0 & \frac{1}{2} & 0 \\ 0 & 0 & 0 & 0 & 0 & \frac{\beta_o}{2} \end{bmatrix} \quad \dots\dots(A-9)$$

where, $[D^{ck}]$ is the stress-strain relations in modeling of crack, E is the modulus of elasticity, R^t is the secant modulus and ν is the poisons ratio.

If the crack closes, then all compressive stresses normal to the crack plane are transmitted across the crack and only shear transfer coefficient β_l for closed crack is introduced. Then $[D^{ck}]$ can be expressed

Appendix A: Finite Element Formulation and Material Modeling

$$[D^{ck}] = \frac{E}{(1+\nu)(1-2\nu)} \begin{bmatrix} (1-\nu) & \nu & \nu & 0 & 0 & 0 \\ \nu & 1-\nu & \nu & 0 & 0 & 0 \\ \nu & \nu & 1-\nu & 0 & 0 & 0 \\ 0 & 0 & 0 & \beta_1 \frac{(1-2\nu)}{2} & 0 & 0 \\ 0 & 0 & 0 & 0 & \frac{(1-2\nu)}{2} & 0 \\ 0 & 0 & 0 & 0 & 0 & \beta_1 \frac{(1-2\nu)}{2} \end{bmatrix} \dots\dots(A-10)$$

The stress-strain relations for concrete that has cracked in two directions are:

$$[D^{ck}] = E \begin{bmatrix} \frac{R^t}{E} & 0 & 0 & 0 & 0 & 0 \\ 0 & \frac{R^t}{E} & 0 & 0 & 0 & 0 \\ 0 & 0 & 1 & 0 & 0 & 0 \\ 0 & 0 & 0 & \frac{\beta_o}{2(1+\nu)} & 0 & 0 \\ 0 & 0 & 0 & 0 & \frac{\beta_o}{2(1+\nu)} & 0 \\ 0 & 0 & 0 & 0 & 0 & \frac{\beta_o}{2(1+\nu)} \end{bmatrix} \dots\dots(A-11)$$

If both directions reclose, then:

$$[D^{ck}] = eq.(B-10) \dots\dots (A-12)$$

and, the stress-strain relations for concrete that has cracked in all three dimensions are:

$$[D^{ck}] = eq.(B-11) \dots\dots (A-13)$$

and, if all three cracks reclose, then;

$$[D^{ck}] = eq.(B-10) \dots\dots (A-14)$$

A.4.1.4: Cracking Criterion:

Three different approaches for crack modeling have been employed in the analytical studies of concrete structures using the numerical technique of the

Appendix A: Finite Element Formulation and Material Modeling

finite element method. These are smeared cracking modeling as shown in Fig. (A-9), discrete cracking modeling as shown in Fig. (A.10), and fracture mechanics modeling. For (*ANSYS 2011*) computer program, crack modeling of concrete depends on smeared cracks. For different states of stresses (tension-tension-tension, tension-tension-compression and tension-compression-compression), the stress-strain matrices for cracked concrete are given in the last section.

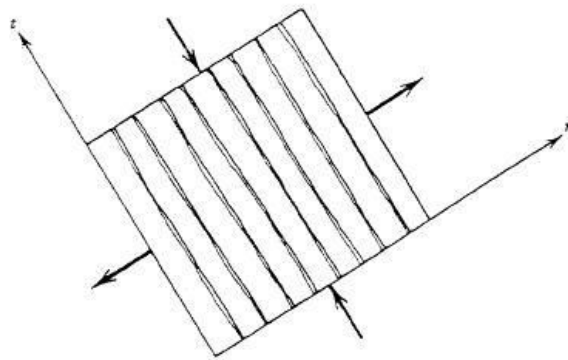


Fig.(A.9):Representation of a Single Crack in The Smeared Crack Modeling Approach(*Owen and Hinton 1980*).

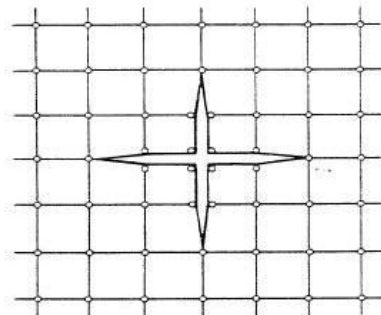


Fig.(A.10):Two Dimensional Cracking Representation in Discrete Crack Modeling Approach(*Owen and Hinton 1980*).

A.4.1.5:Crushing Modeling:

If the material at an integration point fails in uniaxial, biaxial or triaxial compression, the material is assumed to crush at that point. Under this condition,

the material strength at the considered integration point is assumed to have degraded to an extent such that its contribution to the stiffness of an element in question can be ignored (*ANSYS 2011*).

A.4.1.6: Failure Criteria for Concrete

The model is capable of predicting failure of concrete materials. Both cracking and crushing failure modes are accounted for. The two input strength parameters – i.e., ultimate uniaxial tensile and compressive strengths are needed to define a failure surface of the concrete. Consequently, a criterion for failure of the concrete due to a multiaxial stress state can be calculated (*William and Warnke 1975*).

A three-dimensional failure surface for concrete is shown in Fig.(A.11). The most significant nonzero principal stresses are in the x and y directions, represented by σ_{xp} and σ_{yp} , respectively. Three failure surfaces are shown as projections on the σ_{xp} - σ_{yp} plane. The mode of failure is a function of the sign of σ_{zp} (principal stress in the z direction). For example, if σ_{xp} and σ_{yp} are both negative (compressive) and σ_{zp} is slightly positive (tensile), cracking would be predicted in a direction perpendicular to σ_{zp} . However, if σ_{zp} is zero or slightly negative, the material is assumed to crush (*ANSYS 2011*).

In a concrete element, cracking occurs when the principal tensile stress in any direction lies outside the failure surface. After cracking, the elastic modulus of the concrete element is set to zero in the direction parallel to the principal tensile stress direction. Crushing occurs when all principal stresses are compressive and lie outside the failure surface; subsequently, the elastic modulus is set to zero in all directions (*ANSYS 2011*), and the element effectively disappears.

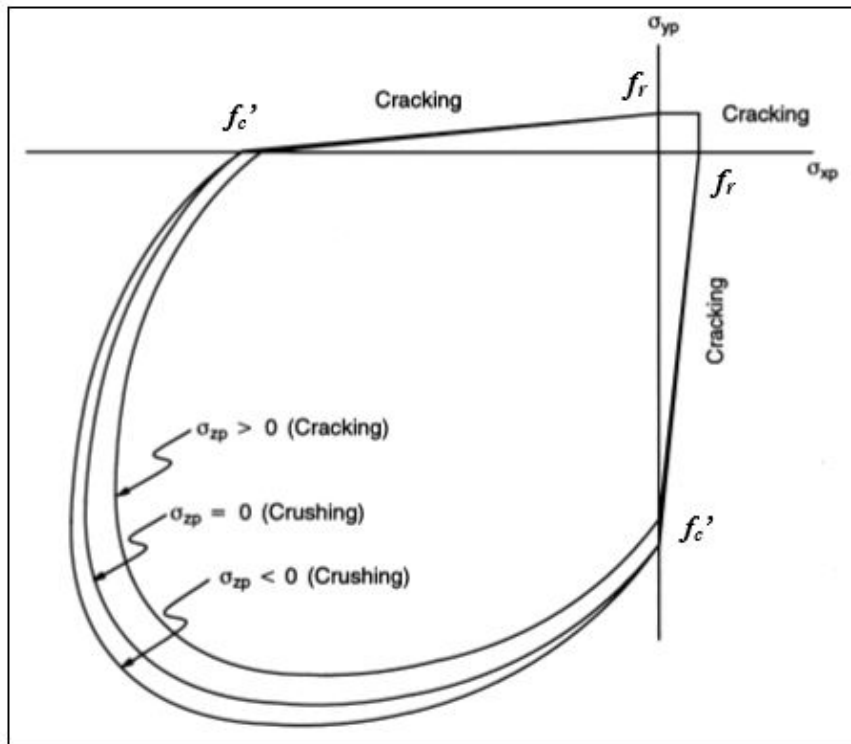


Fig.(A.11):3-D Failure Surface for Concrete(ANSYS 2011).

During this study, it was found that if the crushing capability of the concrete is turned on, the finite element beam models fail prematurely. Crushing of the concrete started to develop in elements located directly under the loads. Subsequently, adjacent concrete elements crushed within several load steps as well, significantly reducing the local stiffness. Finally, the model showed a large displacement, and the solution diverged.

B.4.2: FRP Composites:

In this study, the specially orthotropic material is also transversely isotropic, where the properties of the FRP composites are nearly the same in any direction perpendicular to the fibers. Thus, the properties in the y direction are the same as those in the z direction.

Fig.(A.12) shows the stress-strain curves used in this study for the FRP composites.

Appendix A: Finite Element Formulation and Material Modeling

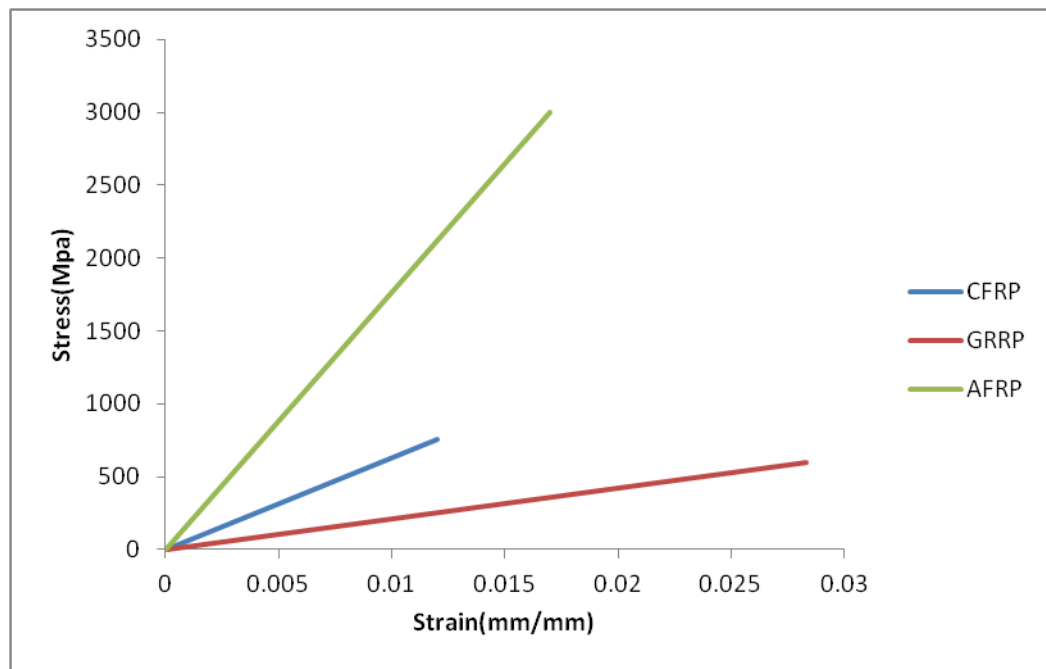


Fig.(A.12): Stress-Strain Curves for FRP

ANSYS program needed data for the FRP composites in the finite element such as:

- Thickness of FRP layer.
- Orientation of the fiber direction.
- Elastic modulus of the FRP composite in three directions (E_x , E_y and E_z).
- Shear modulus of the FRP composite for three planes (G_{xy} , G_{yz} and G_{xz}).
- Major Poisson's ratio for three planes (ν_{xy} , ν_{yz} and ν_{xz}). Note that a local coordinate system for the FRP layered solid elements is defined where the x direction is the same as the fiber direction, while the y and z directions are perpendicular to the x direction.

The properties of isotropic materials, such as elastic modulus and Poisson's ratio, are identical in all directions; therefore, no subscripts are required. This is not the case with specially orthotropic materials. Subscripts are needed to define properties in the various directions. For example, $E_x \neq E_y$ and $\nu_{xy} \neq \nu_{yx}$. E_x is the

Appendix A: Finite Element Formulation and Material Modeling

elastic modulus in the fiber direction, and E_y is the elastic modulus in the y direction perpendicular to the fiber direction. The use of Poisson's ratios for the orthotropic materials causes confusion; therefore, the orthotropic material data are supplied in the ν_{xy} or major Poisson's ratio format for the ANSYS program. The major Poisson's ratio is the ratio of strain in the y direction to strain in the perpendicular x direction when the applied stress is in the x direction. The quantity ν_{yx} is called a minor Poisson's ratio and is smaller than ν_{xy} , whereas E_x is larger than E_y . Eq.(A-15) shows the relationship between ν_{xy} and ν_{yx} (**Kaw 1997**).

$$\nu_{yx} = \frac{E_y}{E_x} \nu_{xy} \quad \text{.....(A-15)}$$

where:

ν_{yx} = Minor Poisson's ratio

E_x = Elastic modulus in the x direction (fiber direction)

E_y = Elastic modulus in the y direction

ν_{xy} = Major Poisson's ratio

B.4.3: Modeling of Reinforcement

Modeling of reinforcement in connecting with the finite element analysis of RC members is much simpler than modeling of concrete. The uniaxial stress-strain relation for reinforcement is idealized in (**ANSYS 11**) as a bilinear curve, representing Elasto-plastic behavior with strain hardening. The relation is assumed to be identical in tension and in compression as shown in Fig. (A.13).

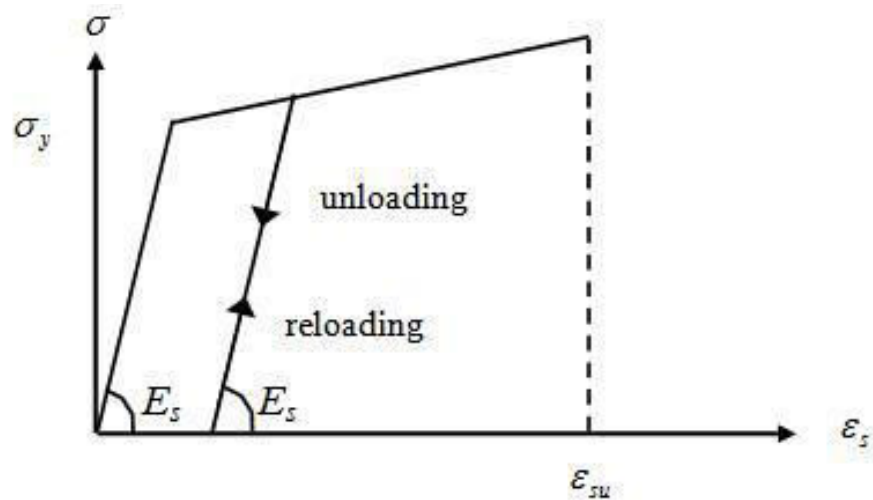


Fig.(A.13): Stress-Strain Relationship of Steel Bar(Hinton and Owen,1980).

A.5: Nonlinear Solution Technique:

In the present research work, only material nonlinearity is considered. In the analysis of RC columns strengthened with FRP strips, the behavior of nonlinear material, including sudden changes in the element stiffness due to cracking, crushing of concrete, yielding of tension steel reinforcement and the plastic deformation of concrete and reinforcement represents the main sources of the nonlinearity. For simple linear elastic problems, the fundamental approach of solution is generally obtained by solving the set of equilibrium equations for the unknown displacements $\{a\}$ of the following form:

$$[K]\{a\} = \{f\} \quad \text{..... (A-16)}$$

This cannot be achieved directly in the cases of nonlinear system where the stiffness matrix $[K]$ is a function of structural displacements,

$$[K] = [K \{a\}] \quad \text{..... (A-17)}$$

Therefore, it cannot exactly be computed before the determination of the unknown displacement vector $\{a\}$.

For the solution of a nonlinear structural problem, the equilibrium equations in the finite element form can be expressed as:

Appendix A: Finite Element Formulation and Material Modeling

$$\{r\} = \{p\} - \{f\} \quad \dots\dots (A-18)$$

where $\{r\}$ is the out of balance force vector, $\{f\}$ is the vector of externally applied nodal loads, and $\{p\}$ represents the vector of the nodal forces equivalent to the internal stress level, which is given by:

$$\{P\} = \int_V [B]^T \{\sigma\} dV \quad \dots\dots (A-19)$$

where $\{\sigma\}$ is the vector of stresses. The integration, which appears in this equation is carried out numerically using the Gaussian-quadrature scheme.

The solution of the set of equilibrium equations (A-16) is based upon obtaining a balance between the external and internal load vectors such that the residual forces are zero. The basic nonlinear solution techniques, which have been used in connection with the finite element analysis, are the incremental technique, iterative technique and a combination of them (incremental-iterative technique).

The incremental-iterative technique is widely used especially in the nonlinear analysis of RC structures. The load is applied incrementally and at each increment of loading successive iterations is performed, as shown in Fig. (A.14), in order to obtain a converged solution (*Turner,1956*). This method yields a higher accuracy, but at a large cost of computational effort.

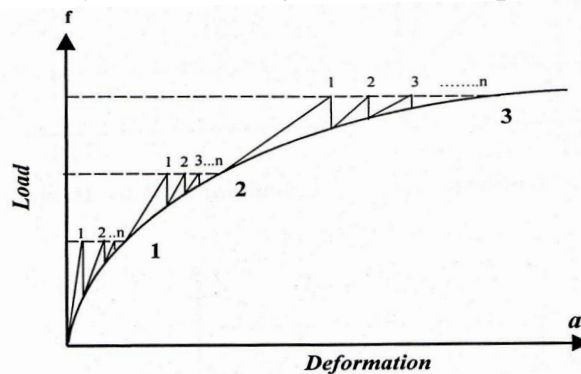


Fig. (A.14) Incremental-Iterative Techniques for The Solution of Nonlinear Equations (*Phillips,1976*)(ANSYS 2011).

Appendix A: Finite Element Formulation and Material Modeling

(*ANSYS 2011*) employs the "Newton-Raphson" approach to solve nonlinear problems. In this approach, the load is subdivided into a series of load increments. The load increments can be applied over several load steps. Fig. (A.15), illustrates the use of Newton-Raphson equilibrium iterations in a single DOF nonlinear analysis.

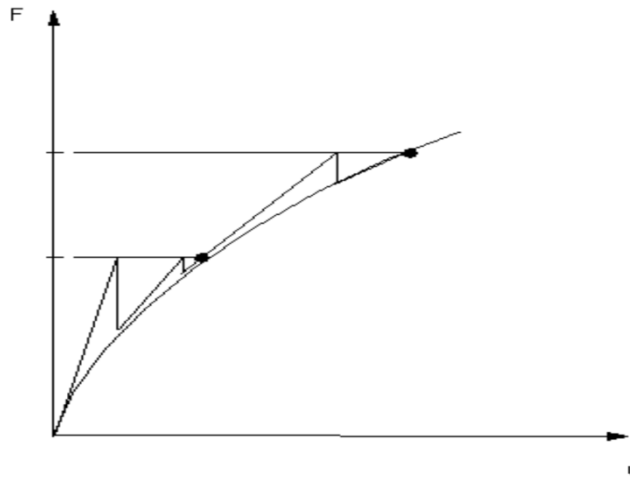


Fig. (A.15) Newton-Raphson Equilibrium Iterations in a Single DOF (*ANSYS 2011*).

To obtain a converged solution for a certain load vector, the Newton-Raphson method evaluates the out of balance load vector, which is the difference between the restoring forces (the loads corresponding to the element stresses) and the applied loads. The program then performs a linear solution, using the out of balance loads, and checks for convergence. If a specified convergence criterion is not satisfied, the out of balance load vector is reevaluated, the stiffness matrix is updated, and a new solution is obtained. This iterative procedure continues until the problem converges. A number of convergence enhancement and recovery features, such as line search and automatic load stepping can be activated to help the problem to converge. If convergence cannot be achieved, then the program attempts to use a smaller load increment. In the present work, the full and modified Newton-Raphson methods have been generally used.

Appendix A: Finite Element Formulation and Material Modeling

From the previous discussion, a nonlinear analysis using the ANSYS computer software can be organized into three levels of operation:

- The "top" level consists of the load steps that it defines explicitly over a "time" span. Loads are assumed to vary linearly within load steps (for static analyses), as shown in Fig. (A.16).
- Within each load step, the program performs several solutions (sub steps or time steps) to apply the load gradually.

At each sub step, the program will perform a number of equilibrium iterations to obtain a converged solution.

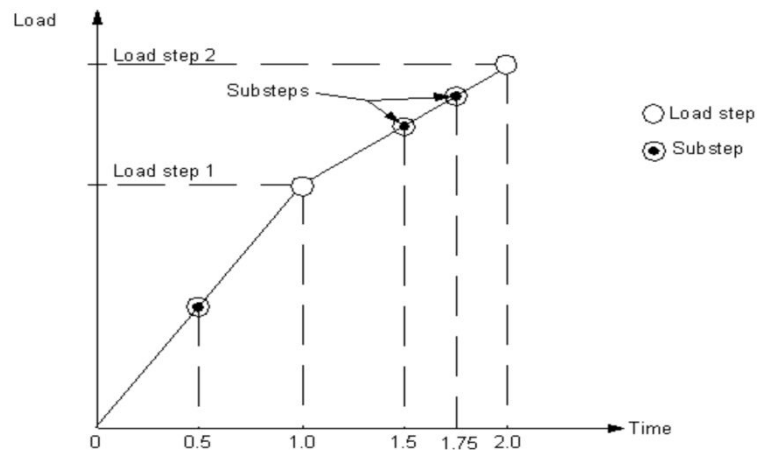


Fig. (A.16) Load Step, Sub Steps and Time (ANSYS 2011).

A.6: Convergence Criteria:

In the nonlinear finite element analysis, convergence is assumed to occur when the difference between the external and internal forces has reached an acceptable small value. Thus a convergence criterion is required in order to terminate the iterative process when the solution is considered to be sufficiently accurate. In general, the main types of convergence criteria for nonlinear structural analysis are the force and the displacement criteria. The force

Appendix A: Finite Element Formulation and Material Modeling

convergence criterion, which has been adopted in the current study, is based on out of balance forces and can be written in the below form:

$$\frac{\|\{r\}\|}{\|\{f\}\|} \times 100 \% \leq \text{TOLER} \quad \text{.....(A-20)}$$

where,

$$\|\{r\}\| = (\{r\}^T \{r\})^{1/2} \quad \text{.....(A-21)}$$

$$\|\{f\}\| = (\{f\}^T \{f\})^{1/2} \quad \text{.....(A-22)}$$

and TOLER is a specified convergence tolerance (*Phillips, 1976*).

Appendix B: Tables and Figures of Parametric Study

Appendix B

B.1 Results of Parametric Study:

Table (B-1): Creep Strain of Models

Models	Creep strain	Models	Creep strain
C.0.7%Pu.30.8	0.002633	G.0.7%Pu.30.8	1.92E-04
C.0.28%Pu.30.8	0.010531	G.0.28%Pu.30.8	7.67E-04
C.0.72%Pu.30.8	0.026328	G.0.72%Pu.30.8	1.92E-03
C.0.26.7%Pu.30.8	0.002382	G.0.26.7%Pu.30.8	1.88E-04
C.0.26.28%Pu.30.8	0.009527	G.0.26.28%Pu.30.8	7.50E-04
C.0.26.72%Pu.30.8	0.023818	G.0.26.72%Pu.30.8	1.88E-03
C.0.46.7%Pu.30.8	0.002338	G.0.46.7%Pu.30.8	2.08E-04
C.0.46.28%Pu.30.8	0.009353	G.0.46.28%Pu.30.8	8.31E-04
C.0.46.72%Pu.30.8	0.023384	G.0.46.72%Pu.30.8	2.08E-03
C.0.7%Pu.30.15	0.002547	G.0.7%Pu.30.15	1.20E-04
C.0.28%Pu.30.15	0.010187	G.0.28%Pu.30.15	4.78E-04
C.0.72%Pu.30.15	0.025467	G.0.72%Pu.30.15	1.20E-03
C.0.26.7%Pu.30.15	0.002404	G.0.26.7%Pu.30.15	1.18E-04
C.0.26.28%Pu.30.15	0.009615	G.0.26.28%Pu.30.15	4.71E-04
C.0.26.72%Pu.30.15	0.024037	G.0.26.72%Pu.30.15	1.18E-03
C.0.46.7%Pu.30.15	0.002378	G.0.46.7%Pu.30.15	1.31E-04
C.0.46.28%Pu.30.15	0.009511	G.0.46.28%Pu.30.15	5.25E-04
C.0.46.72%Pu.30.15	0.023777	G.0.46.72%Pu.30.15	1.31E-03
C.0.7%Pu.30.30	0.002492	G.0.7%Pu.30.30	6.62E-05
C.0.28%Pu.30.30	0.009966	G.0.28%Pu.30.30	2.65E-04
C.0.72%Pu.30.30	0.024915	G.0.72%Pu.30.30	6.62E-04
C.0.26.7%Pu.30.30	0.002409	G.0.26.7%Pu.30.30	6.52E-05
C.0.26.28%Pu.30.30	0.009637	G.0.26.28%Pu.30.30	2.61E-04
C.0.26.72%Pu.30.30	0.024093	G.0.26.72%Pu.30.30	6.52E-04

Appendix B: Tables and Figures of Parametric Study

Table(B-1): Continue.

Models	Creep strain	Models	Creep strain
C.0.46.7%Pu.30.30	0.002387	G. 0.46.7%Pu.30.30	7.26E-05
C.0.46.28%Pu.30.30	0.00955	G.0.46.28%Pu.30.30	2.90E-04
C.0.46.72%Pu.30.30	0.023874	G.0.46.72%Pu.30.30	7.26E-04
C.0.7%Pu.40.8	0.002285	G.0.7%Pu.40.8	1.66E-04
C.0.28%Pu.40.8	0.009141	G.0.28%Pu.40.8	6.66E-04
C.0.72%Pu.40.8	0.022854	G.0.72%Pu.40.8	1.66E-03
C.0.26.7%Pu.40.8	0.002068	G.0.26.7%Pu.40.8	1.63E-04
C.0.26.28%Pu.40.8	0.008271	G.0.26.28%Pu.40.8	6.51E-04
C.0.26.72%Pu.40.8	0.020678	G.0.26.72%Pu.40.8	1.63E-03
C.0.46.7%Pu.40.8	0.00203	G.0.46.7%Pu.40.8	1.80E-04
C.0.46.28%Pu.40.8	0.00812	G.0.46.28%Pu.40.8	7.22E-04
C.0.46.72%Pu.40.8	0.020301	G.0.46.72%Pu.40.8	1.80E-03
C.0.7%Pu.40.15	0.002211	G.0.7%Pu.40.15	1.04E-04
C.0.28%Pu.40.15	0.008843	G.0.28%Pu.40.15	4.15E-04
C.0.72%Pu.40.15	0.022109	G.0.72%Pu.40.15	1.04E-03
C.0.26.7%Pu.40.15	0.002087	G.0.26.7%Pu.40.15	1.02E-04
C.0.26.28%Pu.40.15	0.008348	G.0.26.28%Pu.40.15	4.09E-04
C.0.26.72%Pu.40.15	0.020869	G.0.26.72%Pu.40.15	1.02E-03
C.0.46.7%Pu.40.15	0.002064	G.0.46.7%Pu.40.15	1.14E-04
C.0.46.28%Pu.40.15	0.008257	G.0.46.28%Pu.40.15	4.56E-04
C.0.46.72%Pu.40.15	0.020643	G.0.46.72%Pu.40.15	1.14E-03
C.0.7%Pu.40.30	0.002163	G.0.7%Pu.40.30	5.75E-05
C.0.28%Pu.40.30	0.008652	G.0.28%Pu.40.30	2.30E-04
C.0.72%Pu.40.30	0.021631	G.0.72%Pu.40.30	5.75E-04
C.0.26.7%Pu.40.30	0.002092	G.0.26.7%Pu.40.30	5.67E-05
C.0.26.28%Pu.40.30	0.008367	G.0.26.28%Pu.40.30	2.27E-04
C.0.26.72%Pu.40.30	0.020918	G.0.26.72%Pu.40.30	5.67E-04
C.0.46.7%Pu.40.30	0.002073	G.0.46.7%Pu.40.30	6.31E-05
C.0.46.28%Pu.40.30	0.008291	G.0.46.28%Pu.40.30	2.52E-04

Appendix B: Tables and Figures of Parametric Study

Table(B-1): Continue.

Models	Creep strain	Models	Creep strain
C.0.46.72%Pu.40.30	0.020727	G.0.46.72%Pu.40.30	6.31E-04
C.0.7%Pu.50.8	0.002047	G.0.7%Pu.50.8	1.49E-04
C.0.28%Pu.50.8	0.008189	G.0.28%Pu.50.8	5.97E-04
C.0.72%Pu.50.8	0.020474	G.0.72%Pu.50.8	1.49E-03
C.0.26.7%Pu.50.8	0.001852	G.0.26.7%Pu.50.8	1.46E-04
C.0.26.28%Pu.50.8	0.007411	G.0.26.28%Pu.50.8	5.84E-04
C.0.26.72%Pu.50.8	0.018527	G.0.26.72%Pu.50.8	1.46E-03
C.0.46.7%Pu.50.8	0.001819	G.0.46.7%Pu.50.8	1.62E-04
C.0.46.28%Pu.50.8	0.007275	G.0.46.28%Pu.50.8	6.47E-04
C.0.46.72%Pu.50.8	0.018189	G.0.46.72%Pu.50.8	1.62E-03
C.0.7%Pu.50.15	0.001981	G.0.7%Pu.50.15	9.30E-05
C.0.28%Pu.50.15	0.007923	G.0.28%Pu.50.15	3.72E-04
C.0.72%Pu.50.15	0.019807	G.0.72%Pu.50.15	9.30E-04
C.0.26.7%Pu.50.15	0.00187	G.0.26.7%Pu.50.15	9.17E-05
C.0.26.28%Pu.50.15	0.007479	G.0.26.28%Pu.50.15	3.67E-04
C.0.26.72%Pu.50.15	0.018698	G.0.26.72%Pu.50.15	9.17E-04
C.0.46.7%Pu.50.15	0.00185	G.0.46.7%Pu.50.15	1.02E-04
C.0.46.28%Pu.50.15	0.007398	G.0.46.28%Pu.50.15	4.08E-04
C.0.46.72%Pu.50.15	0.018495	G.0.46.72%Pu.50.15	1.02E-03
C.0.7%Pu.50.30	0.001938	G.0.7%Pu.50.30	5.15E-05
C.0.28%Pu.50.30	0.007752	G.0.28%Pu.50.30	2.06E-04
C.0.72%Pu.50.30	0.01938	G.0.72%Pu.50.30	5.15E-04
C.0.26.7%Pu.50.30	0.001874	G.0.26.7%Pu.50.30	5.08E-05
C.0.26.28%Pu.50.30	0.007497	G.0.26.800.50.30	2.03E-04
C.0.26.72%Pu.50.30	0.018742	G.0.26.72%Pu.50.30	5.08E-04
C.0.46.7%Pu.50.30	0.001857	G.0.46.7%Pu.50.30	5.65E-05
C.0.46.28%Pu.50.30	0.007428	G.0.46.28%Pu.50.30	2.26E-04
C.0.46.72%Pu.50.30	0.018571	G.0.46.72%Pu.50.30	5.08E-04

Appendix B: Tables and Figures of Parametric Study

B.2 Figures of Eccentricity Effect:

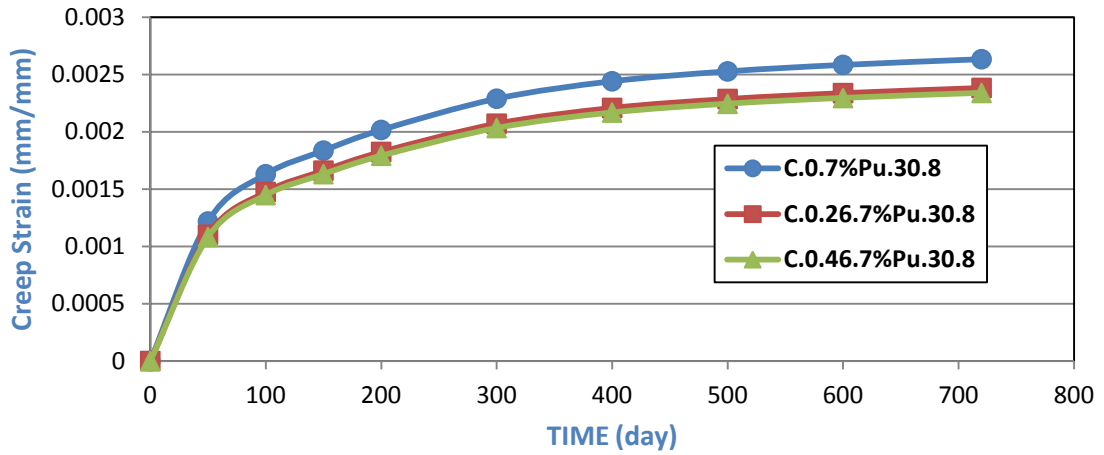


Fig.(B-1) :Time vs Creep Strain Behavior for Models(C.#.7%Pu.30.8)

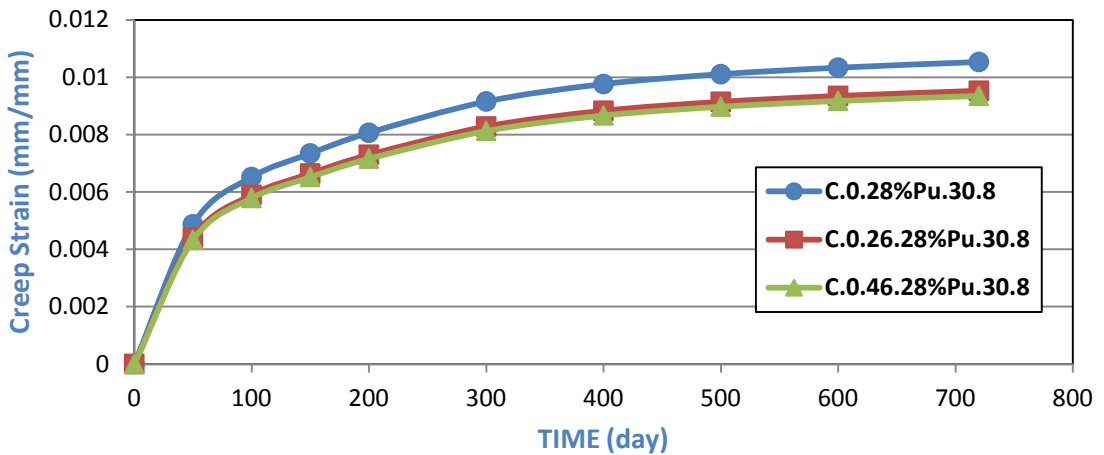


Fig.(B-2) :Time vs Creep Strain Behavior for Models(C.#.28%Pu.30.8)

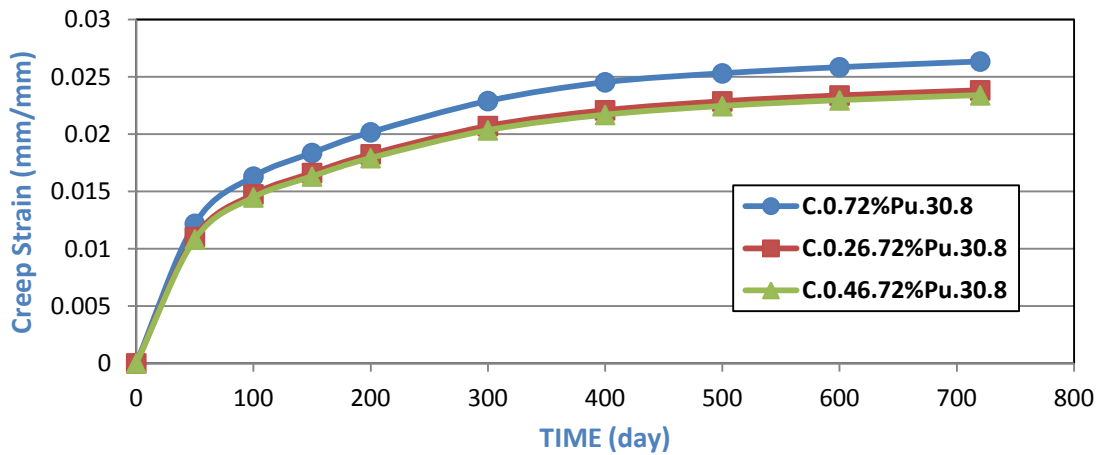


Fig.(B-3) :Time vs Creep Strain Behavior for Models(C.#.72%Pu.30.8)

Appendix B: Tables and Figures of Parametric Study

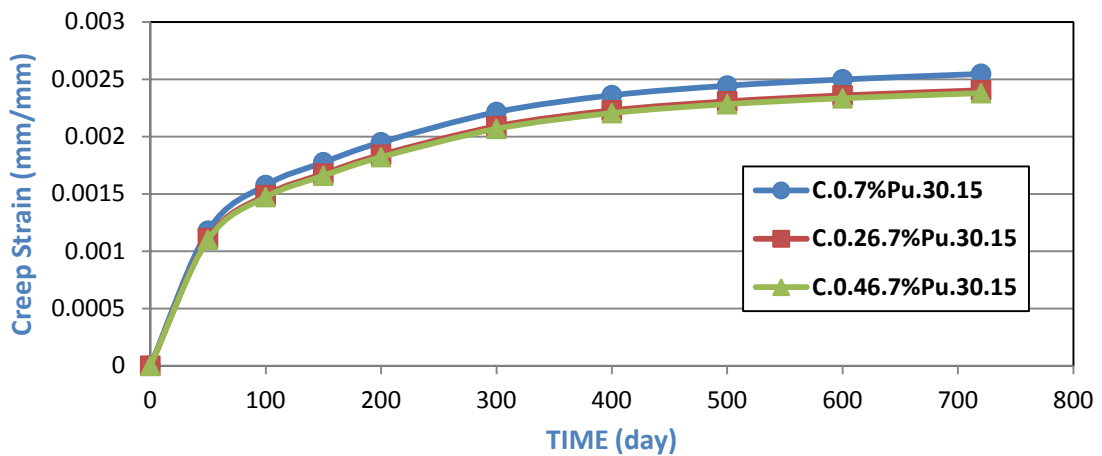


Fig.(B-4) :Time vs Creep Strain Behavior for Models(C.#.7%Pu.30.15)

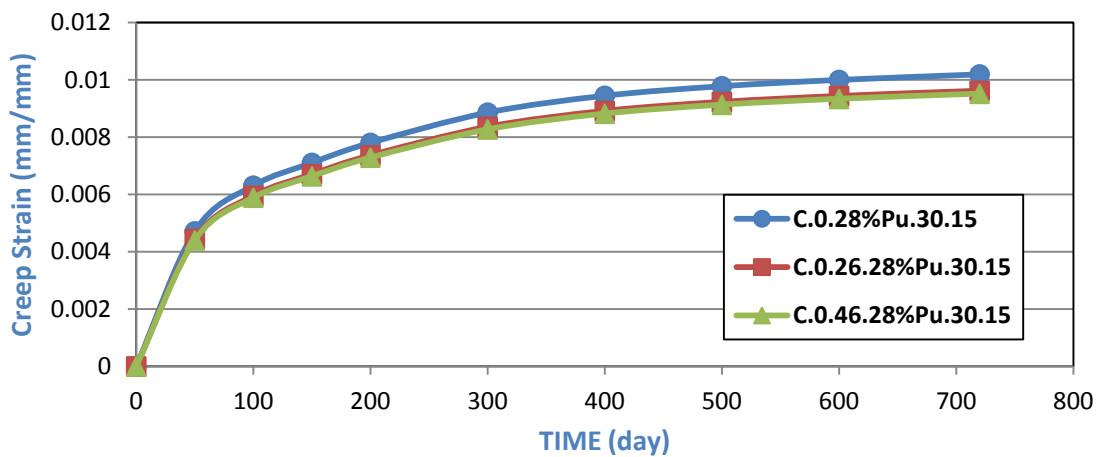


Fig.(B-5) :Time vs Creep Strain Behavior for Models(C.#.28%Pu.30.15)

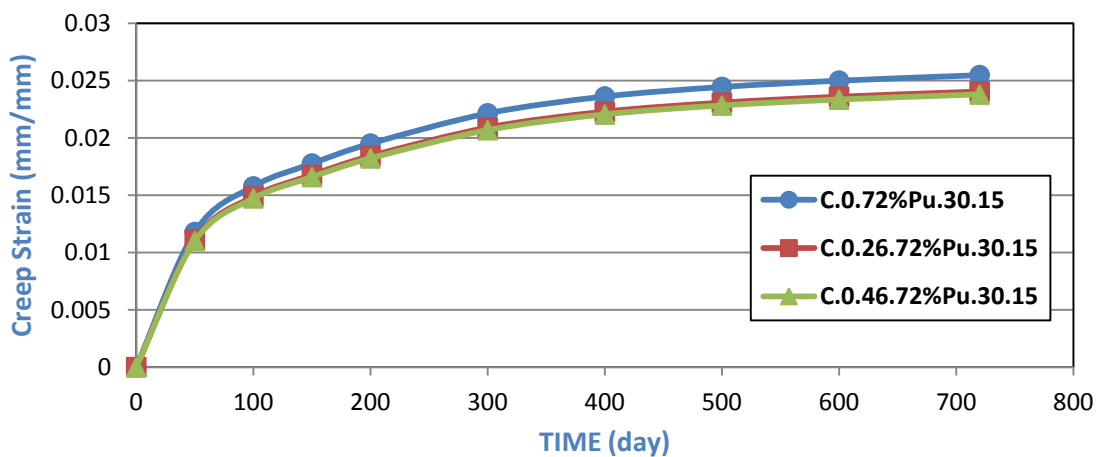


Fig.(B-6) :Time vs Creep Strain Behavior for Models(C.#.72%Pu.30.15)

Appendix B: Tables and Figures of Parametric Study

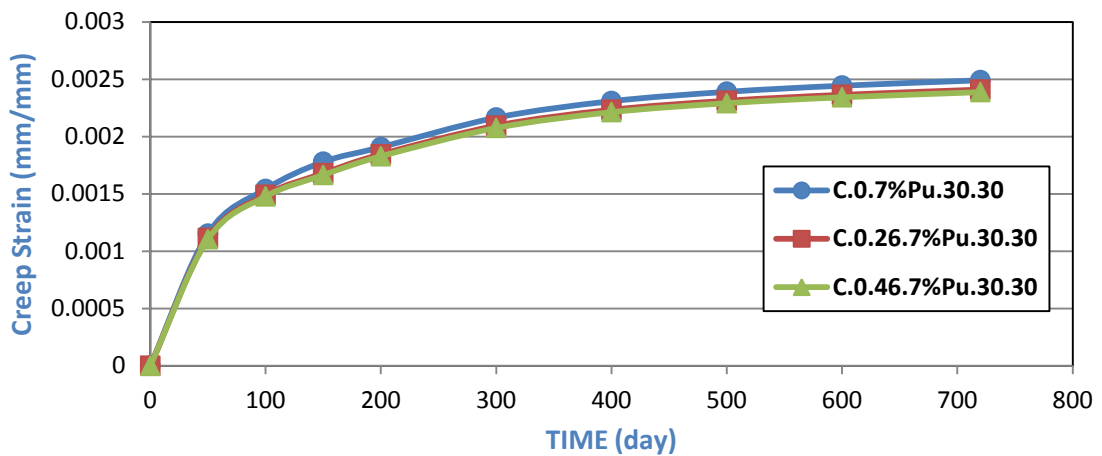


Fig.(B-7) :Time vs Creep Strain Behavior for Models(C.#.7%Pu.30.30)

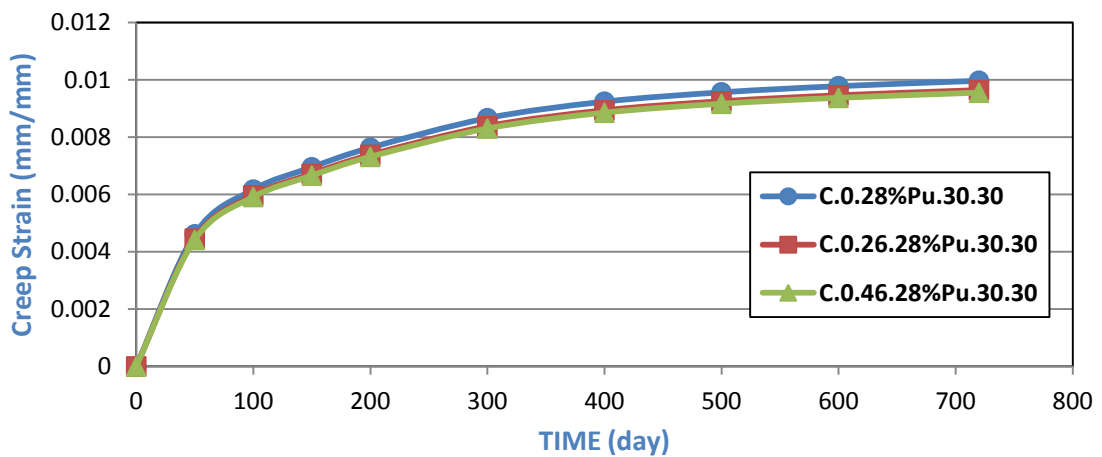


Fig.(B-8) :Time vs Creep Strain Behavior for Models(C.#.28%Pu.30.30)

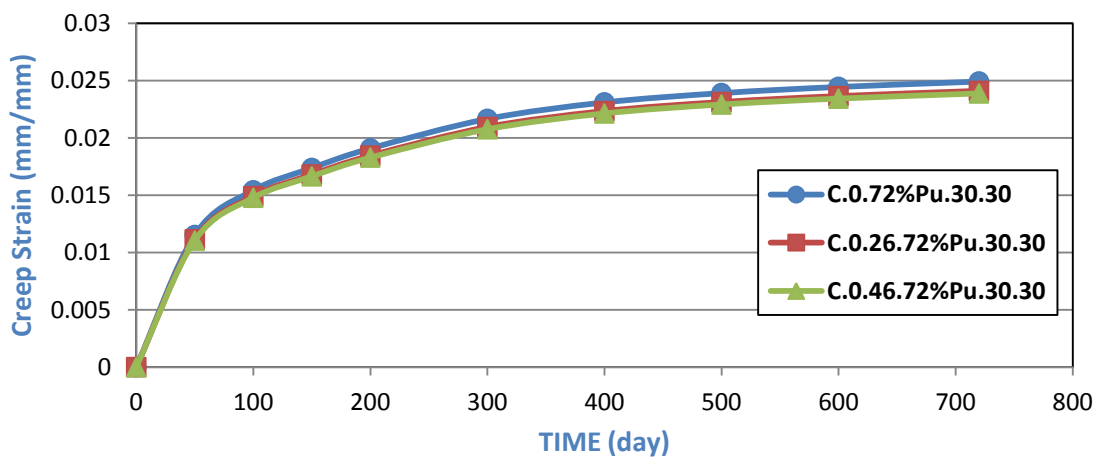


Fig.(B-9) :Time vs Creep Strain Behavior for Models(C.#.72%Pu.30.30)

Appendix B: Tables and Figures of Parametric Study

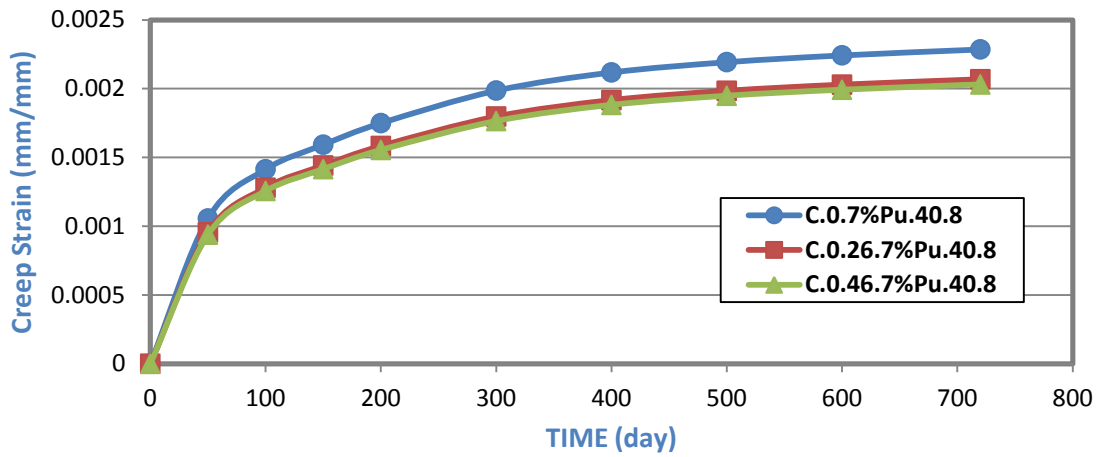


Fig.(B-10) :Time vs Creep Strain Behavior for Models(C.#.7%Pu.40.8)

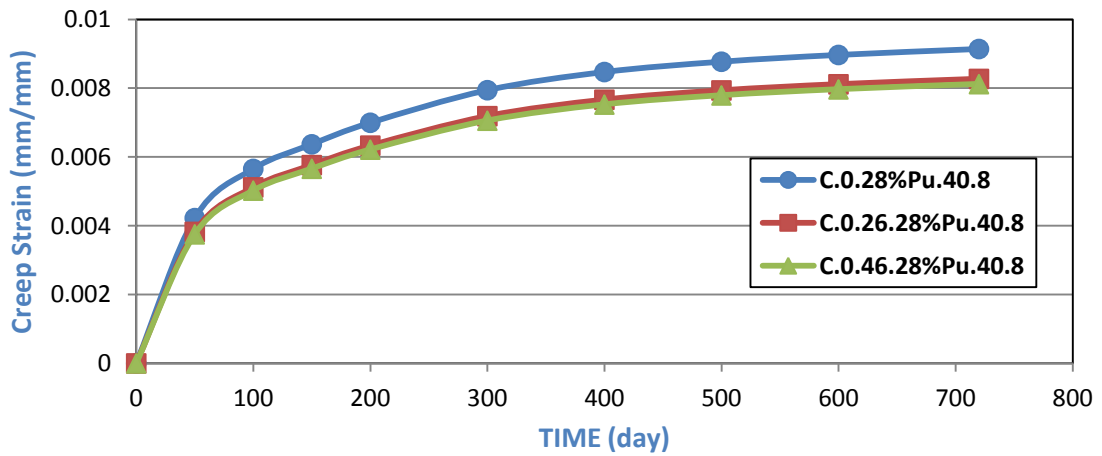


Fig.(B-11) :Time vs Creep Strain Behavior for Models(C.#.28%Pu.40.8)

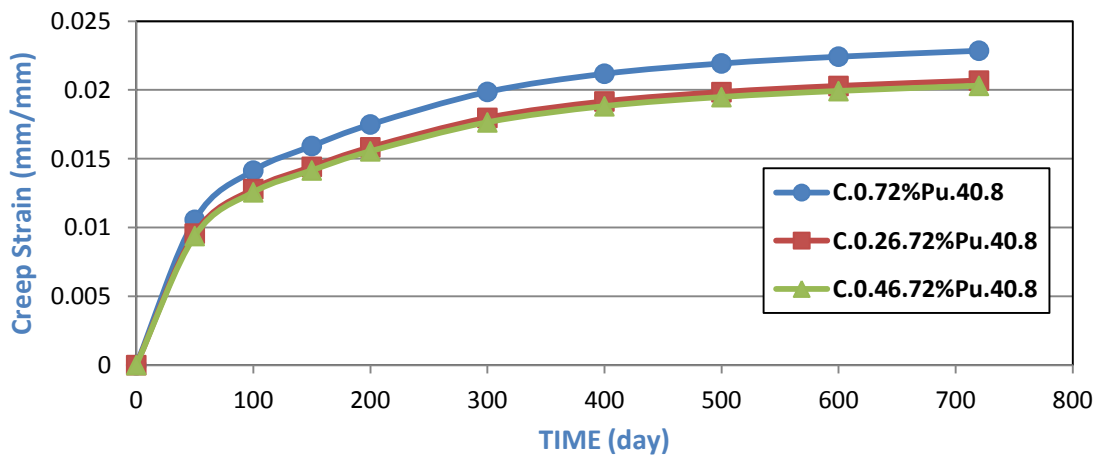


Fig.(B-12) :Time vs Creep Strain Behavior for Models(C.#.72%Pu.40.8)

Appendix B: Tables and Figures of Parametric Study

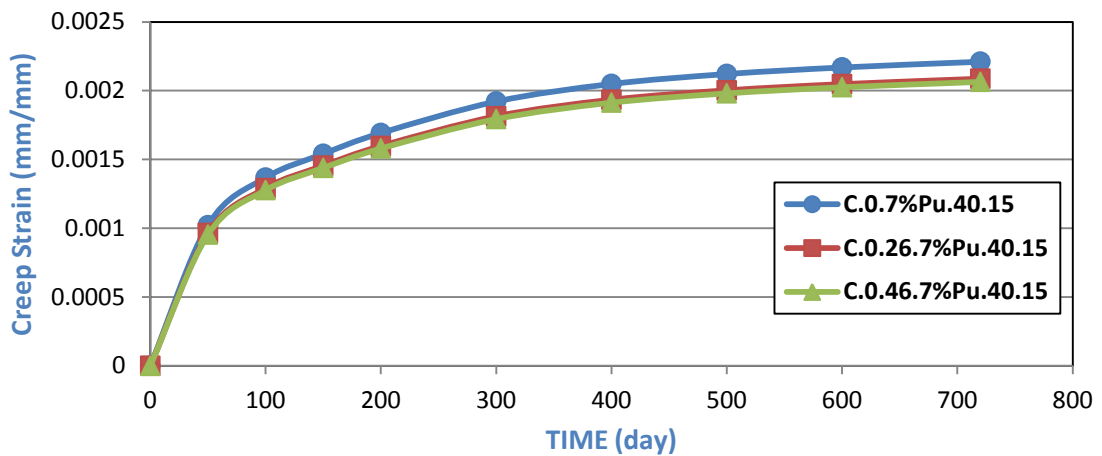


Fig.(B-13) :Time vs Creep Strain Behavior for Models(C.#.7%Pu.40.15)

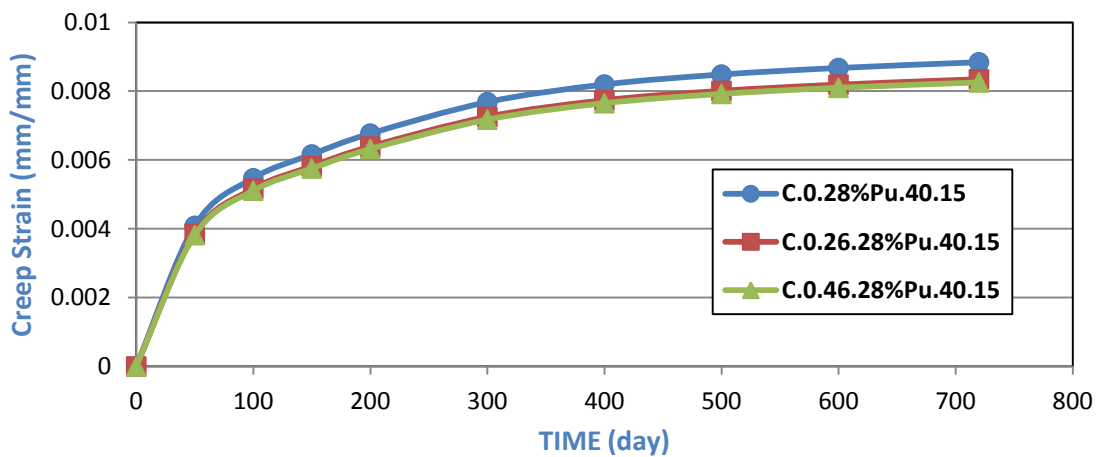


Fig.(B-14) :Time vs Creep Strain Behavior for Models(C.#.28%Pu.40.15)

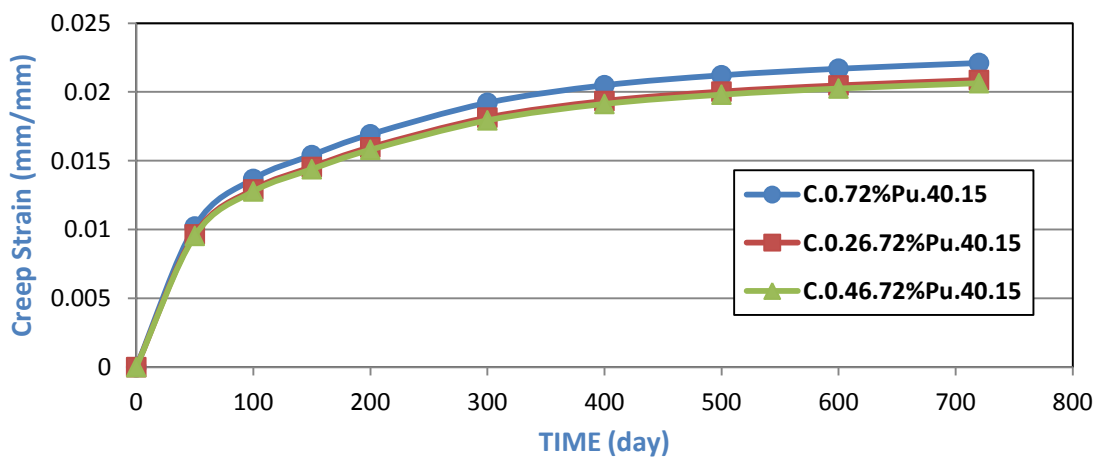


Fig.(B-15) :Time vs Creep Strain Behavior for Models(C.#.72%Pu.40.15)

Appendix B: Tables and Figures of Parametric Study

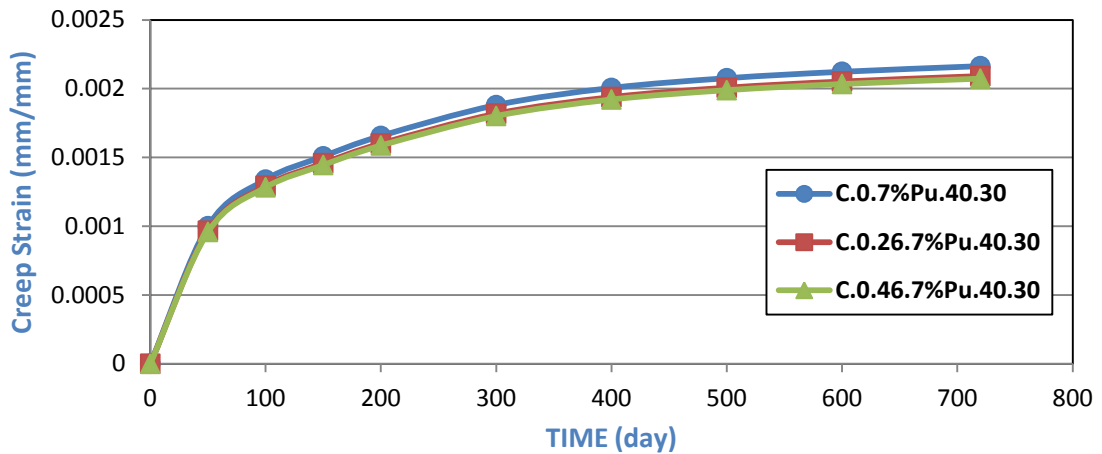


Fig.(B-16) :Time vs Creep Strain Behavior for Models(C.#.7%Pu.40.30)

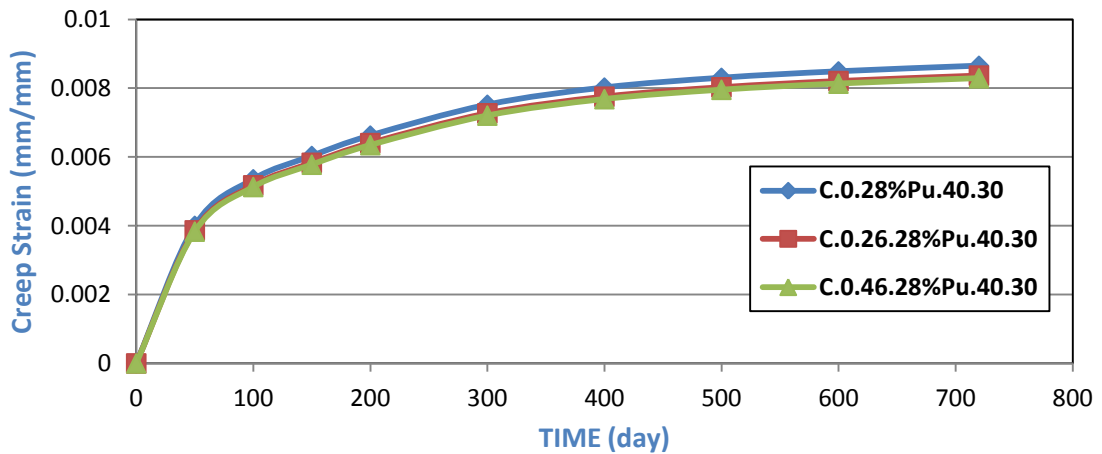


Fig.(B-17) :Time vs Creep Strain Behavior for Models(C.#.28%Pu.40.30)

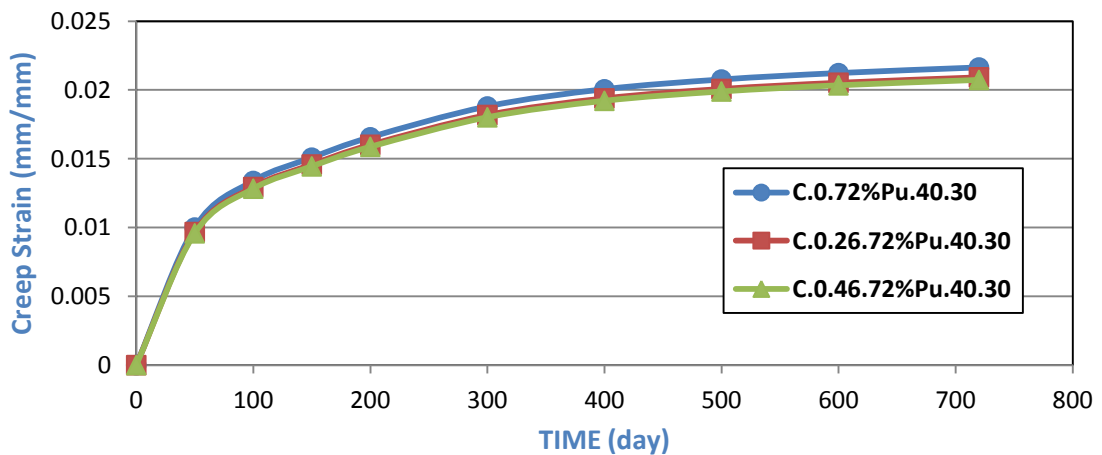


Fig.(B-18) :Time vs Creep Strain Behavior for Models(C.#.72%Pu.40.30)

Appendix B: Tables and Figures of Parametric Study

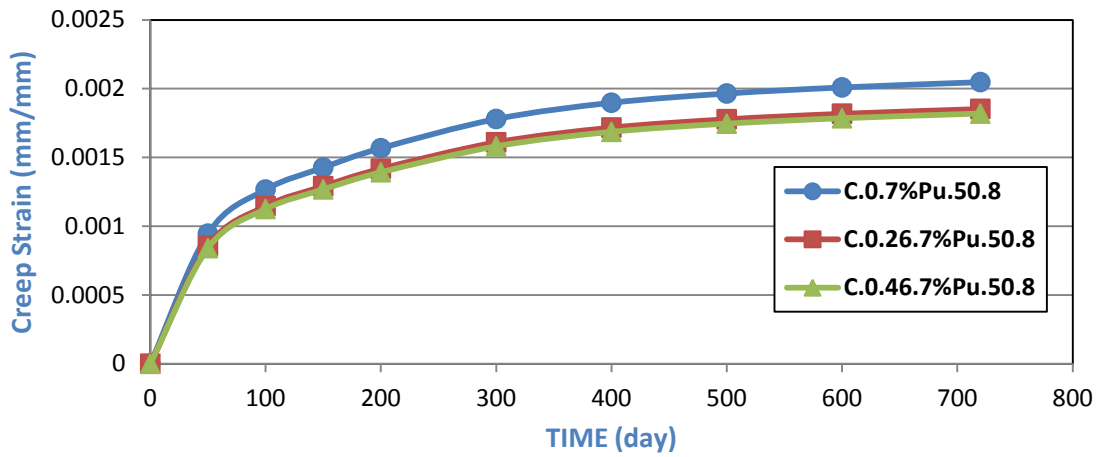


Fig.(B-19) :Time vs Creep Strain Behavior for Models(C.#.7%Pu.50.8)

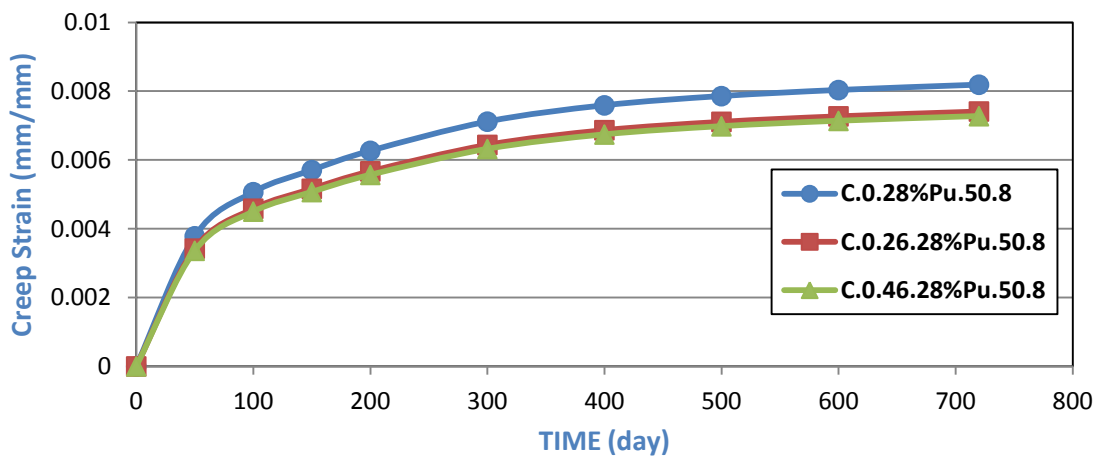


Fig.(B-20) :Time vs Creep Strain Behavior for Models(C.#.28%Pu.50.8)

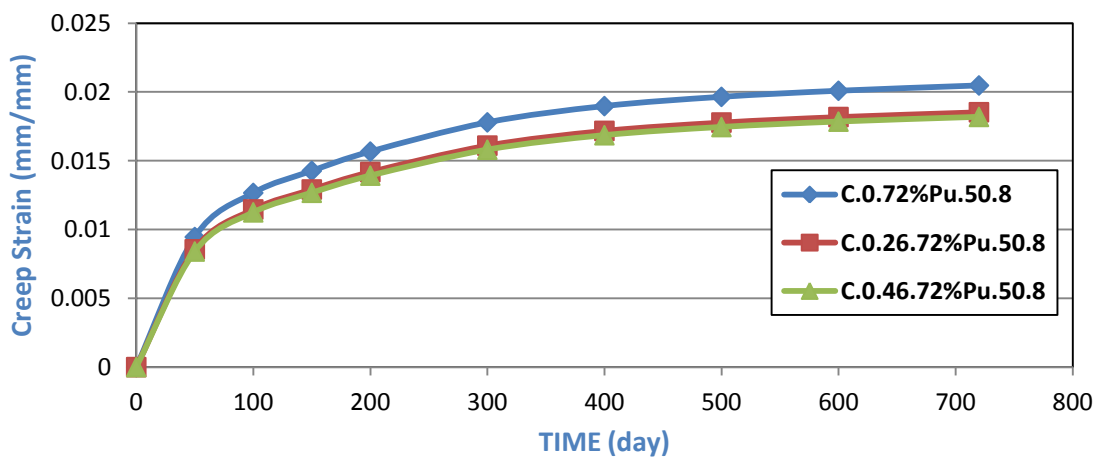


Fig.(B-21) :Time vs Creep Strain Behavior for Models(C.#.72%Pu.50.8)

Appendix B: Tables and Figures of Parametric Study

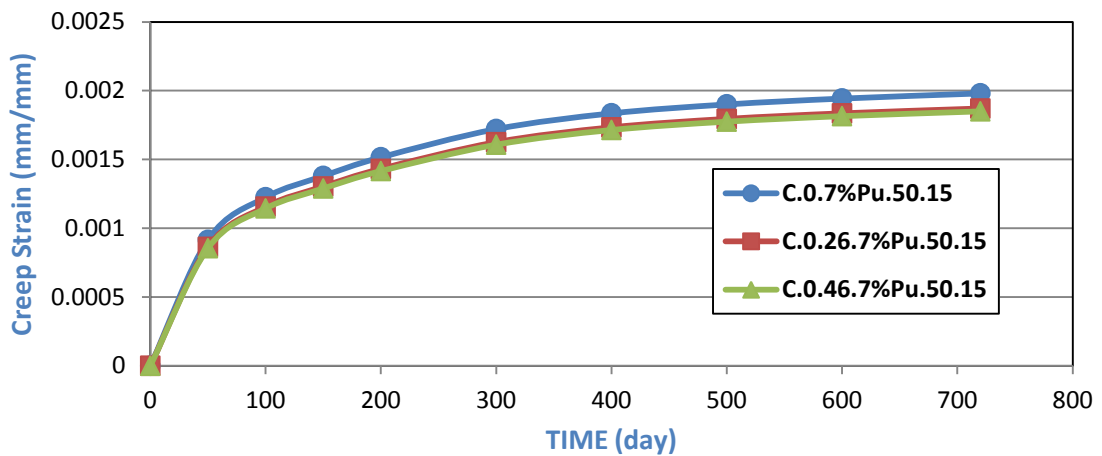


Fig.(B-22) :Time vs Creep Strain Behavior for Models(C.#.7%Pu.50.15)

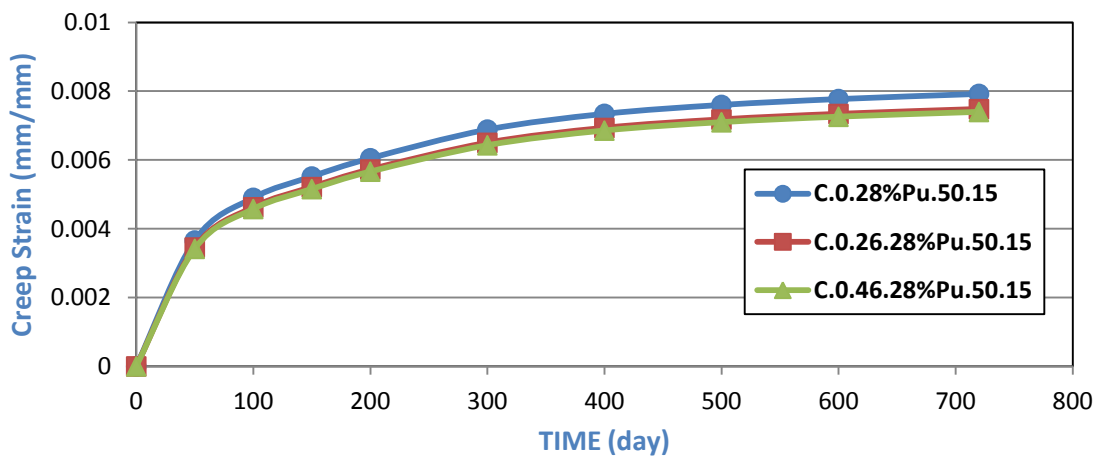


Fig.(B-23) :Time vs Creep Strain Behavior for Models(C.#.28%Pu.50.15)

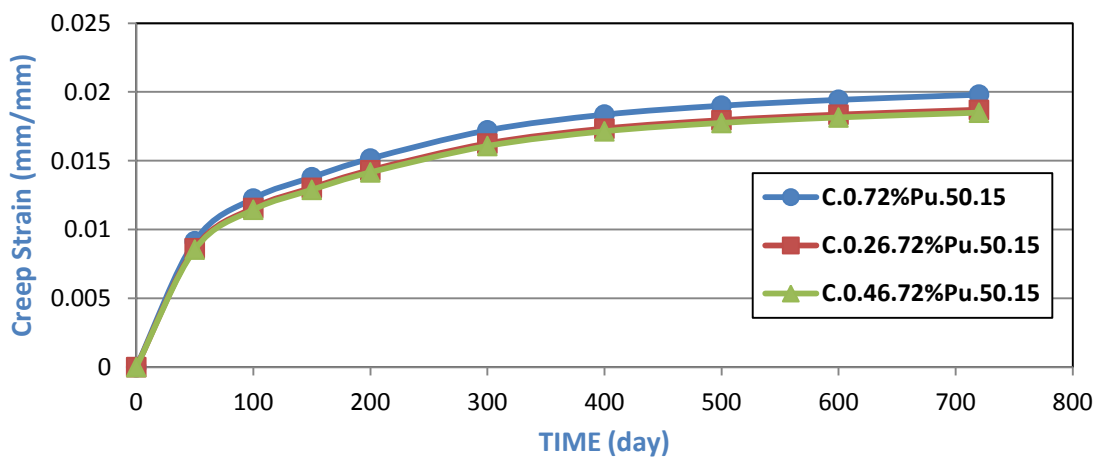


Fig.(B-24) :Time vs Creep Strain Behavior for Models(C.#.72%Pu.50.15)

Appendix B: Tables and Figures of Parametric Study

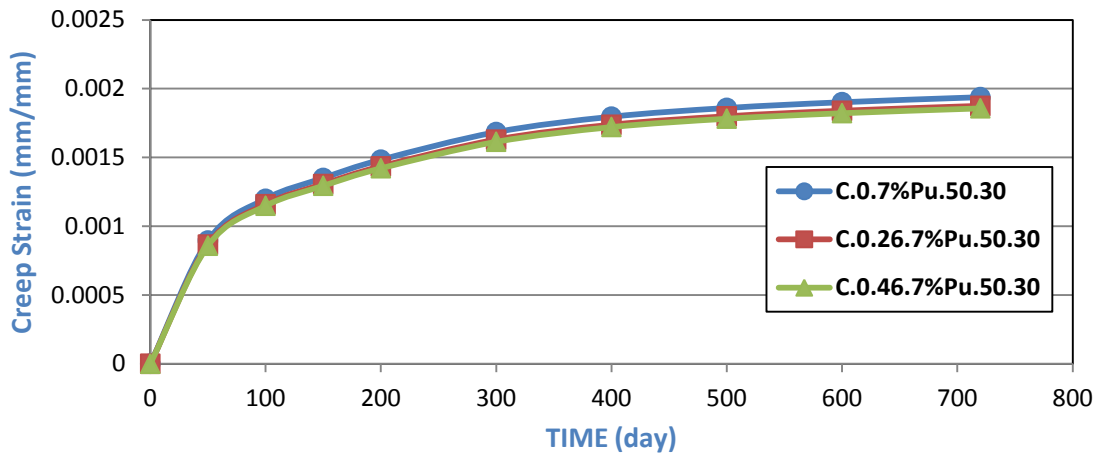


Fig.(B-25) :Time vs Creep Strain Behavior for Models(C.#.7%Pu.50.30)

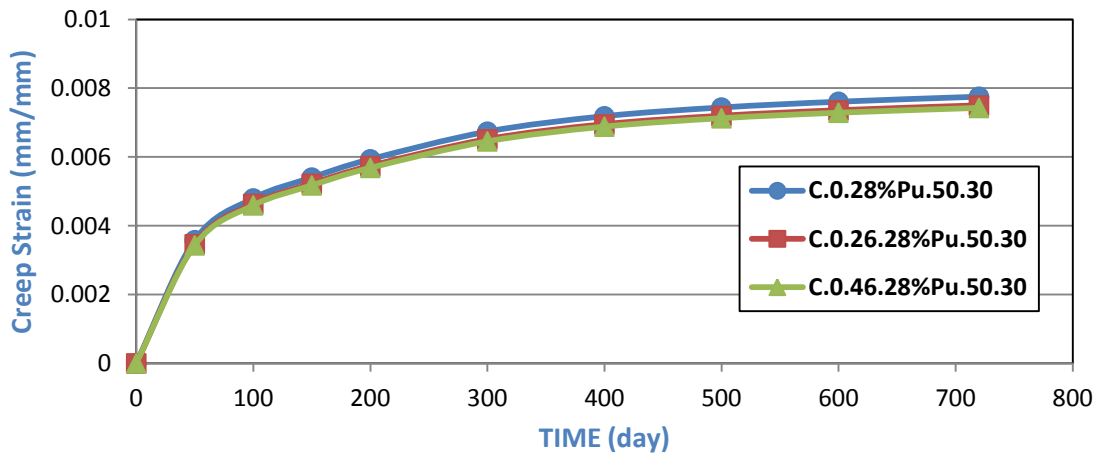


Fig.(B-26) :Time vs Creep Strain Behavior for Models(C.#.28%Pu.50.30)

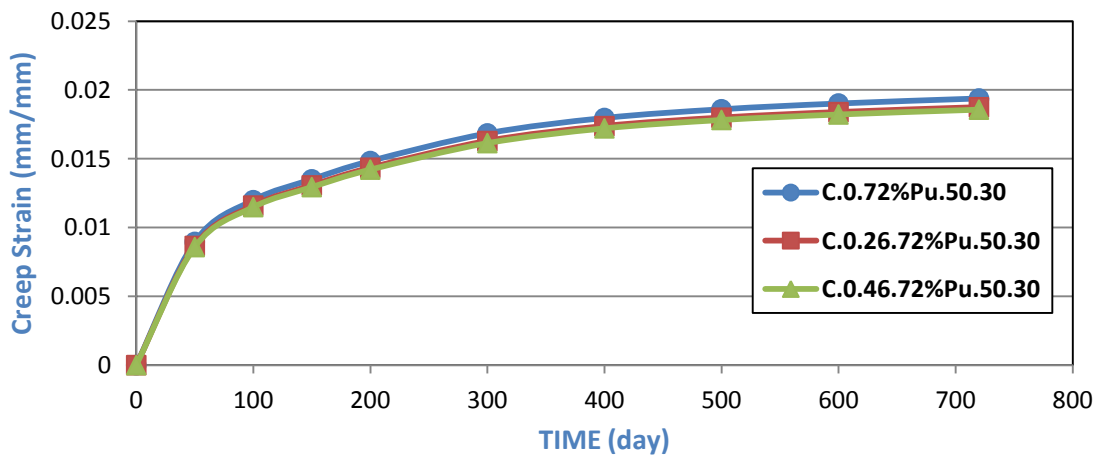


Fig.(B-27) :Time vs Creep Strain Behavior for Models(C.#.72%Pu.50.30)

Appendix B: Tables and Figures of Parametric Study

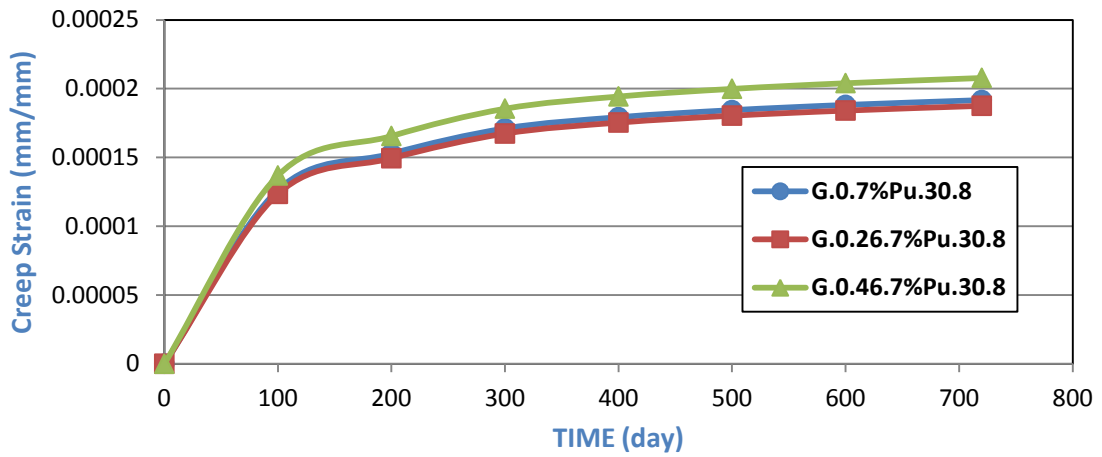


Fig.(B-28) :Time vs Creep Strain Behavior for Models(G.#.7%Pu.30.8)

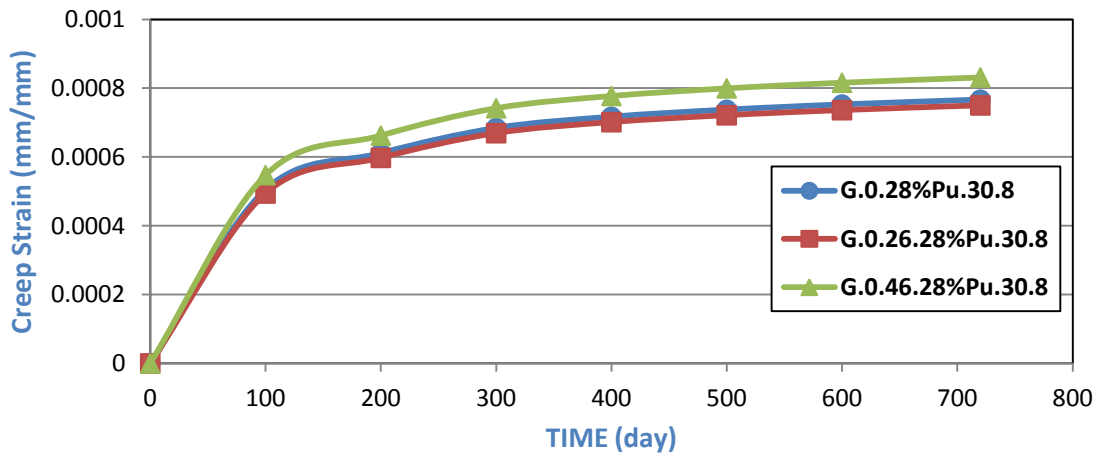


Fig.(B-29) :Time vs Creep Strain Behavior for Models(G.#.28%Pu.30.8)

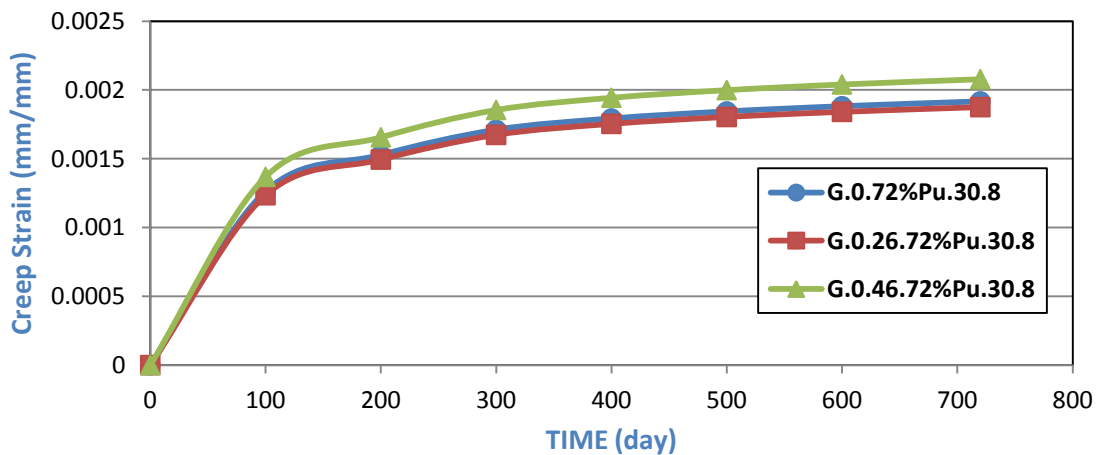


Fig.(B-30) :Time vs Creep Strain Behavior for Models(G.#.72%Pu.30.8)

Appendix B: Tables and Figures of Parametric Study

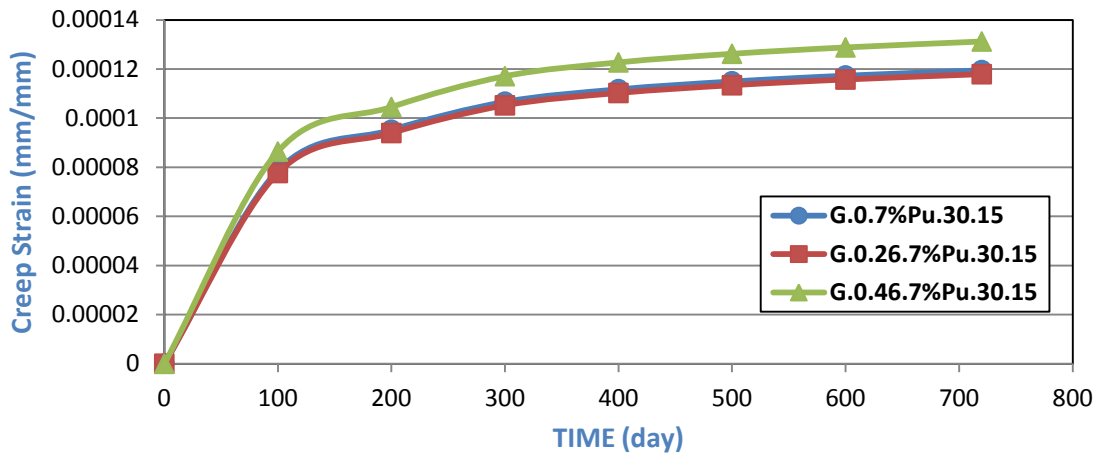


Fig.(B-31) :Time vs Creep Strain Behavior for Models(G.#.7%Pu.30.15)

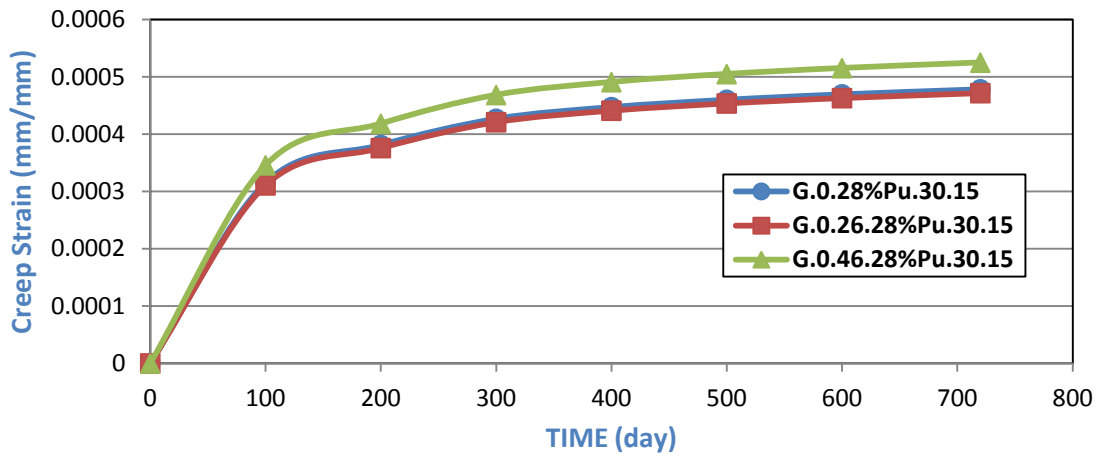


Fig.(B-32) :Time vs Creep Strain Behavior for Models(G.#.28%Pu.30.15)

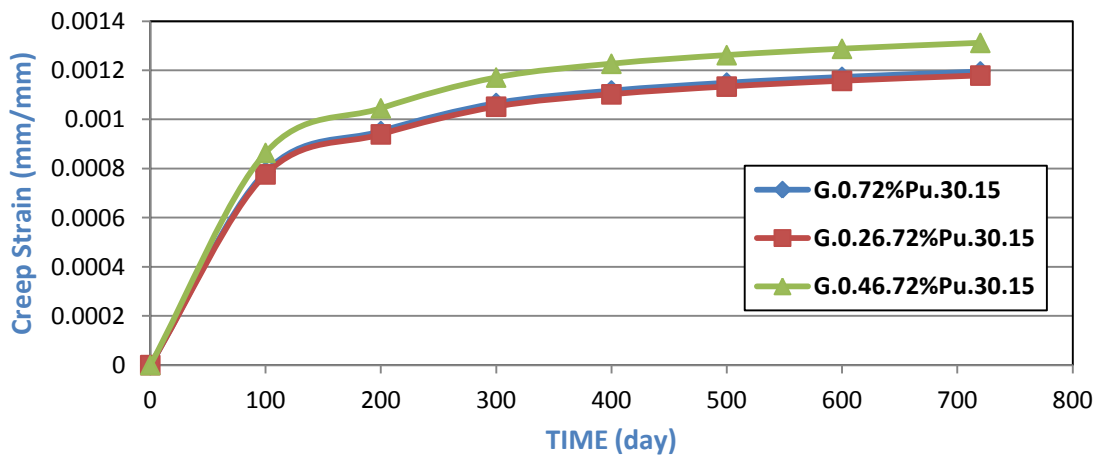


Fig.(B-33) :Time vs Creep Strain Behavior for Models(G.#.72%Pu.30.15)

Appendix B: Tables and Figures of Parametric Study

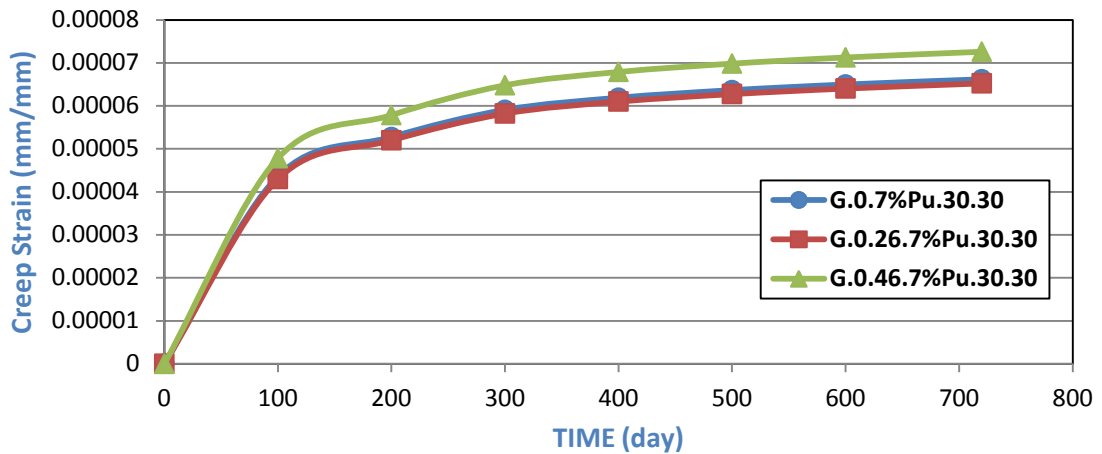


Fig.(B-34) :Time vs Creep Strain Behavior for Models(G.#.7%Pu.30.30)

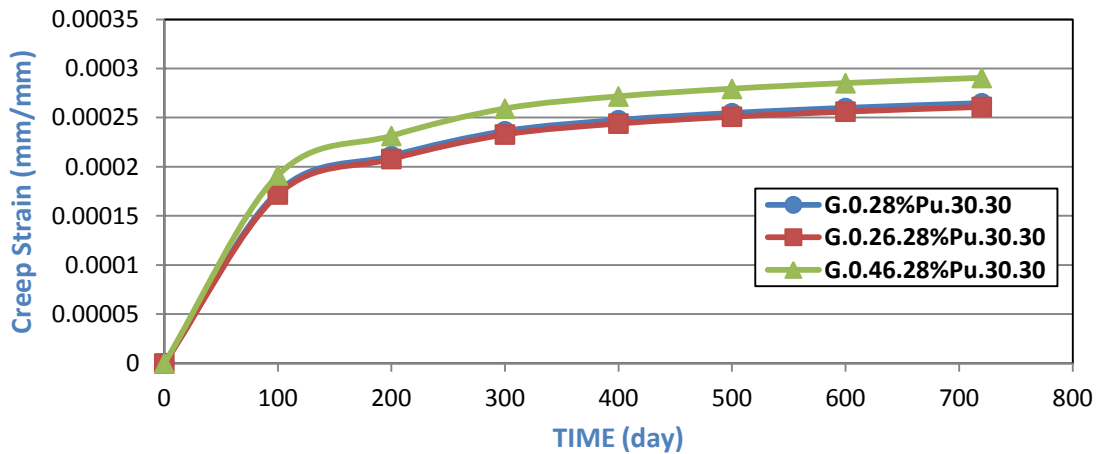


Fig.(B-35) :Time vs Creep Strain Behavior for Models(G.#.28%Pu.30.30)

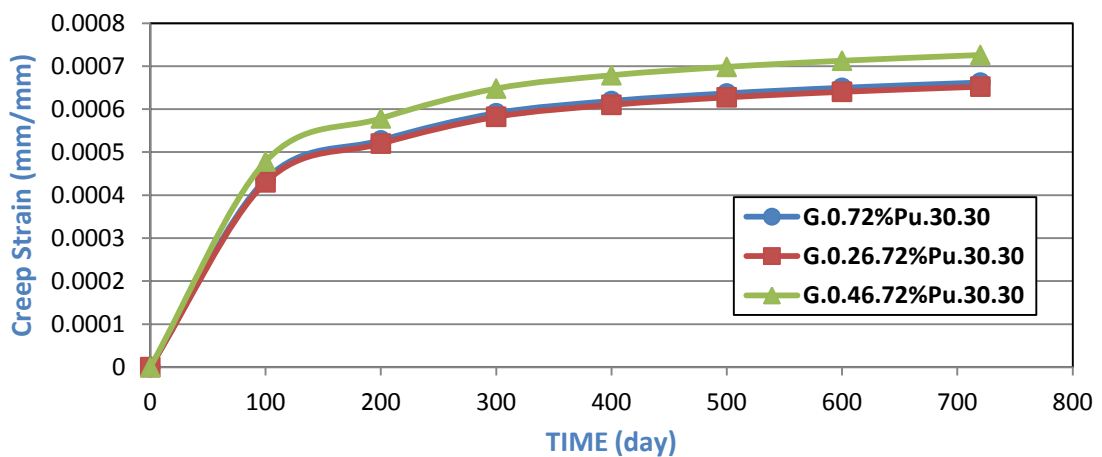


Fig.(B-36) :Time vs Creep Strain Behavior for Models(G.#.72%Pu.30.30)

Appendix B: Tables and Figures of Parametric Study

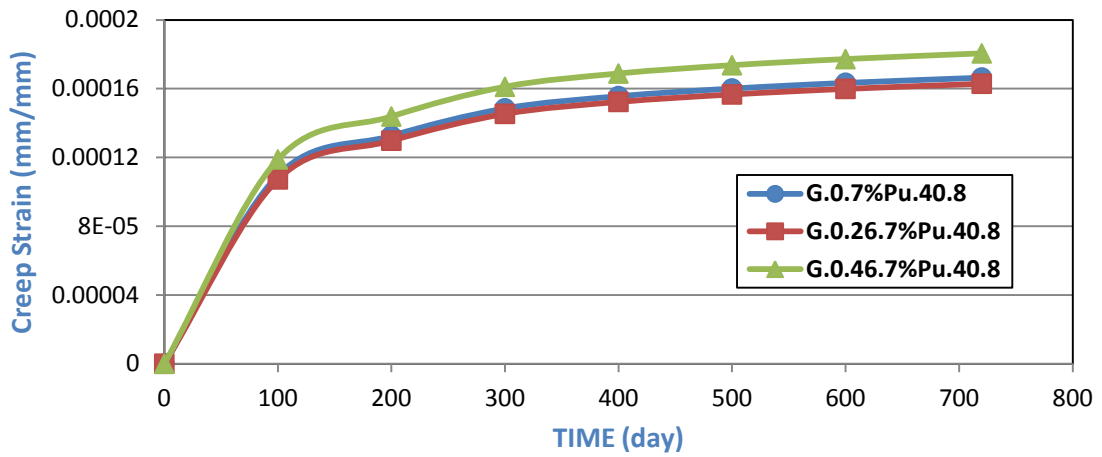


Fig.(B-37) :Time vs Creep Strain Behavior for Models(G.#.7%Pu.40.8)

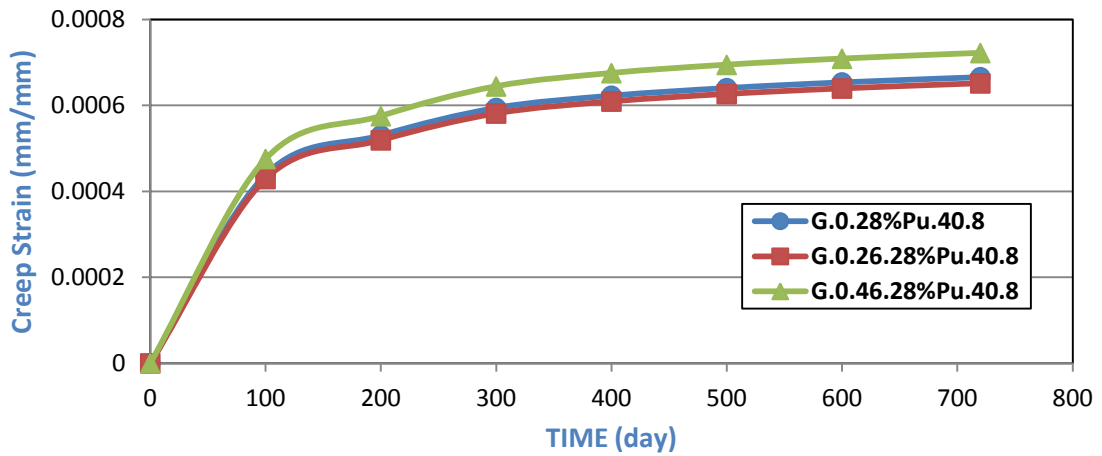


Fig.(B-38) :Time vs Creep Strain Behavior for Models(G.#.28%Pu.40.8)

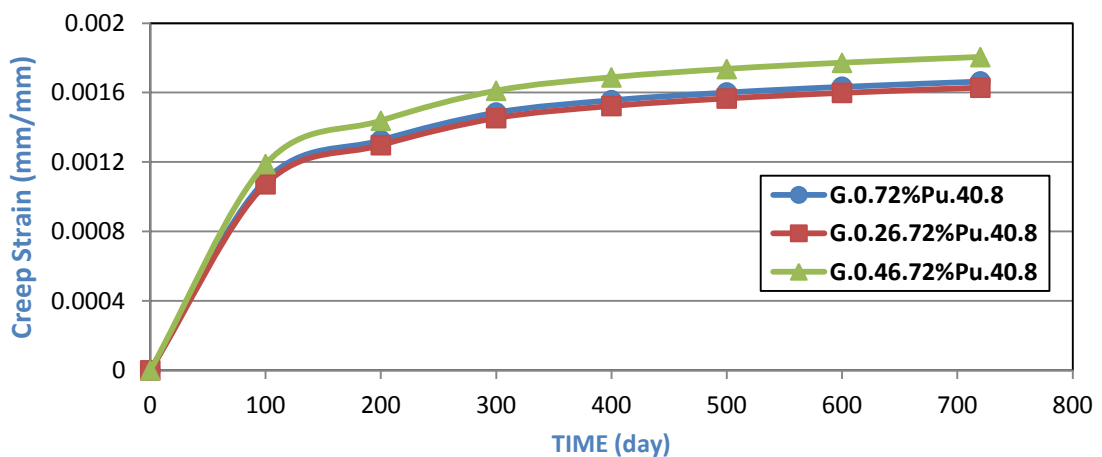


Fig.(B-39) :Time vs Creep Strain Behavior for Models(G.#.72%Pu.40.8)

Appendix B: Tables and Figures of Parametric Study

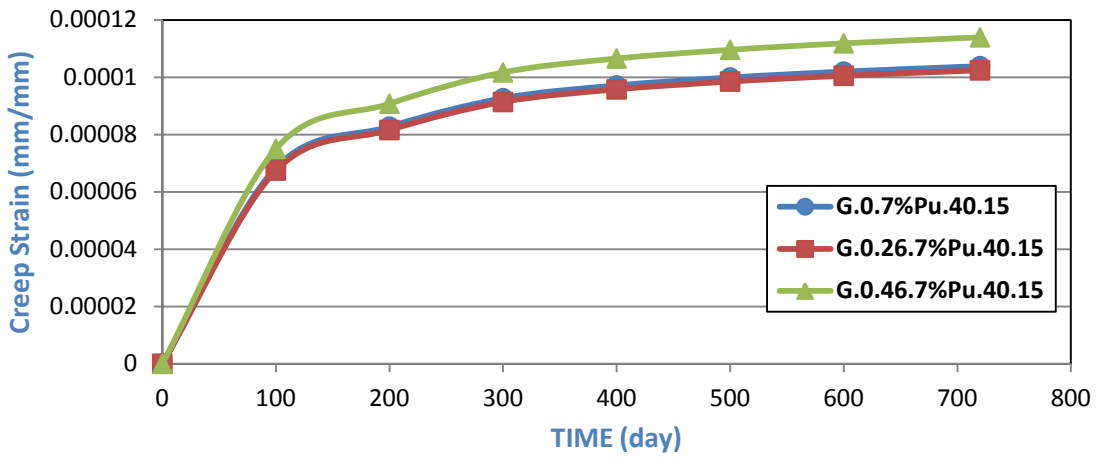


Fig.(B-40) :Time vs Creep Strain Behavior for Models(G.#.7%Pu.40.15)

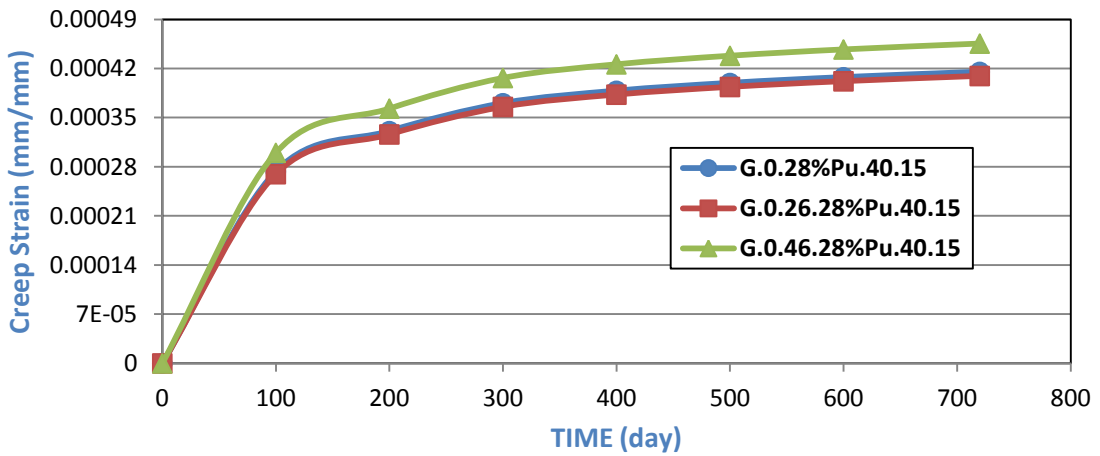


Fig.(B-41) :Time vs Creep Strain Behavior for Models(G.#.28%Pu.40.15)

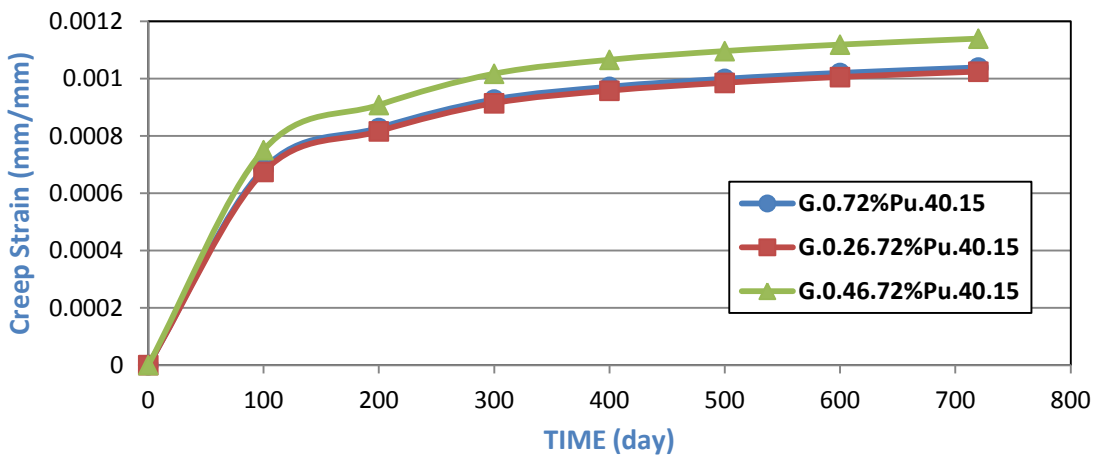


Fig.(B-42) :Time vs Creep Strain Behavior for Models(G.#.72%Pu.40.15)

Appendix B: Tables and Figures of Parametric Study

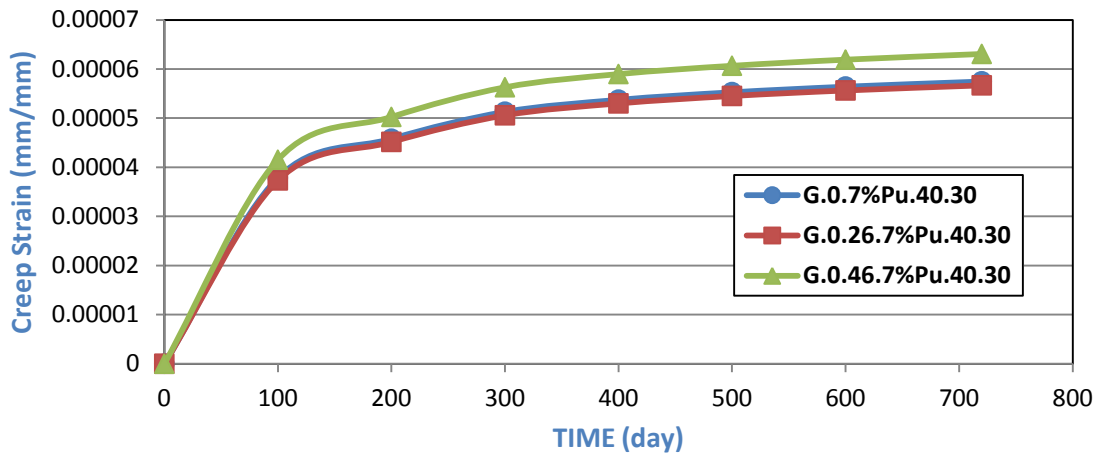


Fig.(B-43) :Time vs Creep Strain Behavior for Models(G.#.7%Pu.40.30)

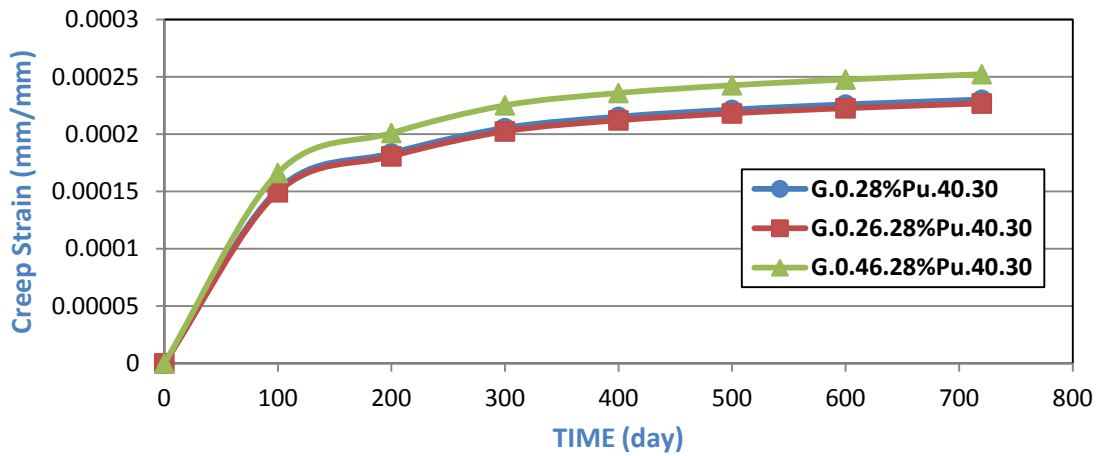


Fig.(B-44) :Time vs Creep Strain Behavior for Models(G.#.28%Pu.40.30)

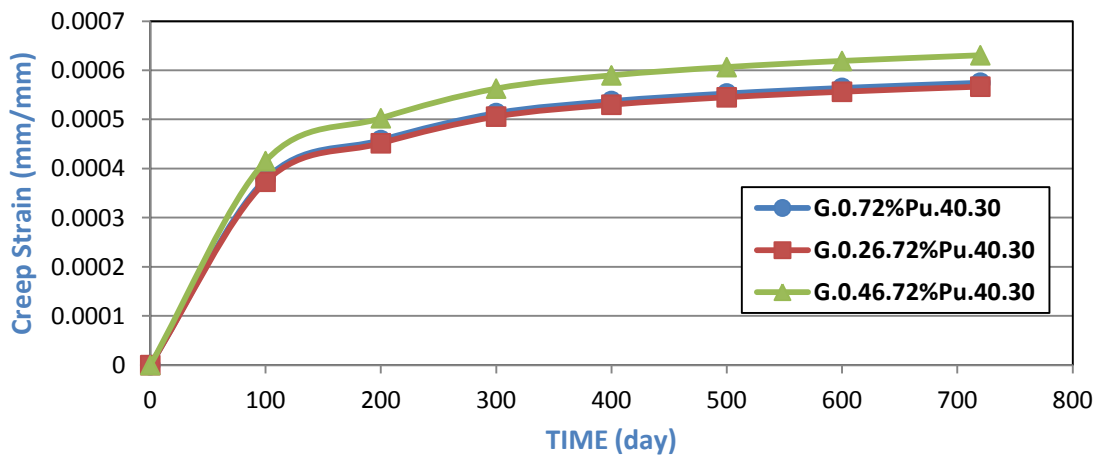


Fig.(B-45) :Time vs Creep Strain Behavior for Models(G.#.72%Pu.40.30)

Appendix B: Tables and Figures of Parametric Study

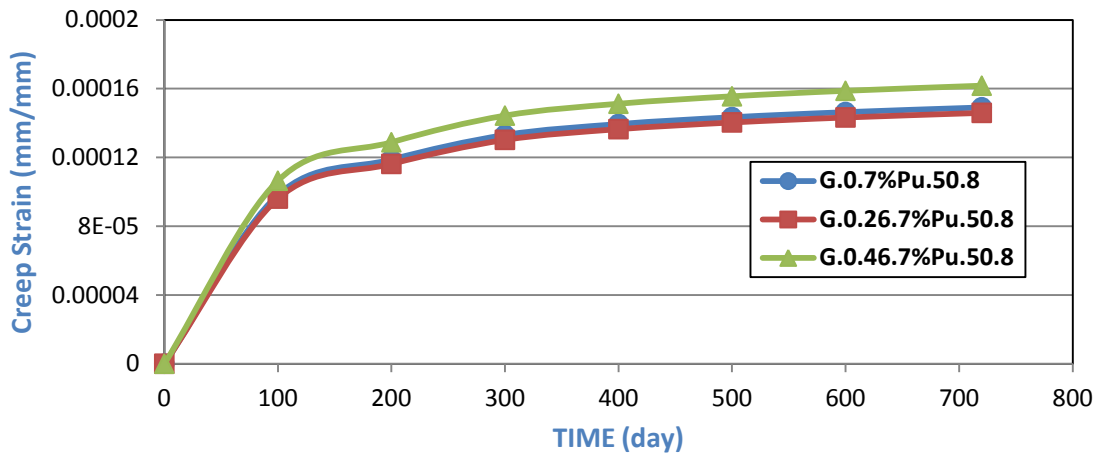


Fig.(B-46) :Time vs Creep Strain Behavior for Models(G.#.7%Pu.50.8)

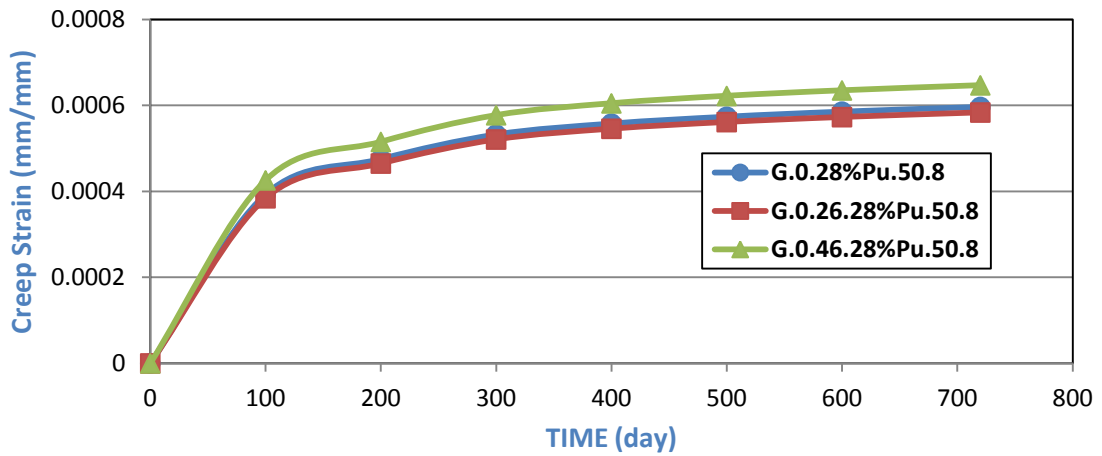


Fig.(B-47) :Time vs Creep Strain Behavior for Models(G.#.28%Pu.50.8)

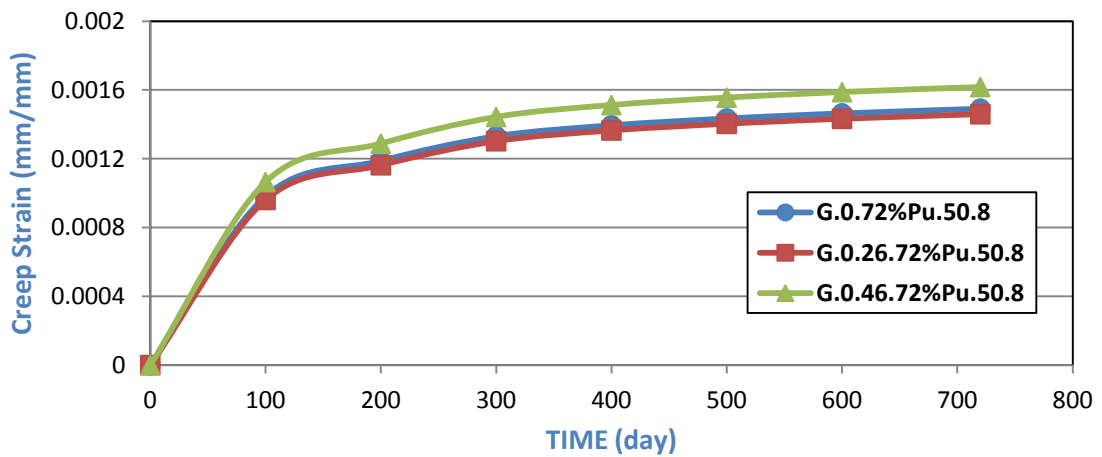


Fig.(B-48) :Time vs Creep Strain Behavior for Models(G.#.72%Pu.50.8)

Appendix B: Tables and Figures of Parametric Study

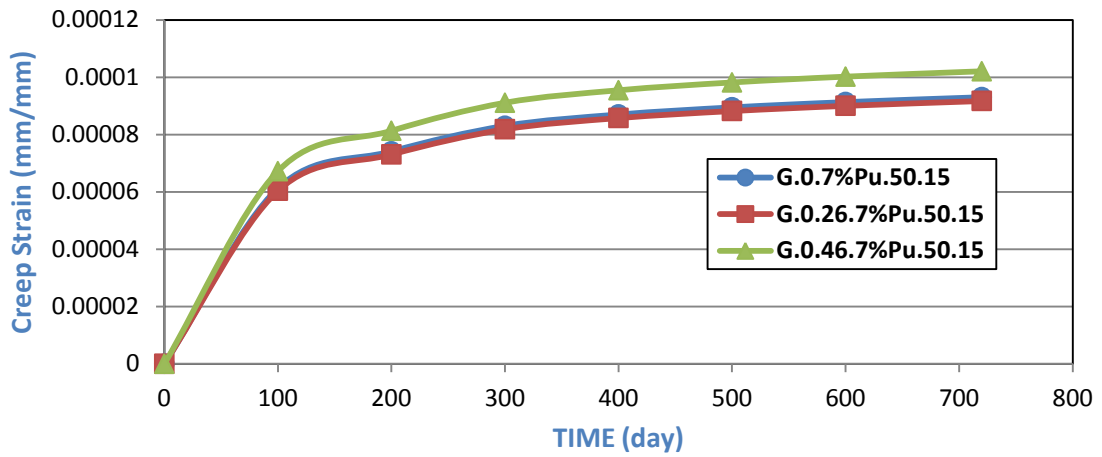


Fig.(B-49) :Time vs Creep Strain Behavior for Models(G.#.7%Pu.50.15)

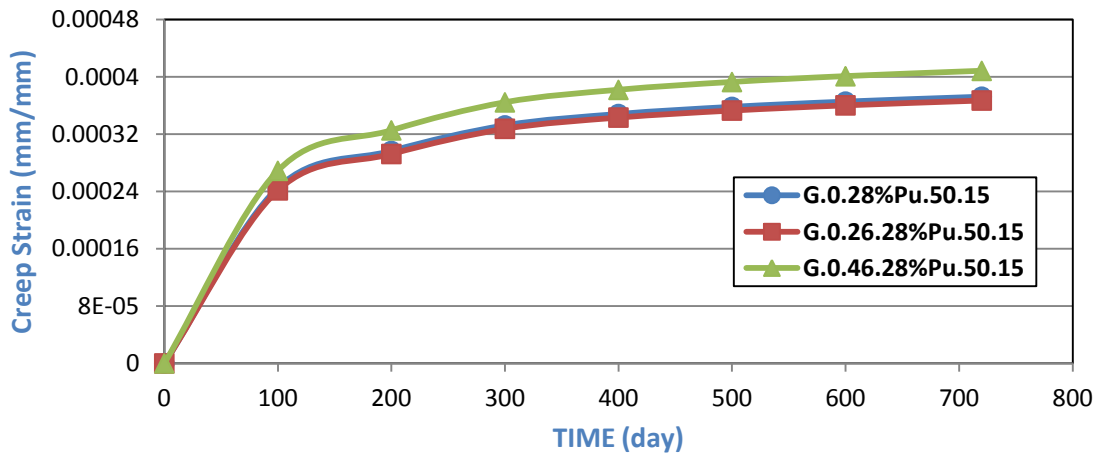


Fig.(B-50) :Time vs Creep strain Behavior for Models(G.#.28%Pu.50.15)

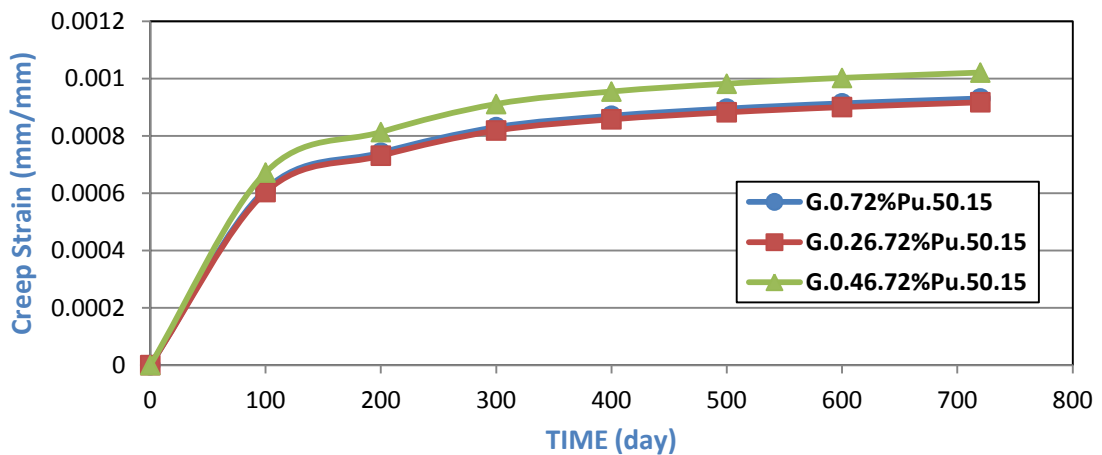


Fig.(B-51) :Time vs Creep Strain Behavior for Models(G.#.72%Pu.50.15)

Appendix B: Tables and Figures of Parametric Study

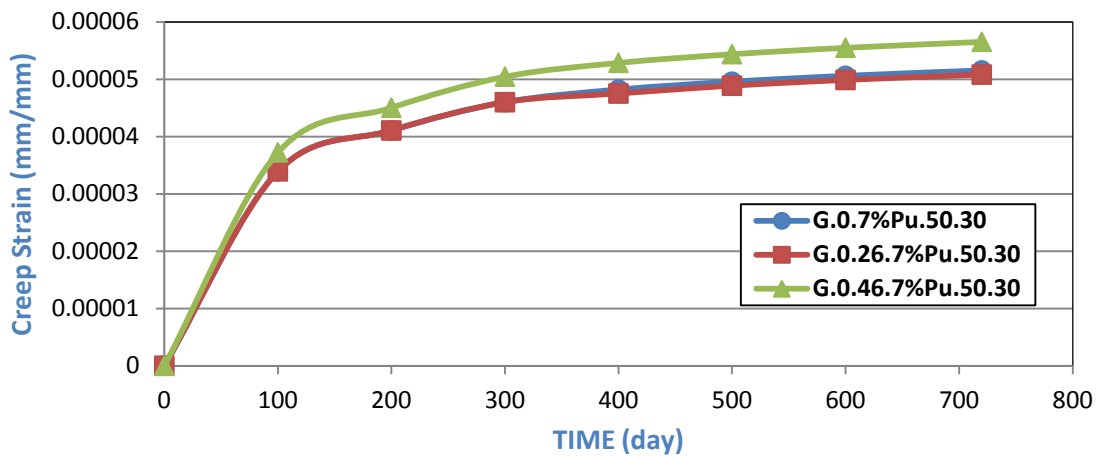


Fig.(B-52) :Time vs Creep Strain Behavior for Models(G.#.7%Pu.50.30)

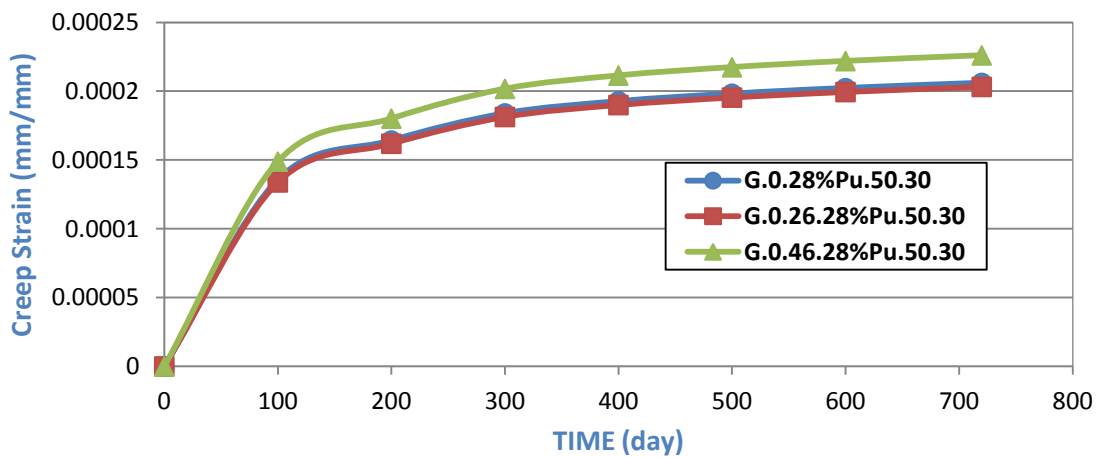


Fig.(B-53) :Time vs Creep Strain Behavior for Models(G.#.28%Pu.50.30)

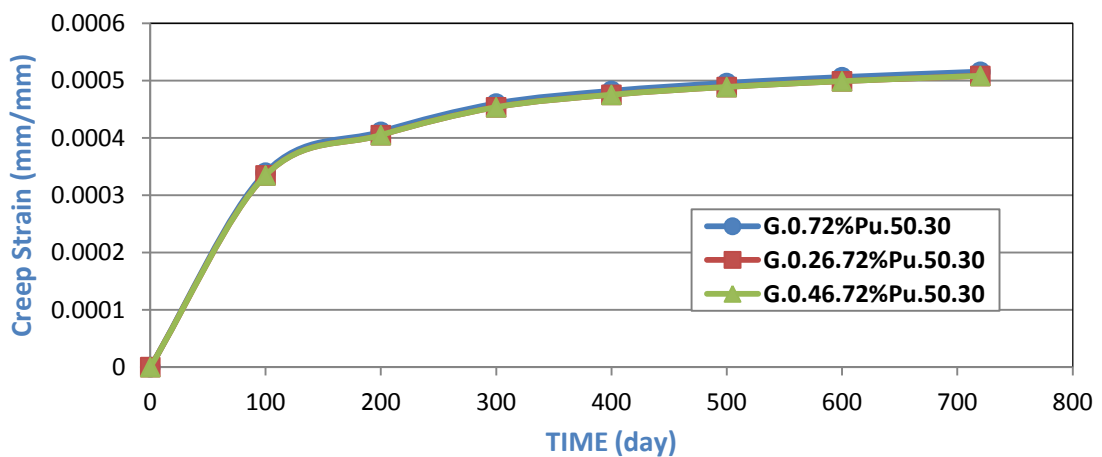


Fig.(B-54) :Time vs Creep Strain Behavior for Models(G.#.72%Pu.50.30)

Appendix B: Tables and Figures of Parametric Study

B.3 Figures of Length Effect:

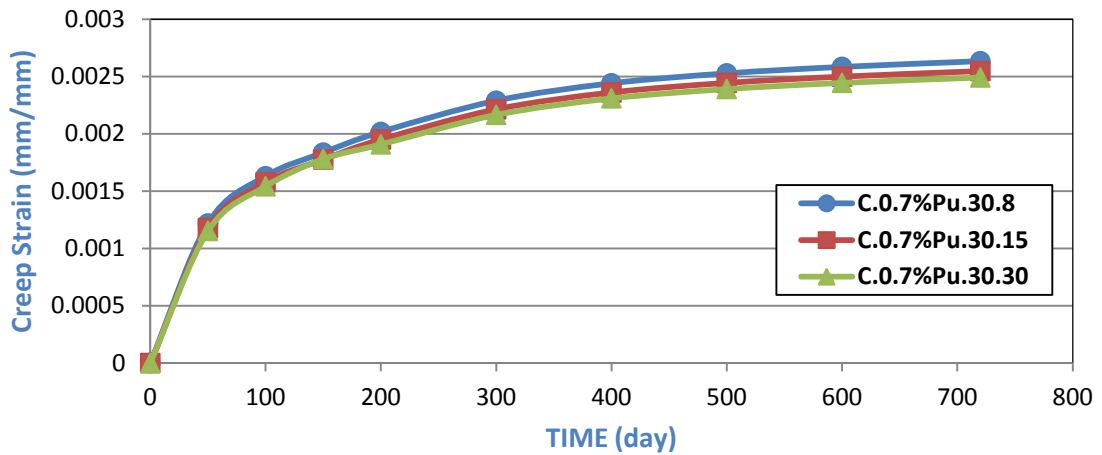


Fig.(B-55):Time vs Creep Strain Behavior for Models(C.0.7%Pu.30.#)

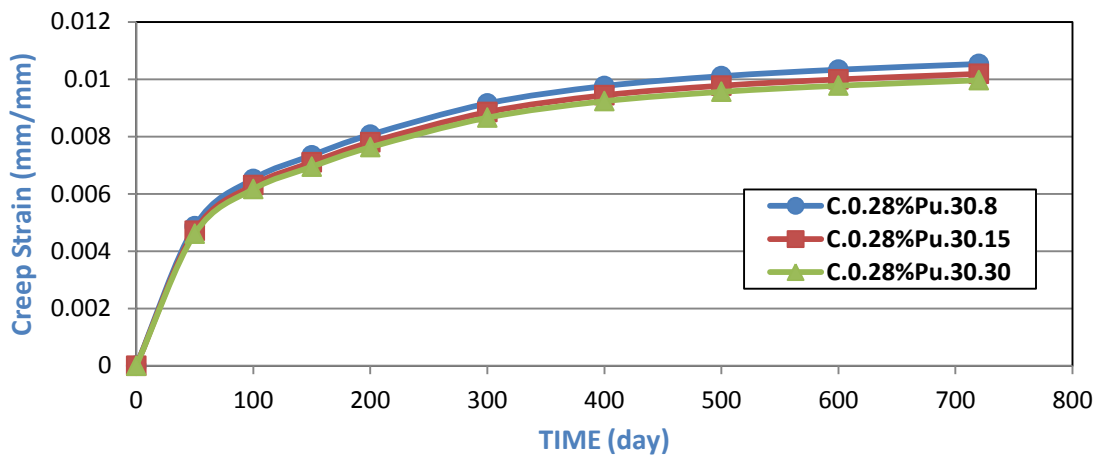


Fig.(B-56) :Time vs Creep Strain Behavior for Models(C.0.28%Pu.30.#)

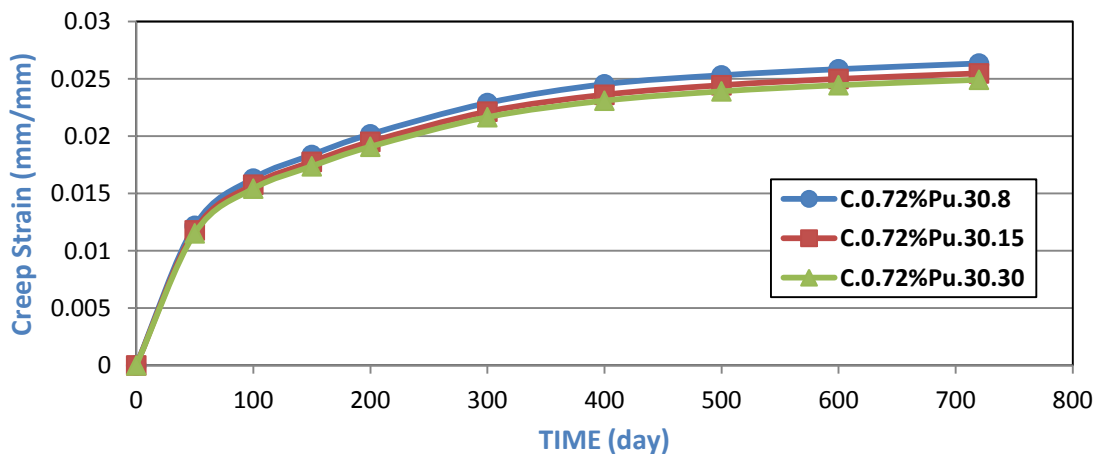


Fig.(B-57) :Time vs Creep Strain Behavior for Models(C.0.72%Pu.30.#)

Appendix B: Tables and Figures of Parametric Study

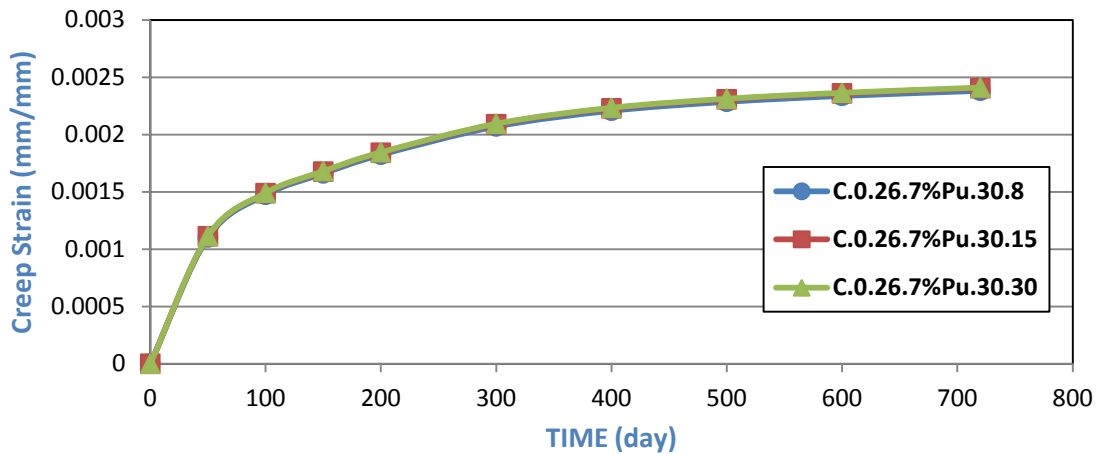


Fig.(B-58) :Time vs Creep Strain Behavior for Models(C.0.26.7%Pu.30.#)

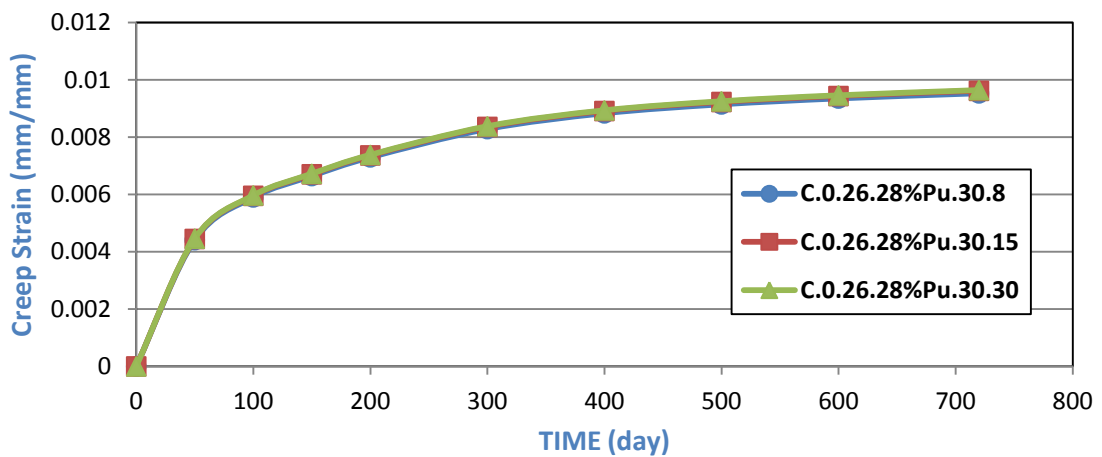


Fig.(B-59) :Time vs Creep Strain Behavior for Models(C.0.26.28%Pu.30.#)

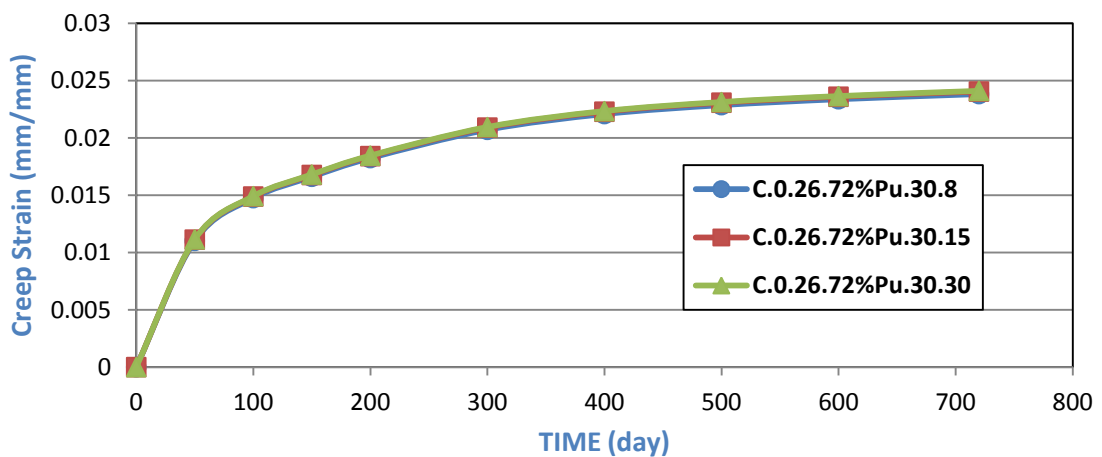


Fig.(B-60) :Time vs Creep Strain Behavior for Models(C.0.26.72%Pu.30.#)

Appendix B: Tables and Figures of Parametric Study

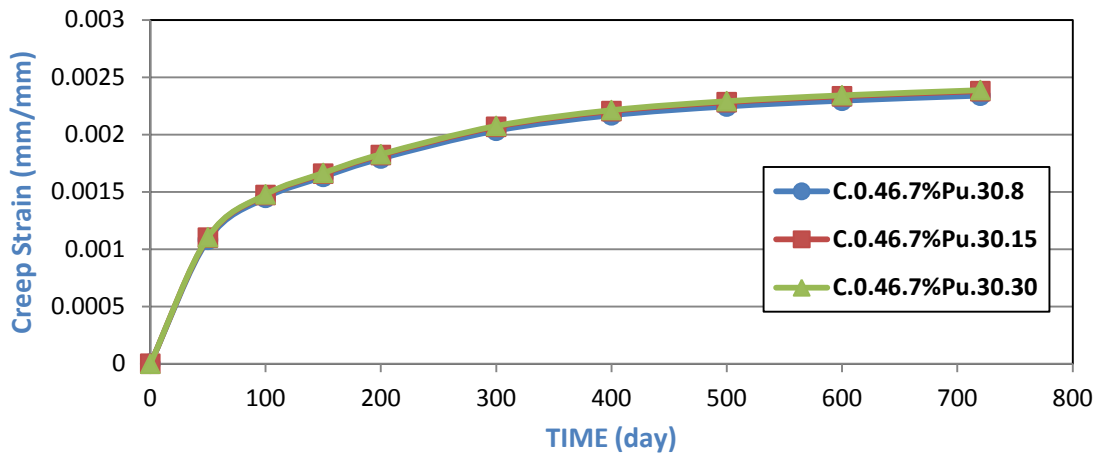


Fig.(B-61) :Time vs Creep Strain Behavior for Models(C.0.46.7%Pu.30.#)

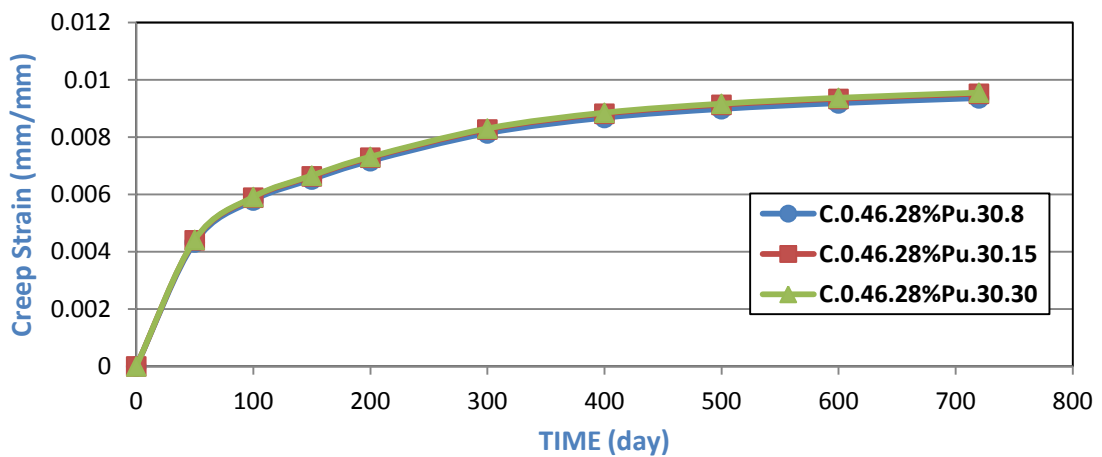


Fig.(B-62) :Time vs Creep Strain Behavior for Models(C.0.46.28%Pu.30.#)

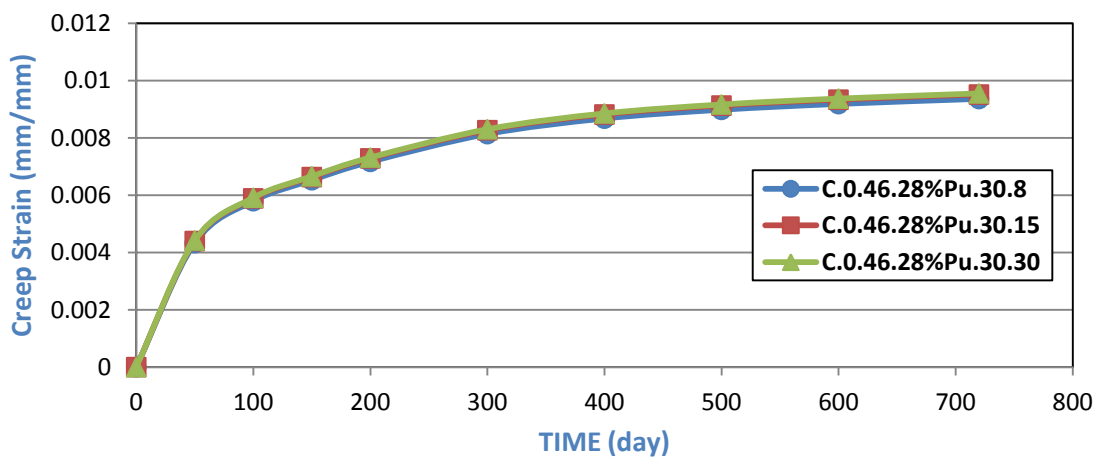


Fig.(B-63) :Time vs Creep Strain Behavior for Models(C.0.46.72%Pu.30.#)

Appendix B: Tables and Figures of Parametric Study

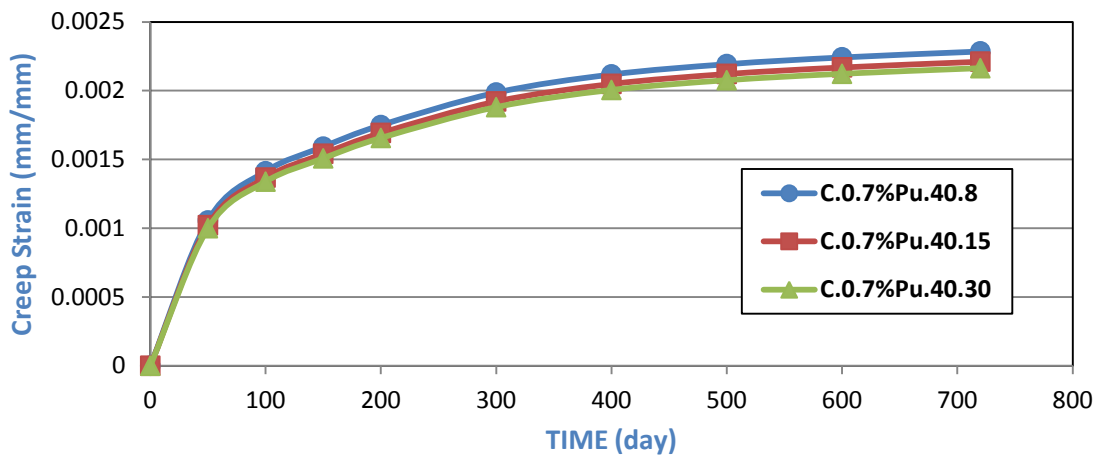


Fig.(B-64) :Time vs Creep Strain Behavior for Models(C.0.7%Pu.40.#)

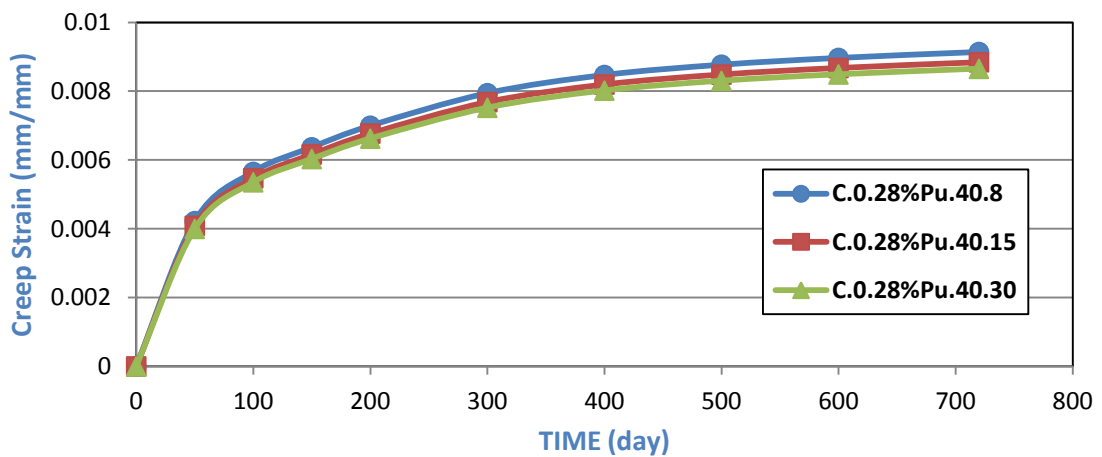


Fig.(B-65) :Time vs Creep Strain Behavior for Models(C.0.28%Pu.40.#)

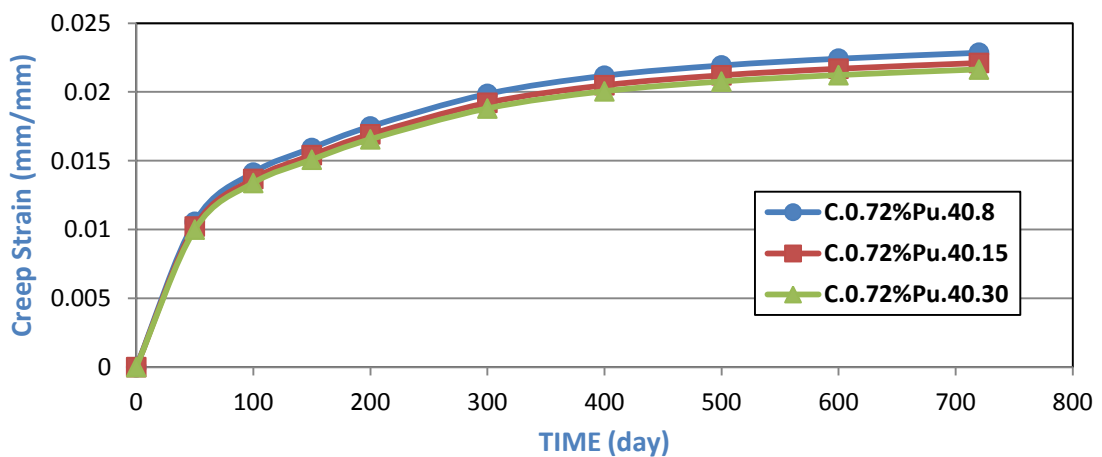


Fig.(B-66) :Time vs Creep Strain Behavior for Models(C.0.72%Pu.40.#)

Appendix B: Tables and Figures of Parametric Study

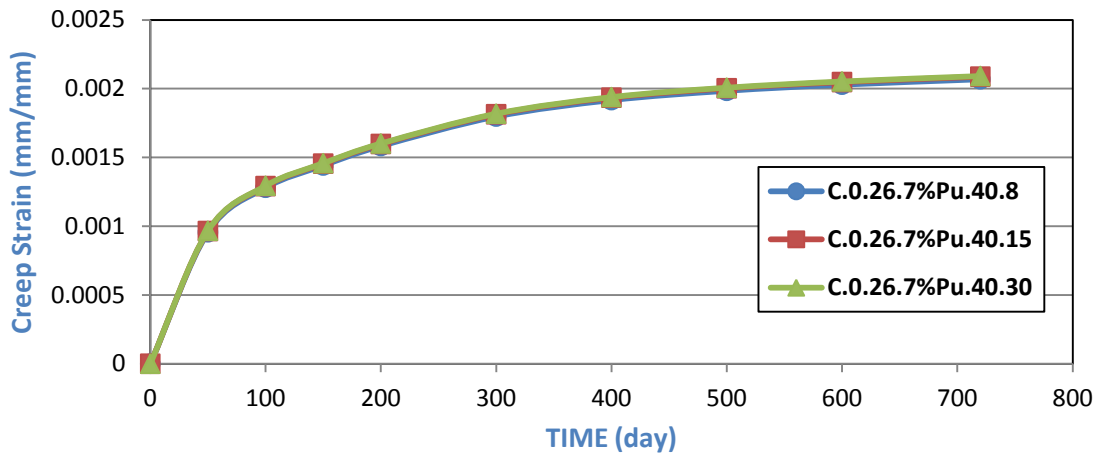


Fig.(B-67) :Time vs Creep Strain Behavior for Models(C.0.26.7%Pu.40.#)

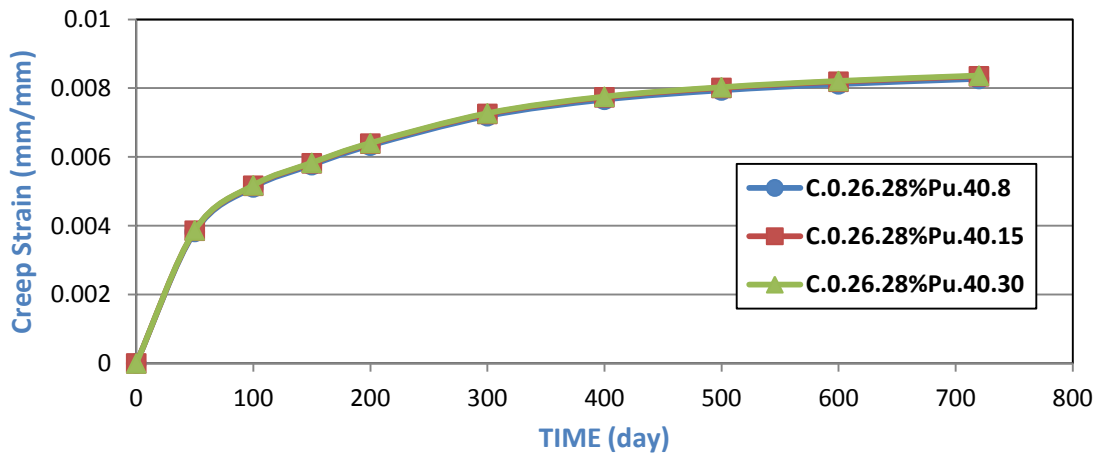


Fig.(B-68) :Time vs Creep Strain Behavior for Models(C.0.26.28%Pu.40.#)

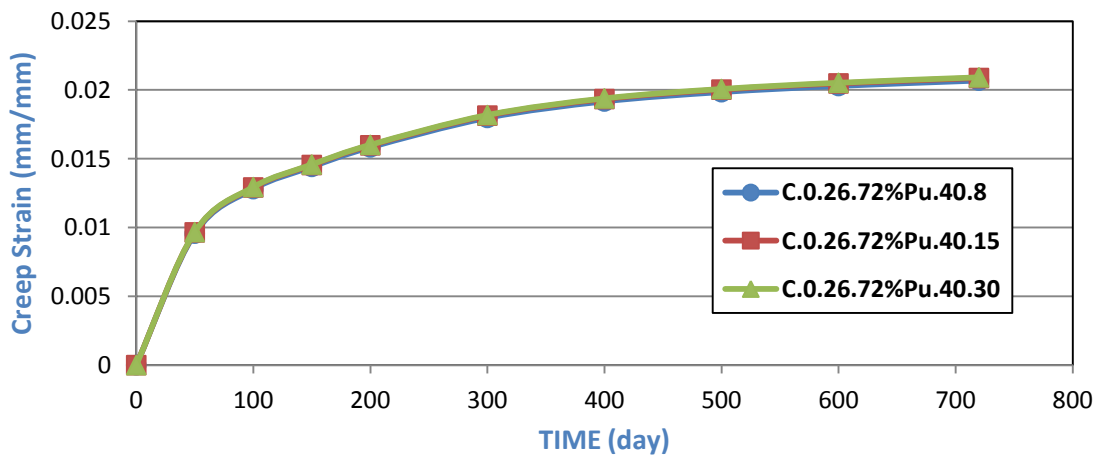


Fig.(B-69) :Time vs Creep Strain Behavior for Models(C.0.26.72%Pu.40.#)

Appendix B: Tables and Figures of Parametric Study

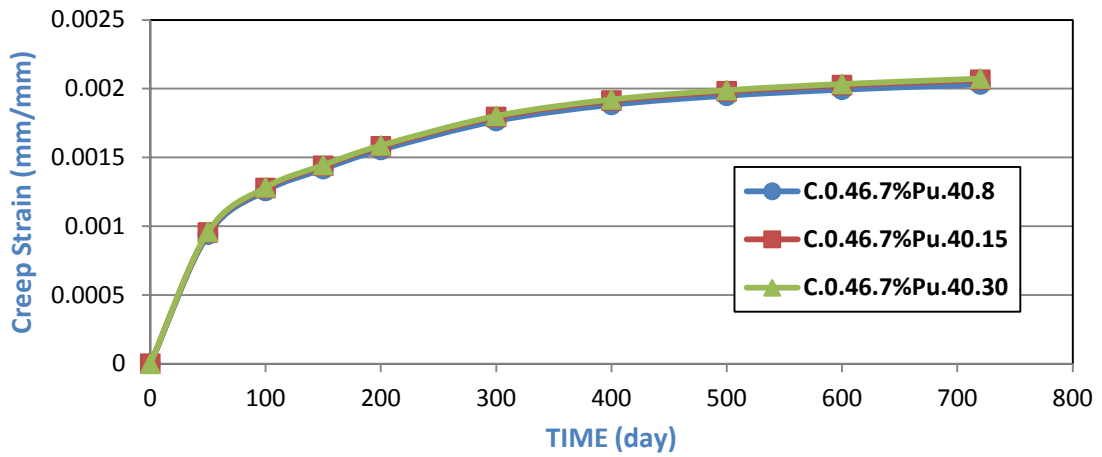


Fig.(B-70) :Time vs Creep Strain Behavior for Models(C.0.46.7%Pu.40.#)

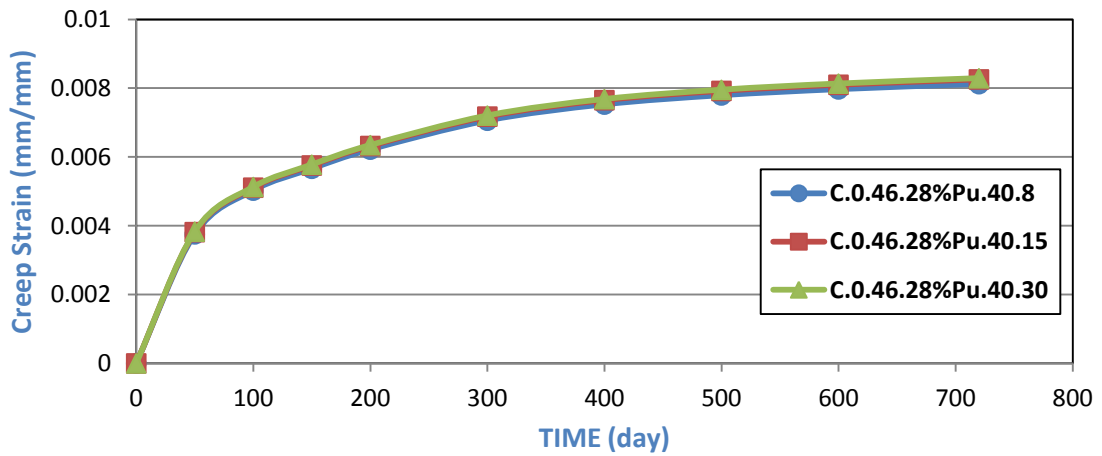


Fig.(B-71) :Time vs Creep Strain Behavior for Models(C.0.46.28%Pu.40.#)

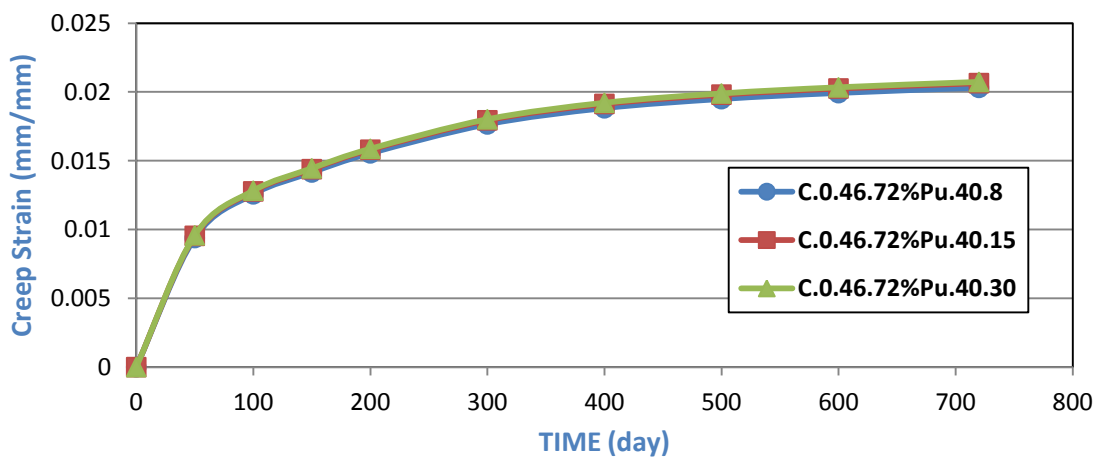


Fig.(B-72) :Time vs Creep Strain Behavior for Models(C.0.46.72%Pu.40.#)

Appendix B: Tables and Figures of Parametric Study

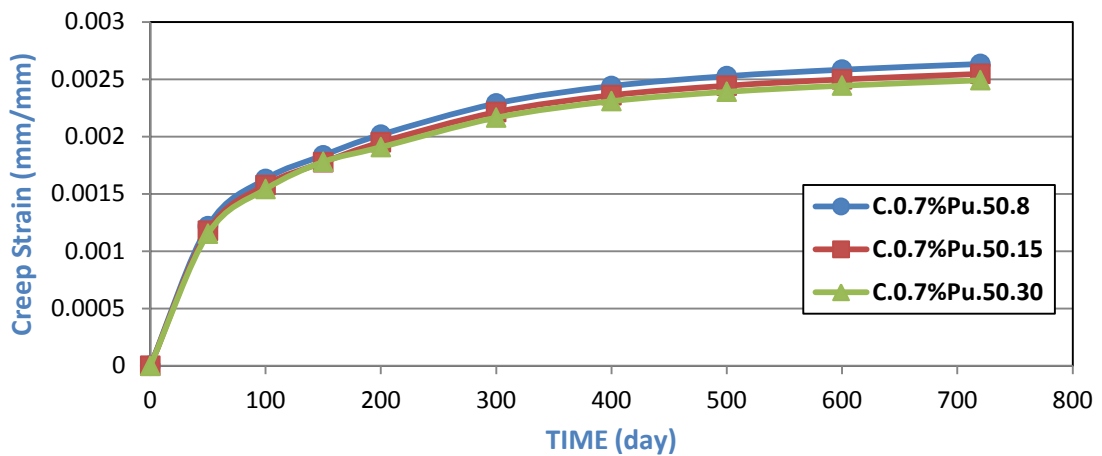


Fig.(B-73) :Time vs Creep Strain Behavior for Models(C.0.7%Pu.50.#)

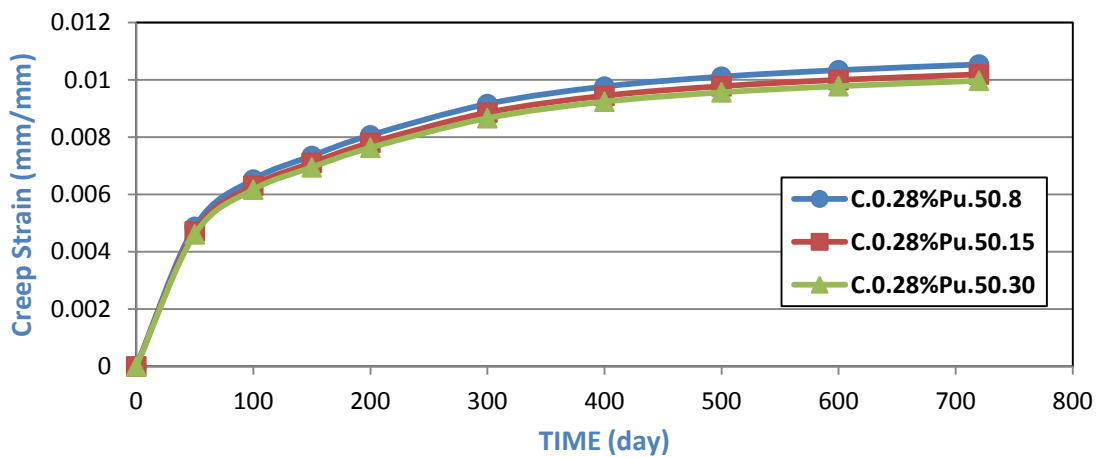


Fig.(B-74) :Time vs Creep Strain Behavior for Models(C.0.28%Pu.50.#)

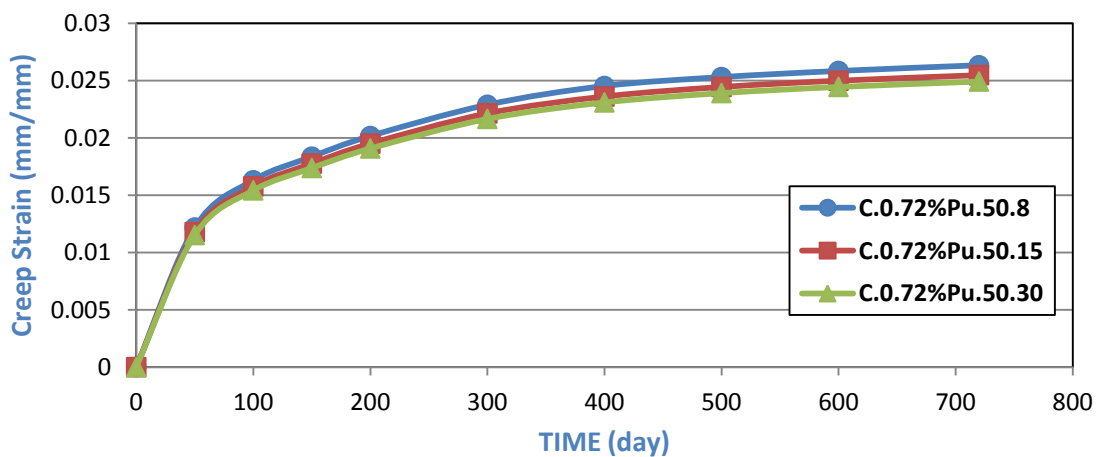


Fig.(B-75) :Time vs Creep Strain Behavior for Models(C.0.72%Pu.50.#)

Appendix B: Tables and Figures of Parametric Study

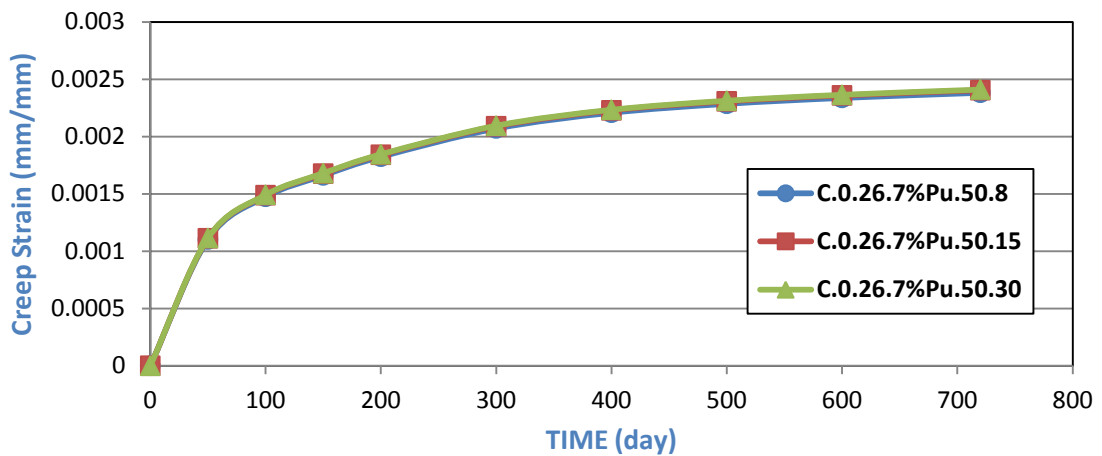


Fig.(B-76) :Time vs Creep Strain Behavior for Models(C.0.26.7%Pu.50.#)

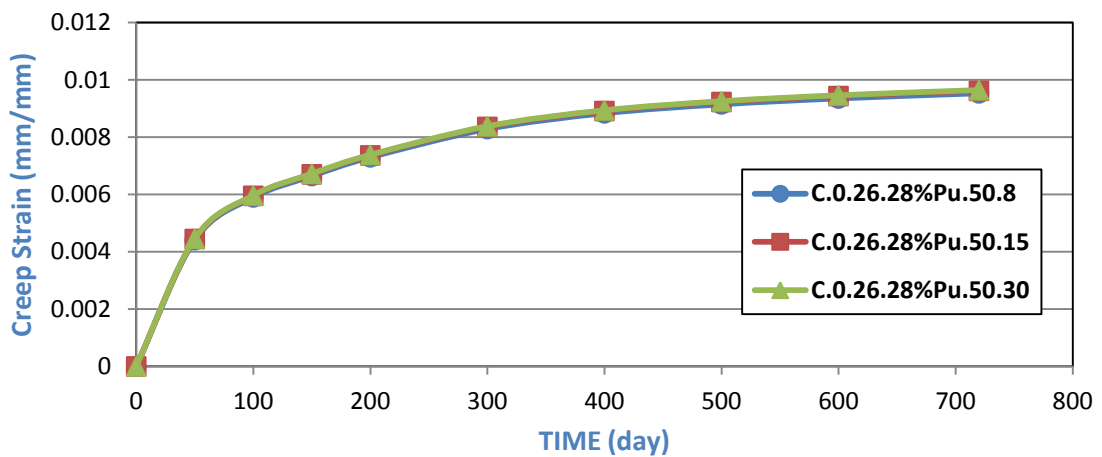


Fig.(B-77) :Time vs Creep Strain Behavior for Models(C.0.26.28%Pu.50.#)

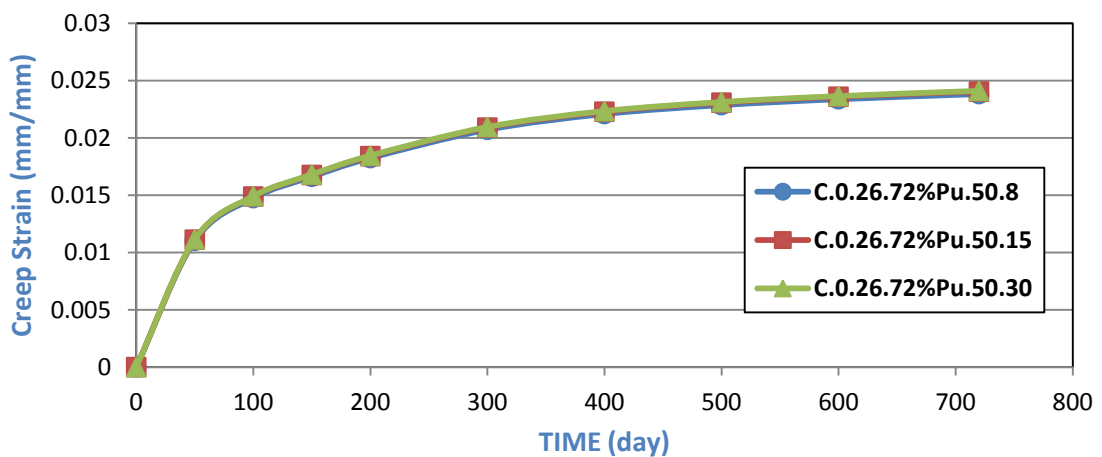


Fig.(B-78) :Time vs Creep Strain Behavior for Models(C.0.26.72%Pu.30.#)

Appendix B: Tables and Figures of Parametric Study

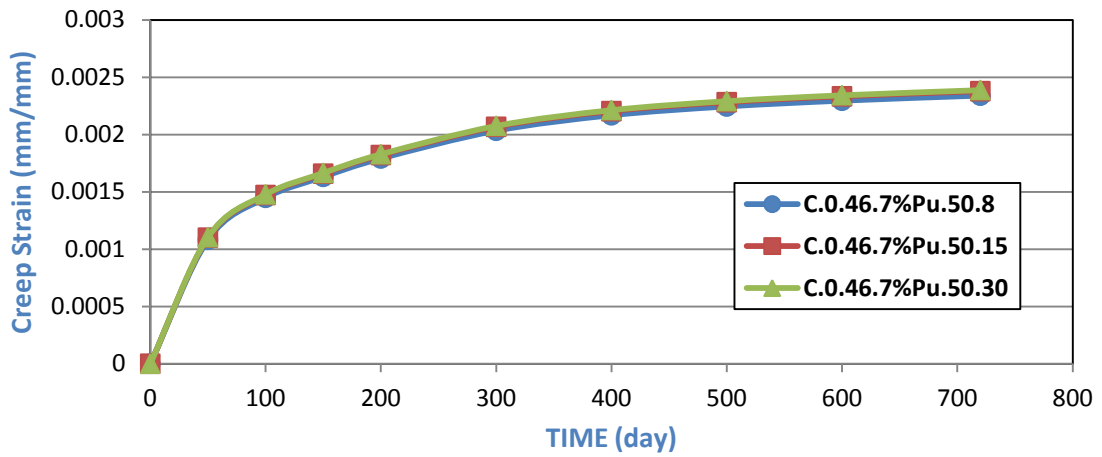


Fig.(B-79) :Time vs Creep Strain Behavior for Models(C.0.46.7%Pu.50.#)

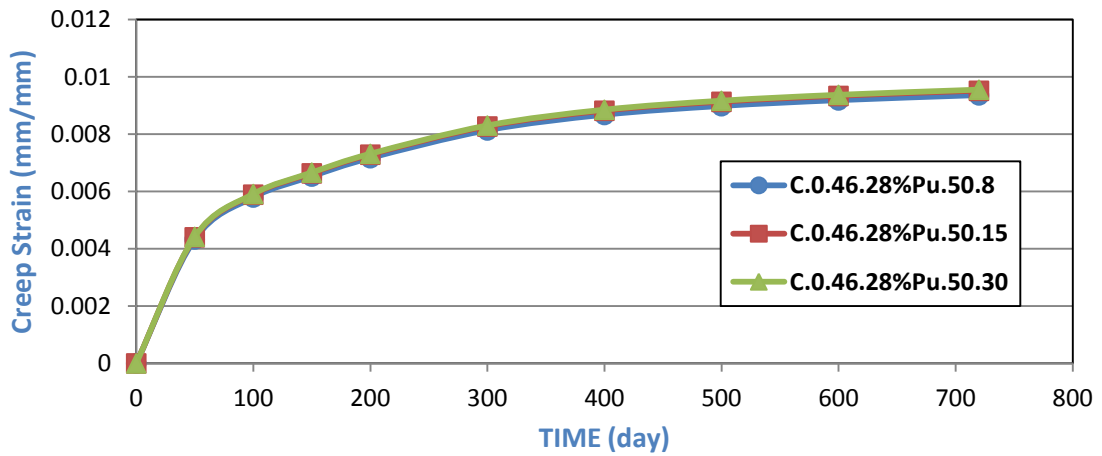


Fig.(B-80) :Time vs Creep Strain Behavior for Models(C.0.46.28%Pu.50.#)

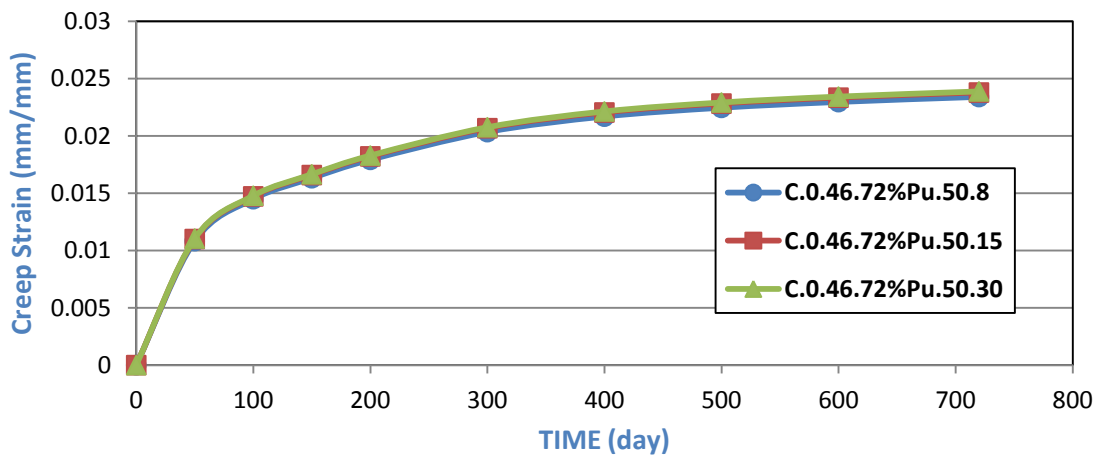


Fig.(B-81) :Time vs Creep Strain Behavior for Models(C.0.46.72%Pu.50.#)

Appendix B: Tables and Figures of Parametric Study

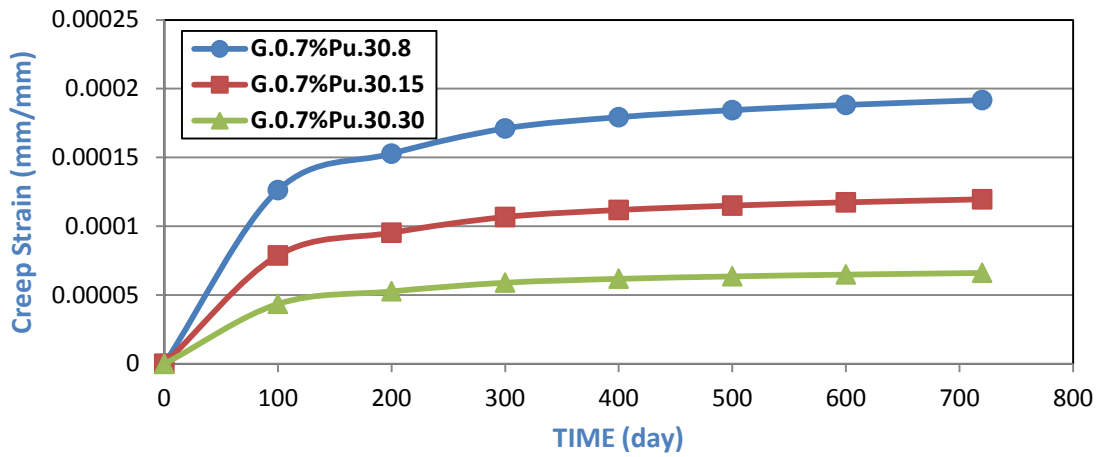


Fig.(B-82) :Time vs Creep Strain Behavior for Models(G.0.7%Pu.30.#)

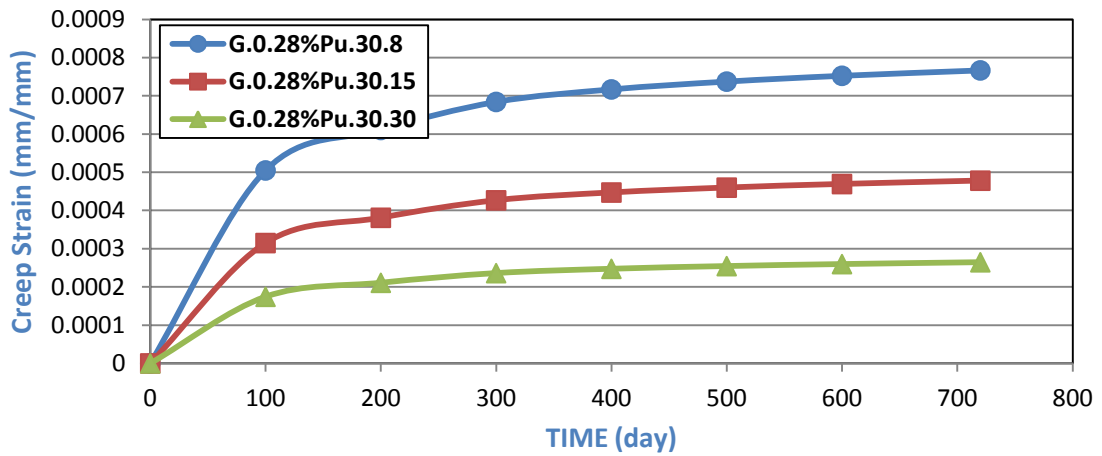


Fig.(B-83) :Time vs Creep Strain Behavior for Models(G.0.28%Pu.30.#)

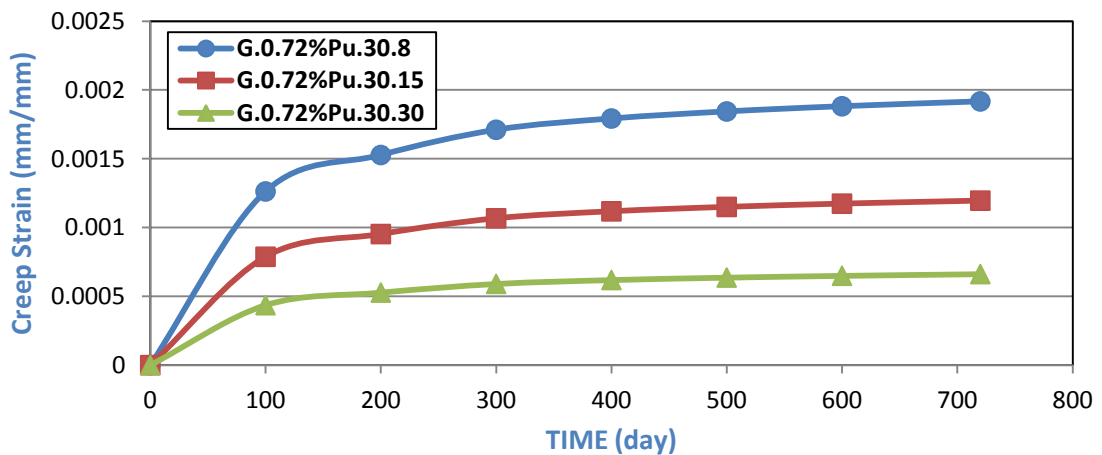


Fig.(B-84) :Time vs Creep Strain Behavior for Models(C.0.72%Pu.30.#)

Appendix B: Tables and Figures of Parametric Study

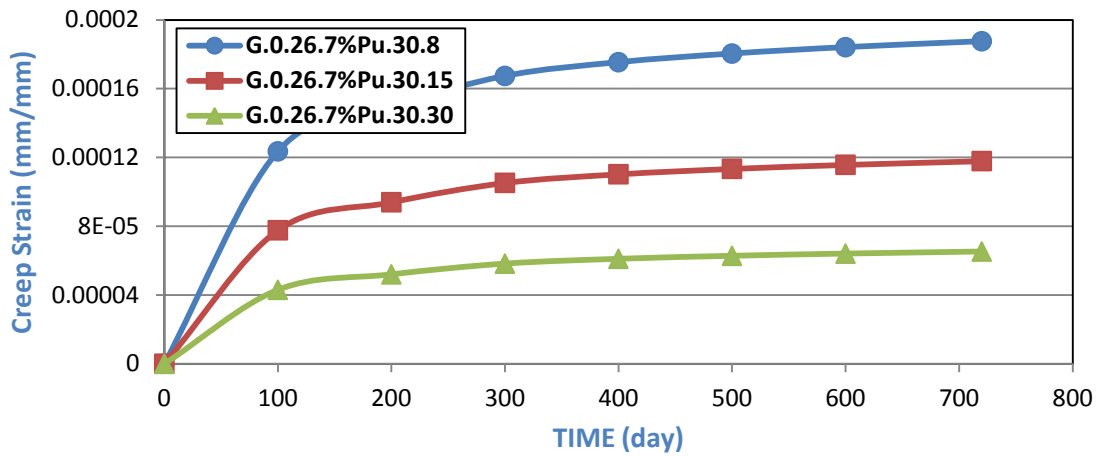


Fig.(B-85) :Time vs Creep Strain Behavior for Models(G.0.26.7%Pu.30.#)

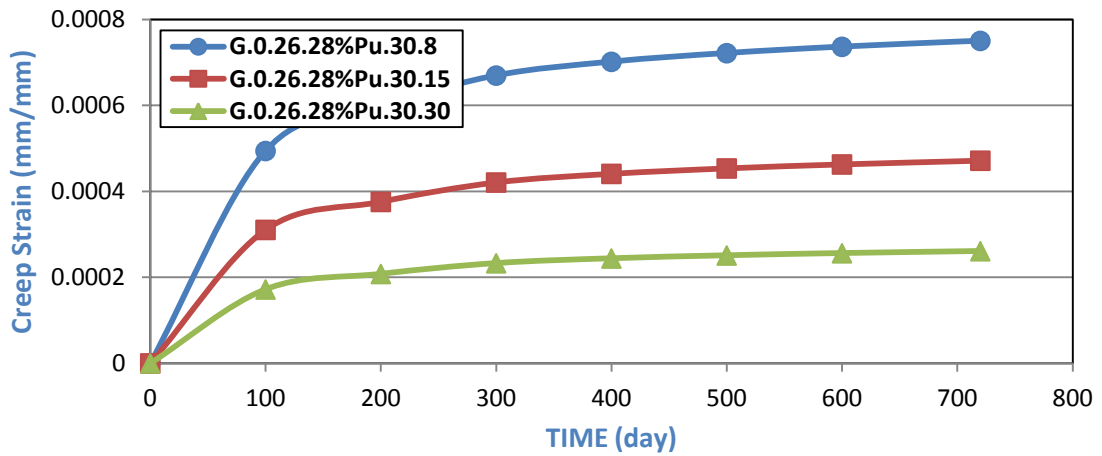


Fig.(B-86) :Time vs Creep Strain Behavior for Models(G.0.26.28%Pu.30.#)

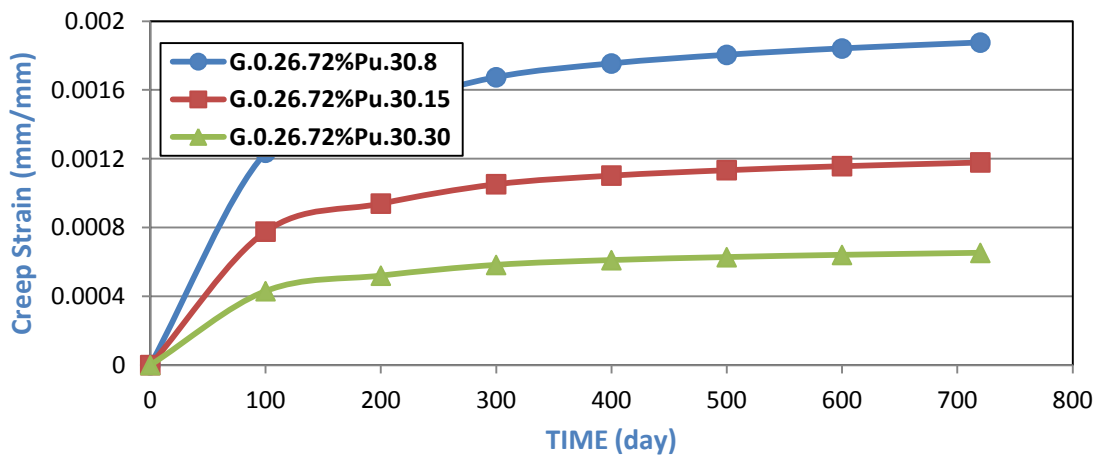


Fig.(B-87) :Time vs Creep Strain Behavior for Models(G.0.26.72%Pu.30.#)

Appendix B: Tables and Figures of Parametric Study

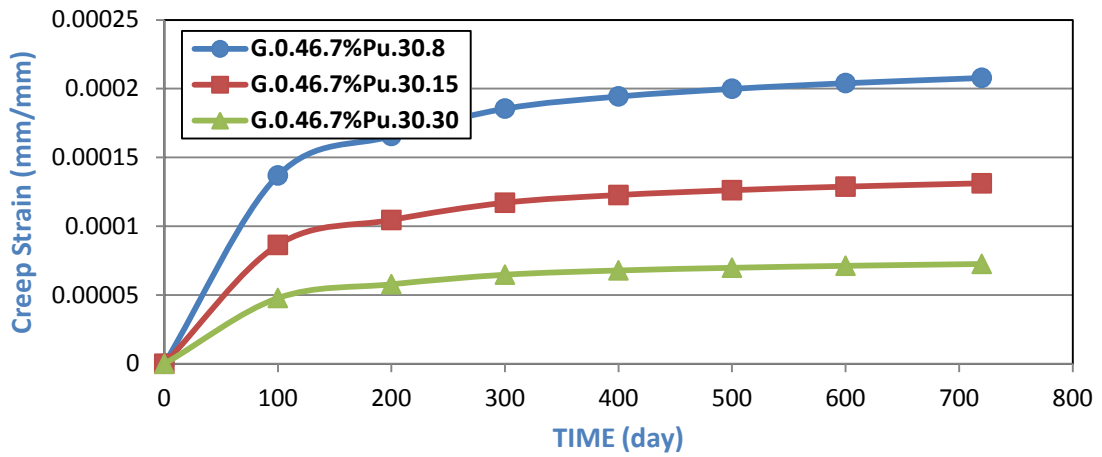


Fig.(B-88) :Time vs Creep Strain Behavior for Models(G.0.46.7%Pu.30.#)

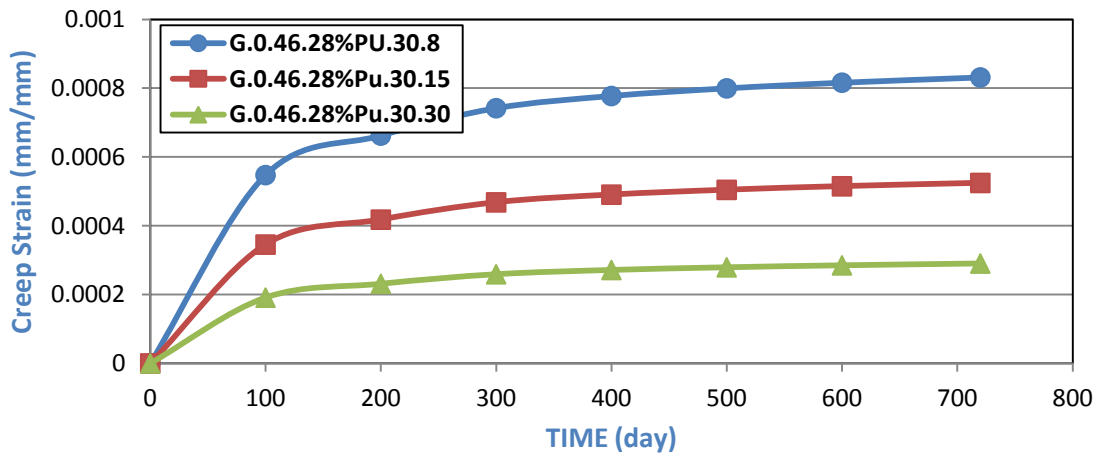


Fig.(B-89) :Time vs Creep Strain Behavior for Models(G.0.46.28%Pu.30.#)

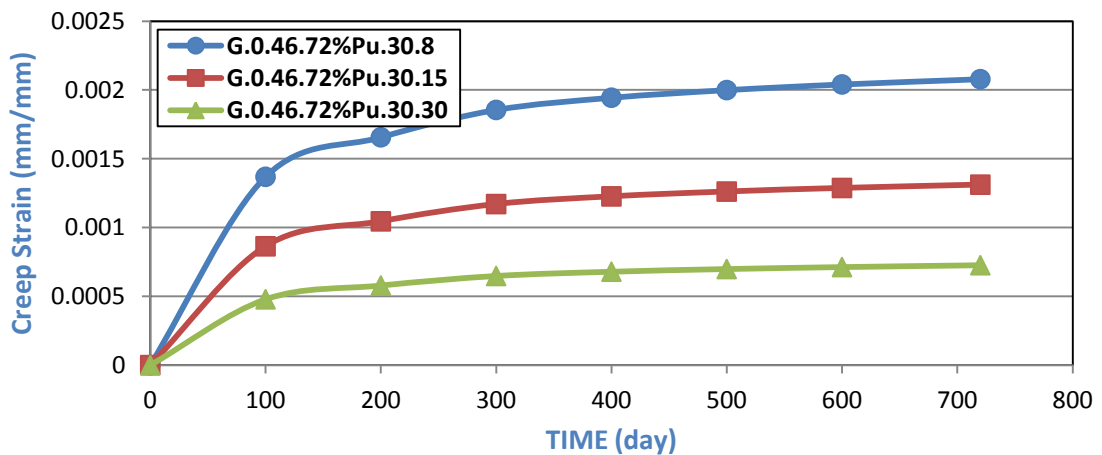


Fig.(B-90) :Time vs Creep Strain Behavior for Models(G.0.46.72%Pu.30.#)

Appendix B: Tables and Figures of Parametric Study

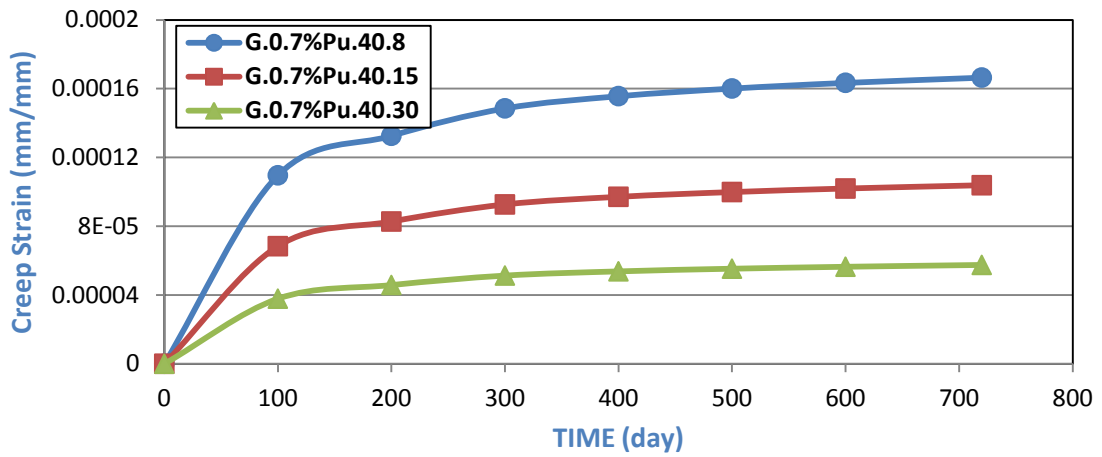


Fig.(B-91) :Time vs Creep Strain Behavior for Models(G.0.7%Pu.40.#)

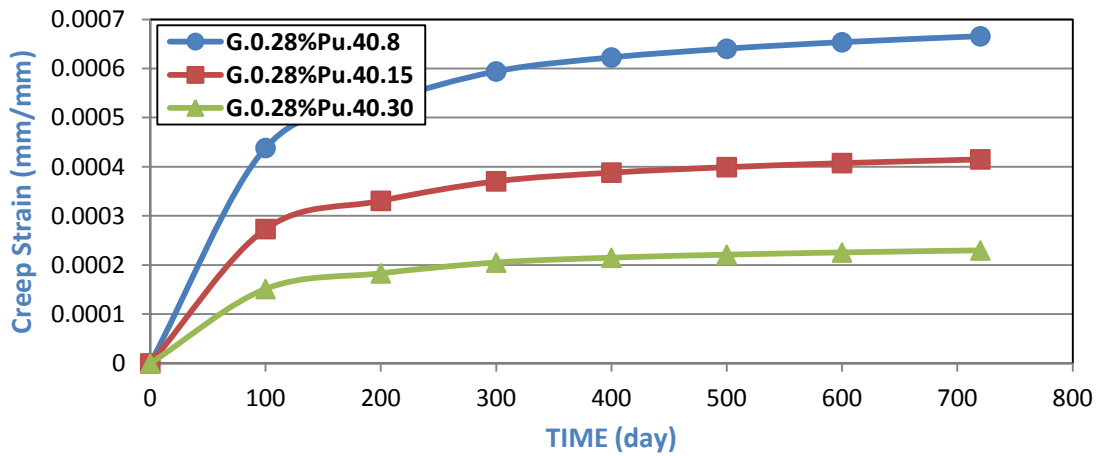


Fig.(B-92) :Time vs Creep Strain Behavior for Models(G.0.28%Pu.40.#)

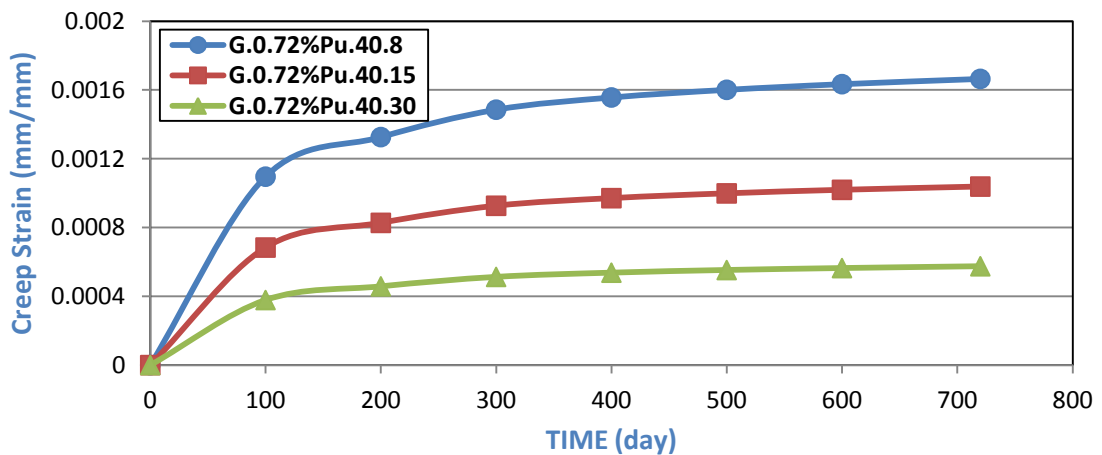


Fig.(B-93) :Time vs Creep Strain Behavior for Models(G.0.72%Pu.40.#)

Appendix B: Tables and Figures of Parametric Study

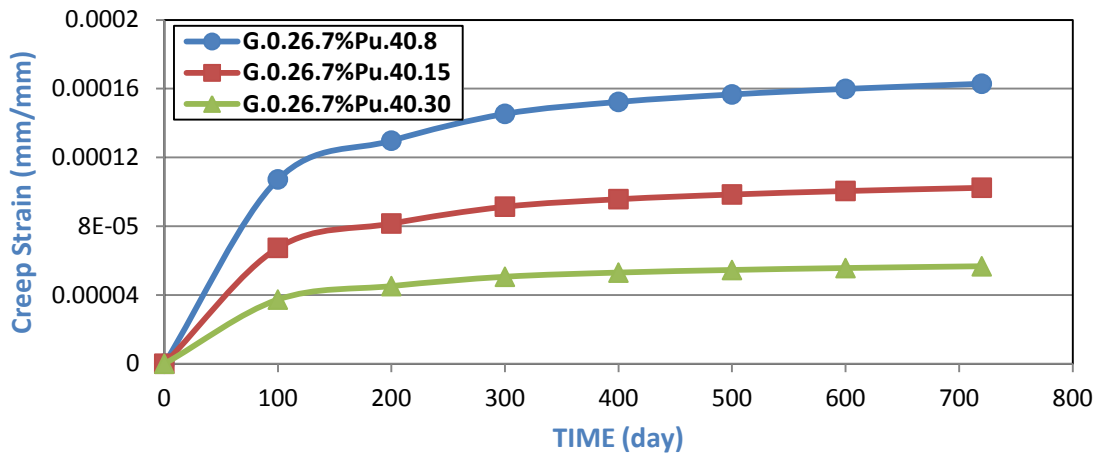


Fig.(B-94) :Time vs Creep Strain Behavior for Models(G.0.26.7%Pu.40.#)

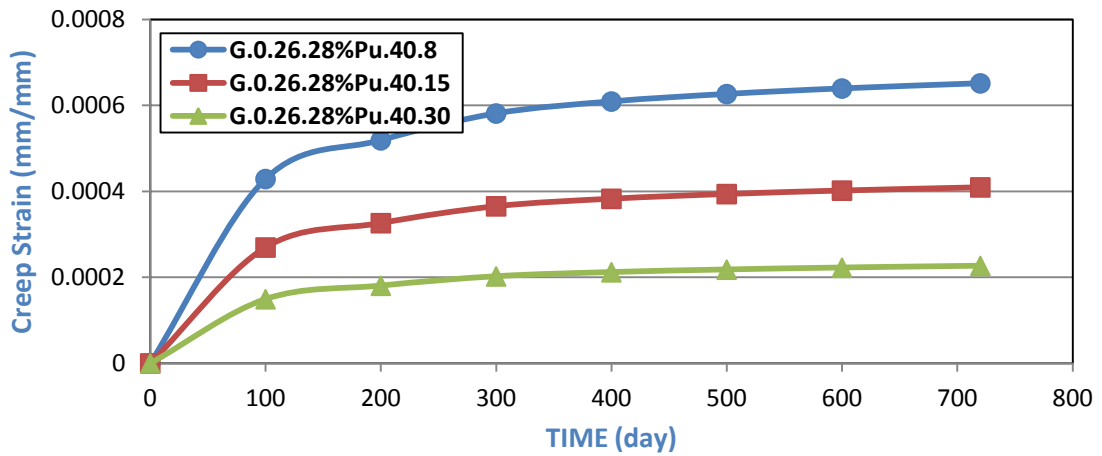


Fig.(B-95) :Time vs Creep Strain Behavior for Models(G.0.26.28%Pu.40.#)

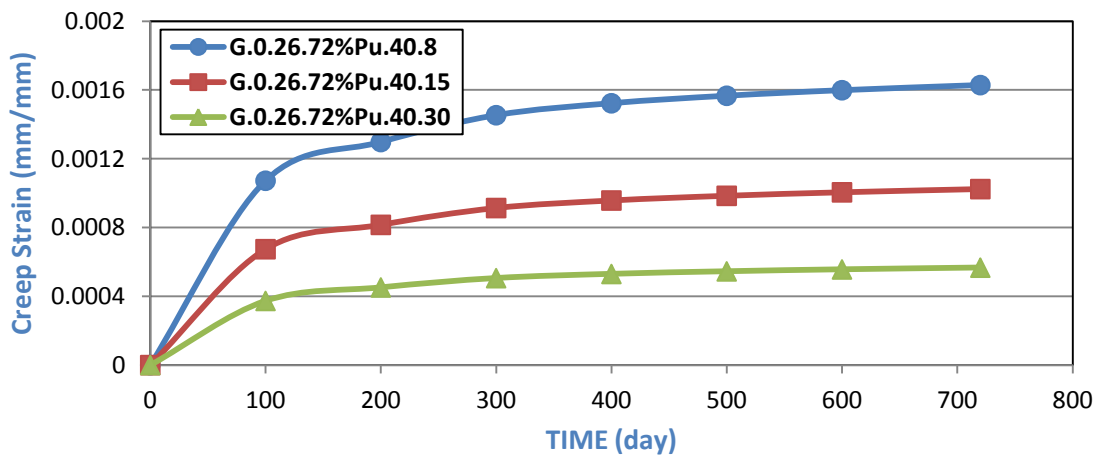


Fig.(B-96) :Time vs Creep Strain Behavior for Models(G.0.26.72%Pu.40.#)

Appendix B: Tables and Figures of Parametric Study

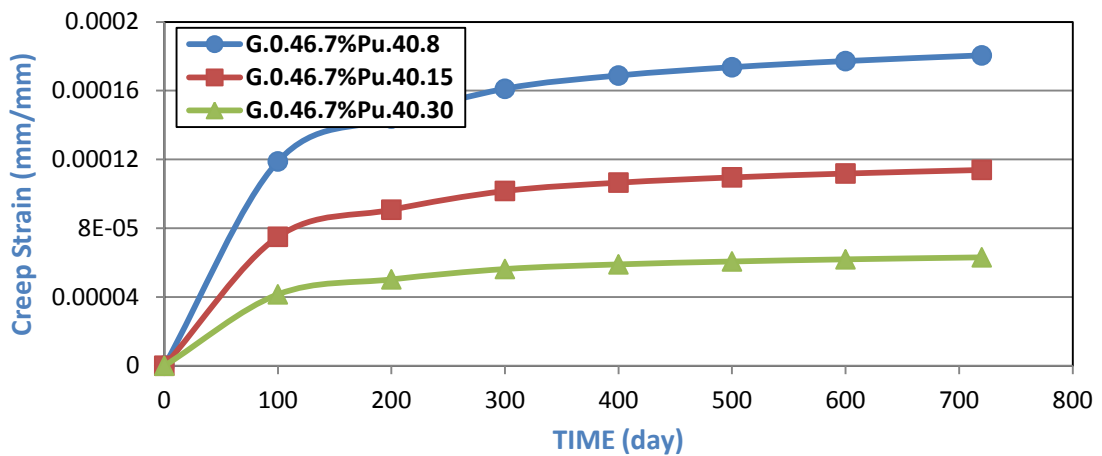


Fig.(B-97) :Time vs Creep Strain Behavior for Models(G.0.46.7%Pu.40.#)

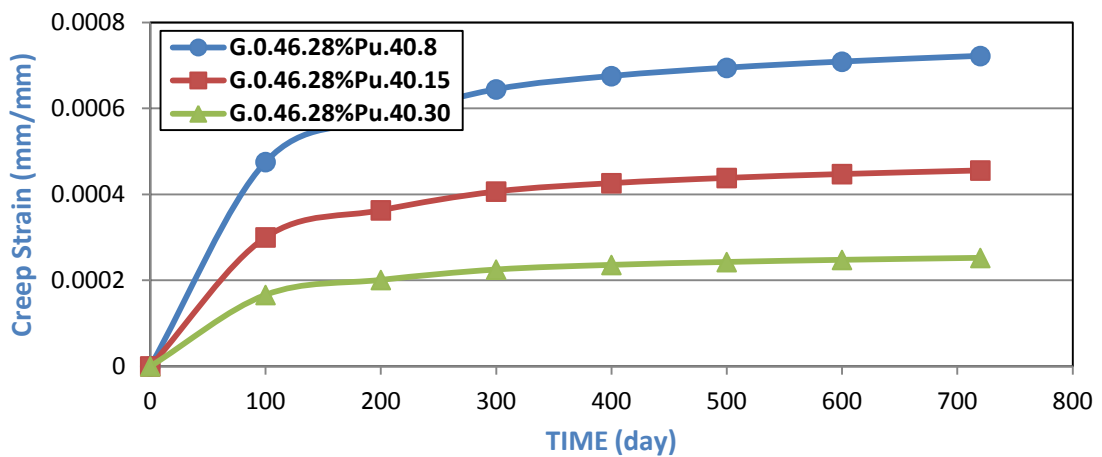


Fig.(B-98) :Time vs Creep Strain Behavior for Models(G.0.46.28%Pu.40.#)

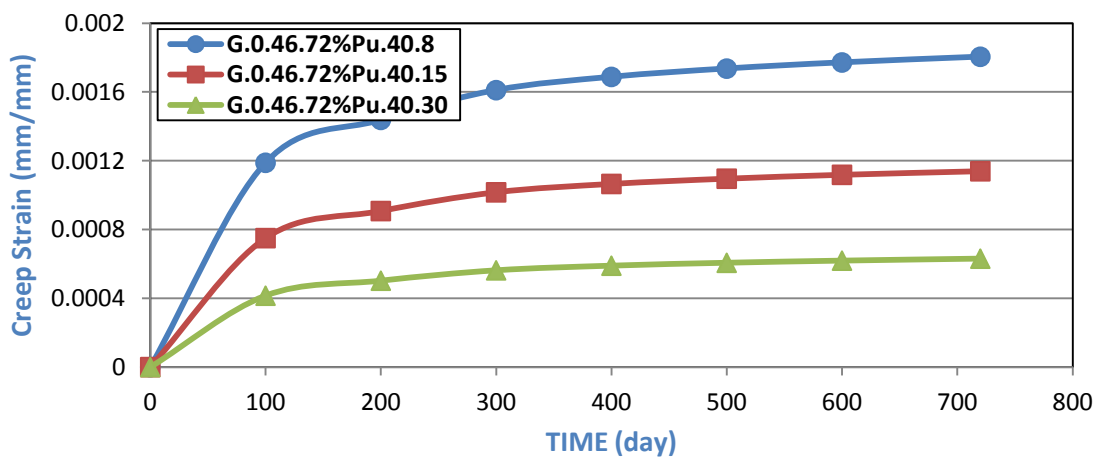


Fig.(B-99) :Time vs Creep Strain Behavior for Models(G.0.46.72%Pu.40.#)

Appendix B: Tables and Figures of Parametric Study

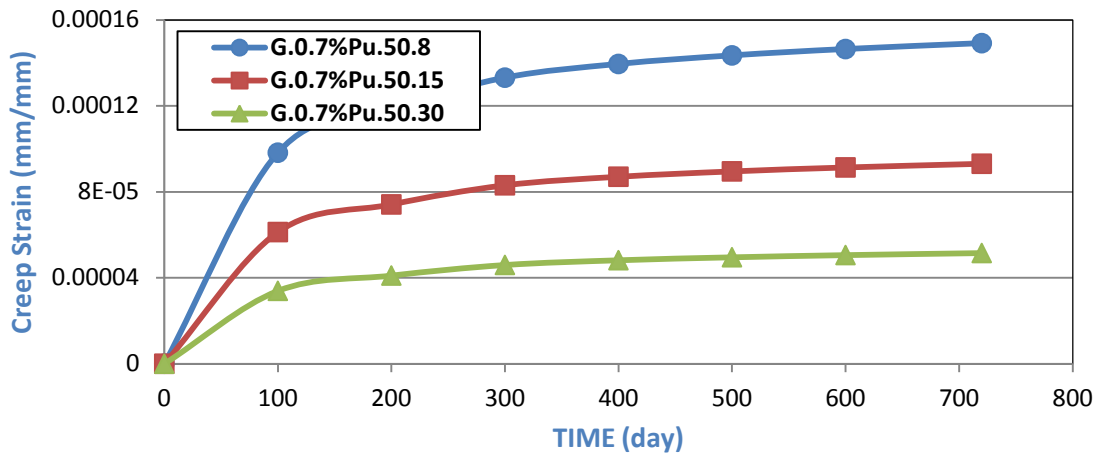


Fig.(B-100) :Time vs Creep Strain Behavior for Models(G.0.7%Pu.50.#)

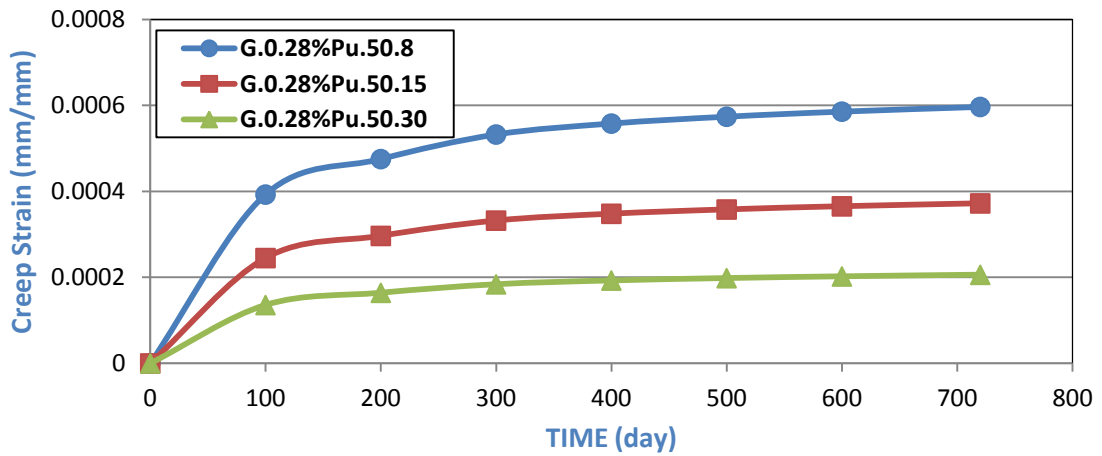


Fig.(B-101) :Time vs Creep Strain Behavior for Models(G.0.28%Pu.50.#)

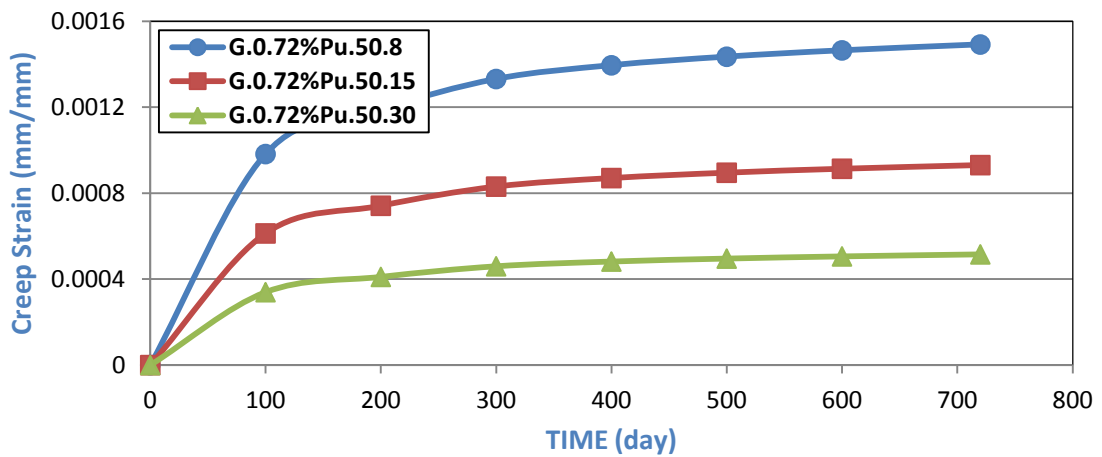


Fig.(B-102) :Time vs Creep Strain Behavior for Models(G.0.72%Pu.50.#)

Appendix B: Tables and Figures of Parametric Study

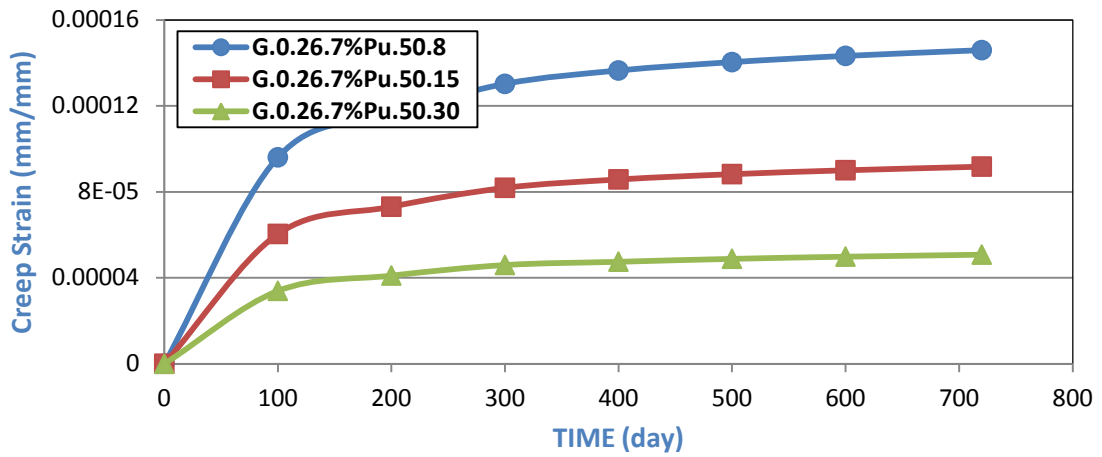


Fig.(B-103) :Time vs Creep Strain Behavior for Models(G.0.26.7%Pu.50.#)

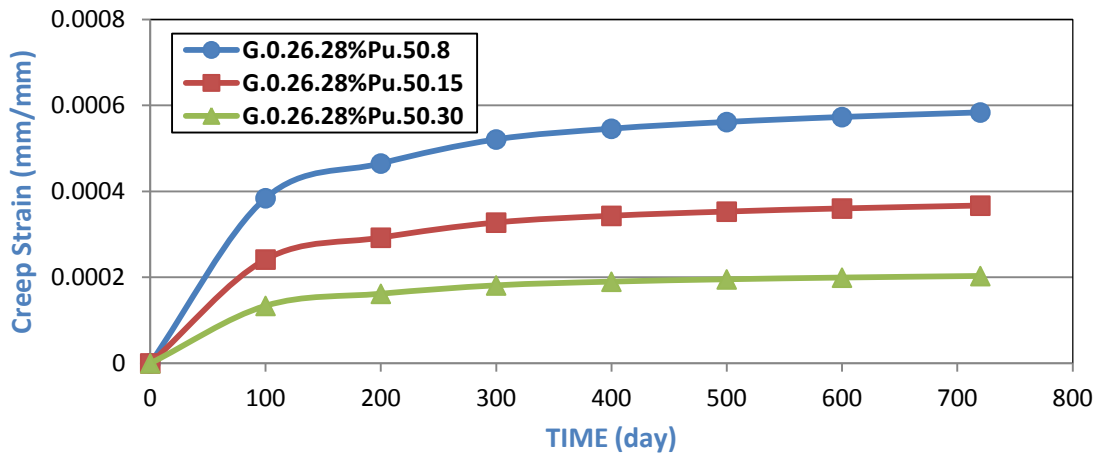


Fig.(B-104) :Time vs Creep Strain Behavior for Models(G.0.26.28%Pu.50.#)

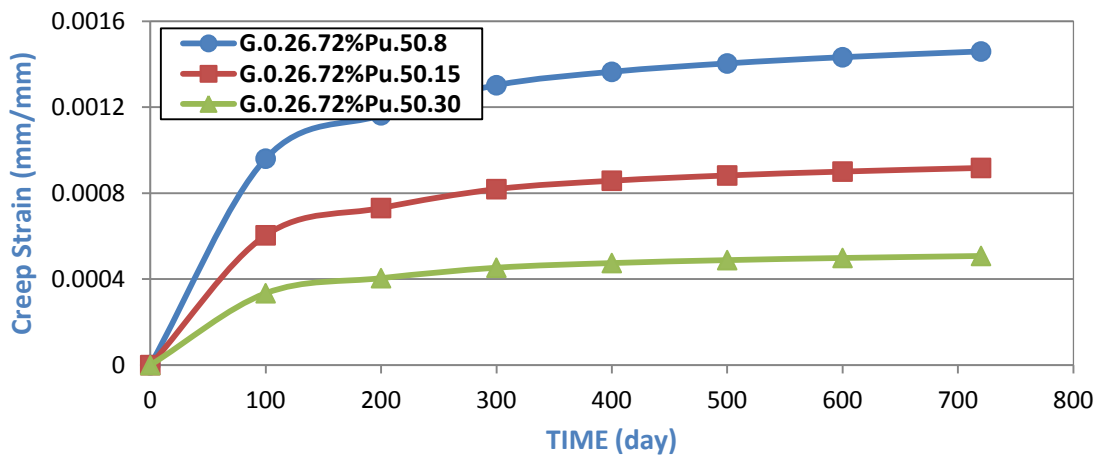


Fig.(B-105) :Time vs Creep Strain Behavior for Models(G.0.26.72%Pu.50.#)

Appendix B: Tables and Figures of Parametric Study

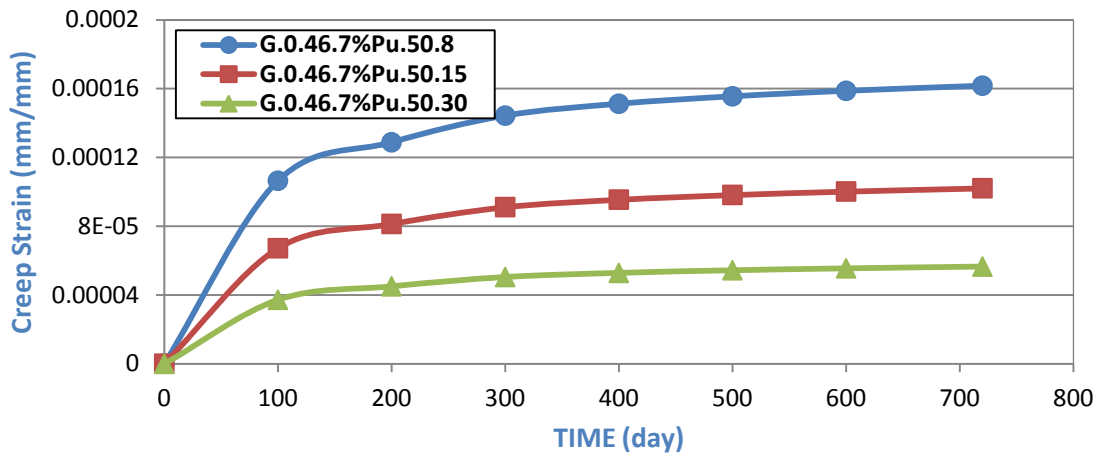


Fig.(B-106) :Time vs Creep Strain Behavior for Models(G.0.46.7%Pu.50.#)

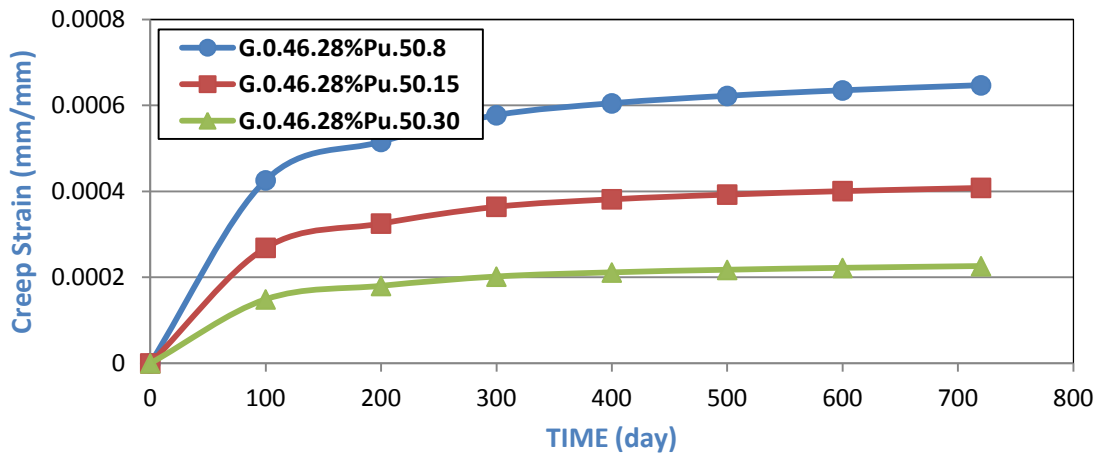


Fig.(B-107) :Time vs Creep Strain Behavior for Models(G.0.46.28%Pu.50.#)

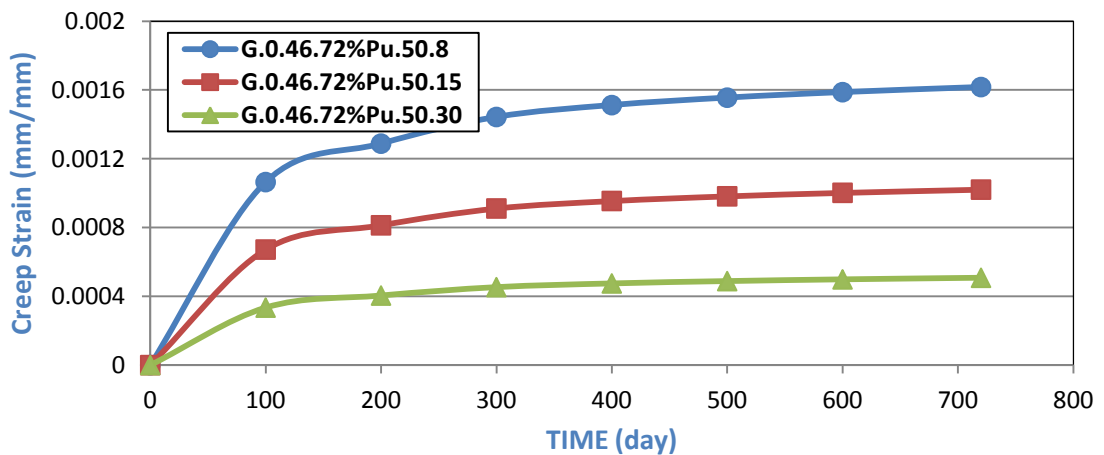


Fig.(B-108) :Time vs Creep Strain Behavior for Models(G.0.46.72%Pu.50.#)